AD-A248 337

Department of the Navy

Office of Naval Research

Electrochemistry in Colloids and Dispersions

Volume III

COLLOIDAL SEMICONDUCTORS

A final report to the Department of the Navy, compiled by the

Division of Colloid and Surface Chemistry

of the American Chemical Society

4 February 1992

92-06924

||||||||||||||||||||||||

92 3 17 046

AD-A248 337

Best
Available
Copy

****

(21) REDOX MECHANISMS IN HETEROGENEOUS PHOTOCATALYSIS.

THE CASE OF HOLES vs. OH°RADICAL OXIDATION AND FREE vs. SURFACE-

BOUND OH°RADICAL OXIDATION PROCESSES

****

Nick Serpone,*[1,2] Darren Lawless,[1] Rita Terzian,[1] and Dan Meisel[3]

[1] Department of Chemistry, Concordia University, 1455 deMaisonneuve
       Blvd. West, Montréal, Québec, Canada H3G 1M8.

[2] Laboratoire de Photocatalyse, Catalyse et Environnement, URA au CNRS,
       Ecole Centrale de Lyon, 69130 Ecully, France.

[3] Chemistry Division, Argonne National Laboratory, 9700 South Cass
       Avenue, Argonne, Illinois, USA 60439.

Accesion For		
NTIS CRA&I	☑	
DTIC TAB	☐	
Unannounced	☐	
Justification		
By		
Dist ibution /		
Availability Codes		
Dist	Avail and/or Special	
A-1		

*Please address all correspondence to Prof. N. Serpone at Concordia
University.*

ABSTRACT

Photo-assisted redox processes mediated by illuminated semiconductor particles find their origin with the electron/hole pair formed subsequent to the light absorption event. This article focusses on those events occurring on TiO_2 particles (anatase form; bandgap energy 3.2 eV) in aqueous media. In particular, the emphasis is placed on the photo-oxidative reactions induced initially by the valence band hole (redox potential at pH ~ 0, ca. 3.0-3.2 V) and which find practical application in the degradation of a variety of organic compounds (aliphatic and aromatic) of varying complexity, as might be found in waste waters or industrial effluents. While the total oxidative mineralization of these compounds has been demonstrated, as evidenced by observation of stoichiometric formation of CO_2 in every case, the intimate details of process kinetics and mechanisms have not been documented. The very nature of the oxidizing species has been invoked by some to be the valence band holes (free or trapped) interacting directly with the organic substrate and by others to be the OH• radical, formed by hole oxidation of the OH⁻ groups or H_2O molecules on the TiO_2 particle surface. As well, taking the OH• radical to be the oxidant, two schools have evolved recently, distinguished by whether oxidation by OH• species occurs at the particle surface or by a free OH• radical which desorbed into the solution bulk. Herein, we present some of the data and arguments germane to the questions raised and present some recent pulse radiolysis results which bear on these issues.

$\mathcal{III}$ - 2

ABSTRACT

This report summarizes the current status of experimental and theoretical studies which address fundamental and applied aspects of electrochemistry in colloids and dispersions. The range of such microheterogeneous fluids examined includes micellar solutions, microemulsions, emulsions, latexes, and dispersions of solids in liquids. Several broad subtopics are described. These topics include electroanalytical methods and applications, solute distribution, diffusion, and transport, electrosynthesis and electrocatalysis, polymers and latexes, and colloidal metals and semiconductors.

This report is presented in three volumes, I, II, and III.

CONTENTS

CONTENTS

CONTENTS

INTRODUCTION

Recent discussions in heterogeneous photocatalyzed mineralization of organic contaminants, mediated by illuminated TiO_2 anatase, have centered on mechanistic details in efforts to improve the photocatalytic activity of the TiO_2 material, and to understand the role and importance of mineralization by *free* versus *surface bound* oxidizing radicals ($OH^•$) on the one hand and versus direct hole oxidation on the other. If the potential of this semiconductor in photocatalytic processes can be maximized, a better understanding of the chemical nature of the photo-formed electrons and holes, together with the role(s) these species play in heterogeneous reactions at the TiO_2/electrolyte interface is required.[1] Despite the various efforts, the mechanism of the photocatalyzed oxidative degradation of organics remains unclear. Even the optical characteristics of the photo-generated valence band holes in illuminated TiO_2 have not been established. Conflicting reports have assigned absorption features which appear in the near UV-visible region to photogenerated holes [see ref.2 for a recent discussion].

Two principal pathways have been proposed in the mineralization of organic substrates or oxidation of inorganic materials. One of these considers the surface OH^- groups and/or molecular water on TiO_2 as the primary target(s) for the reaction of the photogenerated holes, a reaction which yields $OH^•$ radicals. The current prevailing view favors these radicals as the primary oxidizing species, which proceed to react with the substrate.[3] The alternative pathway involves direct hole oxidation of the organic substrate, a view reinforced by a recent study[4] which failed to detect any of the expected OH-adduct intermediates following flash photolysis of several TiO_2/substrate combinations.

3

Added to the issue of the nature of the primary oxidizing species, another problem that has been raised is whether the primary oxidation event implicating the OH[•] radical occurs on the photocatalyst's surface or in solution, subsequent to its desorption.

In this paper, we first discuss the nature of the heterogeneous surface and then some of the more significant results and conclusions reached by others. Subsequently, we look at our recent pulse radiolysis work[5,6] in which we examine the reaction of OH[•] radicals with colloidal (6.5 nm rad.) TiO_2 particles in aqueous media. We find that reaction of the OH[•] radical with the TiO_2 occurs at a diffusion-controlled rate. We conclude that release of OH[•] formed upon illumination of the TiO_2 surface is an unlikely event. We also emphasize that the species produced by reaction of OH[•] with TiO_2 is identical to a trapped hole at the particle surface.

THE NATURE OF THE TiO_2 PARTICLE SURFACE

When a crystal of TiO_2 (e.g., anatase form) is produced, the network of Ti^{IV} and O^{2-} comes to an abrupt end at the gas/solid or liquid/solid interface. This leads to titanium(IV) species at the surface which are coordinatively unsaturated, that is there are dangling orbitals (surface states) on the particle surface which can interact with orbitals of other species present at the interfaces. Exposure of a naked TiO_2 crystal to water vapor or to an aqueous medium causes hydroxylation of the surface by dissociative chemisorption of molecular water to satisfy the coordination of surface Ti^{IV} ions.[3,7] Figure 1 shows schematically the process.

Two types of surface OH^{-} groups result as evidenced by photo-electron spectroscopy:[8] (a) one OH^{-} group bridges two surface vicinal Ti^{IV} ions, becom-

ing a Bronsted acid center, and (b) the other, a terminal Ti^{IV}-OH^- group which has basic character. The TiO_2 particle surface also contains chemisorbed and physisorbed water of hydration. Temperature programmed desorption experiments have placed the number of surface OH^- groups[9] at ca. 5 OH/nm^2, representing less than 50% of surface coverage.[7] A theoretical report puts the number of OH^- groups at 5-10 per nm^2,[10] with the exact number dependent on the type of crystal plane examined.[11-13] The consensus seems to be 7-10 OH^-/nm^2 [12,14-17] for TiO_2 at ambient temperature. Chemisorbed water (H_2O bound directly to surface Ti^{IV} ions) amounts to about 2-3 molecules/nm^2 for rutile TiO_2.[9] Thus, most if not all the Ti^{IV} sites are occupied.

Other species present in the medium can also chemisorb strongly (and irreversibly) on these sites {$H_2PO_4^-$ and/or HPO_4^{2-}, F^- and NO_3^- [7]} displacing some of the terminal OH^- groups to give a surface coverage approaching half a mono-layer.[18-21] Other anions (Cl^-, I^-, and SO_4^{2-}) are reversibly adsorbed. This extrinsic adsorption has important consequences in photocatalyzed oxidat-ions,[22] since anions can potentially block catalytic sites and scavenge redox equivalents. The nonstoichiometry of TiO_2 provides surface Ti^{III} sites on which such electron acceptors as molecular oxygen can adsorb. High-temperature (400-600 C) pre-treatment of TiO_2 in an oxidizing atmosphere (O_2) reduces the number of these sites, while pre-treatment in a reducing atmosphere (H_2) increases their number.

NATURE OF THE SURFACE OF TiO_2 UNDER IRRADIATION

In the absence of light and in a given aqueous electrolyte medium, the particle surface will have certain electronic characteristics and a distinct number of adsorption sites onto which anions, cations, organics, and other

III-5

species present can chemisorb or physisorb, reversibly or irreversibly. In the presence of light, the surface electronic properties will undergo dramatic changes, altering as well the nature of the adsorption sites. Thus, dark adsorption/desorption events will be altered, and additional new events will take place arising from photoadsorption/photodesorption equilibria.

The primary photochemical act, subsequent to near-UV light absorption by TiO_2 particles (wavelengths < 380 nm), is the generation of electron/hole pairs whose separation into conduction band electrons (e^-_{CB}) and valence band holes (h^+_{VB}) is facilitated by the electric field gradient in the space charge region (eqn 1) . Chemically, the hole which is associated with valence bonding

$$TiO_2 + h\nu \longrightarrow TiO_2\{e^-...h^+\} \longrightarrow e^-_{CB} + h^+_{VB} \tag{1}$$
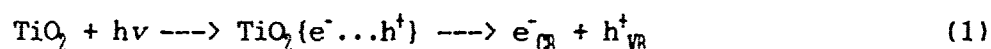
orbitals is constrained at the surface or sub-surface sites in the region where light is absorbed. The greater mobility of the electron,[23] poised at the conduction band potential,[24] facilitates its migration across the particle (Figure 2). Both charge carriers travel rapidly to the surface[2] where they are ultimately trapped by intrinsic sub-surface energy traps $\{Ti^{IV}-O^{2-}-Ti^{IV}\}$ for the hole and surface traps $\{-Ti^{IV}-\}$ for the electrons (eqn 2),[25] and by extrinsic traps via interfacial electron transfer with surface adsorbed electron donors (D_{ads}) and acceptors (A_{ads}), respectively (eqn 3).

$$\{Ti^{IV}-O^{2-}-Ti^{IV}\}_{sub-surface} + h^+_{VB} \longrightarrow \{Ti^{IV}-O^{-\bullet}-Ti^{IV}\}_{sub-surface} \tag{2a}$$

$$\{-Ti^{IV}-\}_{surface} + e^-_{CB} \longrightarrow \{-Ti^{III}-\}_{surface} \tag{2b}$$

$$h^+_{VB} + D_{ads} \longrightarrow D^+_{ads} \tag{3a}$$

$$e^-_{CB} + A_{ads} \longrightarrow A^-_{ads} \tag{3b}$$

III-6
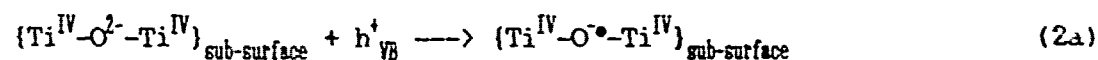
Rapid electron/hole recombination (reverse of eqn 1) necessitates that D and A
be pre-adsorbed prior to light excitation of the TiO_2 photocatalyst. Adsorbed
redox-active solvents can also act as electron donors. In the case of a
hydrated and hydroxylated TiO_2 anatase surface, hole trapping by interfacial
electron transfer occurs via eqn 4 to give surface-bound $OH^\bullet$ radicals.[25-34] The
necessity for pre-adsorbed D and A for efficient charge carrier trapping calls

$$\{Ti^{IV}-O^{2-}-Ti^{IV}\}-OH^- + h^+_{VB} \longrightarrow \{Ti^{IV}-O^{2-}-Ti^{IV}\}-OH^\bullet \qquad (4a)$$

$$\{Ti^{IV}-O^{2-}-Ti^{IV}\}-OH_2 + h^+_{VB} \longrightarrow \{Ti^{IV}-O^{2-}-Ti^{IV}\}-OH^\bullet + H^+ \qquad (4b)$$
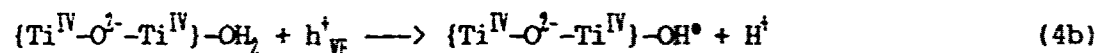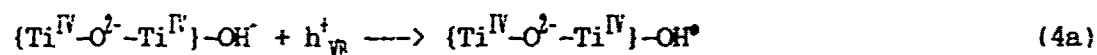
attention to the importance of adsorption/desorption equilibria in photocatal-
ysis. These equilibria and the extent of adsorption will depend on such
factors as the pH of the medium and the point of zero charge for the TiO_2 used
(for anatase, pzc ~ 6.0-6.4 [35-37]), which in turn is highly affected by the
particle environment (nature of ions, ionic strength, among others). In acid
media, the particle surface is positively charged and should enhance adsorpt-
ion of anionic and polar substrates; in alkaline media the surface charge is
negative and should favor adsorption by cationic species.

It should be emphasized that even trapped electrons and holes can
rapidly recombine on the particle surface. To obviate recombination of holes
and electrons, the latter carrier is scavenged by pre-adsorbed (and photo-
adsorbed) molecular oxygen to give the superoxide radical anion, $O_2^{-\bullet}(ads)$,
(eqn 5) which can be reduced further to the peroxide dianion, $O_2^{2-}(ads)$ (eqn
6). Alternatively, surface peroxo species can be formed[36-41] either by hydroxyl
radical (hole) pairing (eqn 7) or by sequential two-hole capture by the same
OH group (eqns 4a and 8) or by dismutation of $O_2^{-\bullet}$ (eqn 9).

III-7

$$O_2(ads) + e^-_{CB} \longrightarrow O_2^{-\bullet}(ads) \qquad (5)$$

$$O_2^{-\bullet}(ads) + e^-_{CB} \longrightarrow (O_2^{2-})_{surface} \qquad (6)$$

$$2(^\bullet OH)_{surface} \longrightarrow (H_2O_2)_{surface} \qquad (7a)$$

$$(H_2O_2)_{surface} \longrightarrow (O_2^{2-})_{surface} + 2H^+ \qquad (7b)$$

$$\{Ti^{IV}-O^{2-}-Ti^{IV}\}-OH^\bullet + h^+_{VB} \xrightarrow{-H^+} (O)_{surface} \longrightarrow O_2(ads) \qquad (8)$$

$$2\, O_2^{-\bullet}(ads) \longrightarrow O_2(ads) + O_2^{2-}(ads) \qquad (9)$$
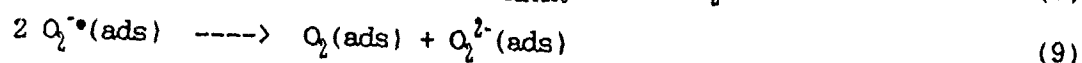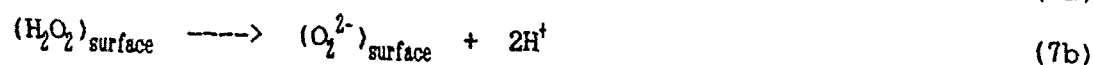
In acidic media (pH 3), in which most photo-oxidative decomposition of organics have been carried out historically, the superoxide radical anion protonates to give the hydroperoxide radical, $HO_2^\bullet$ (pKa 4.88 [42]). Other reactions, among others, that no doubt occur on the TiO_2 particle surface and that are solvent (water) related are summarized in eqns 10 to 15.

$$O_2^{-\bullet}(ads)\ H^+ \longrightarrow HO_2^\bullet(ads) \qquad (10)$$

$$2\, HO_2^\bullet \longrightarrow H_2O_2 + O_2 \qquad (11)$$

$$H_2O_2 + O_2^{-\bullet} \longrightarrow OH^\bullet + OH^- + O_2 \qquad (12)$$

$$H_2O_2 + e^-_{CB} \longrightarrow OH^\bullet + OH^- \qquad (13)$$

$$H_2O_2 + h^+_{VB} \longrightarrow O_2 + 2H^+ \qquad (14)$$

$$O_2^{-\bullet} + HO_2^\bullet \longrightarrow O_2 + HO_2^- \xrightarrow{H^+} H_2O_2 \qquad (15)$$
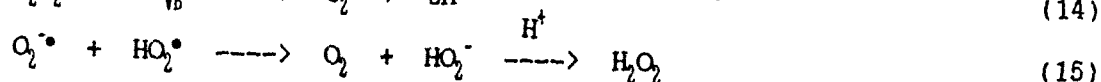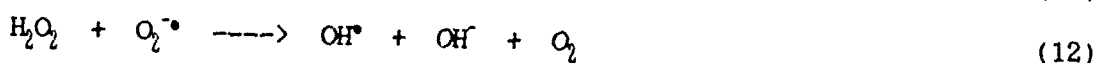
It is evident that under illumination, the electronic characteristics and the very nature of the TiO_2 particle surface have undergone a dramatic change. It will be the extent of these changes, under the conditions used, that will dictate *en premier lieu* the events which take place along the photo-oxidative path of the organic substrates to total mineralization.

THE NATURE OF THE OXIDIZING SPECIES (HOLE vs OH· RADICAL)

The chemical evidence to date supports the notion that the OH· radical is the major oxidizing species involved in the photomineralization of most of the organics examined.[43-47] Such evidence stems from the observation of hydroxylated intermediate products, formed along the course of the photo-oxidation process and which bear close resemblance to products obtained by oxidation with Fenton's reagent.[48] In the oxidation of phenol by light-activated TiO_2 in aqueous media, Okamoto et al.[49] have identified the products shown in Scheme 1, the major components being hydroquinone (HQ), and
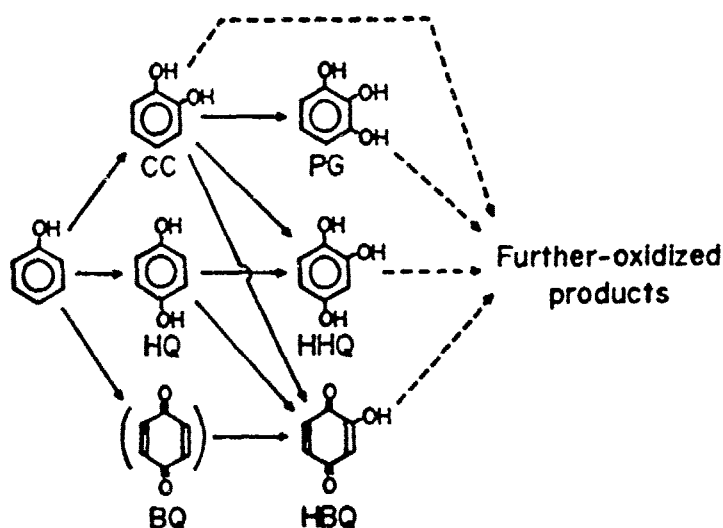
(Scheme 1)

catechol (CC) for 16% conversion. Similar hydroxylated species (3-fluorocatechol, fluorohydroquinone, 4-fluorocatechol, and 1,2,4-trihydroxybenzene) have been identified in the photo-oxidation of 3-fluorophenol.[50] Photo-oxidation of 3-chlorophenol over light-irradiated ZnO in aqueous media gave the hydroxylated intermediates illustrated in Scheme 2, with chlorohydroquinone as the major component for 30% conversion.[51] Added support for OH· as the primary oxidant in aqueous media comes from a recent kinetic deuterium isotope experiment[52] which showed that the rate limiting step in the photo-oxidation

9

of iso-propanol on TiO_2 is formation of active oxygen species through a
reaction involving the solvent water.

(Scheme 2)
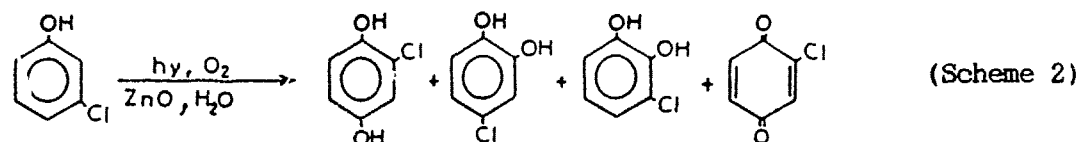
The nature of the intermediates implicated in the photo-oxidation of
water with TiO_2 has been identified in several reports using spin traps by the
electron spin resonance (ESR) technique. Using a pre-reduced anatase powder in
aqueous solutions (pH 4 and 7) at ambient conditions, Jaeger and Bard[32] and
Harbour et al.[53] identified only the anodically formed OH• radical, since
confirmed by other workers.[25-34] A low-temperature (77 K) ESR study identified
the OH• radical (no spin traps);[31] however, this was recently questioned by
Howe and Grätzel[25] who found no evidence for OH• species, even at 4.2 K. These
authors have inferred that the ESR signal seen by Anpo et al.[31] and theirs is
associated with the O⁻• radical anion resulting from trapping of positive
holes at lattice oxide ions (eqn. 2a). They postulated[25] that the OH• radicals
identified by spin trapping methods are not the primary product of hole
trapping, but originate as transient intermediates of photo-oxidation.

Regrettably, ESR investigations have provided no clear picture of the
primary radical intermediate(s) in the TiO_2 assisted photo-oxidation of water.
The nature of the observed radical species appears to depend on the origin and
pre-treatment of the TiO_2 sample, on the conditions and extent of its reduct-
ion, on the extent of surface hydroxylation, and on the presence of molecular
oxygen, among others.[7]

In some cases, the presence of inhibitors (OH• radical scavengers), from
competition experiments, and identification of intermediate products and their

ratios has led some authors to infer that photo-oxidations of organics over light-activated TiO_2 (and ZnO) implicates both OH• radicals and positive holes (eqn 16).[43,51,54-56] THus, oxidation of acetate at illuminated TiO_2/water

$$
\begin{array}{c}
\text{"hole"} \xrightarrow{\text{substrate}} \text{oxidation products} \\
OH^-/H_2O \qquad \text{substrate} \\
OH^•
\end{array}
\tag{16}
$$
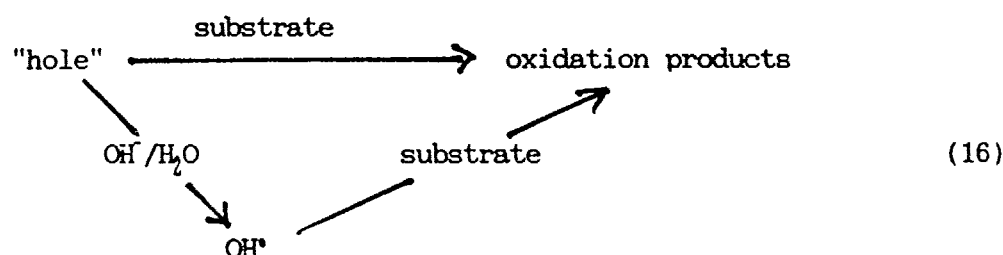
interface produced not only the expected photo-Kolbe products CO_2 and methyl radicals by positive holes, but also glycolate and glyoxylate which originated from oxidation of acetate by hydroxyl radicals via H-atom abstraction at the methyl group.[54] Photo-oxidation of dichlorobenzene over aqueous ZnO dispersions has led to various hydroxylated intermediates, the formation of which is quantitatively inhibited by ethanol which scavenges the OH• radical in the first step of the reaction.[56] This was taken as evidence that the OH• species is the sole oxidant. By contrast, the photo-oxidation of furfuryl alcohol[55] and mono-chlorophenols[51] appears to proceed by both pathways. For the phenols, the major pathway (~ 65%) was oxidation via OH• radicals and the remainder via direct hole oxidation.[51]

It should be remarked that product identification may not lead, if at all, to a delineation of OH• versus hole oxidation, since the products may be identical in both cases. For example, the products identified in the photo-oxidation of phenol (Scheme 1) may originate either by OH• radical attack of the phenol ring, or by direct hole oxidation to give the cation radical which subsequently undergoes hydration in solvent water (Scheme 3). Thus, product analysis alone will in most cases be insufficient to unambiguously establish

11

the process(es) in the primary photochemical event.

(Scheme 3)

hydroxylation product
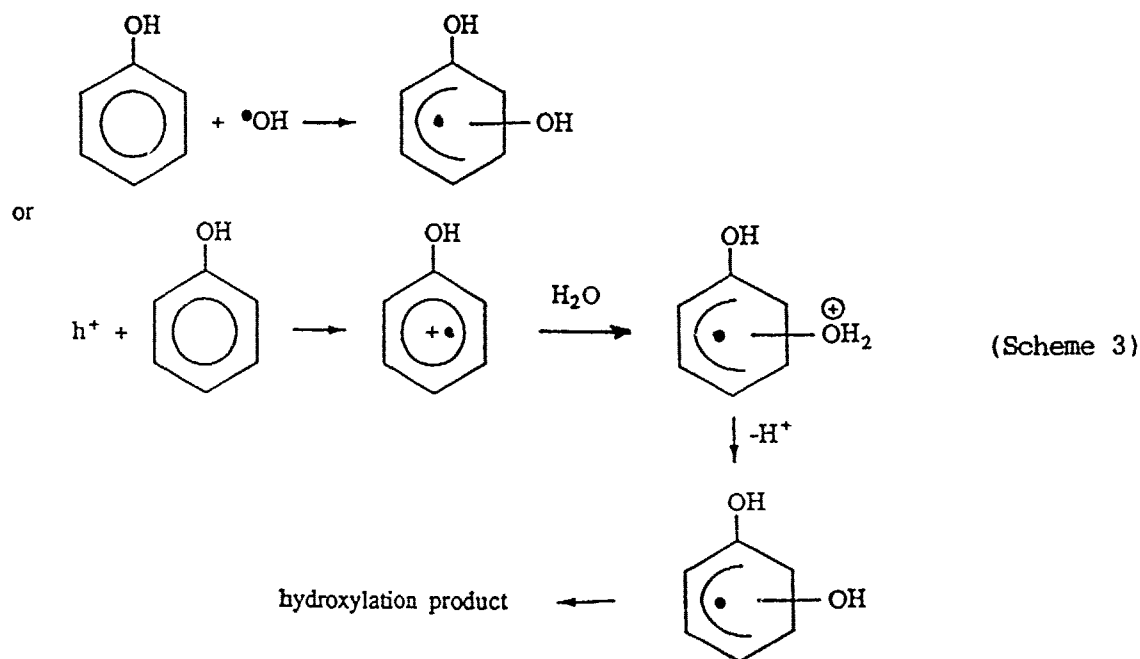
Several years ago, we indicated that complete degradation of organics over light-excited aqueous TiO_2 suspensions did not occur if either H_2O and/or molecular O_2 were absent.[57] Partial oxidations, and not mineralization, are often the rule and not the exception when photo-oxidations are carried out in redox-inert solvents.[24,58] Acetonitrile and dichloromethane have commonly been used. In the absence of water, total mineralization of the organic substrate *does not occur*; only partially oxidized products, often involving photo-oxygenation, have been isolated.[24] In these cases, the primary oxidizing species was described as the positive hole. Reactions 17-19 illustrate some relevant recent examples from the work of Fox and co-workers.[24,48]

$$ \underset{Ph}{\overset{Ph}{\diagup}}\!\!=\!\!CH_2 \quad \xrightarrow[CH_3CN]{TiO_2{}^\bullet} \quad \underset{Ph}{\overset{Ph}{\diagup}}\!\!=\!\!O \qquad (17) $$

~100%

toluene (CH$_3$ on benzene) $\xrightarrow[\substack{PhCH_3 \\ O_2}]{TiO_2{}^{\bullet}}$ benzaldehyde (CHO on benzene) (18)

(4-X-phenyl)–S–(4-X-phenyl) $\xrightarrow[\substack{TiO_2 \\ O_2 \\ CH_3CN}]{h\nu}$ (4-X-phenyl)–S(=O)–(4-X-phenyl) (19)
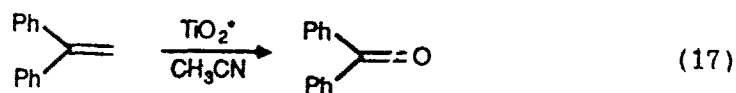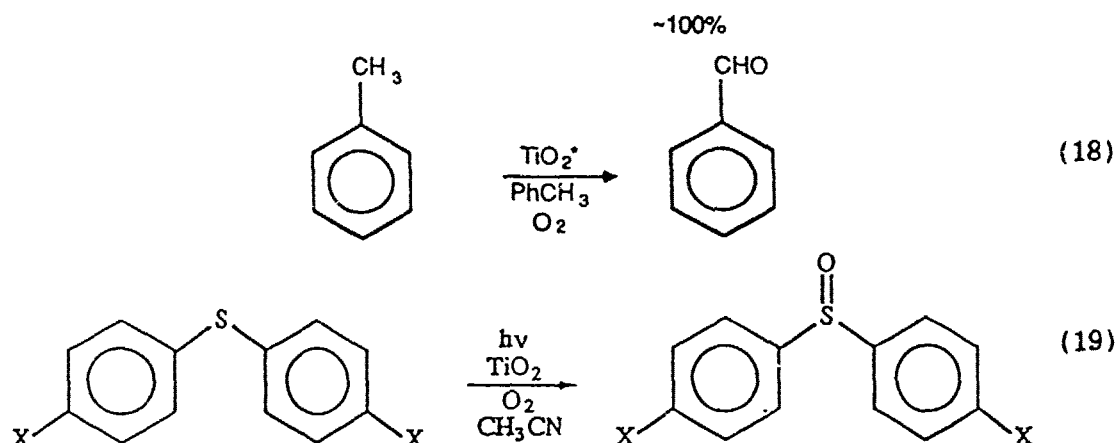
Additional, equally convincing evidence for direct hole oxidation, as the principal step in the photo-oxidation process, was reported in an early study by Boonstra and Mutsaers[59] who concluded that the hydroxyl radical was unlikely to participate in reactions involving TiO_2. Modification of the TiO_2 surface with chlorosilicon compounds led to a decrease in the activity for several photocatalyzed reactions, yet the effect was smaller than the extent of the eliminated hydroxyl groups. The enhanced yield of phenol photo-oxidation in de-oxygenated suspensions of ZnO, containing Hg^{2+} ions as electron scavengers, was taken as conclusive by Domenech et al.[60] for a direct hole oxidation pathway.

Perhaps the strongest evidence for direct hole oxidation comes from a recent study[61] which failed to detect any of the expected hydroxylated inter- mediate OH$^{\bullet}$-adducts following diffuse reflectance flash photolysis of several TiO_2/substrate combinations. Experimental difficulties together with the fact that OH$^{\bullet}$-adducts often possess absorption bands in the UV region where TiO_2 absorption interferes, thereby obstructing observation of such expected hydro- xylated species, do not obviate the intermediacy of OH$^{\bullet}$ radicals (possibly by an electron transfer process) in photo-oxidations. As noted recently by Fox,[24] the possibility that such single electron redox reactions could be mediated by

13

trapped hole equivalents either on the metal oxide surface (as, for example, by a surface bound OH$^\bullet$ radical) or by a sub-surface lattice oxygen situated directly beneath an adsorbed hydroxide ion remains unanswered.

SURFACE vs. SOLUTION REACTIONS

Another issue, often raised in discussions of photocatalyzed mineralization of organic substrates, is whether the initial oxidation of the organic substrate occurs on the photocatalyst's surface or in solution.

In analyzing the kinetic data of photocatalyzed oxidations (and reductions), mediated by photo-activated semiconductor particles, several studies in the 1980's literature have fitted the results to the simple rate expression of the form of eqn. 20.[62-64]

$$r_{initial} = kKC/(1 + KC) \tag{20}$$

Determination of initial rates of oxidation as a function of increased concentration of organic substrate, for a given photocatalyst loading, commonly yields the type of plots illustrated in Figure 3, taken for the photo-oxidation of m-cresol.[65] The similarities of eqn.20 or its more complex form for a multi-component system (eqn.21 [62]), to a Langmuir adsorption

$$r = -\frac{dC}{dt} = \frac{kKC}{1 + \sum_{(all\ reactants)}^{i=1,n} K_i C_i(t) + \sum_{(all\ intermediates)}^{j=1,m} K_j C_j(t) + K_s C_s} \tag{21}$$

isotherm[66] (where k is the observed rate constant, K is the adsorption coefficient and C_0 is the initial concentration of substrate) have led to inferences that the mineralization process takes place on the photocatalyst's

III - 14

14

surface.[67] {Note that the values of k and K are apparent empirical constants which describe the rate of degradation under a given set of experimental conditions covering a range of solute concentrations; they have no absolute meaning}. Similar plots obtain if one considers a bimolecular reaction between reactants X and Y. The initial rate will increase with increase in the concentration of the Y (or X) substrate; the kinetics become pseudo first order. Thus, a Langmuirian type behavior does not guarantee a surface occurring process.

A rigorous treatment[3] of the kinetics involved in the photo-catalyzed oxidations of organic substrates on an irradiated semiconductor under a variety of conditions has recently examined whether it was possible to delineate surface vs. solution bulk reactions. The derived kinetic model considered four cases implicating OH• radical attack of the organic substrate: (i) reaction occurs while both species are adsorbed; (ii) reaction occurs between the adsorbed substrate and the *free* radical; (iii) reaction occurs between surface bound OH• radical and the substrate in solution; and (iv) reaction occurs while both species are in solution. In all cases, the analytical form of the derived complex rate expressions was identical and was similar to that from the Langmuir model. Clearly, kinetic studies alone are silent as to whether photo-oxidations are surface processes or solution processes. An empirical model based on enzyme kinetics confirmed this difficulty.[50,65]

Some studies have sought chemical evidence and inferences to ascertain whether or not the oxidation is a surface process. The selective inhibiting influence of iso-propanol, which modifies only two terms in the kinetic expression that are independent of the furfuryl alcohol (FA) concentration,

15

III - 15

was taken by Lemaire et al.[55] to mean that oxidation of FA by OH• radicals over ZnO dispersions occurs in the homogeneous phase. The relative importance of the formation of glycolate and glyoxylate via OH• oxidation of acetate increases with increasing pH.[54] It was inferred that since in alkaline media little adsorption of acetate takes place on the negatively charged TiO_2 surface, the hydroxyl radicals must diffuse away from the surface of the photocatalyst to oxidize acetate in solution.

In their elegant study, Turchi and Ollis[3] inferred that the photo-oxidative process need not occur at the catalyst's surface, as the reactive OH• species can diffuse several hundred angstroms in the solution. Other workers have suggested that the diffusion length of an OH• radical in the presence of TiO_2 may only be a few atomic distances or less.[68]

A recent photoelectrochemical study[69] is strongly supportive of a solution OH• reactive species in photocatalyzed oxidations. The two important anodic and cathodic reactions on the working metal electrode are embodied in eqns 22. In a slurry photochemical reactor containing an organic substrate,

$$TiO_2^- \longrightarrow TiO_2 + e^- \qquad \text{(anodic)} \qquad (22a)$$

$$OH• \longrightarrow OH^- + h^+ \qquad \text{(cathodic)} \qquad (22b)$$
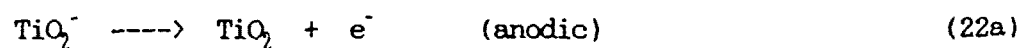
the initial photocurrent was cathodic which rapidly became anodic under steady-state (Figure 4). Immobilization of the TiO_2 onto a conducting carbon paste in a non-uniform manner, in which presumably *no* TiO_2 comes in contact with the electrode, gave similar results as the slurry cell reactor. Nozik et al.[69] inferred from the results that photo-generated surface-originating OH• radicals must diffuse into solution to generate the observed cathodic photo-

current.

By contrast, another (ESR) study[10] concludes that the $OH^\bullet$ radical does all its work on the catalyst's surface, and photo-oxidation is a surface process. Irradiated H_2O_2 is a well-known source of $OH^\bullet$ radicals in homogeneous phase. Variations in the ratio [DMPO-OH]/[DMPO-CO_2] as a function of [Formate]/[DMPO] in a competition experiment between formate and the spin trap used (DMPO) for the $OH^\bullet$ radical, which generates $CO_2^{-\bullet}$ radicals, were followed by the ESR technique.[10] A similar competition experiment was carried out in a heterogeneous system containing TiO_2, formate and DMPO. It was thought that if the $OH^\bullet$ radical produced by illumination of TiO_2 reacted in homogeneous phase, then the variation in [DMPO-OH]/[DMPO-CO_2] would have to overlap that from the H_2O_2 experiment. As noted in Figure 5, the reference system H_2O_2 and the TiO_2 system showed different behavior, taken as evidence[12] that the $OH^\bullet$ radicals react heterogeneously on the surface of the TiO_2 particles.

Unfortunately, these competition experiments remain inconclusive. Considerations of the several complex events (Scheme 4) occurring on the TiO_2 particle and the various other species present on the surface lead us to conclude that the behavior embodied in Figure 5 should *not have been unexpected*. Identical variation of the ratios would *only* have been observed if the parameters describing the steps were identical in both homogeneous and heterogeneous phases. However, the presence of a TiO_2 particle/solution inter-face will, no doubt, influence the kinetics (k') of the various stages in Scheme 4, as one or more may occur on the particle surface, not to mention the differences in the term ϕI_a^b and $\phi I'^b_a$ for the H_2O_2 versus the TiO_2 experiment, respectively.

Scheme 4
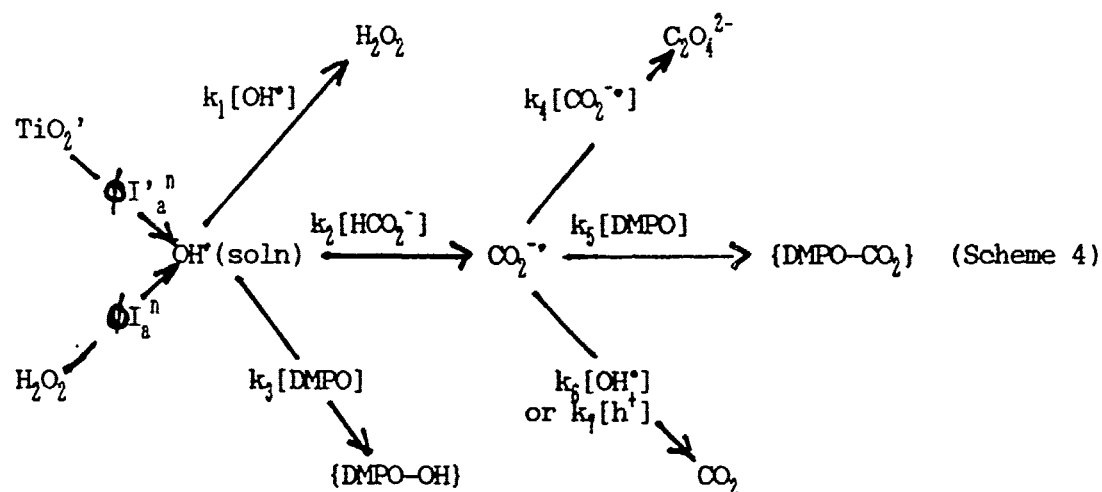
where $\phi_{\{DMPO-OH\}}/\phi_{\{DMPO-CO2\}} = k_3/\{k_2 k_5 [HCO_2^-] \cdot \mathcal{T}_{CO2}\}$

and

$\phi'_{\{DMPO-OH\}}/\phi'_{\{DMPO-CO2\}} = k'_3/\{k'_2 k'_5 [HCO_2^-] \cdot \mathcal{T}_{CO2}\}$

It is clear that one technique alone cannot provide unambiguous conclusions and that other evidence need be obtained, which together with other results might lead to a reasonable understanding of the complex events in photo-oxidation.

Recent time-resolved-microwave-conductivity studies[23] on TiO_2 Degussa P 25 showed a definite increase in the lifetime of the mobile charge carrier (electron) in the presence of iso-propanol, resulting either from (i) scavenging of surface $OH^{\bullet}$ radicals by i-PrOH or (ii) to displacement of a deep surface trap by the alcohol. Observation of a small signal growth in the last pulse of a 100-pulse train (5 Hz) in the TiO_2/i-PrOH sample was inferred to arise from electron ejection from the $CH_3C^{\bullet}(OH)CH_3$ radicals, formed in an irradiated (with 3 MeV from a Van de Graaff accelerator) iso-propanol sol of TiO_2, via eqn. 23. A similar process explained the observed photocurrent doubling effect by alcohols,[71-73] a process which could only take place at the

TiO$_2$ surface.

$$CH_3C^\bullet(OH)CH_3 \ + \ TiO_2 \ \text{------>} \ CH_3C(O)CH_3 \ + \ TiO_2^- \ + \ H^+ \qquad (23)$$
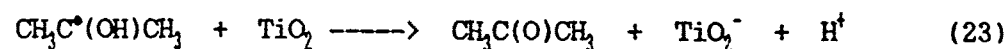
We now discuss our recent pulse radiolysis work,[6] in which we attempted to resolve these two issues by this technique and to clarify the conflicting views regarding the optical features of the photo-generated hole.

PULSE RADIOLYSIS STUDIES

Difficulties encountered in interpreting results from light activated TiO$_2$ could be obviated by the pulse radiolytic method which affords examining the behavior of one of the charge carriers without the interference from the other. We examine[6] the reaction of TiO$_2$ colloids with OH$^\bullet$ radicals produced by irradiation of N$_2$O-saturated aqueous solutions with high energy electrons. The observed growth rate of the product, which we presently define simply as {TiO$_2$ + OH$^\bullet$}, varies linearly with [TiO$_2$] giving k = 6.0 x 10^{11}M^{-1}s^{-1} (concentration in terms of particles). The decay rate of this product increases linearly with [OH$^\bullet$], k = 1.5 x 10^{9}M^{-1}s^{-1}.[6]

Spectral Features of the Hole – Henglein et al.[34,74] have reported an absorption band at 430 nm for the photogenerated trapped hole in platinized TiO$_2$. A more recent study[75] ascribes a band at 630 nm to the photogenerated hole. These conflicting results have been taken up by Bahnemann.[2]

If the trapped hole is an oxidized lattice oxygen as described in eqn. 2a, and to the extent that the O$^-$$^\bullet$ radical in homogeneous phase has a spectral feature at 240 nm,[76] it is difficult to rationalize a 400-nm shift when this

19

radical is bonded to two Ti^{IV} on a TiO$_2$ particle. The issue was resolved[6] by injecting a hole into TiO$_2$ via radiolytically formed OH$^\bullet$ radicals. Figure 6 illustrates the resulting spectrum of the {TiO$_2$ + OH$^\bullet$} product which shows an onset of absorption at ca. 470 nm rising toward the UV region and reaching a maximum at ~ 350 nm, more in line with expectations.

Nature of the {TiO$_2$ + OH$^\bullet$} Product – Molecular oxygen had no effect on the fate of this product. However, SCN$^-$ was oxidized by this product to the SCN$^\bullet$ radical which in the presence of excess SCN$^-$ gave the (SCN)$_2^{-\bullet}$ anion radical (Figure 7). The rate of decay of {TiO$_2$ + OH$^\bullet$} in the presence of thiocyanate could be expressed by eqn 24, where k_1^0 is the intrinsic decay of the

$$\text{Rate} = k_{(decay)}[\{\text{TiO}_2 + \text{OH}^\bullet\}] = (k_1^0 + \frac{k_1 K[\text{SCN}^-]}{1 + K[\text{SCN}^-]})[\{\text{TiO}_2 + \text{OH}^\bullet\}] \quad (24)$$

product ($5.4 \times 10^4 \text{s}^{-1}$), k_1 ($3.7 \times 10^5 \text{s}^{-1}$) is the SCN$^-$ dependent first order decay of {TiO$_2$ + OH$^\bullet$}, and K is the adsorption coefficient of SCN$^-$ on the surface of TiO$_2$ ($1.5 \times 10^4 \text{M}^{-1}$). The suggested mechanism for the oxidation of SCN$^-$ is given by the sequence in eqns 25. The electron transfer reaction 25b occurs between the two species, SCN$^-$ ion and OH$^\bullet$ radical, when both are adsorbed at the surface of the same TiO$_2$ particle.[6]

$$\{\text{TiO}_2\} + \text{SCN}^- \underset{k_{des}}{\overset{k_{ads}}{\rightleftharpoons}} (\text{SCN}^-)_{ads} \quad (25a)$$

$$\{TiO_2 + OH^\cdot\} + (SCN^-)_{ads} \xrightarrow{k_1} \{TiO_2 + OH^-\}\text{-}SCN^\cdot \qquad (25b)$$

$$\{TiO_2 + OH^-\}\text{-}SCN^\cdot \xrightarrow{SCN^-} \{TiO_2\} + SCN_2^{-\cdot} \qquad (25c)$$

Considerations of the yield of this radical dimer permitted defining the redox potential of $\{TiO_2 + OH^\cdot\}$ as 1.5 V, a strongly oxidizing species, yet a rather deep hole trap about 1.3 eV above the valence band of TiO_2. The product is acidic in aqueous media, pKa equal to ca. 2.8–2.9 (eqn. 26).

$$\{Ti(IV)\text{-}O^{2-}\text{-}Ti(IV)\}\text{-}OH^\cdot + H^+ = \{Ti(IV)\text{-}O^{-\cdot}\text{-}Ti(IV)\}\text{-}H_2O \qquad (26)$$

Given that a photogenerated free hole reacts with water or OH^- groups upon arrival at the TiO_2 surface to create, initially, an adsorbed $OH^\cdot$ radical, a process which occurs on a small particle within a few picoseconds, we were unable under our conditions to distinguish between a trapped hole and an adsorbed $OH^\cdot$ radical. We identify the product of the $OH^\cdot$ reaction, $\{TiO_2 + OH^\cdot\}$, as the trapped hole (adsorbed hydroxyl radical), and make no distinction between I and II of eqn.27.[6]

$$\{Ti(IV)\text{-}O^{2-}\text{-}Ti(IV)\} + OH^\cdot \rightarrow \{\{Ti(IV)\text{-}O^{2-}\text{-}Ti(IV)\}\text{-}OH^\cdot \leftrightarrow \{Ti(IV)\text{-}O^{-\cdot}\text{-}Ti(IV)\}\text{-}OH^-\} \qquad (27)$$

$$\qquad\qquad\qquad\qquad\qquad\quad \text{I} \qquad\qquad\qquad \text{II}$$

CONCLUSIONS

Our pulse radiolysis results are consistent with the interpretation that adsorbed OH• radicals (surface trapped holes) are the major oxidants, while free hydroxyl radicals probably play a minor role, if any. Since we find that the OH• radical reacts with TiO_2 at a diffusion controlled rate, the reverse reaction, that is desorption of OH• to the solution, would seem highly unlikely. The surface trapped hole, as defined by eqn 27, accounts for most of the observations which have previously led to the suggestion of OH• radical oxidation. The formation of H_2O_2 and the observations of hydroxylated inter-mediate products can all occur via surface reaction of this species. Although we cannot entirely preclude the remote possibility that a small fraction of the OH• radicals may leak out from the "surface" and mediate the photo-oxidation process in solution, its contribution to the total photo-oxidative process must be minimal.

Further indications that the OH• radical is surface bound, and is unlikely to desorb into the solution, emanates from a recent study[77] which notes that decafluorobiphenyl (DFBP) is tenaciously adsorbed ($\geqslant$ 99%) on metal oxide particle surfaces (Al_2O_3 and TiO_2) and does not undergo facile exchange between the two oxide materials ($\leqslant$ 5%). When adsorbed on the alumina surface in dispersions into which H_2O_2 or a TiO_2 colloidal sol (particle size ca. 0.05 um) is added, followed by uv irradiation, the DFBP is photodegraded. This indicates that the OH• radical from H_2O_2 and TiO_2 sols (particles adsorbed on alumina) migrate to the reaction site on the DFBP/Al_2O_3 system to initiate the photo-oxidative events. By contrast, if TiO_2 beads (size ca. 1000 um) are used *in lieu* of H_2O_2 or the TiO_2 sol to generate the oxidizing species, the photo-degradation is nearly suppressed and is identical to the behavior of the

III-22

DFBP/Al$_2$O$_3$ system alone, irradiated with uv light under otherwise identical conditions. Pentafluorophenol, which readily exchanges between the two metal oxide surfaces, undergoes facile photodegradation under the same conditions. The authors[77] conclude that the photogenerated oxidizing species (OH• radical) does not migrate far from the photogenerated active sites on TiO$_2$, and that the degradation process must occur at the photocatalyst surface or within a few atomic distances from the surface.

ACKNOWLEDGEMENTS

III - 23

REFERENCES

1. Anpo, M. in *"Research in Chemical Intermediates - II"*, Elsevier Science Publications, Amsterdam, p. 67, 1989.

2. Bahnemann, D.W. in *"Photochemical Conversion and Storage of Solar Energy"*, E. Pelizzetti and M. Schiavello, Eds., Kluwer Academic Publishers, Dordrecht, The Netherlands, 1991.

3. Turchi C.S.; Ollis, D.F. *J.Catal.*, 1990, *122*, 178.

4. Draper, R.B.; Fox, M.A. *J.Phys.Chem.*, 1990, *94*, 4628.

5. Lawless, D.; Serpone, N.; Meisel, D. in *"Proc.Symp.Semiconductor Photo-electrochemistry"*, C. Koval, Ed., The Electrochemical Society, Inc., Pennington, N.J., 1991.

6. Lawless, D.; Serpone, N.; Meisel, D. *J.Phys.Chem.*, 1991, *95*, 0000.

7. Augustynski, J. *Structure and Bonding*, 1988, *69*, 1.

8. Sham, T.K.; Lazarus, M.S. *Chem.Phys.Lett.*, 1979, *68*, 426.

9. Munuera, G.; Stone, F.S. *Discuss.Faraday Soc.*, 1971, *52*, 205.

10. Boehm, H.P.; Herrmann, M. *Z.Anorg.Chem.*, 1967, *352*, 156.

11. Boehm, H.P. *Discuss.Faraday Soc.*, 1971, *52*, 264.

12. Suda, Y.; Morimoto, T. *Langmuir*, 1987, *3*, 786.

13. Tanaka, K.; White, J.M. *J.Phys.Chem.*, 1982, *86*, 4708.

14. Morishige, K.; Kanno, F.; Ogawara, S.; Sasaki, S. *J.Phys.Chem.*, 1985, *89*, 4404.

15. Boonstra, A.H.; Mustaers, C.A.H.A. *J.Phys.Chem.*, 1975, *79*, 1694.

16. Mumuera, G.; Rives-Arnau, V.; Saucedo, A. *J.Chem.Soc.Faraday Soc.I*, 1979, *75*, 736.

17. Doremieux-Morin, C.; Enriquez, M.A.; Sanz, J.; Fraissard, J. *J.Colloid Interfac.Sci.*, 1983, *95*, 502.

18. Flaig-Baumann, R.; Herrmann, M.; Boehm, H.P. *Z.Anorg.Chem.*, 1970, *372*, 296.

19. Herrmann, M.; Kaluza, U.; Boehm, H.P. *Z.Anorg.Chem.*, 1970, *372*, 308.

III-24

20. Munuera, G.; Navio, J.A.; Rives-Arnau, V. in *Fourth International Conference on Photochemical Conversion and Storage of Solar Energy"*, J. Rabani, Ed., Jerusalem 1982, p. 141.

21. Munuera, G.; Gonzales-Elipe, A.R.; Rives-Arnau, V.; Navio, J.A.; Malet, P.; Soria, J.; Conesa, J.C.; Sanz, J. in *"Studies in Surface Science and Catalysis"*, M. Che and G.C. Bond, Eds., Elsevier, Amsterdam, 1985, vol. 21, p. 113.

22. Abdullah, M.; Low, G.K.-C.; Matthews, R.W. *J.Phys.Chem.*, **1990**, *94*, 6820.

23. Warman, J.M.; de Haas, M.P.; Serpone, N.; Pichat, P. *J.Phys.Chem.*, submitted for publication.

24. Fox, M.A.; Draper, R.B.; Dulay, M.; O'Shea, K. in *"Photochemical Conversion and Storage of Solar Energy"*, E. Pelizzetti and M. Schiavello, Eds., Kluwer Academic Publishers, Dordrecht, The Netherlands, 1991.

25. Howe, R.F.; Gratzel, M. *J,Phys.Chem.*, **1987**, *91*, 3906.

26. Avudaithai, M.; Kutty, T.R.N. *Mat.Res.Bull.*, **1988**, *23*, 1675.

27. Volz, H.G.; Kaempf, G.; Fitzky, H.G.; Klaeren, A. *ACS Symp.Ser.*, **1981**, *151*, 163.

28. Grätzel, M.; Howe, R.F. *J.Phys.Chem.*, **1990**, *94*, 2566.

29. Maldotti, A.; Amadelli, R.; Bartocci, C.; Carassiti, V. *J.Photochem. Photobiol. A: Chemistry*, **1990**, *53*, 263.

30. Howe, R.F. *Adv.Coll.Interfac.Sci.*, **1982**, *18*, 1.

31. Anpo, M.; Shima, T.; Kubokawa, Y. *Chem.Lett.*, **1985**, 1799.

32. Jaeger, C.D.; Bard, A.J. *J.Phys.Chem.*, **1979**, *83*, 3146.

33. Ceresa, E.M.; Burlamacchi, L.; Visca, M. *J.Mater.Sci.*, **1983**, *18*, 289.

34. Bahnemann, D.W.; Henglein, A.; Spanhel, L. *Faraday Discuss.Chem.Soc.*, **1984**, *78*, 151.

35. Berube, Y.G.; de Bruyn, P.L. *J.Coll.Interfac.Sci.*, **1968**, *27*, 305.

36. Bobyrenko, Y.Y.; Zholnin, A.B.; Konovalova, V.K. *Russ.J.Phys.Chem.*, **1972**, *46*, 749.

37. Schindler, P.W.; Gamsjager, H. *Kolloid Z. und Polymere*, **1972**, *250*, 759.

38. Markham, M.C.; Laidler, J.K. *J.Phys.Chem.*, **1953**, *57*, 363.

III - 25

39. (a) Oosawa, Y.O.; Grätzel, M. *J.Chem.Soc.,Faraday Trans. 1*, 1988, *84*, 197.
    (b) Thampi, K.R.; Rao, M.S.; Schwarz, W.; Grätzel, M.; Kiwi, J.
    J.Chem.Soc.,Faraday Trans.1, 1988, *84*, 1703. (c) Gu, B.; Kiwi, J.;
    Grätzel, M. *Nouv.J.Chim.*, 1985, *9*, 539.

40. Muraki, H.; Saji, T.; Fujihira, M.; Aoyagui, S. *J.Electroanal.Chem.*,
    1984, *169*, 319.

41. Grätzel. C.K.; Jirousek, M.; Grätzel, M. *J.Mol.Catal.*, 1990, *60*, 375.

42. Sawyer, D.T.; Gibian, M.J. *Tetrahedron*, 1979, *35*, 1471.

43. Matthews, R.W. *J.Chem.Soc.Faraday Trans.1*, 1984, *80*, 457.

44. Izumi, I.; Dunn, W.W.; Willbourn, K.O.; Fan, F.F.; Bard, A.J.
    J.Phys.Chem., 1980, *84*, 3207.

45. Izumi, I.; Fan, F.F.; Bard, A.J. *J.Phys.Chem.*, 1981, *85*, 218.

46. Fujihira, M.; Satoh, Y.; Osa, T. *Bull.Chem.Soc.Jpn.*, 1982, *55*, 666.

47. (a) Matthews, R.W. *J.Catal.*, 1986, *97*, 565. (b) Matthews, R.W. *Water Res.*,
    1986, *20*, 569. (c) Matthews, R.W. *J.Phys.Chem.*, 1987, *91*, 3328. (d)
    Matthews, R.W. *Sol.Energy*, 1987, *38*, 405. (e) Matthews, R.W.
    Aust.J.Chem., 1987, *40*, 667.

48. Barbeni, M.; Minero, C.; Pelizzetti, E.; Borgarello, E.; Serpone, N.
    Chemosphere, 1987, *16*, 225.

49. Okamoto, K.; Yamamoto, Y.; Tanaka, H.; Tanaka, M.; Itaya, A.
    Bull.Chem.Soc.Jpn., 1985, *58*, 2015.

50. Minero, C.; Aliberti, C.; Pelizzetti, E.; Terzian, R.; Serpone, N.
    Langmuir, 1991, *in press*.

51. Senili, T.; Boule, P.; Lemaire, J. *J.Photochem.Photobiol.A:Chemistry*,
    1989, *50*, 117.

52. Cunningham, J.; Srijaranai, S. *J.Photochem.Photobiol.A:Chemistry*, 1988,
    43, 329.

53. Harbour, J.R.; Tromp, J.; Hair, M.L. *Can.J.Chem.*, 1985, *63*, 204.

54. Bahnemann, D.W. in *"Proc.Symp.Semiconductor Photoelectrochemistry"*, C.
    Koval, Ed., The Electrochemical Society, Inc., Pennington, N.J., 1991.

55. Richard, C.; Lemaire, J. *J.Photochem.Photobiol.A:Chemistry*, 1990, *55*, 127.

56. Sehili, T.; Boule, P.; Lemaire, J. *J.Photochem.Photobiol.A:Chemistry*,
    1989, *50*, 103.

III-26

57. Barbeni, M.; Pramauro, E.; Pelizzetti, E.; Borgarello, E.; Gratzel, M.; Serpone, N. *Nouv.J.Chim.*, **1984**, *8*, 547.

58. Fox, M.A. in *"Photocatalysis - Fundamentals and Applications"*, N. Serpone and E. Pelizzetti, Eds., Wiley-Interscience, New York, 1989, chapter 13, pp.421-455.

59. Boonstra, H.; Mutsaers, C. *J.Phys.Chem.*, **1975**, *79*, 1940.

60. Peral, J.; Casado, J.; Domenech, J. *J.Photochem.Photobiol.A:Chemistry*, **1988**, *44*, 209.

61. Draper, R.B.; Fox, M.A. *Langmuir*, **1990**, *6*, 1396.

62. Ollis, D.F.; Pelizzetti, E.; Serpone, N. in *"Photocatalysis - Fundamentals and Applications"*, N. Serpone and E. Pelizzetti, Eds., Wiley-Interscience, New York, chapter 18, pp.604-637.

63. Al-Ekabi, H.; Serpone, N. *J.Phys.Chem.*, **1988**, *92*, 5726.

64. Al-Ekabi, H.; Serpone, N.; Pelizzetti, E.; Minero, C.; Fox, M.A.; Draper, R.B. *Langmuir*, **1989**, *5*, 250.

65. Terzian, R.; Serpone, N.; Minero, C.; Pelizzetti, E. *J.Catal.*, **1991**, *128*, 0000.

66. Pichat, P.; Herrmann, J.M. in *"Photocatalysis - Fundamentals and Applications"*, N. Serpone and E. Pelizzetti, Eds., Wiley-Interscience, New York, chapter 8, pp. 218-250.

67. Matthews, R.W. *Water Res.*, **1990**, *24*, 653.

68. Bolton, J.R. personal communication to N. Serpone, 1989.

69. Peterson, M.W.; Turner, J.A.; Nozik, A.J. *J.Phys.Chem.*, **1991**, *95*, 221.

70. Bolton, J.R. *D.O.E. Contractors Meeting*, Golden, CO., June 1989. We thank Prof. Bolton for a preprint.

71. Nosaka, Y.; Sasaki, H.; Norimatsu, K.; Miyama, H. *Chem.Phys.Lett.*, **1984**, *105*, 456.

72. Morrison, S.R.; Freund, T. *J.Chem.Phys.*, **1967**, *47*, 1543.

73. Miyake, M.; Yoneyama, H.; Tamura, H. *Chem.Lett.*, **1976**, 635.

74. Bahnemann, D.W.; Henglein, A.; Lillie, J.; Spanhel, L. *J.Phys.Chem.*, **1984**, *88*, 709.

75. Arbour, C.; Sharma, D.K.; Langford, C.H. *J.Phys.Chem.*, **1990**, *94*, 331.

III-27

76. Hug, G.L. *"Optical Spectra of Nonmetallic Inorganic Transient Species in Aqueous Solution"*, NSRDS-NBS 69, 1981.

77. Minero, C.; Catozzo, F.; Pelizzetti, E. *submitted for publication.*

III-28

FIGURE CAPTIONS

Figure 1.- Surface hydroxyl groups on TiO_2. (a) Hydroxyl-free surface;
(b) physical adsorption of water; (c) dissociation of water to
give rise to two distinct OH^- groups. Adapted from refs. 3 and 7.

Figure 2.- Schematic representation of the formation of an electron/hole pair
and electron transfer reaction at the semiconductor particle.

Figure 3.- (a) Plot showing the effect of the initial concentration on the
initial rate of the photo-oxidative mineralization of m-cresol.
(b) Linear transform of the Langmuir-type isotherm. Reproduced
with permission from ref. 65.

Figure 4.- Transient response for TiO_2 P 25: (a) without HCOOH and (b) with
0.1 M HCOOH. Reproduced from ref. 69.

Figure 5.- Formate competition "cross-over point" analysis; Ratio denotes the
ratio of the ESR peak heights of the DMPO-OH to the $DMPO-CO_2$ spin
adducts. The relative [DMPO] was taken as 1. Adapted from the data
of ref. 70.

Figure 6.- Absorption of the $\{TiO_2 + OH^\bullet\}$ product following reaction of TiO_2
with radiolytically produced $OH^\bullet$ radicals. Reproduced from ref. 6.

Figure 7.- Dependence of the pseudo first order rate constant for the decay of
the $\{TiO_2 + OH^\bullet\}$ product on $[SCN^-]$. The inset shows the Langmuir
analysis of the results. Reproduced from ref. 6.

29

III-29

Fig 1

Proton

Oxygen

Titanium ion

Lattice oxygen

(a)

(b)

(c)

(001)
Surface

III-30

Fig 2

ELECTROLYTE

TiO₂ particle

Fig. 3

m-Cresol

TiO_2 2 g/L; pH 3
air equilibrated
aqueous solutions

A

Initial Rate (μM/min)

Initial Concentration (μM)

B

$[In. Rate]^{-1}$, $(μM/min)^{-1}$

$[m-Cresol]^{-1}$, $(μM)^{-1}$

Fig 4

Fig5

Formate/DMPO Competition Experiments

TiO_2

H_2O_2

[DMPO]/[Formate]

2.6

.8

2.5

RATIO

.5

20

III-34

Fig.6

Fig.7

III-36

(22) Surface Intervalence Enhanced Raman

Scattering from $Fe(CN)_6^{4-}$ on Colloidal Titanium Dioxide.

A Mode-by-Mode Description of the Franck-Condon

Barrier to Interfacial Charge Transfer

Robert L. Blackbourn, Christopher S. Johnson,

and Joseph T. Hupp[*]

Department of Chemistry

Northwestern University

Evanston, Illinois 60208-3113

Prepared for publication in J Am Chem Soc.   III-37

Surface Intervalence Enhanced Raman

Scattering from $Fe(CN)_6^{4-}$ on Colloidal Titanium Dioxide.

A Mode-by-Mode Description of the Franck-Condon

Barrier to Interfacial Charge Transfer

Robert L. Blackbourn, Christopher S. Johnson,

and Joseph T. Hupp[*]

Department of Chemistry

Northwestern University

Evanston, Illinois 60208-3113

IV-38

Abstract: The first experimental observation of "surface intervalence enhanced" Raman scattering (*not* SERS) is reported. The transition giving rise to the enhancement is a heterogeneous charge tr nsfer between $Fe(CN)_6^{4+}$ and colloidal titanium dioxide (Vrachnou, et al. $I.$ E^1 .nal. Chem., 1989, 258, 193). Enhancement effects in the scattering spectrum are interpreted with t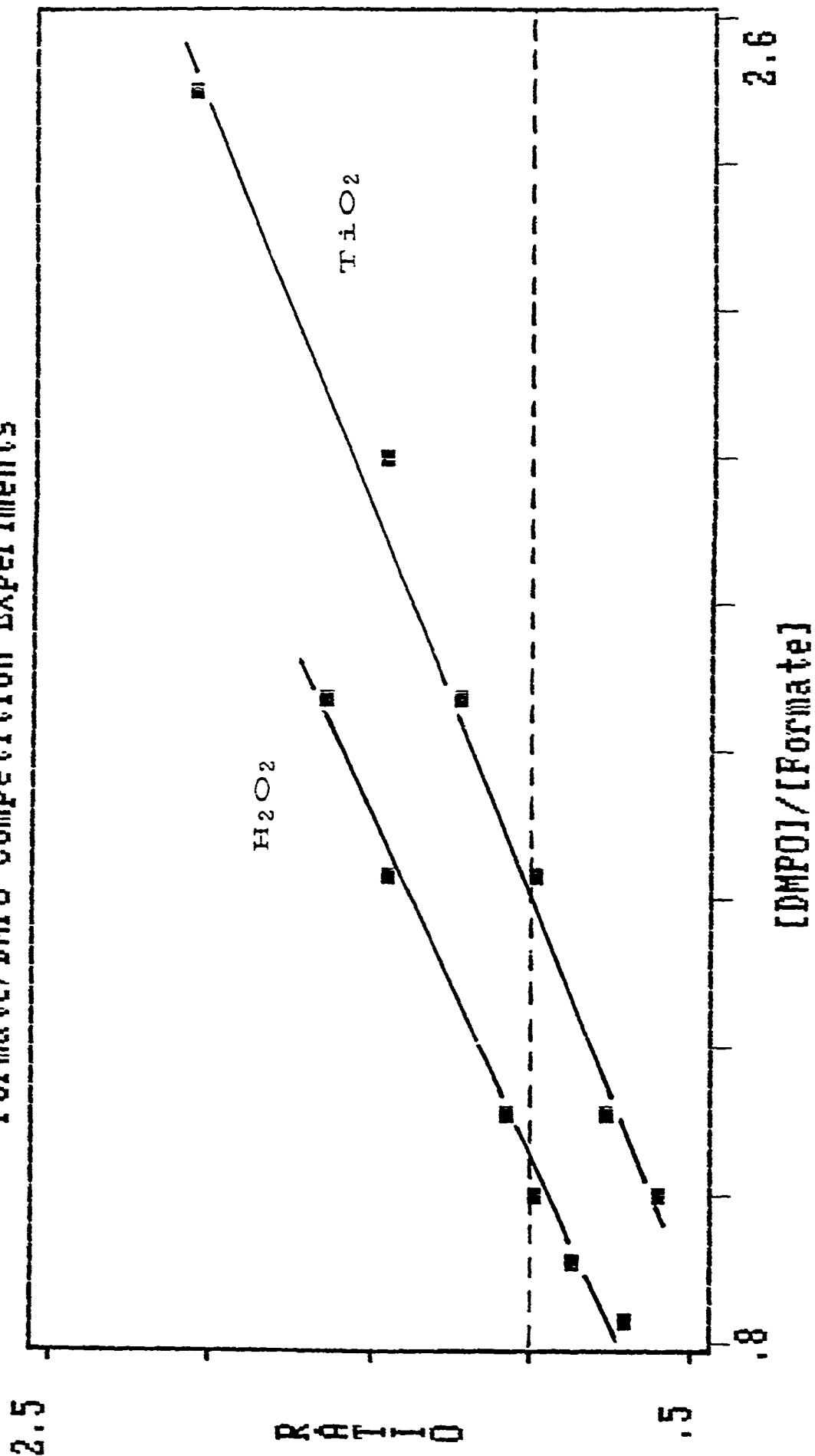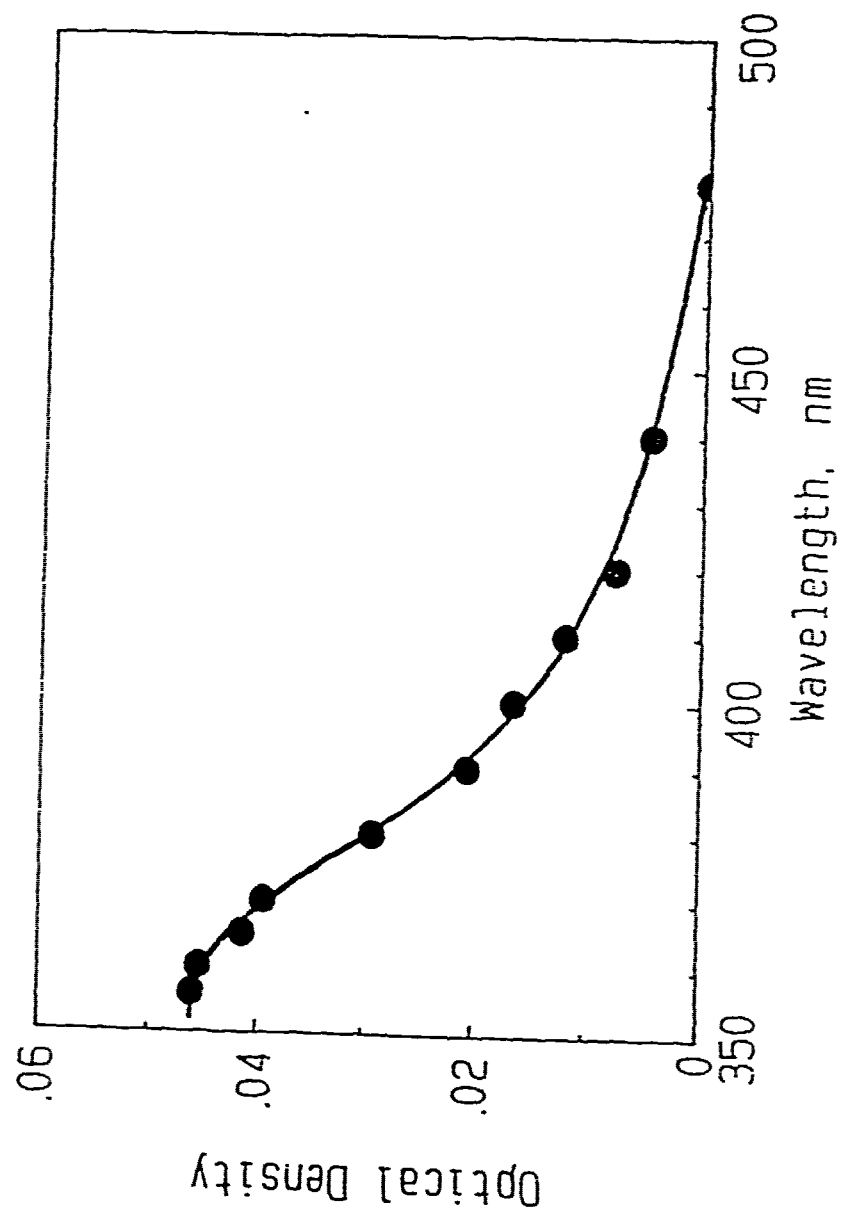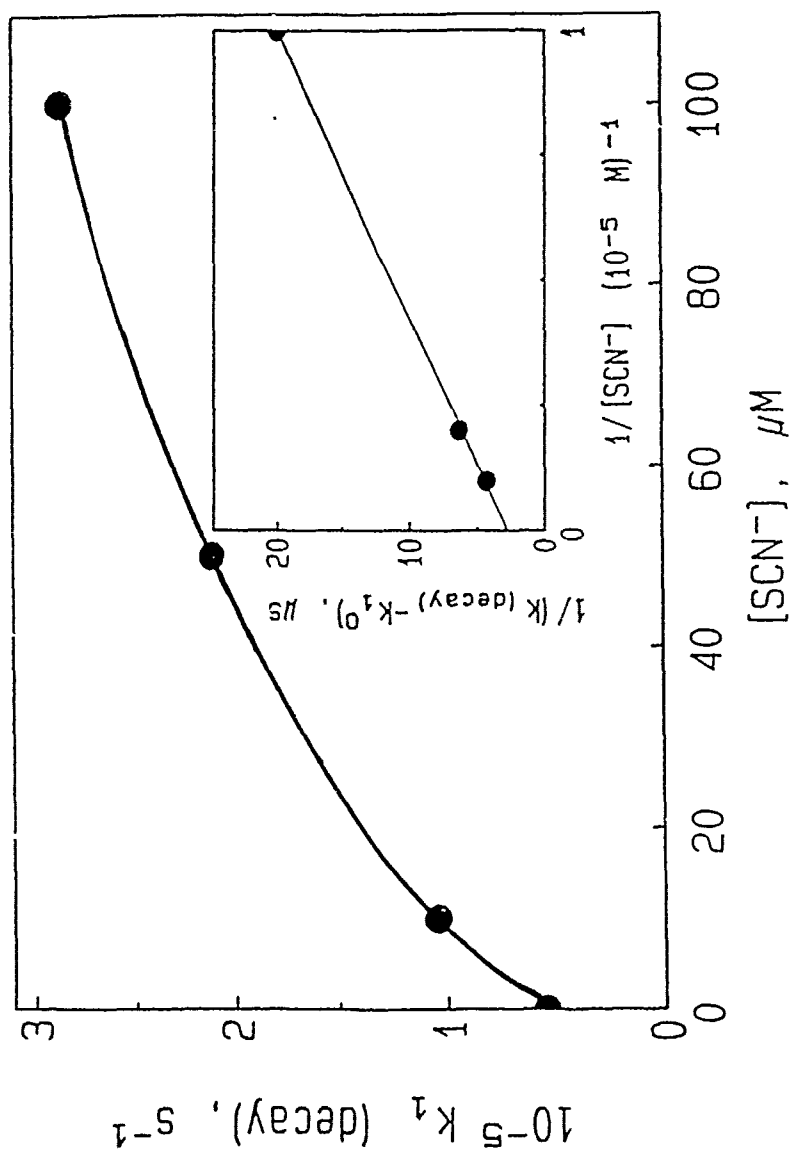he aid of recently developed time-dependent analyses. From the analyses a complete, quantitative description of charge-transfer induced vibrational reorganization is obtained (i.e. all force constants, all normal coordinate displacements, and all single-mode components of the vibrational Franck-Condon barrier to charge-transfer are obtained). For the $Fe(CN)_6^{4+}$/colloidal-TiO_2 system, the most significant findings are: a) that a total of ten modes are displaced during interfacial electron transfer, b) that the largest single displacement occurs in a mode associated with a bridging cyanide ligand, and c) that three *surface* modes (Ti-O vibrations) are activated during optical electron transfer.

One of the key requirements in any quantitative description of electron transfer

kinetics, in any environment, is an accurate estimate of internal or vibrational

reorganization energetics.[1] We have recently shown that complete mode-by-mode

descriptions of vibrational reorganization for selected metal-to-ligand[2] and metal-to-

metal (or intervalence)[3] charge-transfer events in solution can be obtained by

applying time-dependent scattering theory[4,5] to pre- or post-resonance Raman

spectra.[6] The quantities obtained are redox-induced normal coordinate displacements

(Δ), force constants (f) and individual components (χ_i') of the total vibrational

reorganization energy (χ_v). We now wish to report an extension of this methodology

to an *interfacial* charge transfer reaction.

The reaction chosen was optical electron transfer from $Fe(CN)_6^{4-}$ to colloidal

titanium dioxide:[7,8]

$$Fe(CN)_6^{4-} \atop Fe(CN)_6^{4-} \atop Fe(CN)_6^{4-} \atop Fe(CN)_6^{4-} \Bigg\} TiO_2 \quad \xrightarrow{\text{INTERVALENCE EXCITATION}} \quad Fe(CN)_6^{3-} \atop Fe(CN)_6^{3-} \atop Fe(CN)_6^{4-} \atop Fe(CN)_6^{3-} \Bigg\{ \begin{array}{c} e^- \\ e^- \\ TiO_2 \\ e^- \end{array} \tag{1}$$

Following Vrachnou and co-workers,[7] we find that an intense optical absorption

exists ($\lambda_{max} = 410$ nm, $\varepsilon \approx 5{,}000$ M^{-1} cm^{-1}) for the "surface intervalence" charge

transfer reaction in eq. 1. We further find (fig. 1) that Raman scattering spectra can

be readily obtained based on near-resonant excitation (488 nm).[9] Control experiments

at 514.5 nm (nominally preresonant), at 647.1 nm (off resonance), with ferrocyanide alone, or with colloidal TiO_2 alone, all show the scattering in fig. 1 to be resonantly enhanced (e.g. enhancement factors of at least 20 for the highest energy modes).[10]

The observation of enhancement is of central importance: within the context of the time-dependent theory,[4,5] resonance enhancement (Albrecht A-term scattering) indicates the displacement of normal coordinates in direct response to the pertinent electronic transition (in our case, eq. 1). In the simplest case, the quantitative relationships between scattering intensity (I) and molecular structural changes are:[4]

$$I_1 / I_2 = \omega_1^2 \Delta_1^2 / \omega_2^2 \Delta_2^2 \qquad (2)$$

and

$$\chi_4 = 0.5 \sum_k \Delta_k^2 (\omega_k / 2\pi) \qquad (3)$$

where ω is 2π times the vibrational frequency and the summation is over all modes which are significantly resonantly enhanced. If a local mode approximation is appropriate, absolute bond length changes ($|\Delta a|$) can also be obtained:[24]

$$(|\Delta a|) = \left(\Delta^2 \hbar / \mu \omega b \right)^{\frac{1}{2}} \qquad (4)$$

In eq. 4, μ is the reduced mass and b is the bond degeneracy.

Table 1 lists the relative intensities, unitless normal coordinate displacements and bond-length changes obtained for resonance enhanced modes. Absolute Δ and Δa values were derived by assuming that the changes in length for nonbridging Fe-C bonds equalled those determined crystallographically for free $Fe(CN)_6^{3-/4-}$.[12] Mode assignments were made by analogy to $Fe(CN)_6^{4-}$,[13] $(H_3N)_5Ru\text{-}NC\text{-}Fe(CN)_5^{1-}$, $(H_3N)_5Os\text{-}$

NC-Fe(CN)$_5^{1-}$ and related systems,[3] and will be described in greater detail elsewhere. From the table, a number of points are worth noting: 1) The total number of modes (or types of bonds) displaced is surprisingly large (ten) indicating that even the simplest of interfacial redox reactions may entail substantial complexity in vibrational activation. 2) As seen for related binuclear metal systems (in solution),[3] bridging modes suffer the greatest displacement, with the C≡N bridging mode providing the largest single contribution to the vibrational barrier. 3) Remarkably, three *surface* modes are enhanced and therefore displaced during optical electron transfer. This last observation is unprecedented experimentally and is at odds with most, if not all, existing theoretical views of interfacial electron transfer.

While the mode assignments in Table 1 are reasonably well established, questions do arise regarding the possibility of more than one type of binding geometry (e.g. doubly-bridged) and the degree of protonation of the bound ferrocyanide. We performed a number of control experiments where: (1) Fe(CN)$_6^{4-}$ and colloidal TiO$_2$ concentrations were substantially varied. (2) The pH was varied between 1 and 3. (3) Multiple excitation wavelengths were used in resonance. (4) An isotope study using a 7:1 dilution in D$_2$SO$_4$/D$_2$O was completed.[14] Interestingly, all of these experiments led to no change in relative Raman intensities or frequency shifts. These results, therefore, tend to support the notion that only one type of complexed ferrocyanide species exists, which apparently is unprotonated, and is bound to titanium via a single-cyanide ligand.[14]

6

Finally, the possibility of unwanted scattering from either a Prussian blue or titanate/$Fe(CN)_6^{4-}$ species was considered. We eliminated the Prussian blue problem by: (a) using $Os(CN)_6^{4-}$ in place of $Fe(CN)_6^{4-}$ with similar results, (b) purposely making the Prussian blue complex which absorbs in the red and showing that it is not present in our absorption spectrum, and (c) proving that no enhancement occurs in the $Fe(CN)_6^{4-}$/colloidal-TiO_2 solution at 647.1 nm (where Prussian blue would absorb). The second problem, titanate formation during preparative $TiCl_4$ hydrolysis, can be effectively eliminated by dialysis.[7] This was confirmed by an electrochemical experiment (supplementary material) in which redox-active $Fe(CN)_6^{4-}$ (i.e. free or titanate bound) was shown to be absent from $Fe(CN)_6^{4-}$/dialyzed-colloid solutions, but present in intentionally prepared $Fe(CN)_6^{4-}$/titanate solutions.[15]

Supplementary Material Available: One figure showing differential pulse voltammograms for $Fe(CN)_6^{4-}$/colloidal-TiO_2 and $Fe(CN)_6^{4-}$/titanate solutions. Ordering information is given on any current masthead page.

$\overline{II}$-43

References

1. For general reviews see: (a) Sutin, N. Prog. Inorg. Chem., 1983, 30, 441. (b) Marcus, R. A.; Sutin, N. Biochim. Biophys. Acta 1985, 811, 265. (c) Newton, M. D.; Sutin, N. Ann. Rev. Phys. Chem., 1984, 35, 437.

2. Doorn, S. K.; Hupp, J. T. J. Am. Chem. Soc., 1989, 111, 4704.

3. (a) Doorn, S. K.; Hupp, J. T. J. Am. Chem. Soc., 1989, 111, 1142. (b) Doorn, S. K. Ph.D. Dissertation, Northwestern University, 1990.

4. (a) Heller, E. J.; Sundberg, R. L.; Tannor, D. J. Phys. Chem. 1982, 86, 1822, (b) Tannor, D. J.; Heller, E. J. J. Chem. Phys. 1982, 77, 202. (c) Lee, S. Y.; Heller, E. J. J. Chem. Phys. 1977, 71, 4777. (d) Heller, E. J. Acc. Chem. Res. 1981, 14, 368. (e) Morris, D. E.; Woodruff, W. H. J. Phys. Chem., 1985, 89, 5795.

5. See also: (a) Warshel, A.; Dauber, P. J. Chem. Phys. 1977, 66, 5477. (b) Myers, A. B.; Mathies, R. A. in "Biological Applications of Raman Spectroscopy", T. G. Spiro, Ed.; John Wiley and Sons: New York, 1987; Vol. 2. (c) Schomacher, K. T.; Bangcharoenpaurpong, O.; Champion, P. M. J. Chem. Phys., 1984, 80, 4701. (d) Hizhnyakov, V.; Tehver, I. J. Raman Spectrosc. 1988, 19, 383.

6. Related experimental applications of time-dependent Raman scattering theory: (a) Tutt, L.; Zink, J. I. J. Am. Chem. Soc., 1986, 108, 5830. (b) Zink, J. I.; Tutt, L.; Yang, Y. Y. ACS Symp. Ser. 1986, 307, 39. (c) Yang, Y. Y.; Zink, J. I. J. Am. Chem. Soc. 1985, 107, 4799. (d) Tutt, L.; Tannor D.; Heller, E. J.; Zink, J. I. Inorg. Chem. 1982, 21, 3858. (e) Zink, J. I. Coord. Chem. Rev. 1985, 64, 93. (f)

Truhlson, M. O.; Dollinger, G. D.; Mathies, R. A. J. Am. Chem. Soc. 1987, 109, 586.

7.   Vrachnou, E.; Grätzel, M.; McEvoy, A. J. J. Electroanal. Chem. 1989, 258, 193.

8.   Colloidal TiO_2 sols were prepared following the method used in ref. 7. We found that agitation and slow addition of potassium ferrocyanide solutions to the dialyzed and diluted colloid produced stable charge transfer assemblies. For Raman studies (excitation at 457.9, 488.0, 514.5 and 647.1 nm) the colloidal sols contained approximately 10^{-4} moles of $Fe(CN)_6^{4-}$ per gram of TiO_2; higher loadings led to sol aggregation then precipitation. Ferrocyanide concentrations ranged from 0.1 to 1.0 mM. In a few experiments NO_3^- or methanol was added as an internal intensity standard. The sol pH was varied between 1 and 3 (chiefly by varying dialysis times and the number of dialysis steps) with no variations found in the enhanced scattering spectra. It should be noted that at the low pH's used in this study, polyvinyl alcohol (a common colloid stabilizer) was not needed.

9.   Raman spectra were obtained with a windowless flow cell under an argon blanket. Chromophore concentrations were chosen so as to minimize complications from self absorption. Typically, a bandpass of 9 cm^{-1} was employed with 40 to 60 mW of incident excitation power. For weak portions of the spectrum, signals were sometimes averaged (with appropriate checks for system drift) for as long as twenty hours. We note further that background counts in the low energy end of the spectrum (ca. 750 to 300 cm^{-1}; see fig. 1)

were often as high as 5,000 per second, rendering signal extraction somewhat difficult.

Our results stand in marked contrast to those of Umapathy, McQuillan and Hester (Chem. Phys. Lett., 1990, 170, 128) who very recently reported observing only the two highest frequency modes seen in our spectrum. The precautions described above no doubt account for the exceptional differences between our findings and those reported elsewhere.

10. In addition, very weak, unenhanced modes at 656 and 920 cm^{-1} were occasionally found, as was a stronger mode (also unenhanced) at 1641 cm^{-1}. Lack of enhancement indicates lack of participation of these modes in vibrational reorganization.

11. Intensities have been corrected for residual self absorption (Shriver, D. F.; Dunn, J. B. R. Appl. Spectrosc. 1974, 28, 319) and for ν^4 attenuation effects.

12. Swanson, B. I.; Hamburg, S. I.; Ryan, R. R. Inorg. Chem., 1974, 13, 1685.

13. Jones, L. H.; Memering, M. N.; Swanson, B. I. J. Chem. Phys., 1971, 54, 4666.

14. If, in fact, two cyanide ligands serve as bridges, Δa (ν_{C-N} bridge) decreases to 0.032 Å; most other Δa values would be diminished by about 10%.

15. The source of titanate was the outer portion of a colloidal-TiO_2 dialysis solution. See ref. 7 for related experiments.

III-46

10

Table 1. Spectroscopic, structural and reorganizational parameters for electron transfer from Fe(CN)$_6^{4-}$ to colloidal TiO$_2$.

Mode	Relative Intensity[a,b]	Δ^2	$|\Delta a|$	χ_i	Assignment
2118 cm^{-1}	20.0	0.95[c]	0.048 Å	1000 cm^{-1}	ν_{C-N} bridge
2072	6.61	0.33	0.014	340	ν_{C-N} radial
2058	5.44	0.27	0.026	280	ν_{C-N} terminal
720	0.27	0.11	?	40	?
598	1.00	0.59	0.026[d]	180	ν_{Fe-C}
540	0.33	0.24	0.039	60	ν_{Fe-C} bridge
516	1.12	0.89	e	230	ν_{Ti-O}
484	0.90	0.82	e	200	ν_{Ti-O}
418	0.56	0.69	e	140	ν_{Ti-O}
364	0.27	0.43	0.059	80	ν_{Ti-N}

a. Depolarization studies indicate that all modes, with the possible exception of modes at 540 and 720 cm^{-1} (too weak to determine with certainty), are totally symmetric. b. Within the experimental uncertainty, *relative* intensities are unaffected by changes in excitation wavelength. c. All values scaled to the value for Δ^2 at 598 cm^{-1}. d. Taken from (or taken as) the crystallographically determined value[12] for Fe(CN)$_6^{4-/3-}$. e. Value not determined, since the measured normal coordinate displacement (Δ) may entail more than one type of bond length displacement (i.e., a local-mode approximation may not be appropriate).

Caption for Figure 1

Figure 1.   Preresonance Raman spectrum of 0.6 mM $Fe(CN)_6^{4-}$/5.8g/L TiO_2 colloid at pH = 2.0 with 488.0 nm excitation. The asterisk at 656 cm^{-1} denotes an unenhanced E_g mode of TiO_2. The mode at 540 cm^{-1} is real and is more convincingly resolved in experiments performed at 457.9 nm.

WAVENUMBERS (cm⁻¹)

INTENSITY
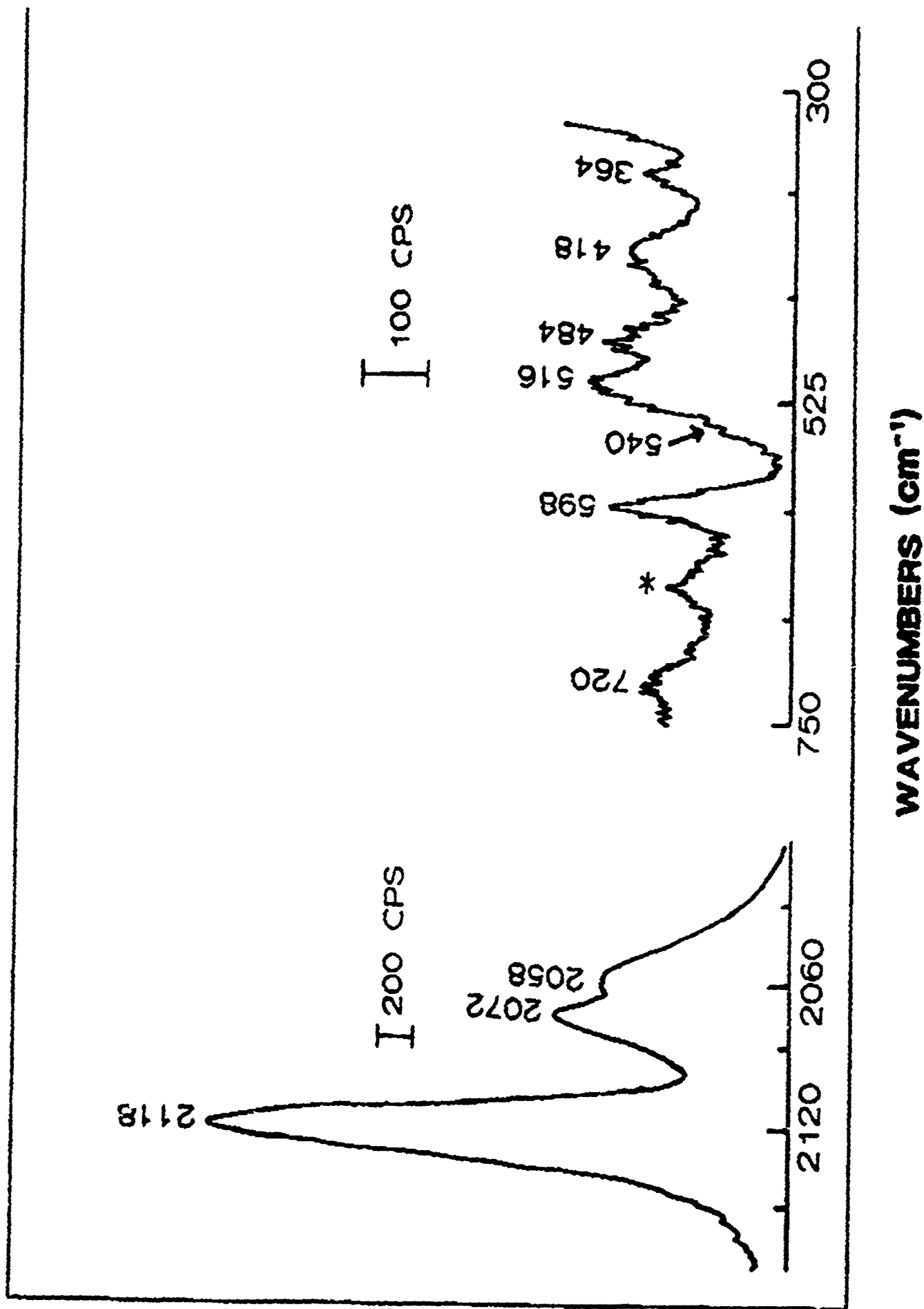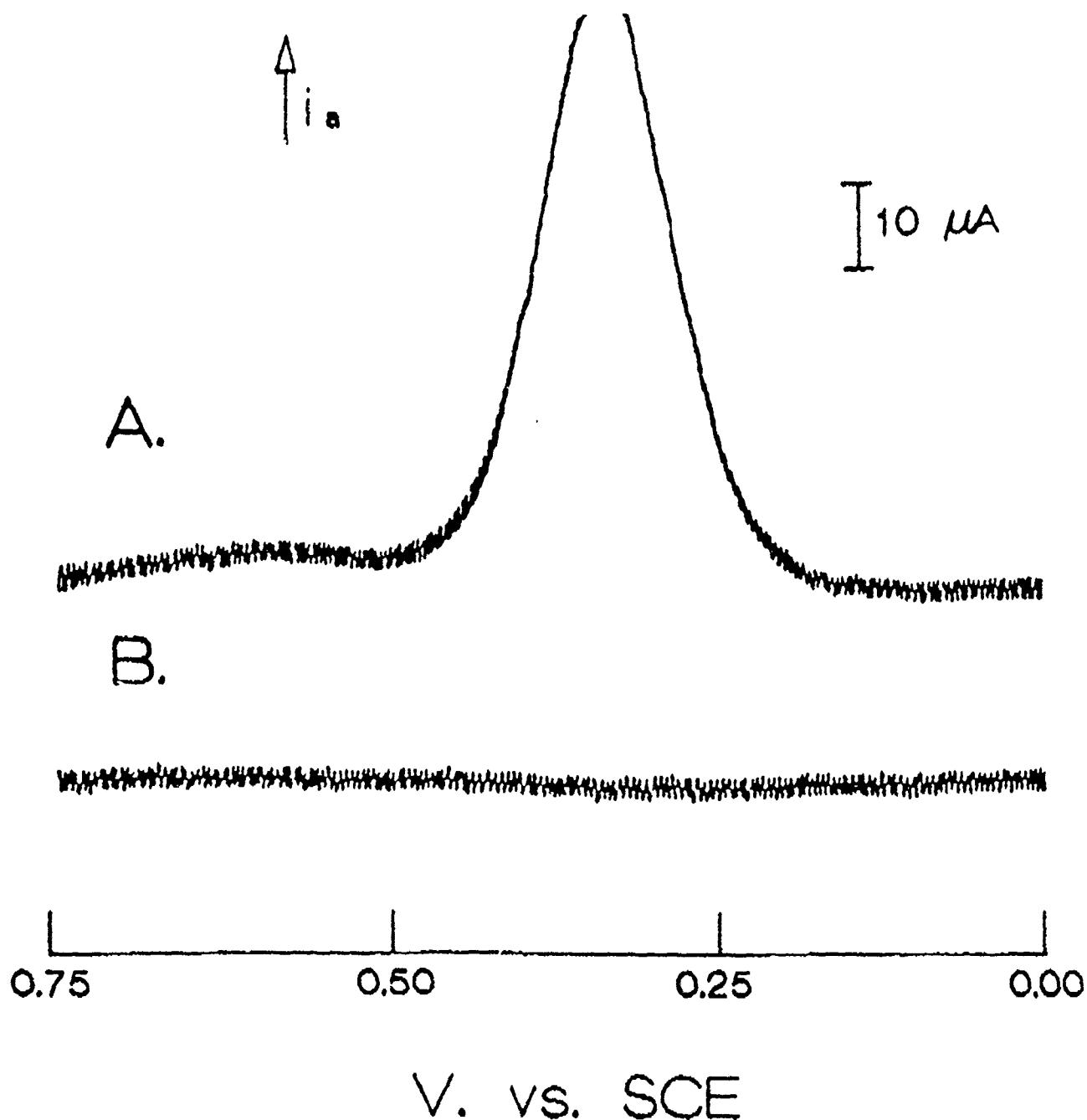
Supplemental Figure. Differential pulse voltammograms of (A) $Fe(CN)_6^{4-}$/titanate solution prepared from the outer dialysis water, pH = 2.0, 0.65 mM $Fe(CN)_6^{4-}$, $E_{1/2}^{ox}$ = 0.33 V; (B) $Fe(CN)_6^{4-}$/Colloidal-TiO_2 assembly prepared from the inner dialyzed solution. The experimental conditions are as follows: scan/rate = 5 mV s^{-1}, pulse amplitude = 5 mV, pulse width = 0.5 sec. The electrode material used was glassy carbon.

III-50

(23) # PHOTOINDUCED ELECTRON TRANSFER IN A COVALENTLY LINKED PORPHYRIN-RuO$_2$ CLUSTER: PHOTOCATALYSIS IN AN ORGANIC-INORGANIC COMPOSITE

Ute Resch and Marye Anne Fox*

Department of Chemistry, University of Texas at Austin, Austin, Texas 78712

The spectroscopic characterization of a series of surfactant-like tris-meso-(p-octoxyphenyl)porphyrins (MP, M = 2 H, Zn, 4H^{2+}) covalently linked through a meso-p-phenoxyalkyl group of varying numbers of methylene group (CH$_2$)$_n$ and (n = 1,4-7) terminated by a bipyridine ligand (B) to a RuO$_2$ cluster (R), MPB$_n$R, are discussed. Thus, a one-electron photocatalyst is covalently bound through a well-known ligand for transition metals to a multi-electron dark catalyst capable of either oxygen or hydrogen evolution.

The variable length of the alkyl chain linking the photoresponsive porphyrin to the RuO$_2$ cluster allows for a shift in populational preferences for folded or extended conformers. The observed photocatalytic activity in these systems derives from photoinduced electron transfer from the porphyrin excited singlet.

A unique design feature of MPB$_n$R is their potential utility in microemulsions. In either an anionic or cationic microemulsion, the water-insoluble porphyrin (M = 2H, Zn) resides in the organic phase or at the interface. Upon photoexcitation, it can transfer charge across the phase boundary to the hydrophilic RuO$_2$ catalyst held in the aqueous phase.

Introduction

The construction of multi-component systems which feature a light-responsive photosensitizing unit bound chemically to a catalyst which is active in inducing redox reactivity represents a viable method for preparing arrays with many practical applications in material science. If monomeric or polymeric organic ligands are employed, such materials constitute organic-inorganic composites, an area of burgeoning importance in macromolecular chemistry. If the attached organic unit is itself photoactive, the resulting photosensitive composite will exhibit characteristics favorable for interfacial charge separation, a problem important in photolithography and xerography.

Such multi-component systems are also important in providing synthetically accessible systems which can mimic many of the features of natural photosynthesis. For example, the covalently linked donor-acceptor systems have been employed as redox-active catalysts by several groups (1-3). In order to achieve high efficiency in such photoconversions, the array must comprise a light absorbing unit which is responsive both in the visible and infrared regions, as well as a mechanism by which the excited state can communicate (usually via charge migration) with a catalytically active site. This mechanism, in general, will allow conversion of light energy into cnarged equivalents (a photogenerated electron-hole pair), which interact with the catalytic site so as to allow a second step in which the transformation of these charged carriers into chemically oxidized and reduced discrete species can occur. In such a synthetic composite, the efficiency with which incident light is converted to chemically stored energy will depend on the efficiency for formation of the charge separated pair and on the ratio of the rates for product formation and back electron transfer (which would consume the photogenerated electron-hole pair). The practical utility of such composites obviously requires, therefore, that the parameters which control electron transfer must be well-defined and that the structure of the composite be synthetically manipulable.

Previous investigations have elaborated the dependence of electron transfer rates on the driving force (free energy charge), solvation, and distance between the electron donor and acceptor

III-52

in both covalently linked systems and between intermolecular reaction partners (4-13). Intermolecular electron transfer in rigid media (9) shows a similar distance dependence to that exhibited in intramolecular redox reactions in which the donor and acceptor are separated by rigid spacers (10,11), or by flexible chains (12,13). The latter allow variation of both distance and orientation between the donors and acceptors and can act effectively as probes for assigning conformational populations (12,13), but rigid spacers offer the advantage of defined distance and orientation (10,11).

Many examples have clearly shown that electron transfer can take place either through bond (possibly involving contributions of superexchange along a linking chain) or through space (by direct interaction, possibly involving intervening solvent molecules between the donor and acceptor in an accessible conformation which places them physically within convenient electron transfer distances) (14,15). The relative contributions of the through-space and through-bond interactions will clearly depend on the conformational populations of the donor and acceptor systems (2c,16).

Since efficiency can be improved either by enhancing charge separation or by inhibiting back electron transfer within the charge separated pair, significant effort has been exerted to define those factors which permit retardation of back electron transfer (17,18). A principal means to achieve this inhibition is to conduct the electron transfer reaction within a heterogeneously dispersed medium involving molecular organizates such as microemulsions, vesicles, bilayers, micelles, etc. (17,18). In such non-homogeneous media, the electric field which develops at the interface between solvent regions can assist in the separation of the primary charge pair and, thus, inhibit back electron transfer. Furthermore, such non-homogeneous media permit preferential solubility of reactants or products into separate spatial regions, thereby enhancing charge separation and prolonging the lifetime of the components of the redox pair in separate microphases (18).

We have found that the photophysical characteristics of a series of covalently linked meso-tris(octoxyphenyl)porphyrin-RuO_2 composite clusters (MPB$_n$R) correlate, as expected, with the catalytic properties of these composites. With these multi-component systems, a synthetic porphyrin (as either free base, acid, or zinc-coordinated species) modified by the attachment of

long chain alkyl groups to a meso-p-phenoxy substituent acts as a photosensitizer. This porphyrin is covalently attached through an alkyl chain composed of a varying number of methylene units (n = 1, 4-7) to a terminal bipyridine group. This group, in turn, acts as a ligand to coordinate a transition metal such as ruthenium, which can be hydrolyzed under standard conditions to form a RuO_2 cluster (R). RuO_2 clusters have been previously demonstrated to exhibit characteristic multi-electron catalysis in the oxidation of water (with evolution of oxygen) or in the reduction of water (with evolution of hydrogen) ([19,20]).

These composite clusters, when dispersed in non-homogeneous media, e.g., in a water-in-oil microemulsion, are arranged so that the neutral water-insoluble porphyrin (as either free base or metallated form) will be found either in the organic phase or at the interface, while the much more polar RuO_2 cluster would be held in the aqueous phase ([21,22]). The desired transformation, initiated by photoexcitation, would then involve transfer of charge across the phase boundary, with the expectation that this phase inhomogeneity could be exploited as a means to enhance charge separation in the photogenerated electron-hole pair and thus to retard energy dissipative electron-hole recombination.

In these composites, either oxidative or reductive photo-mediated catalysis could be expected depending on the identity of the porphyrin sensitizer ([21-23]). For example, the excited singlet state of zinc tetraphenylporphyrin has been clearly shown to be a very active reducing agent (excited state oxidation potential = -1.4 V vs. SCE) ([24,25]), whereas the excited singlet state of the free, bis-protonated ($H_4^{2+}P$) porphyrin has been shown similarly to be a strong oxidant (excited state reduction potential = +1.5 V vs. SCE, from the diacid form of octaethylporphyrin) ([25]). Thus, photoinduced electron transfer from the zinc porphyrin to RuO_2 should result in hydrogen evolution in a water-containing system, whereas hole transfer, mediated by excitation of free acid porphyrin, should initiate oxygen formation, provided in both cases that appropriate redox electron transfer relays are available ([21-23]).

III-54

Synthesis

The synthesis of these composites has been described in detail elsewhere (21-23) and is represented in Scheme 1. The porphyrin components of these materials were obtained by condensation of pyrrole with a 3:1 ratio (Scheme 1) of substituted to unsubstituted benzaldehydes (substitution by attachment in the para-position of an OC_8H_{17} group) and purified by chromatography (21). The non-functionalized meso-phenol group was allowed to react 4-(ω-bromoalkyl)-4-'-methyl-2,2'-bipyridine. The resulting ligand functionalized porphyrin was then treated with $RuCl_3$ in a 3:1 mixture of THF:methanol, and heated under reflux for 60 min under nitrogen. Upon treatment of the bound complex with aqueous base, hydrolysis occurred to generate porphyrin-complexed RuO_2 particles (21,22). Spectral characteristics of such particles are reported elsewhere (21-23).

$ZnPB_nR$ was obtained by treatment of free base porphyrin with $Zn(OAc)_2$. MPB_n and MPB_nR (M = 2H, Zn) are redispersable powders readily soluble in chlorinated solvents, tetrahydrofuran (THF), pyridine, xylene-pentanol mixtures, and in both anionic and cationic microemulsions (21-23). The diacid porphyrin derivatives ($H4^{2+}PB_nR$) were obtained by treating the free base or zinc porphyrins with strong acid (hydrochloric or trifluoroacetic acid), as previously described (21-23). The free acid composites are readily soluble in chlorinated solvents, THF, and in either cationic or anionic microemulsions (21-23).

Microemulsions. The anionic microemulsion was prepared by mixing p-xylene, n-pentanol, water, and sodium dodecylsulfate in a 57:20:12:11 wt % ratio. The corresponding cationic microemulsion was similarly prepared as a mixture of 55 wt. % p-xylene, 20% n-pentanol, 12% water, and 13 wt. % dodecyl trimethylammonium bromide. Light scattering experiments were used to define the resulting hydrodynamic radius of the resultant water droplets as 43 + 3 Å (26).

<u>Preparation of a Model RuO2 Cluster.</u> A model dimethyl bipyridine-capped RuO2 cluster Me2bpy-RuO2 was prepared by a parallel route, involving the substitution of 4,4'-dimethyl-2,2'-bipyridine for the ligand-functionalized free base, Scheme 2 (22). After basic hydrolysis, the resulting clusters were found to be soluble in water, methanol, and anionic and cationic microemulsions, but were insoluble in chlorinated solvents, p-xylene, and p-xylene-n-pentanol mixtures (22).

<u>Results and Discussion</u>

<u>Cyclic Voltammery of the Model RuO2 Cluster</u> (22). The dimethylbipyridine surface-derivatized RuO2 clusters exhibit a catalytic oxidation current at potentials positive of +1.2 V (vs. SCE), i.e., it shows only a modest overpotential (ca. 200 mV) for the evolution of oxygen. The observed cyclic voltammeric behavior is consistent with previous descriptions of such clusters as effective catalysts for the 4-electron oxidation of water (19). Me2bpy-RuO2 also displays moderate catalytic activity for the reduction of water to hydrogen, Figure 1. A similar behavior has been reported for a RuO2-coated TiO2 substrate (27).

<u>Characterization of MPB$_n$R (M = 2H, Zn, 4H2+)</u> (21-23). In the composites, the surface of the RuO2 cluster is functionalized by covalent attachment of the bipyridine ligating site, resulting in a transition metal oxide cluster protected against further growth and agglomeration into larger particles by its organic coating (28,29). When imaged by transmission electron microscopy, these clusters show an average size of 21 ± 7 Å which seems to be independent of the linking chain length, making them among the smallest RuO2 clusters yet reported (22,23).

This chemical sequestering of the RuO2 cluster produces an enhanced solubility in chlorinated and other non-polar solvents. That is, the solubility properties of the composite reflect solvation interactions with the attached porphyrin rather than with the hydrophilic RuO2 cluster. Previous reports of chemically modified CdSe and CdS crystallites bound to surface-attached phenyl groups similarly exhibit alterations of their hydrophobic character and, hence, solubility,

compared with native bulk CdSe or CdS clusters (28). As with these crystallites, the synthesis of re-disperable powders of colloidal semiconductor clusters which employ synthetic routes involving organometallic reagents (28), or polymeric sodium polyphosphate (29) as a stabilizing surfactant have been reported.

Spectral Dependence of These Porphyrin RuO_2 Composite Clusters on Spacer Chain Length. (23) The absorption spectra of MPB_n (M = 2H, $4H^{2+}$) are not influenced by coordination to $RuCl_3$, although the quantum yields for fluorescence are strongly attenuated, Figure 2. The magnitude of the fluorescence quenching is dependent on the spacer length of the flexible alkyl chain connecting the porphyrin and the RuO_2 cluster, Table 1. Hydrolysis of the MPB_n-coordinated $RuCl_3$ to the MPB_nR composite (M = 2H, $4H^{2+}$), however, results in a broadening of the Soret band, although without shift in the band positions. Further diminution of the fluorescence of the composite is observed after hydrolysis.

Both the magnitude of the Soret broadening and the further decrease in fluorescence intensity upon formation of RuO_2 are likewise dependent on chain length, Table 1. For composites in which the metal oxide cluster is rigidly attached to the photosensitizer (n = 1) or where substantial entropic disorder in the linking chain makes folding of the photosensitizing porphyrin over the metal oxide cluster unlikely (n = 7), only a slight broadening can be observed. For composites of intermediate connecting chain length (n = 4-6), more extensive broadening is notable. Similarly, only minor changes in the relative fluorescence quantum yields are observed upon conversion of the complexed $RuCl_3$ to a RuO_2 cluster for n = 1 or 7.

Porphyrin aggregation cannot be responsible for the observed spectral broadening in MPB_nR, since the absorption spectra of redissolved MPB_nR are unaffected by concentration over a wide range (4×10^{-8} to 2×10^{-4} M) (22,23). Porphyrin aggregation has previously been reported to result either in a splitting (30) or bathochromic shift (31) of the Soret band, depending on the relative orientation of the two strongly interactive porphyrins. Nonetheless, analogous perturbations of absorption spectra have been described for meso-tetratolyl porphyrins linked to

quinones and hydroquinones through amide bonds of variable length (12c) There, the broadened absorption spectra were assigned to strongly perturbed conformers in which the quinone folds over the pi system of the porphyrin, causing strong electronic interaction between these groups, i.e., to the formation of an intramolecular complex. Such complexed donor/acceptor conformations exhibited lower fluorescence efficiency and perturbed emission spectra compared to extended conformations which lack this intramolecular complexation (12c).

A parallel interpretation of our data would suggest that conformational folding is optimal for $n = 4$-6, whereas entropic effects become dominant for longer chains (e.g., $n = 7$) and steric inhibition precludes folding for $n = 1$.

Rates of Photoinduced Electron Transfer (21-23). The lower fluorescence quantum yields observed in MPB_nR compared to MP and MPB_n are predominantly caused by electron transfer. A control experiment involving a soluble porphyrin and a separately dispersed RuO_2 cluster show that, at the concentrations of this experiment, interaction (adsorption or energy transfer) between the porphyrin of one MPB_nR cannot be invoked as an explanation for diminished fluorescence emission (22). The absence of low energy absorption bands in the Me_2 bpy-RuO_2 clusters argues against a highly efficient intramolecular energy transfer mechanism as a significant route for fluorescence quenching (21,22). The possibility that the observed fluorescence quenching is caused by enhanced spin-orbital coupling mediated by the heavy effect of a ruthenium in MPB_nR is rendered unlikely since complexation of MPB_n to RuO_2 leads to a decrease in the porphyrin triplet yield, but the triplet lifetime is unaffected (21-23). We conclude, therefore, that electron transfer from the excited singlet state of the porphyrin sensitizer to the RuO_2 moiety in these composite clusters constitutes a dominant route for fluorescence decay of the photogenerated excited singlet state at least in the non-complexed conformations.

If so, then the rate constants for electron transfer can be determined from the relative fluorescence quantum yields of the composites and the fluorescence lifetimes of the unbound porphyrins MPB_n. As shown in Tables 1 and 2, both the relative fluorescence yields and these

ZII—Sd

rate constants depend sensitively on the spacer length separating the photosensitizer from the covalently-attached metal oxide cluster. Somewhat slower electron transfer rates are observed for the free base than for the zinc porphyrin, an effect which can be assigned by differences in the excited state redox potentials in the two substrates. In the free acid porphyrin, hole transfer (i.e., electron transfer from RuO_2 to the porphyrin) is assumed to be the dominant relaxation process, given the potential measurements discussed earlier.

Influence of Spacer Length on Triplet Lifetime in MPB$_n$R (23). In parallel to the shortened singlet lifetime observed as described above, a similar decrease in the triplet yield is observed (see triplet yields in pyridine, Table 2). Two transient species with lifetimes of 160 ns and 280 ms, respectively, are observed upon flash photolysis of MPB$_n$R (n = 4-7). Virtually identical transient absorption spectra are observed irrespective of solvent, and the absorption spectra of both transients closely resemble that of the triplet of the uncomplexed porphyrin (26). The length of the linking chain does not influence the lifetime, but the relative contributions of the short- and long-lived components are affected. With n = 4-6, higher amounts of the short lived species are observed, compared to n = 7 (a species which, from fluorescence quenching measurements, we concluded had smaller contributions from the folded conformers). For n = 1, where most likely no folding occurs, only a single long-lived component is observed.

The observation of two triplets in the loosely tethered clusters is thought to derive from the conformational inhomogeneity within MPB$_n$R consistent with their absorption and fluorescence properties. The folded conformer which display a Soret broadening and are most likely non-fluorescent also correlate with a faster triplet decay, whereas the slower component of triplet decay is assigned to the extended, non-perturbed porphyrin triplet state. The substantial decrease in the triplet state lifetime in the folded conformers is probably better explained by enhanced intersystem crossing caused by the heavy atom effect of ruthenium than by electron trasnfer emanating from the triplet state. Enhanced intersystem crossing most likely also accounts for the more or less complete fluorescence quenching in the complexed conformers.

Blocking Conformational Folding by Pyridine Ligation (23). Axial ligation of pyridine to the core metal in cofacial zinc porphyrin dimers has been found to reverse aggregation and, thus, the magnitude of both exciton coupling (i.e., broadened spectral bands) and fluorescence quenching (32). The interference with agglomeration of such porphyrins was mainly attributed to a steric effect, i.e., the blocking of the pi face of the porphyrin by a ligating pyridine solvent molecule, thus preventing intermolecular pi-pi interaction between the two porphyrins (32a). Similar attachment of an electron donor molecule to a vacant apical coordination site in zinc tetraphenylporphyrin has been reported to affect both its ground state absorption (33-35) and fluorescence spectrum (36) and to cause shifts in its redox potential (37), without influencing either the fluorescence quantum yield or lifetime (36). Pyridine does not quench the triplet state of zinc tetraphenylporphyrin (38).

Both the absorption and fluorescence spectra of MPB_n and MPB_nR exhibit bathochromic shifts in pyridine (absorption 434, 568, and 608 nm; fluorescence spectra 619 and 699 nm, respectively) compared to the same bands measured in a p-xylene-n-pentanol mixture (430, 560, and 602 nm; 610 and 660 nm, respectively). For $ZnPB_nR$, fluorescence quenching in pyridine is less efficient than that in p-xylene, n-pentanol, Table 2. In contrast, the free base derivative H_2PB_nR (where no pyridine ligation can occur) displays nearly identical Soret bandwidths, as well as fluorescence quantum yields, in either pyridine or in xylene-pentanol mixtures. Thus, the absence of spectral broadening and the increase in the relative fluorescence quantum yields of $ZnPB_nR$ in pyridine implicate axial ligation of pyridine at zinc rather than dielectric effects on its excited state properties. In parallel, this same pyridine ligation significantly diminishes the contribution observed from the short-lived triplet, i.e., it seems to prevent the RuO_2 cluster from folding over the porphyrin pi chain by flexing of the appended alkyl chain (39).

The Soret band-broadening, the increase in relative fluorescence quantum yield, and the decrease in the short-lived triplet component similarly depend on spacer length, with most significant effect being observed where n = 4-6, and reduced effects prevailing for n = 7. This

result suggests that a much smaller fraction of the complexed conformers exists for n = 7 than for n = 4-6. This interpretation finds further support in the much lower fluorescence quenching observed for ZnPBR (n = 1) where most likely no folding occurs in the presence and absence of pyridine. However, in pyridine, where intramolecular complexation seems to be minimal for ZnPB$_N$R, both the porphyrin fluorescence intensity and triplet yield are substantially lower than for ZnPB$_n$. Thus, an additional route, most likely electron transfer from the porphyrin excited triplet state to RuO$_2$, must account for the fluorescence quenching.

Effect of Spacer Length on Fluorescence Lifetimes in ZnPB$_n$R (23). Time-resolved single photon counting can be used to measure excited singlet state lifetimes of ZnPB$_n$R. Comparison of the fluorescence lifetimes observed in p-xylene-n-pentanol and in n-pyridine would allow clear distinction between contributions from the complexed conformers to the fluorescence decay kinetics.

In MPB$_n$, single exponential fits could effectively describe the observed fluorescence decay, but in the presence of the RuO$_2$ cluster (in MPB$_n$R), more complex triple exponential fits were required giving lifetimes of 0.03-0.09 ns (τ_1), 0.15-0.56 ns (τ_2), and 1.2-1.3 ns (τ_3) with relative amplitudes of 0.6-0.9 (A_1), 0.1-0.2 (A_2), and 0.02-0.2 (A_3). For all ZnPB$_n$R, the fluorescence decay is dominated by the short-lived component, but the relative contributions from the long-lived components depend on the length of the bridging chain. As the chain length is decreased, the relative importance of the short-lived component increases.

The observation of nearly identical fluorescence lifetimes and relative amplitudes of ZnPB$_n$R in these two solvents indicates that negligible fluorescence derives from the complexed conformers. That is to say, in the complexed conformers, the porphyrin fluorescence is completely quenched. The multi-exponentiality observed in the flourescence kinetics derives entirely from the non-complexed (fluorescent) conformers.

The multi-exponential singlet decay kinetics can thus be best explained by electron transfer from non-complexed conformations which do not equilibrate on the sub-nanosecond timescale

(12c). Small spatial separation between the absorptive porphyrin excited state and the RuO_2 cluster favors rapid forward electron transfer, but also a similar acceleration of back electron transfer (15,40). This rapid recombination obviously influences our ability to observe even transient formation of a radical cation with transient absorption spectroscopy, the expected intermediate formed in these redox transformations.

Photolysis of ZnPBR in the Presence of a Sacrificial Electron Acceptor (22). A transient absorption spectrum for ZnPBR recorded in the presence of persulfate (as a sacrifical electron acceptor) in a cationic microemulsion is shown as Figure 3. When observed 7 ms after the initial excitation, the transient spectrum, which is identical to that expected for a porphyrin radical cation, does not decay over a period of at least 1 ms. This transient cannot derive from thermal oxidation of the porphyrin by persulfate, since the ground state absorption spectrum does not permanently change. Similar evidence for the formation of a porphyrin radical cation in the presence of persulfate is also observed for ZnPBR but to a smaller conversion (only about 30% of the intensity observed is ZnPBR) (22).

Likewise, laser excitation of ZnPBR in an anionic microemulsion in the presence of protons similarly generates a porphyrin cation radical (22). Thus, protons apparently are capable of acting as effective electronic acceptors (in a parallel role with that shown with persulfate), involving ultimately the probable formation of molecular hydrogen.

Conclusions

Metal oxide-sensitizer composites with an average RuO_2 cluster size of 21 ± 7 Å can be prepared by covalently attaching bipyridine units, which are linked through an alkyl chain to a meso-tris(octyloxyphenyl)porphyrins, to RuO_2 cluster. The steady state fluorescence intensity of the resulting composite is decreased compared to that of the non-complexed porphyrin. The magnitude of the fluorescence quenching depends on the flexible spacer length between the sensitizer and the metal oxide cluster.

III - 62

13

The Soret broadening and observation of two distinct triplets of disparate lifetimes in MPB_nR suggest the involvement of two distinct families of conformers: (1) complexed conformers in which folding of the RuO_2 moiety over the prophyrin macrocycle leads to intramolecular complexation between the two chromophores of the alkyl chain places the RuO_2 moiety spatially in an apical position over the porphyrin pi system; and (2) one more extended (non-complexed) conformer. The complexed conformers are not fluorescent, but do exhibit broadened absorption spectra and reduced triplet lifetimes compared to the non-complexed conformers. When the metal oxide cluster is spatially close to the first sensitizer, electronic interaction between the porphyrin and the redox catalyst via spin-orbital coupling leads to a substantial decrease in the observed porphyrin triplet lifetime. Absorption spectra, fluorescence quenching, and triplet decay kinetics indicate that the distribution of conformers between these two families depends sensitively on the length of the flexible linkage.

Ring size effects are consistent with a predominance of folded conformers with alkyl chains containing four to six carbons, with smaller fractions of folded conformers being attained for alkyl chains containing 1 or 7 methylene units.

Solvent coordination by pyridine blocks the apical site of the porphyrin, correspondingly reducing the contribution of complexed conformers as the solvent wins in the competition (with the metal oxide clusters) for this preferred complexation site. In pyridine therefore, absorption spectra are unaltered by the presence or absence of a covalently attached metal oxide cluster, and higher relative fluorescence quantum yields and a smaller fraction of the fast decaying porphyrin triplet are observed. With $ZnPB_nR$ in pyridine, however, the fluorescence intensity, triplet yield, and the singlet lifetime are still substantially shortened relative to the unbound solvent-ligated porphyrin whereas the triplet lifetime is unaffected. This suggests that in the non-complexed conformers a major decay process operative from the singlet state may be photoinduced electron transfer.

A lower fluorescence intensity is observed in $H_4^{2+}PB_nR$ than in the free acid porphyrin itself. By analogy, this spectral perturbation of its excited state photophysics is likely to be attributable to hole transfer, in which an electron shifts from the metal oxide to the diacid

porphyrin, as would be suggested by the relative redox potential of the free acid in previously described models. In the complexed, non-fluorescent conform.ers very fast intersystem crossing (rather than electron transfer) is probably the dominant decay pathway.

Thus, in MPB$_n$R electron transfer can occur either by direct interaction between the porphyrin and metal oxide in a non-complexed conformer which brings these two moieties to within direct spatial interaction distance, or, with lowered facility, by through-bond interaction along the alkyl linking chain. The observation of relatively small changes in singlet lifetimes upon changing the length of the interconnecting alkyl chain supports the possibility that electron transfer occurs at least partially through space.

References

(1)   (a) Tabushi, I; Koga, N; Yanagita, M. *Tetrahedron Lett.* **1979**, 257-260. (b) Kong, J. L. Y.; Loach, P. A. *Nature* **1980**, *286*, 254-256. (c) Migita, M; Okada,T; Mataga, N. *Chem. Phys. Lett.* **1981**, *84*, 263- 56. (d) Kong, J. L. Y.; Spears, P. A.; Loach, P. A. *Photochem. Photobiol.* **1982**, *35*, 545-553. (e) Bergkamp, M. A.; Dalton, J.; Netzel, T. L. *J. Am. Chem. Soc.* **1982**, *104*, 253-259. (f) Nishitani, S.; Kurata, N.; Sakata, Y.; Misumi, S. *J. Am. Chem. Soc.* **1983**, *105*, 7771-7772. (g) Mataga, N.; Karen, A.; Okada, T.; Nishitani, S. *J. Phys. Chem.* **1984**, *88*. 5138- 5141. (h) Wasielewski, M. R.; Niemczyk, M. P.; Svec, W.A.; Pewitt, E. B. *J. Am. Chem. Soc.* **1985**, *107*, 1080-1082. (i) Leland, B. A.; Joran, A. D.; Felker, P. M.; Hopfield, J. J.; Zewail, A. H.; Dervan, P. B. *J. Phys. Chem.* **1985**, *89*, 5571-5573. (j) Sessler, J. L.; Johnson, M. R.; Lin, T.-Y.; Creager, S. E. *J. Am. Chem. Soc.* **1988**, *110*, 3659-3661.

(2)   (a) Harriman, A.; Porter, G.; Wilowska, A. *J. Chem. Soc., Faraday Trans. 2* **1984**, *80*, 191-204. (b) Blondel, G.; De Keukeleire, D.; Harriman, A.; Milgrom, L. R.*Chem. Phys. Lett* **1985**, *118*, 77-82. (c) Kanda, Y.; Sato, H.; Okada, T.; Mataga, N. *Chem. Phys. Lett.* **1986**, *129*, 306-309. (d) Kaji, N.; Aono, S.; Okura, I. *J. Mol. Catal.* **1986**, *36*, 201-203.

(3)   (a) Elliott, C. M.; Freitag, R. A.; Blaney, D. D. *J. Am. Chem. Soc.* **1985**, *107*, 4647-4655. (b) Danielson, E.; Elliott, C. M.; Merkert, J. M.; Meyer, T. J. *J. Am. Chem. Soc.* **1987**, *109*, 2519- 2520.

III-64

(4)   (a) Marcus, R. A.; Sutin, N. *Biochim. Biophys. Acta* 1985, *811*, 265-282. (b) Closs, G. L.; Miller, J. R. *Science* 1988, *240*, 440-447.

(5)   (a) Rehm, D.; Weller, A. *Ber. Bunsenges. Phys. Chem.* 1969, *73*, 834-839. (b) Rehm, D.; Weller, A. *Isr. J. Chem.* 1970, *8*, 259-271. (c) Greiner, G.; Pasquini, P.; Weiland, R.; Orthwein, H.; Rau, H. *J. Photochem. Photobiol., A : Chem.* 1990, *51*, 179-195. (d) Ohno, T.; Yoshimura, A.; Mataga, N.; *J. Phys. Chem.* 1990, *94*, 4871-4876.

(6)   Miller, J. R.; Beitz, J. V.; Huddleston, R. K. *J. Am. Chem. Soc.* 1984, *106*, 5057-5068.

(7)   (a) Miller, J. R.; Calcaterra, L. T.; Closs, G. L. *J. Am. Chem. Soc.* 1984, *106*, 3047-3049. (b) Schmidt, J. A.; Siemiarczuk, A.; Weedon, A. C.; Bolton, J. R. *J. Am. Chem. Soc.* 1985, *107*, 6112-6114. (c) Bolton, J. R.; Ho, T.-F.; Liauw, S.; Siemiarczuk, A.; Wan, C. S.; Weedon, A. C. *J. Chem. Soc., Chem. Commun.* 1985, 559-560. (d) Irvine, M. P.; Harrison, R. J.; Beddard, G. S.; Leigthon, P. · Sanders, J. K. M. *Chem. Phys.* 1986, *104*, 315-324. (e) Oevering, H.; Paddon-Row, M J.; Heppener, M.; Oliver, A. M.; Cotsaris, E.; Verhoeven, J. W.; Hush, N. S. *J. Am. Chem. Soc.* 1987, *109*, 3258-3269. (f) Finckh, P.; Heitele, H.; Michel-Beyerle, M. E. *Chem. Phys.* 1989, *138*, 1-10.

(8)   (a) Miller, J. R. *Nouv. J. Chim.* 1987, *11*, 83-89. (b) Joran, A. D.; Leland, B. A.; Felker, P. M.; Zewail, A. H.; Hopfield, J. J.; Dervan, P. B. *Nature* 1987, *327*, 508-511.

(9)   (a) Miller, J. R. *Science* 1975, *189*, 221-222. (b) Miller, J. R.; Peeples, J. A.; Schmitt, M. J.; Closs, G. L. *J. Am. Chem. Soc.* 1982, *104*, 6488-6493. (c) Strauch, S.; McLendon, G.; McGuire, M.; Guarr, T. *J. Phys. Chem.* 1983, *87*, 3579-3581.

(10)   Calcaterra, L. T.; Closs, G. L.; Miller, J. R. *J. Am. Chem. Soc.* 1983, *105*, 670-671. (b) Wasielewski, M. R.; Niemczyk, M. R. *J. Am. Chem. Soc.* 1984, *106*, 5043-5045. (c) Joran, A. D.; Leland, B. A.; Geller, G. G.; Hopfield, J. J.; Dervan, P. B. *J. Am. Chem. Soc.* 1984, *106*, 6090-6092. (d) Closs, G. L.; Calcaterra, L. T.; Green, N. J.; Penfield, K. W.; Miller, J. R. *J. Phys. Chem.* 1986, *90*, 3673-3683. (e) Verhoeven, J. W. *Pure Appl. Chem.* 1986, *58*, 1285-1290. (f) Heiler, D.; McLendon, G.; Rogalski, P. *J. Am. Chem. Soc.* 1987, *109*, 604-606. (g) Paddon-Row, M. N.; Oliver, A. M.; Warman, J. M.; Smit, J. K.; de Haas, M. P.; Oevering, H.; Verhoeven, J. W. *J. Phys. Chem.* 1988, *92*, 6958-6962. (h) Johnson, M. D.; Miller, J. R.; Green, N. S.; Closs, G. L. *J. Phys. Chem.* 1989, *93*, 1173-1176. (i) Sakata, Y.; Nakashima, S.; Goto, Y.; Tatemitsu, H.; Misumi, S. *J. Am. Chem. Soc.* 1989, *111*, 8979-8981.

III-65

(11) (a) Lindsey, J. S.; Mauzerall, D. C. *J. Am. Chem. Soc.* **1982**, *104*, 4498-4500. (b) Lindsey, J. S.; Mauzerall, D. C. *J. Am. Chem. Soc.* **1983**, *105*, 6528-6529.

(12) (a) Ho, T.-F.; McIntosh, A. R.; Bolton, J. R. *Nature* **1980**, *286*, 254-256. (b) McIntosh, A. R.; Siemiarczuk, A.; Bolton, J. R.; Stillman, M. J.; Ho, T.-F.; Weedon, A. C. *J. Am. Chem. Soc.* **1983**, *105*, 7215-7223. (c) Siemiarczuk, A.; McIntosh, A. R.; Ho, T.-F.; Stillman, M. J.; Roach, K. J.; Weedon, A. C.; Bolton, J. R.; Connolly, J. S. *J. Am. Chem. Soc.* **1983**, *105*, 7224-7230.

(13) (a) Harriman, A. *Inorg. Chim. Acta* **1984**, *88*, 213-216. (b) Nakamura, H.; Uehata, A.; Motonaga, A.; Ogata, T.; Matsuo, T. *Chem. Lett.* **1987**, 543-546. (c) Saito, T.; Hirata, Y.; Sato, H.; Yoshida, T.; Mataga, N.; *Bull. Chem. Soc. Jpn.* **1988**, *61*, 1925-1931.

(14) Schmidt, J. A.; McIntosh, A. R.; Weedon, A. C.; Bolton, J. R.; Connolly, J. S.; Hurley, J. K.; Wasielewski, M. R. *J. Am. Chem. Soc.* **1988**, *110*, 1733-1740.

(15) Batteas, J. D.; Harriman, A.; Kanda, Y.; Mataga, N.; Nowak, A. K. *J. Am. Chem. Soc.* **1990**, *112*, 126-133.

(16) Gnaedig, K.; Eisenthal, K. B. *Chem. Phys. Lett.* **1977**, *46*, 339-342.

(17) (a) Fendler, J. H. *Acc. Chem. Res.* **1976**, *9*, 153-161. (b) Brugger, P.-A.; Infelta,P. P.; Braun, A. M.; Graetzel, M. *J. Am. Chem. Soc.* **1981**, *103*, 320-326. (c) Graetzel, M. *Energy Resources Through Photochemistry and Catalysis*, Ed., Academic : New York, **1983**. (d) Mandler, D.; Degani, Y.; Willner, I. J. *J. Phys. Chem.* **1984**, *88*, 4366-4370. (e) Steinmueller, F.; Rau, H. *J. Photochem.* **1985**, *28*, 297-308. (f) Seta, P.; Bienvenue, E.; Moore, A. L.; Mathis, P.; Bensasson, R. V.; Liddel, P.; Pessiki, P. J.; Joy, A.; Moore, T. A.; Gust, D. *Nature* **1985**, *316*, 653-655. (g) Matsuo, T. *J. Photochem.* **1985**, *29*, 41-54. (h) Nagamura, T.; Takeyama, N.; Tanaka, K.; Matsuo, T. *J. Phys. Chem.* **1986**, *90*, 2247-2251. (i) Colaneri, M. J.; Kevan, L.; Schmehl, R. *J. Phys. Chem.* **1989**, *93*, 397-401.

(18) (a) Willner, I.; Ford, W. E.; Otvos, J. W.; Calvin, M. *Nature* **1979**, *280*, 823-824. (b) Turro, N. J.; Graetzel, M.; Braun, A. M. *Angew. Chem.* **1980**, *92*, 712-734. (c) Willner, I.; Goren, Z.; Mandler, D.; Maidan, R.; Degani, Y. *J. Photochem.* **1985**, *28*, 215-228.

(19) (a) Kiwi, J. *J. Chem. Soc., Faraday Trans. 2*, **1982**, *78*, 339-345. (b) Christensen, P. A.; Harriman, A.; Porter, G. *J. Chem. Soc., Faraday Trans. 2*, **1984**, *80*, 1451-1464. (c) Mills, A.; McMurray, N. *J. Chem. Soc., Faraday Trans.1*, **1988**, *84*, 379-390.

(20) (a) Amouyal, E.; Keller, P.; Moradpour, A. *J. Chem. Soc., Chem. Commun.* **1980**, 1019-1020. (b) Keller, P.; Moradpour, A.; Amouyal, E. *J. Chem. Soc., Faraday Trans. 1*, **1982**, 3331-3340. (c) Amouyal, E.; Koffi, P. *J. Photochem.* **1985**, *29*, 227-242. (d) Kleijn, J. M.; Lyklema, J. *Coll. Polym. Sci.* **1987**, *265*, 1105-1113. (e) Kleijn, J. M.; Rouwendal, e.; Van Leeuwen, H. P.; Lyklema, J. *J. Photochem. Photobiol., A : Chem.*, **1988**, *44*, 29-50.

(21) Gregg, B. A.; Fox, M. A.; Bard, A. J. *Tetrahedron* **1989**,*45*, 4707-4716.

(22) Resch, U.; Fox, M. A. *J. Phys. Chem.* **1990**, accepted for publication.

(23) Resch, U.; Fox, M. A. *J. Phys. Chem.* **1990**, accepted for publication.

(24) Darwent, J. R.; Douglas, P.; Harriman, A.; Porter, G.; Richoux, M.- C. *Coord. Chem. Rev.* **1982**, *44*, 83-126.

(25) Dolphin, D., Ed., " *The Porphyrins,* " Vol. 3, Academic Press, New York, 1978.

(26) Resch, U.; Hubig, S. M.; Fox, M. A. *Langmuir.* **1990**, accepted for publication.

(27) Goodenough, J. B.; Manoharan, R.; Parantham, M. *J. Am. Chem. Soc.* **1990**, *112*, 2076-2082.

(28) (a) Steigerwald, M. L.; Alivasitos, A. P.; Gibson, J. M.; Harris, T. D.; Kortan, R.; Muller, A.J.; Thayer, A. M.; Duncan, T. M.; Douglass, D. C.; Brus, L. E. *J. Am. Chem. Soc.* **1988**, *110*, 3046-3050. (b) Herron, N.; Wang, Y.; Eckert, H. *J. Am. Chem. Soc.* **1990**, *112*, 1322-1326.

(29) Fojtik, A.; Weller, H.; Koch, U.; Henglein, A. *Ber. Bunsenges. Phys. Chem.* **1984**, *88*, 969-977.

(30) Kasha, M.; Rawls, H. R.; Ashraf el-Bayoumi, M. *Pure Appl. Chem.* **1965**, *11*, 371-393.

(31) Brochette, P.; Pileni, M. P. *Nouv. J. Chim.* **1985**, *9*, 551-554.

III - 67

(32) (a) Hunter, C. A.; Leighton, P.; Sanders, J. K. M. *J. Chem. Soc., PerkinTrans. 1*, **1989**, 547-552. (b) Hunter, C. A.; Sanders, J. K. M. *J. Am. Chem. Soc.* **1990**,*112*, 5525-5534.

(33) Nappa, M.; Valentine, J. S. *J. Am. Chem. Soc.* **1978**, *100*, 5075-5080.

(34) (a) Miller, J. R.; Dorough, G. D. *J. Am. Chem. Soc.* **1952**, *74*, 3977-3981. (b) Becker, D. S.; Hayes, R. G. *Inorg. Chem.* **1983**, *22*, 3050-3053.

(35) (a) Kirksey, C. H.; Hambright, P.; Storm, C. B. *Inorg. Chem.* **1969**, *8*, 2141-2144. (b) Kirksey, C. H.; Hambright, P. *Inorg. Chem.* **1969**, *9*, 958-960. (c) Vogel, G. C.; Beckmann, B. A. *Inorg. Chem.* **1976**, *15*, 483-484.

(36) Humphry-Baker, R.; Kalyanasundaram, K. *J. Photochem.* **1985**, *31*, 105-112.

(37) Kadish, K. M.; Shiue, L. R.; Rhodes, R. K.; Bottomley, L. A. *Inorg. Chem.* **1981**, *20*, 1274-1277.

(38) Pekkarinen, L.; Linschitz, H. *J. Am. Chem. Soc.* **1960**, *82*, 2407-2411.

(39) Boxer, S. G.; Bucks, R. R. *J. Am. Chem. Soc.* **1979**, *101*, 1883-1885.

(40) Harriman, A.; Nowak, A. K. *Pure Appl. Chem.* **1990**, *62*, 1107-1110.

III - 68

Table 1. Soret Bandwidth (FWHM), Relative Fluorescence Quantum Yields of MPB_n Coordinated to Either $RuCl_3$ or RuO_2 (MPB_nR), and Calculated Intramolecular Electron Transfer Rate Constants (k_{et}) in Tetrahydrofuran.

		$RuCl_3$[a]		RuO_2[a]		
M	n	$FWHM$[b] (nm)	Φ_f/Φ_f^{0}[c,d]	$FWHM$[b] (nm)	Φ_f/Φ_f^{0}[c,e]	k_{et}[e,f] $\times 10^{-9}$ (s^{-1})
2H	1	13	0.05	14	0.05	1.9
2H	4	13	0.20	17	0.07	1.3
2H	5	13	0.25	17	0.11	0.79
2H	6	13	0.30	16	0.15	0.56
2H	7	13	0.35	14	0.30	0.23
$4H^{2+}$	1	16	0.09	17	0.09	4.8
$4H^{2+}$	4	16	0.29	20	0.17	2.3
$4H^{2+}$	5	16	0.37	20	0.23	1.6
$4H^{2+}$	6	16	0.42	19	0.30	1.1
$4H^{2+}$	7	16	0.48	17	0.44	0.61

[a] Porphyrin-to-ruthenium ratio, $c_{Ru}/c_P = 1 : 3$

[b] Full width at half height of the maximum absorption of the Soret band:
$FWHM(H_2PB_n) = 13$ nm; $FWHM(ZnPB_n) = 11$ nm; $FWHM(H_4^{2+}PB_n) = 16$ nm, all independent of solvent

[c] Fluorescence quantum yield of ruthenium-coordinated MPB_n (Φ_f) relative to the fluorescence quantum yield of uncomplexed MPB_n (Φ_f^0)

[d] Complexed to $RuCl_3$

[e] Complexed to RuO_2

[f] k_{et} was calculated from the relative fluorescence quantum yields of MPB_nR and the experimental fluorescence lifetime of MPB_n, assuming a single conformation

Table 2. Soret Bandwidth (FWHM), Relative Fluorescence Quantum Yields, and Calculated Intramolecular Electron Transfer Rate Constants (k_{et}) for $ZnPB_nR$ and H_2PB_5R in p-Xylene/n-Pentanol (x-/n-p) and Pyridine (py).

M py	n	x-/n-p FWHM	x-/n-p Φ_f/Φ_f^0 [b]	x-/n-p $k_{et}^c \times 10^{-9}$ (s^{-1})	py FWHM[a] (nm)	py Φ_f/Φ_f^0 [b]	py $k_{et}^c \times 10^{-9}$ (s^{-1})	triplet yield in py $\Delta OD_T/\Delta OD^0_T$
Zn	1	13	0.03	23	11	0.04	17	0.05
Zn	4	16	0.06	11	12	0.16	4.0	0.15
Zn	5	16	0.09	7.2	12	0.20	3.1	0.20
ZH	5	17	0.11	--	17	0.10	0.88	--
Zn	6	15	0.14	4.4	11	0.25	2.3	0.24
Zn	7	13	0.27	1.9	11	0.32	1.6	0.34

[a] Full width at half height of the absorption maximum of the Soret band

[b] Fluorescence quantum yield of RuO_2-coordinated MPB_n (Φ_f) relative to the fluorescence quantum yield of uncomplexed MPB_n (Φ_f^0)

[c] k_{et} was calculated from the relative fluorescence quantum yields of MPB_nR and the experimental fluorescence lifetime of MPB_n, assuming a singke conformation.

Scheme 1

III-71
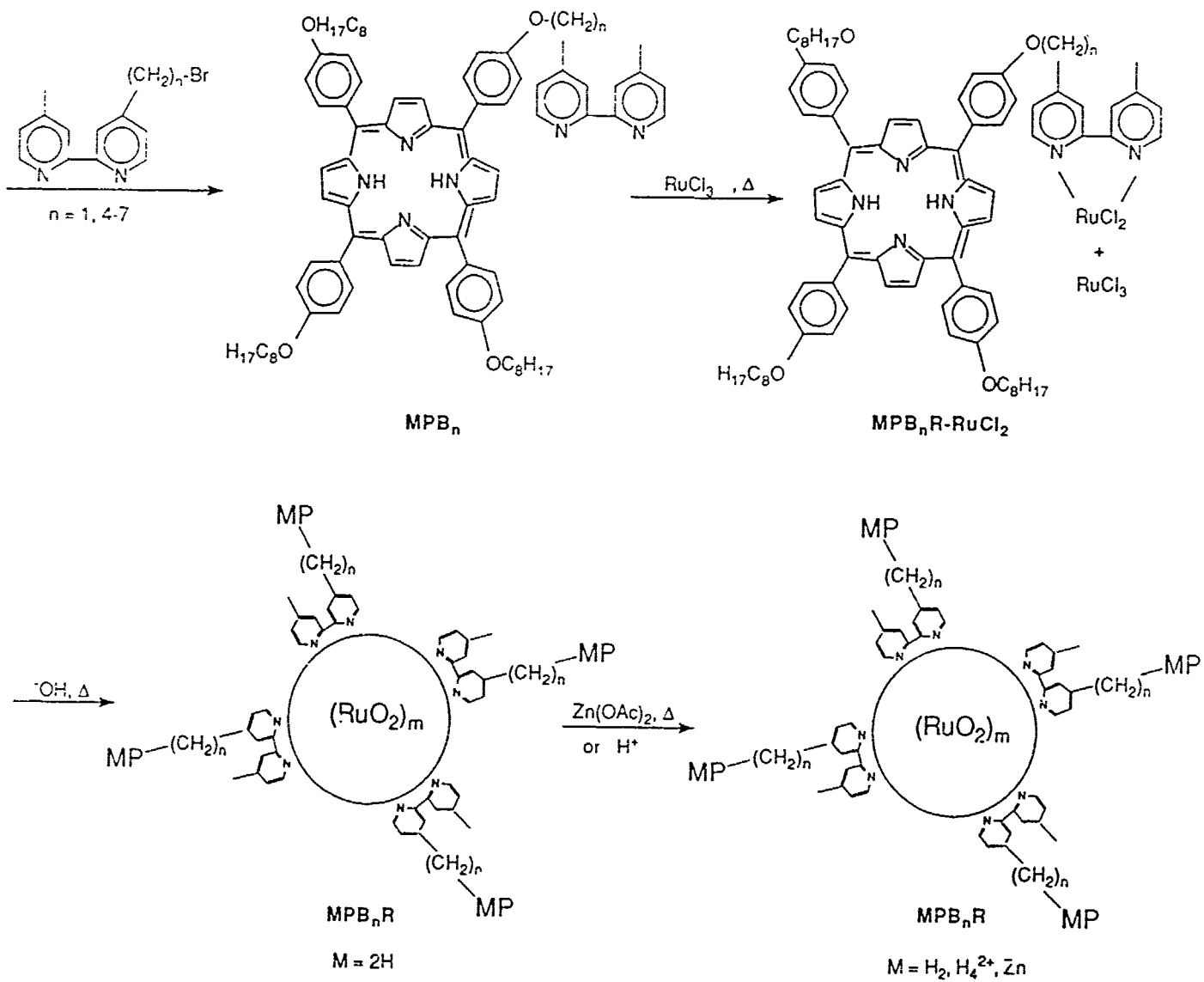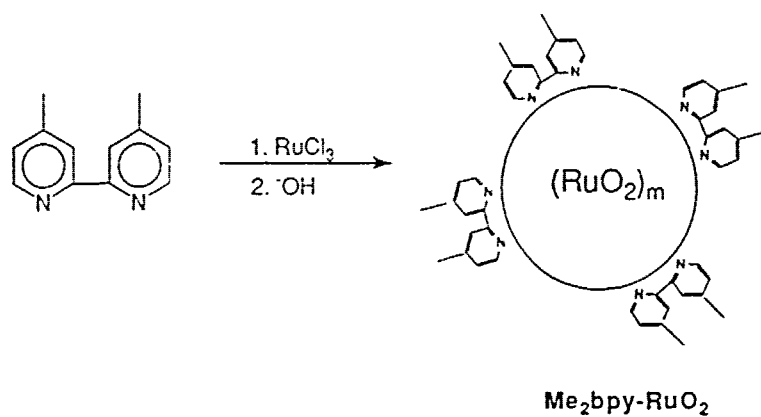
Me$_2$bpy-RuO$_2$

Scheme 2

III-72

Figure captions

Fig.1. Cyclic voltammogram of $Me_2bpy-RuO_2$ in 1M H_2SO_4: the dashed line shows the background. Scan rate: 100 mV/s, potential vs. SCE. The electrode was a vitreous carbon disk; anodic currents are plotted up.

Fig.2. Relative fluorescence quantum yield (Φ_f/Φ_f^0) of H_2PB_5 in THF as a function of the molar ratio of ruthenium to porphyrin (c_{Ru}/c_P): $RuCl_3$; RuO_2; RuO_2 (hydrolysis under dilute conditions : dilution by a factor of 100). Inset: Absorption spectra (Soret region) of H_2PB_5, complexed to $RuCl_3$ ( ) and RuO_2 (- - -); $c_{Ru}/c_P = 3 : 1$. The $RuCl_3$-coordinated species shows the same absorption spectrum (Soret region) as the uncomplexed porphyrin H_2PB_5.

Fig.3. Transient absorption spectrum of the porphyrin radical cation obtained for ZnPBR in the anionic microemulsion with persulfate as electron acceptor. The spectrum was recorded in air-saturated solution 7 μs after excitation at 532 nm. Inset: transient absorption spectrum observed for ZnPBR in the anionic microemulsion in the presence of protons 7 μs after excitation.

Fig.1

III-74
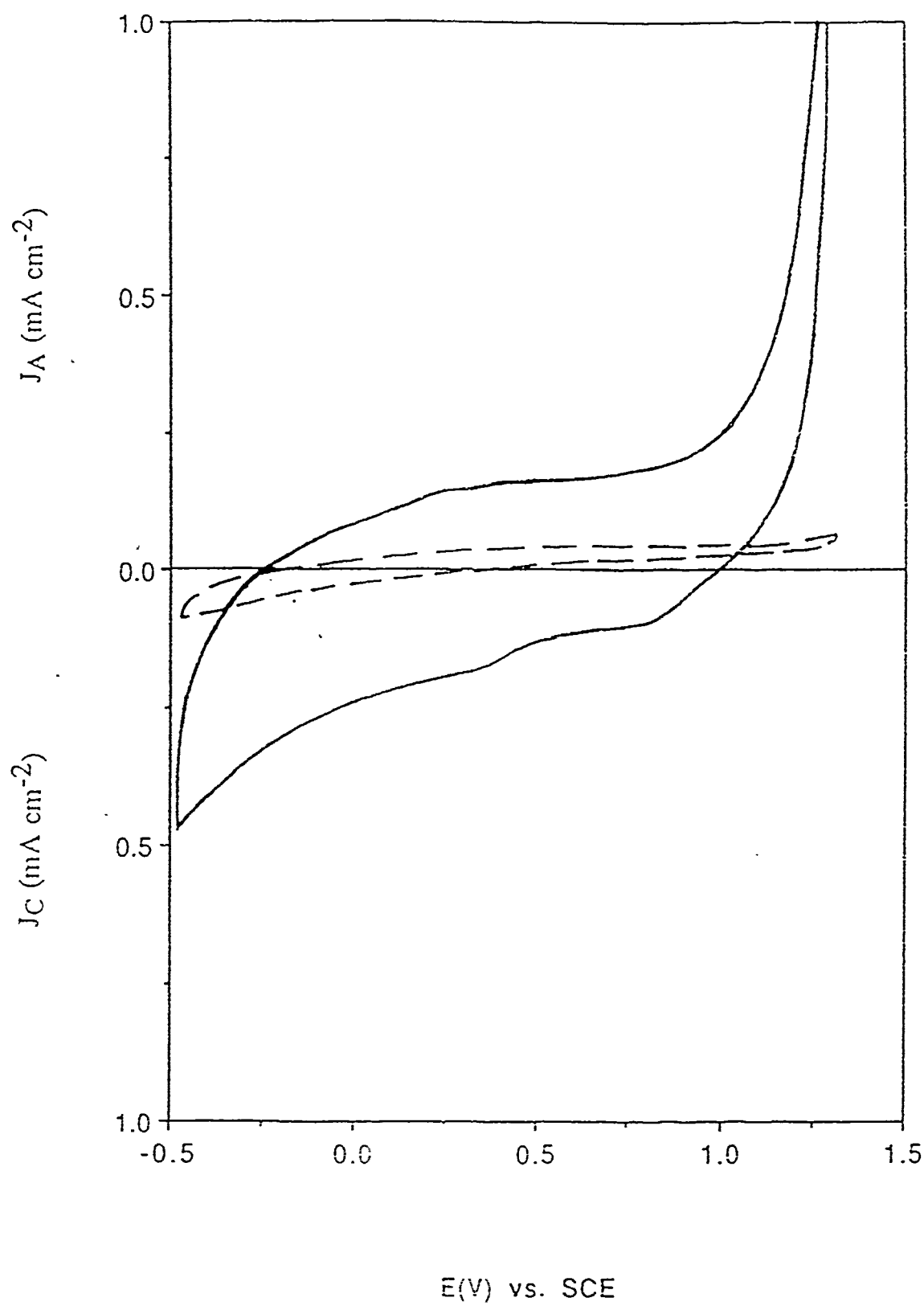
Fig. 2
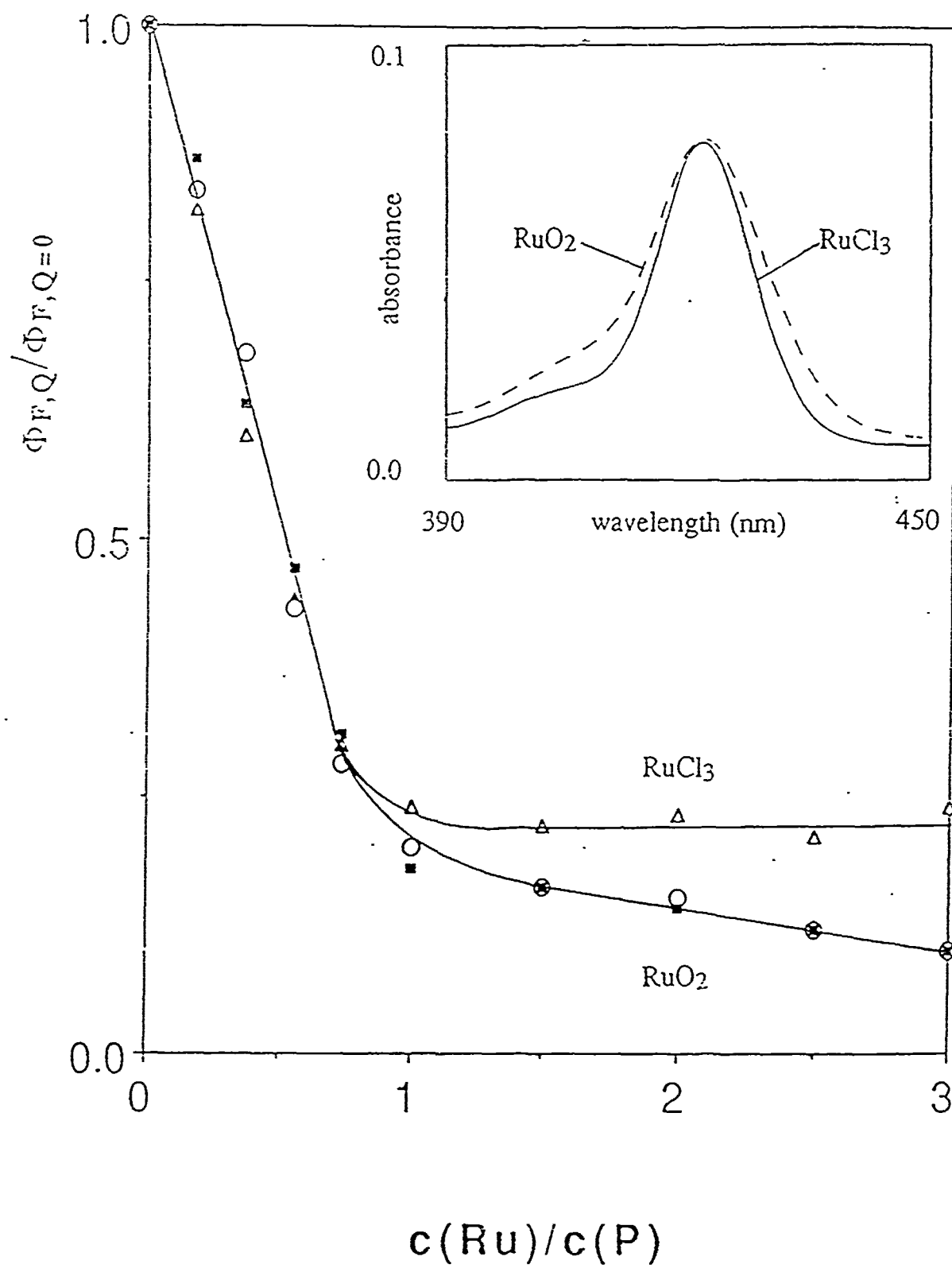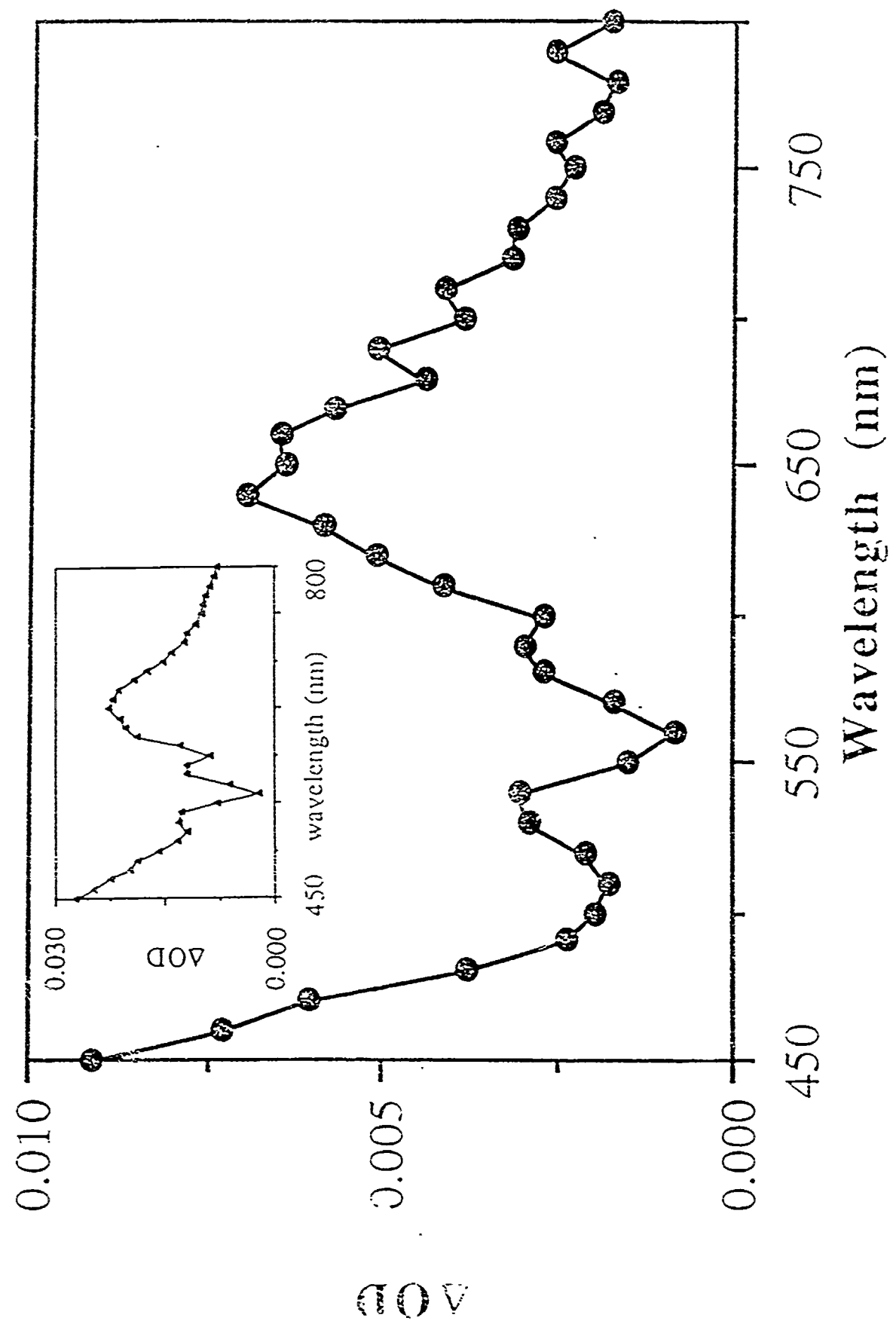
Fig. 3

(24) Redox Catalysis using RuO_2 Dispersions and the Electrochemical Model:

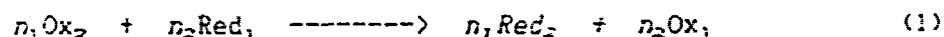the Oxidation of Water by $Ru(bpy)_3^{3+}$ ions

Andrew Mills and Tom Russell,

Department of Chemistry, University College of Swansea, Singleton Park,

Swansea, SA2 8PP, UK.

Abstract

The kinetics of the oxidation of water by $Ru(bpy)_3^{3+}$ ions, mediated by $RuO_2.yH_2O^*$, are studied. In all cases the rate was found to be independant of $[Ru(bpy)_3^{2+}]$. Over the pH range 3-5 the initial rate is largely independent of pH and the kinetics of $Ru(bpy)_3^{3+}$ reduction are first order with respect to $[Ru(bpy)_3^{3+}]$ and $[RuO_2.yH_2O^*]$, with an activation energy of 20 ± 1 kJ mol^{-1}. At pH values below 3 the initial rate of reaction decreases with decreasing pH and the kinetics appear to be 1.6 order with respect to $[Ru(bpy)_3^{3+}]$ although first order with respect to $[RuO_2.yH_2O^*]$ and with an activation energy of $34 \pm .$ kJ mol^{-1}. An electrochemical model of redox catalysis, in which the reduction of $Ru(bpy)_3^{3+}$ and the concomitant oxidation of water to O_2 are considered as two electrochemical 1.reversible processes coupled together *via* the redox catalyst, is used to interpret the results.
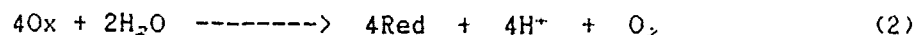
Introduction

There are many redox reactions of the type:

$$n_1 Ox_2 + n_2 Red_1 \longrightarrow n_1 Red_2 + n_2 Ox_1 \qquad (1)$$

which, although thermodynamically feasible. do not proceed at a discernible rate under ambient conditions [1]. For example, in the oxidation of water

- 1 -

to oxygen by a suitably strong oxidising agent, Ox, *i.e.*

$$4Ox + 2H_2O \text{ --------> } 4Red + 4H^+ + O_2 \qquad (2)$$

(where $Ox = Ru(bpy)_3^{3+}$, MnO_4^- or Ce^{IV} ions for example) reaction (2) does not usually proceed. Lack of reaction in (2) has the advantage that aqueous acidic solutions of the oxidants named above are stable over long periods of time and, in the case of MnO_4^- and Ce^{IV} ions, this attractive feature, amongst others, has led to their widespread use in aqueous redox analytical chemistry [2].

In other situations, however, the lack of reaction in a thermodynamically feasible reaction can be an undesirable feature. For example, a great deal of solar energy research has been directed towards the development of an efficient photosystem for the cleavage of water [3]. In such a system reaction (2) must occur at some stage using an oxidising agent, *i.e.* Ox, which has been photogenerated directly or indirectly. Thus, the recognised improbability of reaction (2) occuring in homogeneous solution for most oxidants poses a major problem to the development of an overall water-splitting photochemical system [4,5].

It is possible to facilitate many of the redox reactions described by reaction (1) through the use of a redox catalyst [1,6]. Research carried out by our group has shown that reaction (2), with $Ox = Ce^{IV}$ ions, is mediated by a partially dehydrated form of ruthenium dioxide hydrate ($\%H_2O$ *ca.* 10%), which we have called 'thermally activated ruthenium dioxide hydrate', or $RuO_2.yH_2O^*$ for short [7]. $RuO_2.yH_2O^*$ is prepared by annealing highly hydrated ruthenium dioxide hydrate (the usual form of this oxide hydrate available commercially; $\%H_2O \geqslant 24\%$) in air (or nitrogen for that matter) for 5h at 144°C.

The results of a detailed study of the kinetics of reaction (2),

- 2 -

mediated by $RuO_2 \cdot yH_2O^*$ with $Ox = Ce^{IV}$ ions, were interpreted using an electrochemical model in which the redox catalyst particles were considered to act as microelectrodes mediating electron transfer between a Nernstian reduction reaction ($Ce^{IV} \longrightarrow Ce^{III}$) and an irreversible oxidation reaction ($H_2O \longrightarrow 2H^+ + \frac{1}{2}O_2$) [8].

One of the most popular photosensitisers todate used in solar energy to chemical energy conversion systems, including both sacrificial and 'true' water-splitting photosystems in which O_2 is evolved, is $Ru(bpy)_3^{2+}$ and simple derivatives thereof [9]. In its use as a photosensitiser for water splitting invariably the oxidised form of $Ru(bpy)_3^{2+}$, i.e. $Ru(bpy)_3^{3+}$, is the species Ox in reaction (2) and the O_2 catalyst is either heterogeneous, such as RuO_2 or IrO_2, or homogeneous, such as $Co(II)$ ions or certain Ru oxo-bridged dimers.

Despite the widespread use of $Ru(bpy)_3^{3+}$ as the oxidant in the redox-catalysed reaction (2), there have been few studies of the kinetics of this reaction. In this paper we report the results of a detailed study of the kinetics of reaction (2), where $Ox = Ru(bpy)_3^{3+}$, mediated by $RuO_2 \cdot yH_2O^*$.

Experimental

Materials

The oxygen catalyst, $RuO_2 \cdot yH_2O^*$, was prepared from highly hydrated ruthenium dioxide hydrate obtained from Johnson Matthey. The $Ru(bpy)_2^{3+}$ was purchased as its hydrated chloride salt from Strem. All other chemicals were obtained from BDH in AnalaR form. All water used in the preparation of solutions was doubly distilled and deionised.

III - 79

Methods

The experimental system used to monitor the reduction of the oxidant, Ox, and concomitant evolution of O_2, as a function of time is illustrated in fig. 1. The reaction vessel comprised a thermostated quartz cell (30 ± 0.05°C) with an oxygen membrane polarographic detector (O_2-MPD) incorporated into its base. A potentiostat was used to polarise the Pt working electrode of the O_2-MPD at −0.8 V *vs.* the Ag/AgCl counter electrode. Under these conditions the current which flows between the two electrodes is proportional to the concentration of dissolved oxygen in the liquid phase in the reaction vessel. The potentiostat converts this current into a voltage which is then monitored continuously *via* an x/t chart recorder (Servogore model 210).

Each Ru(bpy)$_2$$^{3+}$ stock solution used (typically 2.31×10^{-2} mol dm^{-3}, with suffcient H_2SO_4 so that the solution pH was 0.45) was made up from a Ru(bpy)$_2$$^{2+}$ solution of the same concentration, using PbO_2 as the oxidant. PbO_2-free aliquats of the stock solution, for use in the kinetic study, were obtained through use of a syringe fitted with an in-line 0.2 μm membrane filter (Schleicher and Schüell). The kinetics of Ru(bpy)$_2$$^{3+}$ reduction were monitored spectrophotometrically *via* the disappearance of its absorption band at 675 nm (ε(Ru(bpy)$_3$$^{3+}$)$_{675}$ = 440 mol^{-1} dm^3 cm^{-1}). The concentration of catalyst dispersion was, typically, 77 μg cm^{-3} made up in an (acetic acid + acetate) buffer concentration with an overall concentration of 0.025 mol dm^{-3}, the desired pH of the final solution, *i.e.* after mixing with the injected Ru(bpy)$_3$$^{3+}$ solution, determined the ratio of acetic acid to acetate in the initial catalyst dispersion. The observed kinetics of Ru(bpy)$_3$$^{3+}$ reduction, with or without catalyst, were largely the same if no buffer was present and the solution pH was adjusted to the

- 4 -

desired pH using strong solutions of H_2SO_4 or NaOH.

In a typical experiment 65 cm^3 of a catalyst dispersion were placed in the reaction vessel and nitrogen purged for 20 min. The kinetic run was started by injecting, through the rubber septum, a small volume (typically 1.0 cm^3) of the oxidant stock solution using a gas-tight syringe. Spectrophotometric monitoring of the oxidant concentration was achieved using using the optical system illustrated in fig. 1, *i.e.* light source, monochromator, amplifier and microcomputer; cell path length 3.2 cm. The absorbance *vs.* time profile was recorded, stored and subsequently analysed using an Achimedes BBC microcomputer. The concentration of dissolved O_2 in the reaction vessel was monitored as a function of time using the O_2-MPD.

The electrochemical model of redox catalysis

In the catalysis of many redox reactions of the type identified by reaction (1), it has been found that the observed kinetics are readily rationalised in terms of an electrochemical model of redox catalysis in which the redox catalyst acts simply to provide a medium through which electron transfer from the one redox couple to the other can take place [1,5,6]. Provided the two redox couples act independently of each other, the electrochemical model of redox catalysis allows for the prediction of the kinetics of reaction (1) from the current-voltage curves for the two contributing couples (the Wagner-Traud Additivity Principle).

In the electrochemical model, at any time t during the course of catalysis the redox catalyst adopts a mixture potential, $E_{mix, t}$, at which the cathodic current, $i_{c, t}$, due to the reduction of Ox_2 is exactly balanced by the anodic current, $i_{a, t}$, due to the oxidation of Red_1. Although the net current is zero, the numerical magnitude of each component current is

$III-81$

ne same and is called the mixture current, $i_{mix, t}$, where

$$i_{mix, t} = i_{a, t} = -i_{c, t} \tag{3}$$

In our study of the catalysis of the redox reaction (2), with $Ox_2 =$ Ru(bpy)$_3^{3+}$, by particles of $RuO_2 \cdot yH_2O^*$ dispersed in solution, the particles can be envisaged as acting as a collection of micro-electrodes.

The current-voltage curve for the oxidation of Red$_1$ to Ox$_1$, where Red$_1$ = H_2O and Ox$_1$ = O_2, is, for most materials including RuO_2, adequately described by a Tafel-type equation, i.e.

$$i_a = i_{o1} \exp(\alpha_1 F\eta_1 / RT) \tag{4}$$

where α_1 is the transfer coefficient and η_1 is the overpotential. The overpotential is given by

$$\eta_1 = E_{mix} - E_1 \tag{5}$$

where E_1 is the equilibrium potential for the Ox$_1$/Red$_1$ couple.

The stoichiometric electrode process of any given redox couple can be written as.

$$v_a S_a + v_b S_b + \ldots + v_j S_j + ne^- = 0 \tag{6}$$

where S_j represents the formula of species j and where the stoichiometric coefficients, v_j are positive for oxidants and negative for reductants. In the presence of an excess of inert supporting electrolyte the corresponding Nernst equation for the equilibrium potential, E, is then:

$$E = E^\circ + (RT/nF)\Sigma v_j \ln(c_j) \tag{7}$$

In the concomitant reduction of Ox$_2$ to Red$_2$ it is possible that the reduction is irreversible for the case when $Ox_2 = $ Ru(bpy)$_3^{3+}$ and, as a result, the current-voltage curve of interest is given by a Tafel-type expression.

$$i_c = i_{o2} \exp(\gamma_2 F\eta_2 / RT) \tag{8}$$

The exchange current densities, i_{o1} and i_{o2}, are given by the following two

III - 82

respective expressions:

$$\ln(i_{o1}) = \ln(i_{oo1}) + (\theta_1 + \alpha_1 v_1/n_1)\ln[Red_1] \tag{9}$$

$$\ln(i_{o2}) = \ln(i_{oo2}) + (\theta_2 - \alpha_2 v_2/n_2)\ln[Red_2] \tag{10}$$

where θ_1 and θ_2 are, respectively, the electrochemical reaction orders of Red_1 and Ox_2 in the anodic and cathodic processes occuring on the surface of the redox catalyst. The terms i_{oo1} and i_{oo2} are the standard exchange current densities for the couples Ox_1/Red_1 and Ox_2/Red_2, respectively.

Fig. 2(a) provides a schematic illustration of the current-voltage curves when the two couples in reaction (1) are highly irreversible and coupled together by a redox catalyst. Spiro has considered this particular electrochemical model of redox catalysis [10] and shown that the mixture current at any time t during the reaction will be given by:

$$i_{mix,t} = i_{oo1}{}^{r_2} \cdot i_{oo2}{}^{r_1} \cdot [Red_1]^{\theta_1 r_2} \cdot [Ox_2]^{\theta_2 r_1} \cdot \exp\{\alpha_2 r_1 F(E_2{}^\circ - E_1{}^\circ)/RT\} \tag{11}$$

where r_1 and r_2 are as follows:

$$r_1 = \alpha_1/(\alpha_1 + \alpha_2); \qquad r_2 = \alpha_2/(\alpha_1 + \alpha_2) \tag{12}$$

In the case of reaction (2), eqn (11) reduces to:

$$i_{mix,t} = i_{oo1}{}^{r_2} \cdot i_{oo2}{}^{r_1} \cdot [Ox_2]^{\theta_2 r_1} \cdot \exp\{\alpha_2 r_1 F(E_2{}^\circ - E_1{}^\circ)/RT\} \tag{13}$$

From eqn (13) it can be seen that one of the interesting features of this particular electrochemical model of a redox catalysed reaction is that when the mixture current lies in the Tafel regions of both couples current-voltage curves, the concentrations of products play no role in the forward kinetics. Such kinetics are very different to those observed for reaction (2) mediated by $RuO_2 \cdot yH_2O^*$ using Ce^{IV} ions as the oxidant in 0.5 mol dm^{-3} H_2SO_4. In this latter case Ce^{III} ions had a marked inhibitory effect on the rate of Ce^{IV} reduction and, as noted earlier, the kinetics were interpreted in terms of an electrochemical model in which the current-voltage curve for the Ce^{IV}/Ce^{III} couple was that for a Nernstian reaction

- 7 -

$\overline{III} - \cancel{f}3$

and the current-voltage curve for the oxidation of water obeyed a Tafel-type equation.

If the overpotential for the Ox_2/Red_2 couple is made sufficiently large the current-voltage curve will level out and the cathodic current arising from the reduction of Ox_2 at the microelectrode particles will attain a limiting, diffusion-controlled value, $i_{c,1}$, where:

$$i_{mix} = -i_{c,1} = n_2 FD[Ox_2]/(v_2 \delta) \tag{14}$$

where D is the trace diffusion constant of Ox_2 in the reaction medium and δ is the thickness of the diffusion layer; the latter parameter depends upon the hydrodynamic conditions within the reaction cell and, in our work, these are fixed through the use of a constant stirring rate.   Fig. 2(b) provides a schematic illustration of the current-voltage curves for this particular example of redox catalysis.

For any kinetic run a $[Ox_2]$ vs. time decay trace is generated and the rate of reduction of Ox_2 at any time t is r(t), where $r(t) = -dOx_2/dt$, and this term is related directly to $i_{mix,t}$ by the expression:

$$r(t) = i_{mix,t}/F \tag{15}$$

In the electrochemical model of redox catalysis, if the kinetics of reaction (1), or (2), are controlled by the rate of diffusion of the oxidant Ox_2 to the surface of the redox catalyst then the rate at any time t will be given by:

$$r(t) = k_1[Ox_2] \tag{16}$$

where k_1 is the first order rate constant.   If the kinetics of Ox_2 reduction are diffusion-controlled the gradient of a first order plot of the data from a kinetic run, i.e. $\ln[Ox_2]$ vs. time, is $= -k_1$, and equivalent to $n_2 FD/(v_2 \delta)$.

- 8 -

II - 84

Results

The $Ru(bpy)_3^{3+}/Ru(bpy)_3^{2+}$ couple has a formal redox potential of 1.26 V $vs.$
NHE in aqueous solution and thus the oxidation of water by $Ru(bpy)_3^{3+}$

$$4Ru(bpy)_3^{3+} + 2H_2O \text{--------}> 4Ru(bpy)_3^{2+} + 4H^+ + O_2 \qquad (17)$$
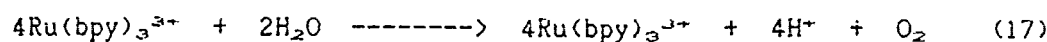
is thermodynamically feasible even at pH 0 and becomes increasingly
feasible as the pH is increased. However, in practice, aqueous solutions
of $Ru(bpy)_3^{3+}$ at pH 0 to 1 are kinetically stable ($i.e.$ reaction (17) does
not proceed at a measurable rate) in the absence of a redox catalyst and
this allows for the preparation and handling of $Ru(bpy)_3^{3+}$ stock solutions,
such as the ones used in our kinetic study.

In a first set of experiments, the initial rate of $Ru(bpy)_3^{3+}$
reduction ($[Ru(bpy)_3^{3+}]_{t=0} = 3.55 \times 10^{-4}$ mol dm^{-3}), in the absence and
presence of $RuO_2 \cdot yH_2O^+$ (77 μg cm^{-3}), was monitored as a function of pH
(varied by altering the acetic acid/acetate ratio, with [acetic acid +
acetate] = 0.025 mol dm^{-3}) over the range pH 0.5 to pH $ca.$ 5.5; the results
of this work are illustrated in fig. 3(a) by curves (i) and (ii),
respectively.

In a second set of experiments, using identical reaction conditions as
above and in the presence of $RuO_2 \cdot yH_2O^*$, the overall %O_2 yields ($i.e.$ at
the end of reaction) were determined as a function of pH and the results
are illustrated in fig. 3(b). In this latter work, in all cases the
kinetics of O_2 generation were that of $Ru(bpy)_3^{3+}$ reduction. It was
further observed that <u>at all pH's the kinetics of $Ru(bpy)_3^{3+}$ reduction were</u>
<u>unaffected by the initial concentration of $Ru(bpy)_3^{2+}$ present even when</u>
<u>using $[Ru(bpy)_3^{2+}]$'s upto ten times that of the initial $[Ru(bpy)_3^{3+}]$.</u>

From the data illustrated in fig. 3, curve (b), it appears that at pH
values from $ca.$ 3 to 5 the kinetics of reaction (17) are largely pH

- 9 -

independent and rapid; above pH 5 the homogeneous reduction of $Ru(bpy)_3^{3+}$ to $Ru(bpy)_3^{2+}$, *via* the hydroxide- or water-initiated oxidative degradation of a small fraction of the $Ru(bpy)_3^{3+}$ present, becomes increasingly important with increasing pH. From the same results it also appears that as the pH of the reaction mixture is decreased from pH 3 to pH 0.5, the kinetics of reaction (17) are slowed down markedly, even though the $\%O_2$ yield remains quite high (see fig. 3(b)). As a result of this observation, the kinetics of reaction (17), mediated by $RuO_2 . yH_2O^*$, were studied in detail at two different pH's, *i.e.* pH 3.9 and pH 2, chosen to correspond to the apparent two different types of kinetics.

Fig. 4(a) illustrates the change in absorbance spectrum due to $Ru(bpy)_3^{3+}$ (3.55×10^{-4} mol dm^{-3}) as a function of time for a typical kinetic run carried out at pH 3.9 after mixing with a $RuO_2 . yH_2O^*$ catalyst dispersion (final concentration = 77 mg cm^{-3}). For the same kinetic run, fig. 4(b) illustrates the variation of absorbance due to $Ru(bpy)_3^{3+}$ (λ = 675 nm, $\varepsilon(Ru(bpy)_3^{3+})_{675}$ = 440 mol^{-1} $dm^3)$ cm^{-1}) and overall $\%O_2$ yield as a function of time. A first order analaysis of the absorbance-time data contained in fig. 4(b) gives a good straight line, illustrated in fig. 4(c), indicating that the kinetics of reaction (17) are first-order with respect to $[Ru(bpy)_3^{3+}]$ at pH 3.9.

Using a pH of 3.9, an initial $[Ru(bpy)_3^{3+}]$ = 3.55×10^{-4} mol dm^{-3} and a reaction temperature of 30°C the kinetics of reaction (17) mediated by $RuO_2 . yH_2O^*$ were studied as a function of $[RuO_2 . xH_2O]$ over the range 0 – 154 μg cm^{-3}. In all cases the kinetics were found to be good first-order (*i.e.* r > 0.9990, over at least 2 half-lives); the resultant plot of the first order rate constant k_1 *vs.* $[RuO_2 . xH_2O]$ is illustrated in fig. 5.

Under the same conditions of pH and initial $[Ru(bpy)_3^{3+}]$, the

III - 86

variation of k, for reaction (17) mediated by $RuO_2 \cdot yH_2O^*$ was determined as a function of temperature over the range 5°C to 50°C and fig. 6 illustrates the subsequent Arrhenius plot of the results, from the gradient of which an activation energy of 20 ± 1 kJ mol^{-1} was calculated.

When reaction (17) was carried out at pH 2, the kinetics of $Ru(bpy)_3^{3+}$ ($[Ru(bpy)_3^{3+}]$ at $t=0 = 3.55 \times 10^{-4}$ mol dm^{-3}) were found not only to be slower but also more complex than those found at pH 3.9. From the derivative of a typical $Ru(bpy)_3^{3+}$ absorbance $vs.$ time profile at pH 2 it appears that the rate of $Ru(bpy)_3^{3+}$ reduction depends directly upon $[Ru(bpy)_3^{3+}]^\gamma$, where γ $ca.$ 1.6. Thus, although the reduction of $Ru(bpy)_3^{3+}$ via reaction (17) at pH 2 gives quite a good fit to second-order kinetics, a better fit is obtained using a γ value in of $ca.$ 1.6. In two subsequent pieces of work the kinetics of $Ru(bpy)_3^{3+}$ reduction in reaction (17), mediated by $RuO_2 \cdot yH_2O^*$, at pH 2 were studied both as a function of $[PuO_2 \cdot yH_2O^*]$ (0 to 300 µg cm^{-3}) and temperature (5 to 60°C), respectively; the results of the analysis of the results of this work are discussed in detail in the Discussion section.

Discussion

The few reports [11-14] which provide some description of the kinetics of reaction (17) mediated by a heterogeneous catalyst such as RuO_2, are listed in table 1. The results illustrated in fig. 3(a) for the pH range 0.5 - 5.5 and in the absence of a O_2 catalyst, appear in broad agreement with the findings of others [14,15], $i.e.$ (i) no O_2 evolution over the entire pH range studied and (ii) above pH 5, $Ru(bpy)_3^{2+}$ reduction increasing rapidly with increasing pH (due to the previously mentioned homogeneous reduction of $Ru(bpy)_3^{3+}$ to $Ru(bpy)_3^{2+}$, via a hydroxide- or water-initiated oxidative

degradation of a small fraction of the $Ru(bpy)_3^{3+}$ present.

The observed variation in $\%O_2$ yield, arising from reaction (17) using $RuO_2 \cdot yH_2O^+$ as the redox catalyst, as a function of pH is illustrated in fig. 3(b) and shows that although the $\%O_2$ yield remains high (i.e. > 50%) over the pH range studied, it peaks at ca. pH 4. The decrease in $\%O_2$ yield with both increasing and decreasing pH from pH 4 is most likely due to competing, possibly redox-catalysed, acid and base catalysed oxidative degradation reactions involving $Ru(bpy)_3^{3+}$. The results of this work are supported by the findings of others [16-18].

The reports on the variation in the kinetics of reaction (1) mediated by a heterogeneous O_2 catalyst as a function of pH are disparate. For example, Minero and his co-workers, using an RuO_2 colloid, supported by polybrene, report that the kinetics are 'not simply first order'; interestlingly, however, their reported trend in initial rate as a function of pH is not dissimilar to that illustrated in fig. 3(a), i.e. decreasing rate with decreasing pH below pH 3, and, approximately, pH independent kinetics over the pH range 3-5. However, in the same paper, Minero et al. also indicate that the kinetics of reaction (17) mediated by a TiO_2/RuO_2 colloid are simple first order and pH independent over the range pH 1 to pH 6 [11]. A similar trend, with much lower rates (70-80 fold less) was also observed by these workers in the absence of a redox catalyst [11]. Juris and Moggi [14] also report a parallel trend in k_1 vs. pH with, and without, an RuO_2 catalyst; however, in this case k_1 appears to increase nearly exponentially with increasing pH over the pH range 0.5 to 6, and the addition of the the redox catalyst does not have a marked effect on the rate (ca. 2 fold increase).

It is worth noting at this stage that in none of the kinetic studies

III-84

referenced above or in table 1 were the kinetics and overall %O_2 yields also monitored as a function of pH;, *i.e.* O_2 evolution was always assumed to proceed with the same kinetics as $Ru(bpy)_3^{3+}$ reduction and with an overall stoichiometric yield. However, on occasions this assumption can prove to be invalid, as we have demonstrated recently from the results of a study of the 'apparent' catalysis of reaction (2), with Ox = Ce^{IV}, using the RuO_2/polybrene colloid of Minero *et al.* [11]. In a previous paper Minero *et al.* had reported the results of a similar kinetic study of Ce^{IV} reduction in which stoichiometric O_2 evolution was assumed [11]. From the results of our work, however, carried out under the same reaction conditions as used by Minero *et al.* [11] we were unable to observe any O_2 evolution and it appeared that the kinetics of Ce^{IV} reduction were those for the oxidation of the polybrene support and not water.

Thus, although $Ru(bpy)_3^{3+}$ is not as strong an oxidising agent as Ce^{IV} ions (and, therefore, less likely to oxidise the support, catalyst or any adventitious impurities) the kinetics of $Ru(bpy)_3^{3+}$ reduction should not automatically be assumed to be due to reaction (17). For example, Shafirovich and Strelets have studied reaction (17) as a function of pH, using an unsupported RuO_2 colloid as the redox catalyst and found that the %O_2 yield was only 16% at pH 1.8 and decreased to 3% at pH 1.2 [18]. In addition, over this same pH range, they found that the amount of CO_2 liberated due to the 'deep' disintegration of a small fraction of $Ru(bpy)_3^{3+}$ increased markedly with decreasing pH. These workers also noted that $Ru(bpy)_3^{3+}$ was able to oxidise some, albeit only *ca.* 1%, of the RuO_2 to RuO_4 even at pH values up to pH 2.8. Although, in our work no evidence was found for this latter reaction this may simply reflect the greater efficacy of $RuO_2 \cdot yH_2O^*$ as a O_2 catalyst.

From the results illustrated in fig. 3 and our previous general
observation that at all pH's tested the kinetics of O_2 generation appeared
to parallel those of $Ru(bpy)_3^{3+}$ reduction it appears that $RuO_2 . yH_2O^*$ is
able to mediate reaction (17). The general shape of the variation in
initial rate of $Ru(bpy)_3^{3+}$ reduction *vs.* pH, with redox catalyst present,
illustrated in fig. 3 (a), can be readily interpreted using the specific
electrochemical model described earlier. In this model of redox catalysis
the initial rate of reduction of $Ru(bpy)_3^{2+}$ will reach a limiting,
diffusion controlled value when the two current-voltage curves are well
separated. The formal redox potential of the O_2/H_2O couple decreases with
increasing pH, *i. e.* $E^\circ = (1.23 - 0.059 \times pH)$ V *vs.* NHE and, since the formal
potential of the $Ru(bpy)_3^{3+}/Ru(bpy)_3^{2+}$ couple is pH independent, it can be
seen that as the solution pH is increased so will the separation in the
equilibrium potentials for the two redox couples involved increase, and
eventually diffusion-controlled kinetics will be achieved. Given the
electrochemical model, from the results illustrated in fig. 3(a) it appears
that over the pH range 3-5 the kinetics are diffusion-controlled and, as a
result, the rate is directly related to i_{max}, where i_{max} is given by eqn
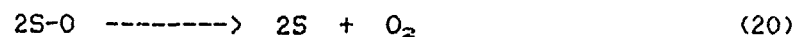(14).

It also appears from the results illustrated in fig. 3(a) that at pH
values below pH 3, the separation in equilibrium potentials for the two
redox couples (which decreases with decreasing pH) is not sufficiently
large to render the kinetics of $Ru(bpy)_3^{3+}$ diffusion controlled. It is
suggested that at pH values << pH 3, such as pH 2, the rate of $Ru(bpy)_3^{3+}$
reduction at any time t during the course of the reaction is related
directly to $i_{max, t}$, where $i_{max, t}$ is given by eqn (13). In order to test
these ideas further the kinetics of reaction (17) were studied at pH 3.9

- 14 -

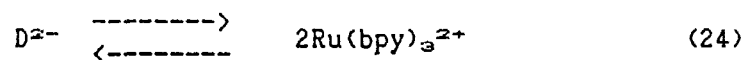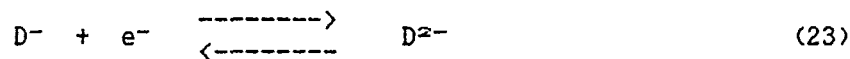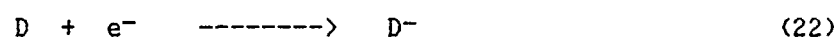and 2, corresponding to the two different types of kinetics predicted by eqns (14) and (13), respectively.
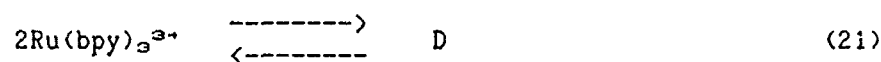
The results of the kinetic study of reaction (17) mediated by $RuO_2 \cdot yH_2O^*$ at pH 3.9 are illustrated in figs. 4-6. At this pH the kinetics of $Ru(bpy)_3^{3+}$ reduction are first order with respect to $[Ru(bpy)_3^{3+}]$ over 2 half lives, as illustrated by straight line first-order plot in fig 4(c). This finding is as expected from eqn (14) of the electrochemical model, which also predicts that k_1 should be proportional to $[RuO_2 \cdot yH_2O^*]$, since $i_{m.1}$ will depend directly upon electrode area and which depends directly upon $[RuO_2 \cdot yH_2O^*]$. The direct dependence of k_1 upon $[RuO_2 \cdot yH_2O^*]$ is confirmed by the results of the study illustrated in fig. 5. From the results of the Arrhenius plot ilustrated in fig. 6 an activation energy of 20 ± 1 kJ mol^{-1} was calculated which compares favourably with the value of 15-19 kJ mol^{-1} which is expected for a diffusion-controlled reaction [5]. Overall, from the results of the kinetic study of reaction (17) mediated by $RuO_2 \cdot yH_2O^*$ at pH 3.9 the reaction appears diffusion-controlled and well described by eqn (14) of the electrochemical model.

As noted earlier, the kinetics of reaction (17) mediated by $RuO_2 \cdot yH_2O^*$ at pH 2 are not first order but rather appear to depend directly upon $[Ru(bpy)_3^{3+}]^\gamma$, where $\gamma = 1.6$ (see the results illustrated in figs. 7(a) and (b)) . If at pH 2 eqn (13) of the electrochemical model is applicable then, from these initial findings it would appear that the term $\theta_{2.1} = 1.6$. From previous electrochemical studies of the oxidation of water using highly defective RuO_2 anodes it appears that the water oxidation occurs via the 'oxide' pathway, i.e.

$$S + H_2O \longrightarrow S-OH + H^+ + e^- \qquad (18)$$

$$2S-OH \longrightarrow S-O + S + H_2O \qquad (19)$$

- 15 -

$$2S-O \ \text{---------} > \ 2S \ + \ O_2 \qquad (20)$$

where S is the active site, with reaction (19) as the rate determining step, i.e. $\alpha_1 = 2$. In our study of the kinetics of reaction (2) with Ox = Ce^{IV}, mediated by $RuO_2 \cdot yH_2O^*$ the same mechanism and rate determing step for water oxidation appeared applicable. Thus, it appears reasonable to assume that this is also the case for reaction (17) mediated by $RuO_2 \cdot yH_2O^*$ and, as a result, we can take $\alpha_1 = 2$ in eqn (12). It can be seen that the term $\theta_2 r_1$ will equal the desired value of 1.6 if $\alpha_2 = \frac{1}{2}$ and $\theta_2 = 2$. One scheme in which this would be the case is as follows:

$$2Ru(bpy)_3^{3+} \ \ \underset{<--------}{\overset{-------->}{}} \ \ D \qquad (21)$$

$$D \ + \ e^- \ \ \text{--------} > \ \ D^- \qquad (22)$$

$$D^- \ + \ e^- \ \ \underset{<--------}{\overset{-------->}{}} \ \ D^{2-} \qquad (23)$$

$$D^{2-} \ \ \underset{<--------}{\overset{-------->}{}} \ \ 2Ru(bpy)_3^{2+} \qquad (24)$$

with eqn (22) as the rate determining step. In this latter case the current-voltage curve would be given by:

$$i_c \ = \ Fk_{22}K_{21}[Ru(bpy)_3^{3+}]^2 \cdot \exp(-\beta FE_{mix}/RT) \qquad (25)$$

where k_{22} is the rate constant for the rate determining step, K_{21} is an equilibrium constant for reaction (21) and β = symmetry factor, which may be taken as = $\frac{1}{2}$.

In the above reaction scheme the electroactive species in the oxidation of water is a dimeric form of $Ru(bpy)_3^{3+}$. The formation of dimers in acid solution is not unknown in the chemistry of derivatives of $Ru(bpy)_3^{3+}$. Thus, Grätzel and his co-workers have found that thermolysis (at 80°C) or photolysis of a solution of RuL_3^{2+} (where L = 2,2'-bipyridyl-

- 16 -

5,5′-dicarboxylic acid) in 0.5 mol dm^{-3} H$_2$SO$_4$ in the presence of persulphate generates oxo-bridged dimers of the type L$_2$(H$_2$O)Ru^{III}-O-Ru^{III}(OH$_2$)L$_2$ which can act as homogeneous O$_2$ catalysts [19,20].

Dimerisation of Ru(bpy)$_3$$^{3+}$ does not appear to occur to any measurable extent in bulk solution under the experimental conditions of our work, since the Ru(bpy)$_3$$^{3+}$ solutions were found to exhibit no deviation from Beer's law. No evidence was found in the bulk solution for the formation of a permanent homogeneous O$_2$ catalyst; Ru(bpy)$_3$$^{2+}$ solutions arising from the catalysed decay of a Ru(bpy)$_3$$^{3+}$ solution were very stable at pH 2 when separated from the RuO$_2$.yH$_2$O* catalyst and then re-oxidised to Ru(bpy)$_3$$^{3+}$ with PbO$_2$.

An important feature of the kinetics at pH 2 which is also predicted by the electrochemical model is the independence of the rate upon [Ru(bpy)$_3$$^{2+}$]. In this respect the kinetics of reaction (17) mediated by RuO$_2$.yH$_2$O* are quite different to those reported by Sutin and his co-workers for the same reaction catalysed by aquocobalt (II) ions; in this latter case r(t) was found to depend not only upon [Ru(bpy)$_3$$^{3+}$]^2 and [Co(II)], but also [Ru(bpy)$_3$$^{2+}$]$^{-1}$ at low [Ru(bpy)$_3$$^{3+}$]/[Co(II)] ratios and low [Co(II)].

Since the kinetics of reaction (17) at pH 2 appear to depend upon [Ru(bpy)$_3$$^{3+}$]$^{1.6}$, a measure of the rate constant can be gleaned from the gradient, = $k'_{1.6}$, of a plot of A$^{-0.6}$ vs. time. From the electrochemical model, $i_{mix, t}$ is directly related to $i_{001}r^2$.$i_{002}r^1$.exp{$\alpha_2 r_1$F(E$_2$^{o} - E$_1$^{o})/RT} which in turn should be directly related to $k'_{1.6}$. Despite the complexity of the kinetics predicted by the electrochemical model via eqn (13), $i_{mix, t}$ will still depend directly upon the total electrode area and, therefore,

- 17 -

[$RuO_2 \cdot yH_2O^*$]. Thus, according to the electrochemical model, at pH 2 a plot of $k'_{1.6}$ vs. [$RuO_2 \cdot yH_2O^*$] should be a straight line and this prediction is confirmed by the results illustrated in fig. 8. From the gradient of the Arrhenius plot illustrated in fig. 9 an activation energy of 34 ± 1 kJ mol^{-1} for reaction (17), carried out at pH 2 and mediated by $RuO_2 \cdot yH_2O^*$, was calculated.

Conclusion

$RuO_2 \cdot yH_2O^*$ is able to mediate the oxidation of water by $Ru(bpy)_3^{3+}$ ions with high %O_2 yields, over a wide pH range. Over the pH range 3-5 the initial rate is largely independent of pH and the kinetics of $Ru(bpy)_3^{3+}$ reduction are first order with respect to [$Ru(bpy)_3^{3+}$] and [$RuO_2 \cdot yH_2O^*$] with an activation energy of 20 ± 1 kJ mol^{-1}. At pH values below 3 the initial rate of reaction decreases with decreasing pH and the kinetics appear to be 1.6 order with respect to [$Ru(bpy)_3^{3+}$] although first order with respect to [$RuO_2 \cdot yH_2O^*$] and with an activation energy of 34 ± 1 kJ mol^{-1}. An electrochemical model of redox catalysis, in which the reduction of $Ru(bpy)_3^{3+}$ and the concomitant oxidation of water to O_2 are considered as two electrochemical irreversible processes coupled together *via* the redox catalyst, can be used to rationalise the findings. Using this model to interepret the results at low pH (pH 2) it appears that electron transfer from a dimer of $Ru(bpy)_3^{3+}$ to the redox catalyst may be the rate determining step. Over the pH range 3 < pH < 5 the kinetics of $Ru(bpy)_3^{3+}$ reduction are diffusion-controlled. As predicted by the electrochemical model the kinetics of $Ru(bpy)_3^{3+}$ reduction were always found to be independent of [$Ru(bpy)_3^{2+}$]. The same electrochemical model can be used to interpret the kinetics of catalysis of reaction (2) with Ox = MnO_4^- [21],

Acknowledgements

III-95

References

(1)   Spiro, M.; Ravnö, A.B. <u>J. Chem. Soc.</u> 1965, 78-96.

(2)   Vogel, A.I. In <u>Quantitative Inorganic Analysis</u>; 3rd Edition;
Longmans: London, 1962; pp. 277-303.

(3)   <u>Energy Resources through Photochemistry and Catalysis</u>: Grätzel, M.,
Ed.; Academic Press, New York, 1983.

(4)   Mills, A. <u>Univ. Wales Sci. Tech. Rev.</u> 1988, <u>4</u>, 39-51.

(5)   Mills, A. <u>Chem. Soc. Rev.</u> 1989, <u>18</u>, 285-316.

(6)   Spiro, M. <u>Chem. Soc. Rev.</u> 1986, <u>15</u>, 141-165.

(7)   Mills, A.; Giddings, S.; Patel, I; Lawrence, C. <u>J. Chem. Soc. Faraday
Trans. 1</u> 1987, <u>83</u>, 2331-2345.

(8)   Mills, A.; McMurray, N. <u>J. Chem. Soc. Faraday Trans. 1</u> 1989, <u>85</u>,
2055-2070.

(9)   Kalyanasundaram, K. <u>Coord. Chem. Rev.</u>, 1982, <u>49</u>, 159-245.

(10)   Spiro, M. <u>J. Chem. Soc.</u> 1979, <u>79</u>, 1507-1512.

(11)   Minero, C.; Lorenzi, E.; Pramauro, E.; Pelizzetti, E. <u>Inorg. Chim.
Acta,</u> 1984, <u>91</u>, 301-305.

(12)   Humphry-Baker, R.; Lilie, J.; Gätzel, M. <u>J. Am. Chem. Soc.</u> 1982, <u>104</u>,
422-425.

(13)   Neumann-Spallart, M. <u>J. Chem. Soc. Faraday Trans. 1</u> 1985, <u>81</u>, 601-
608.

(14)   Juris, A; Moggi, L. <u>Int. J. Solar Energy</u> 1983, <u>1</u>, 273-284.

(15)   Ghosh, P.K.; Brunschwig, B.S.; Chou, C.; Creutz, C.; Sutin, N. <u>J. Am.
Chem. Soc.</u> 1984, <u>106</u>, 4772-4783.

(16)   Collin, J.P.; Lehn, J.M.; Ziessel, R. <u>Nouv. J. Chim.</u> 1982, <u>6</u>, 405-
410.

$\overline{III}$ - 96

-95

(17) Lehn, J. M.; Sauvage, SJ. P.; Ziessel, R. <u>Nouv. J. Chim.</u> 1980, <u>4</u>, 355–358.

(18) Shafirovich, V. Y.; Strelets, V. V. <u>Nouv. J. Chim.</u> 1982, <u>6</u>, 183–186.

(19) Desilvestro, J.; Duonghong, D.; Kleijn, M.; Grätzel, M. <u>Chimia</u> 1985, <u>39</u>, 102–103.

(20) Rotzinger, F. P., Munavalli, S.; Compte, P.; Hurst, J. K.; Grätzel, M.; Pern, F. J.; Frank, A. J. <u>J. Am. Chem. Soc.</u> 1987, <u>106</u>, 6619–6626.

(21) Mills, A.; Russell, T. <u>J. Chem. Soc., Dalton Trans.</u> submitted for publication.

III-97

(1) Schematic illustration of the experimental system used to monitor simultaneously the reduction of $Ru(bpy)_3^{3+}$ ions and the oxidation of water to O_2. The system comprised the following: (a) quartz-iodide light source, (b) monochromator (set at 675 nm), (c) photomultiplier, (d) amplifier, (e) Teflon-coated stirrer flea, (f) stirrer motor, (g) O_2-MPD base, (h) potentiostat and (i) syringe. The effective path length of the reaction vessel was 3.2 cm.

(2) Schematic illustrations of the relevant current-voltage curves for the redox couples Ox_1/Red_1 and Ox_2/Red_2 using the redox catalyst as the working electrode. In the case of redox catalysis of reaction (2) the redox catalyst adopts a mixture potential at which $i_a = -i_c = i_{mix}$. In (a) the mixture current lies in the Tafel region of both current-voltage curves, whereas in (b) i_{mix} lies in the diffusion-controlled region of the current-voltage curve for the Ox_2/Red_2 couple.

(3) (a) Initial rate of $Ru(bpy)_3^{3+}$ reduction vs. pH profile determined using: $[Ru(bpy)_3^{3+}]_{t=0} = 3.55 \times 10^{-4}$ mol dm^{-3}, $[RuO_2 \cdot yH_2O^*] = 77$ μg cm^{-3}, $([HOAc] + [AcO^-]) = 0.025$ mol dm^{-3} and $T = 30°C$.
(b) %O_2 yield vs. pH profile recorded using the same conditions as in (a).

(4)   (a) Changes the visible absorption spectrum due to $Ru(bpy)_3^{3+}$ as a function of time using the same reaction conditions as in fig. 3 (a) but with the pH = 3.9 and using a 1 cm quartz cell; the spectra were recorded (from top to bottom) at the following times after initiation of the reaction: 0, 18, 45, 80, 115, 300, 400 s.

(b) Plots of Absorbance (at 675 nm) due to $Ru(bpy)_3^{3+}$ and dissolved $[O_2]$ as a function of time using the same reaction conditions as in (a) ; $\varepsilon(Ru(bpy)_3^{3+})_{675}$ = 440 mol^{-1} dm^3 cm^{-1}. At t = 500 s the $\%O_2$ yield is $ca.$ 67%.

(c) First-order plot over 2½ half-lives of the absorbance-time data illustrated in (b); the results of a least squares analysis are as follows: gradient (m) = $-(1.04 \pm 0.02) \times 10^{-2}$ s^{-1}, intercept (c) = -0.77 ± 0.02 and correlation coefficient (r) = 0.9992.

(5)   Plot of k_1 $vs.$ $[RuO_2 \cdot yH_2O^*]$. The different values for k_1 were determined using the reaction condtions described for for fig. 4, but with $[RuO_2 \cdot yH_2O^*]$ varied over the range 0 −154 μg cm^{-3}; the results of a least squares analysis are as follows: m = $0..121 \pm 0.005$ s^{-1} mg^{-1} cm^3, c = $(1.2 \pm 0.4) \times 10^{-3}$ s^{-1} and r = 0.9958.

(6)   Arrhenius plot of $\ln(k_1)$ $vs.$ T^{-1}. The different values for k_1 were determined using the reaction condtions described for fig. 4, but with T varied over the range 5 − 50°C; the results of a least squares analysis are as follows: m = $-(2.4 \pm 0.2) \times 10^3$ K, c = 3.6 ±0.5 and r = 0.9949.
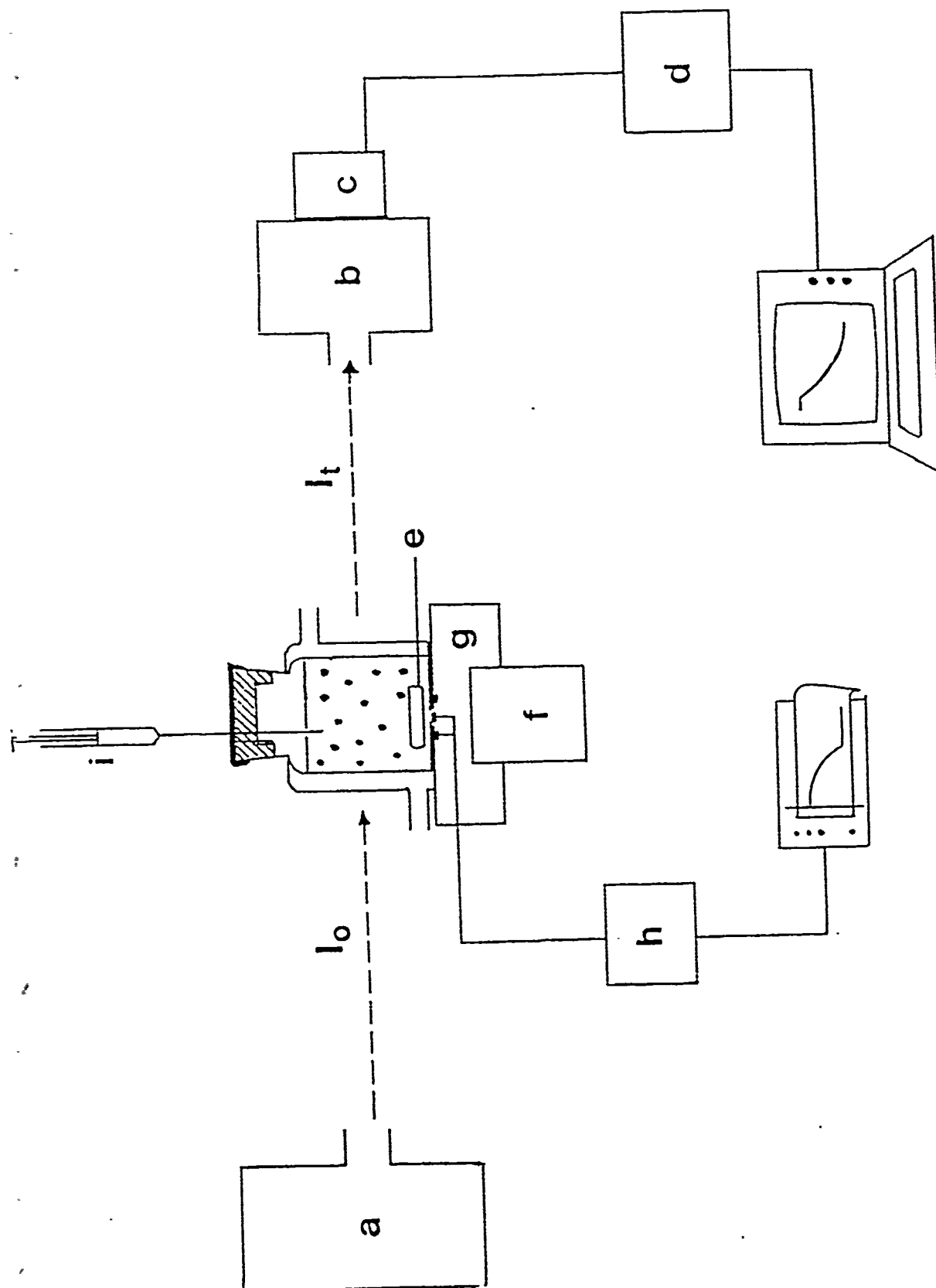
III-99

(7)   (a) Plots of Absorbance (at 675 nm) due to $Ru(bpy)_3^{2+}$ and dissolved

$[O_2]$ as a function of time using the same reaction conditions as in

fig. 3(a) but with at pH 2; $\epsilon(Ru(bpy)_3^{2+})_{675}$ = 440 mol^{-1} dm^3 cm^{-1}.

At t = 500 s the $\%O_2$ yield is ca. 55%

(b) 1.6-order plot (i.e. $(absorbance)^{-0.6}$ vs. t) over 2½ half-lives

of the absorbance-time data illustrated in (a);   the results of a

least squares analysis are as follows: m (= k'_1) = $(1.13 \pm 0.02) \times 10^{-2}$

$(absorbance\ units)^{0.6}$ s^{-1}, c = 1.50 ±0.02 $(absorbance\ units)^{0.6}$ and r

= 0.9989.

(8)   Plot of k'_1 vs. $[RuO_2. yH_2O^*]$.   The different values for k'_1 were

determined using the reaction condtions described for fig. 7, but with

$[RuO_2. yH_2O^*]$ varied over the range 0 –300 μg cm^{-3}; the results of a

least squares analysis are as follows: m = 1.27 ± 0.03 (absorbance

$units)^{0.6}$ s^{-1} mg^{-1} cm^3, c = $(1.7 \pm 0.7) \times 10^{-3}$ $(absorbance\ units)^{0.6}$ s^{-1}

and r = 0.9990.

(9)   Arrhenius plot of $\ln(k'_1)$ vs. T^{-1}.   The different values for k'_1 were

determined using the reaction condtions described for fig. 8, but

with T varied over the range 5 – 60°C; the results of a least squares

analysis are as follows: m = $-(4.1 \pm 0.2) \times 10^3$ K, c = 8.9 ± 0.7 and r

= 0.9964.

Table 1: Kinetic Studies of the Heterogeneous Redox-catalysed

Oxidation of H_2O by $Ru(bpy)_3^{3+}$

Method of $Ru(bpy)_3^{3+}$ Generation	Catalyst	Kinetic Technique*	pH range	Ref.
electrochemically	RuO_2/polybrene colloid	rapid mixing & stopped flow	1-12	11
electrochemically	RuO_2/TiO_2 colloid	rapid mixing & stopped flow	1-12	11
photochemically $(Ru(bpy)_3^{2+}/S_2O_8^{2-})$	RuO_2/TiO_2 colloid	μs flash photolysis	2-7	12
photochemically $(Ru(bpy)_3^{2+}/S_2O_8^{2-})$	RuO_2 and RuO_2/TiO_2 colloids	photochemical relaxation method	-	13
photochemically $(Ru(bpy)_3^{2+}/Co(NH_3)_5Cl^{2+})$	RuO_2 powder	rapid mixing	2-7	14

*: in all cases the $[Ru(bpy)_3^{3+}]$ was monitored spectrphotometrically.

- 25 -
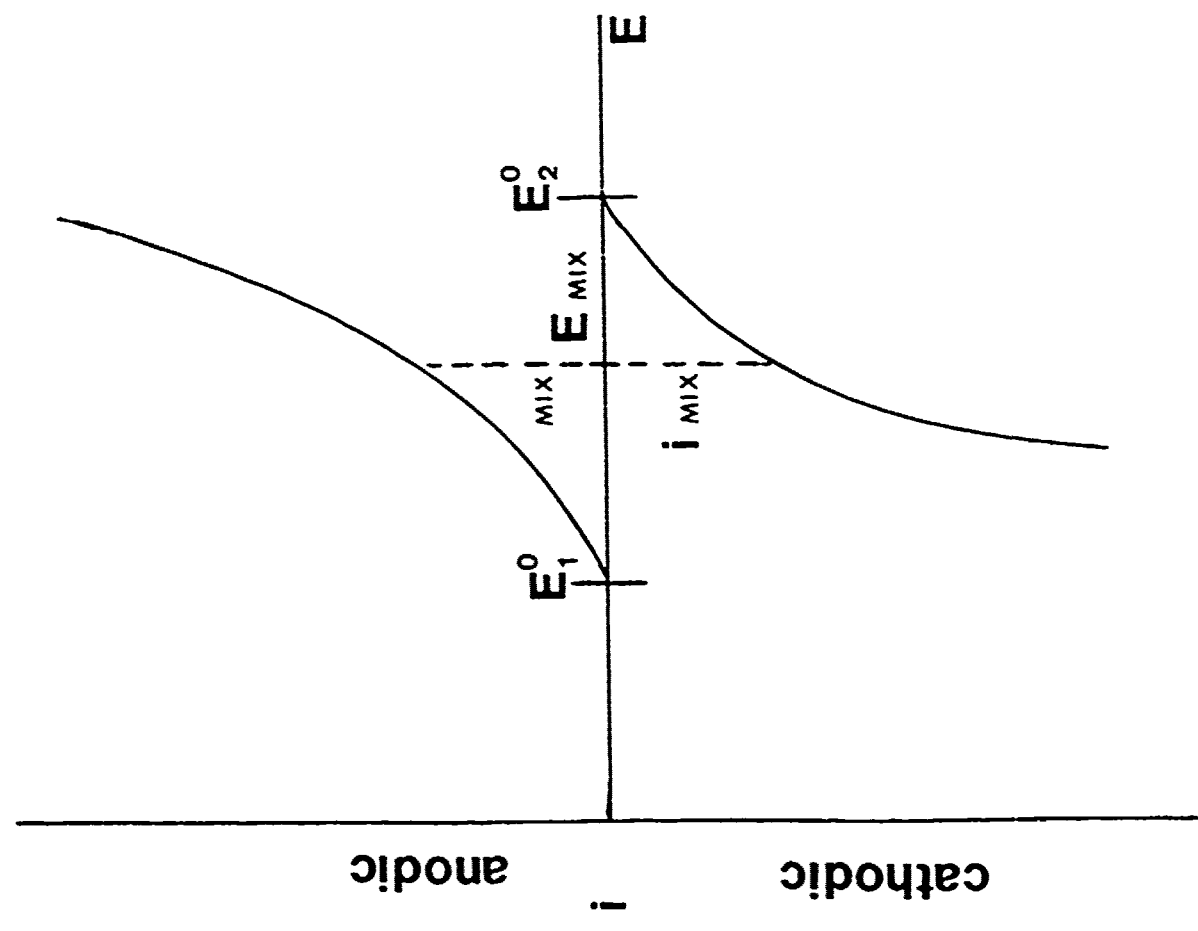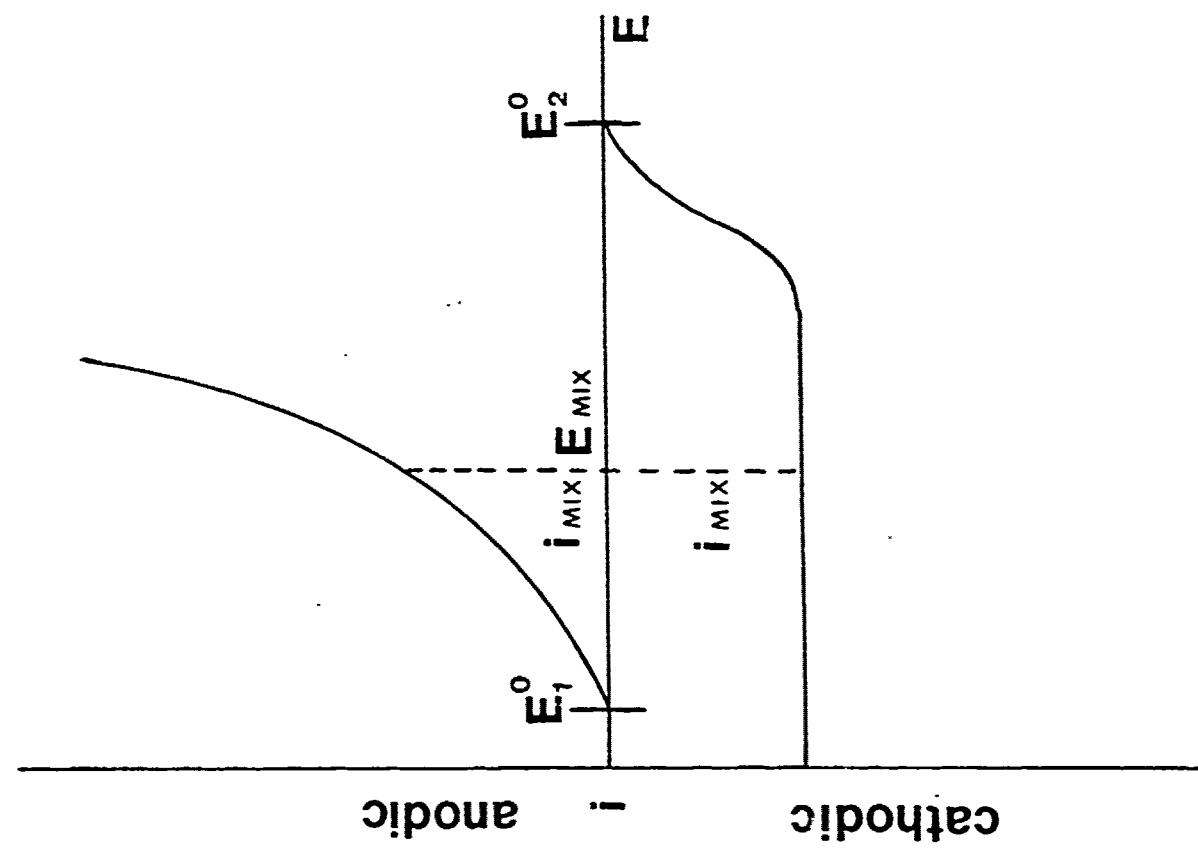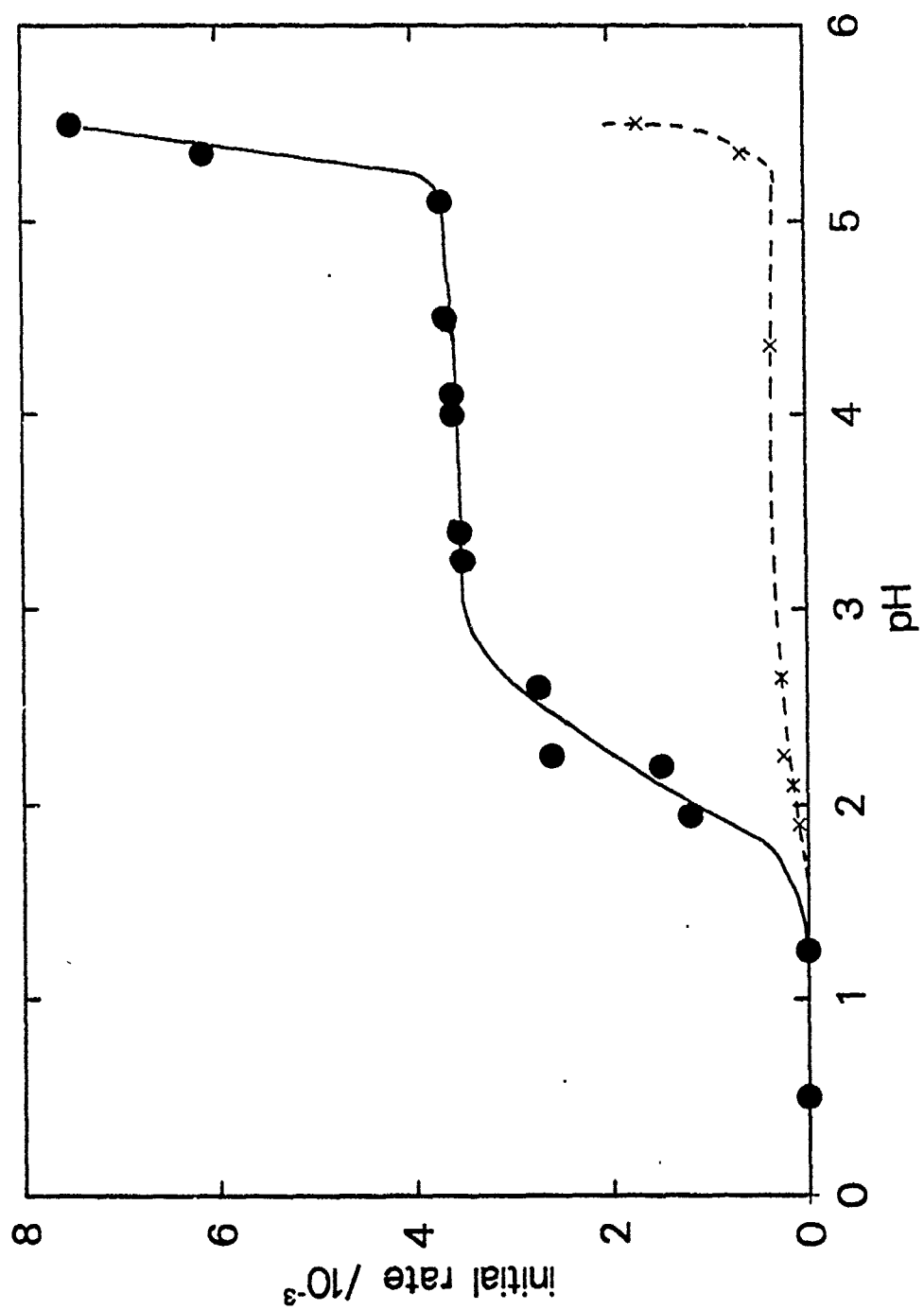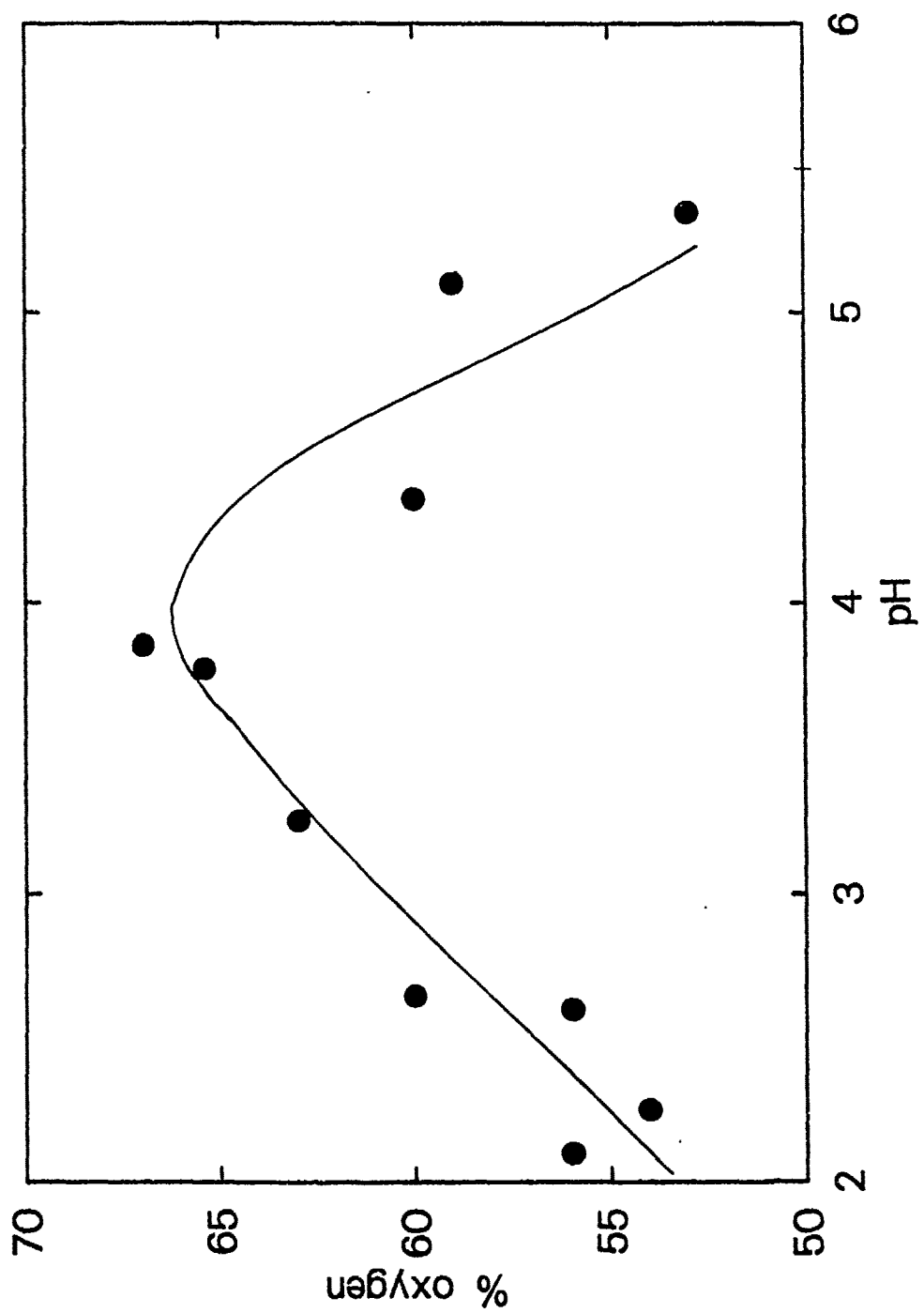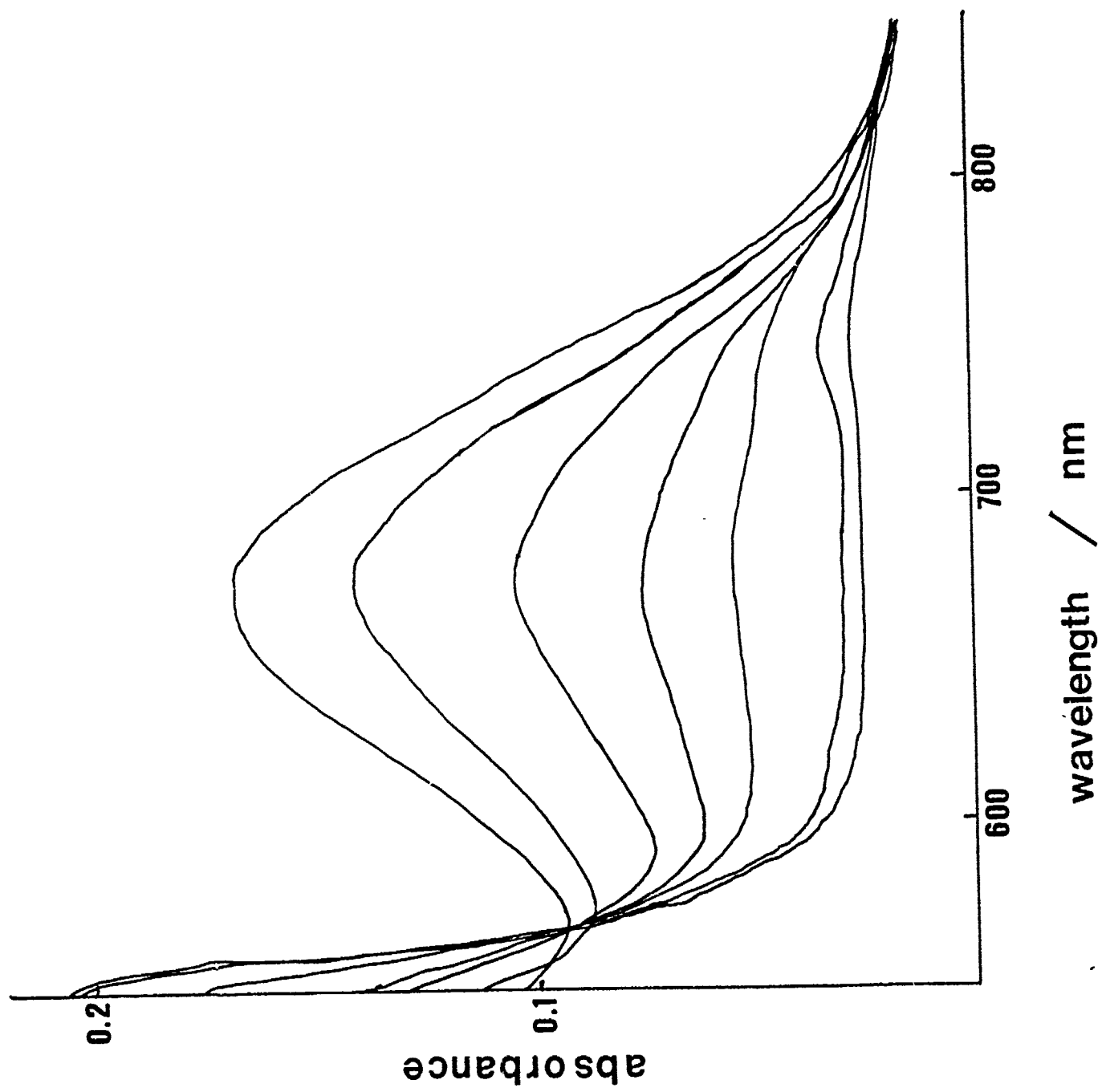
b

E_2^0

E

E_{MIX}

i_{MIX}

i_{MIX}

E_1^0

anodic

cathodic

a

E_2^0

E

E_{MIX}

$_{MIX}$

i_{MIX}

E_1^0

anodic

cathodic

Ⅲ-105

wavelength / nm

$[O_2]$ / 10^{-5} mol dm^{-3}

Time /sec

A

$[O_2]$ / 10^{-5} mol dm^{-3}

Time /sec

A

y-axis: $k'_{1.6} / 10^{-2}$

x-axis: [catalyst] /(mg cm^{-3})
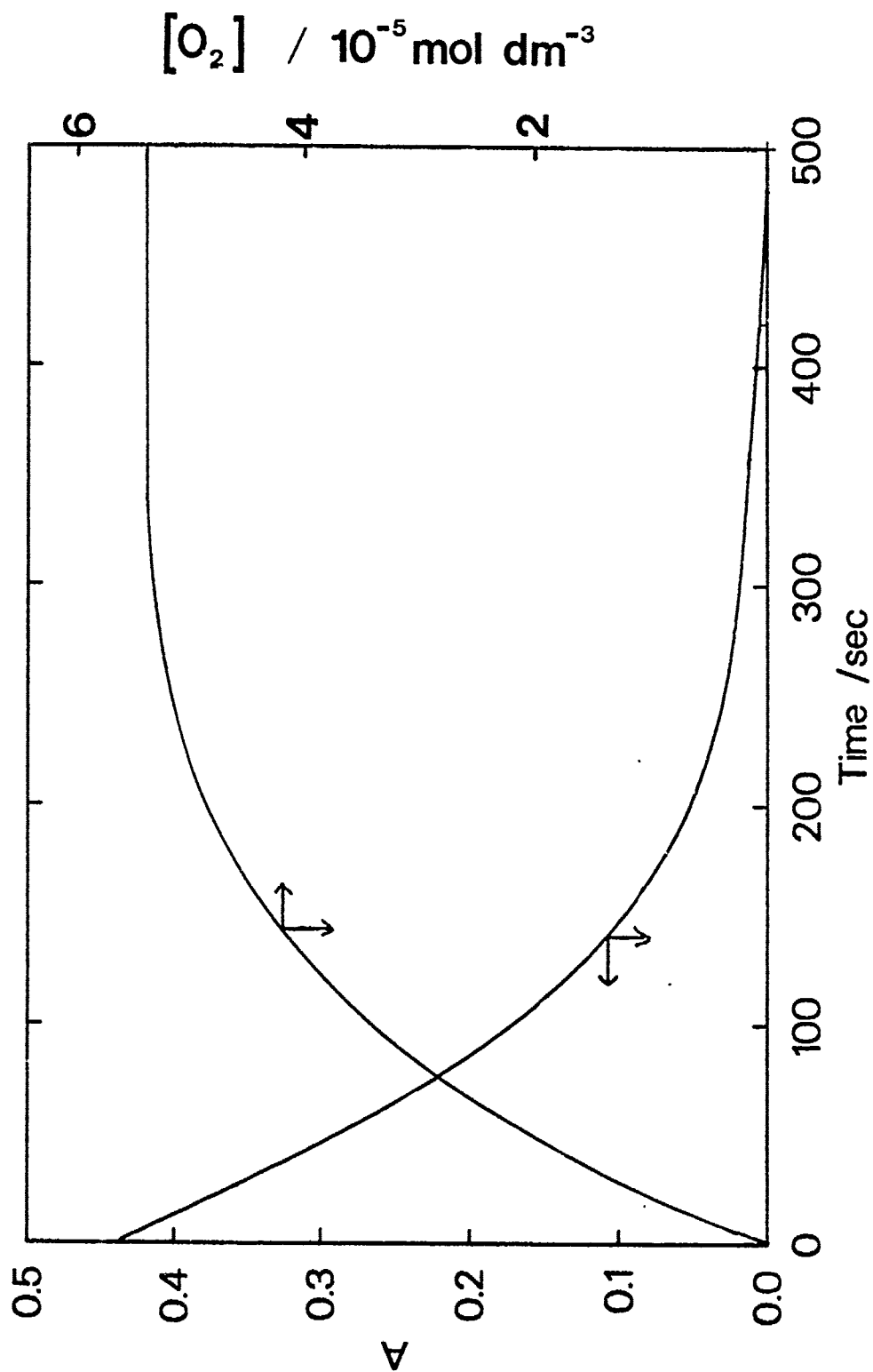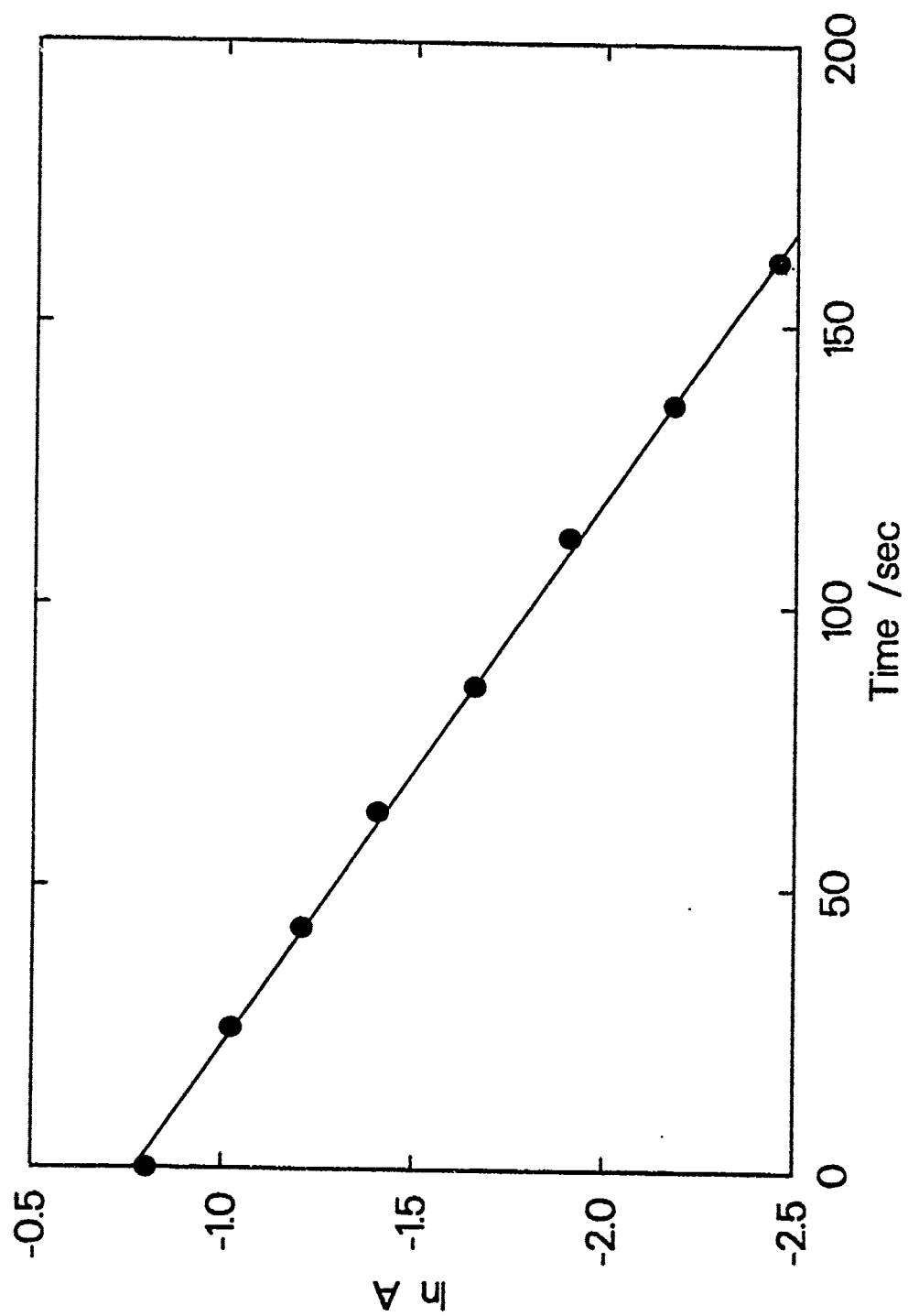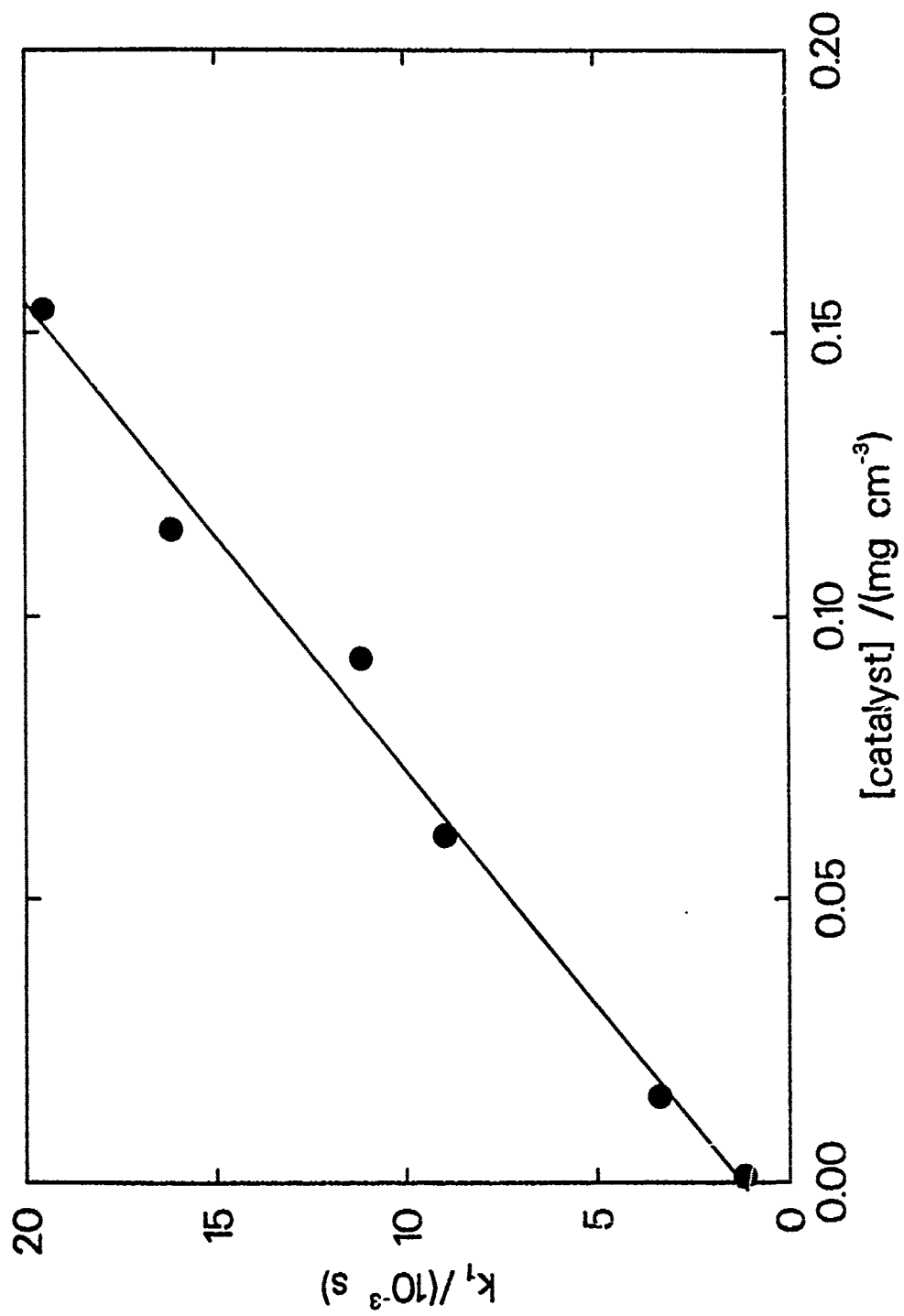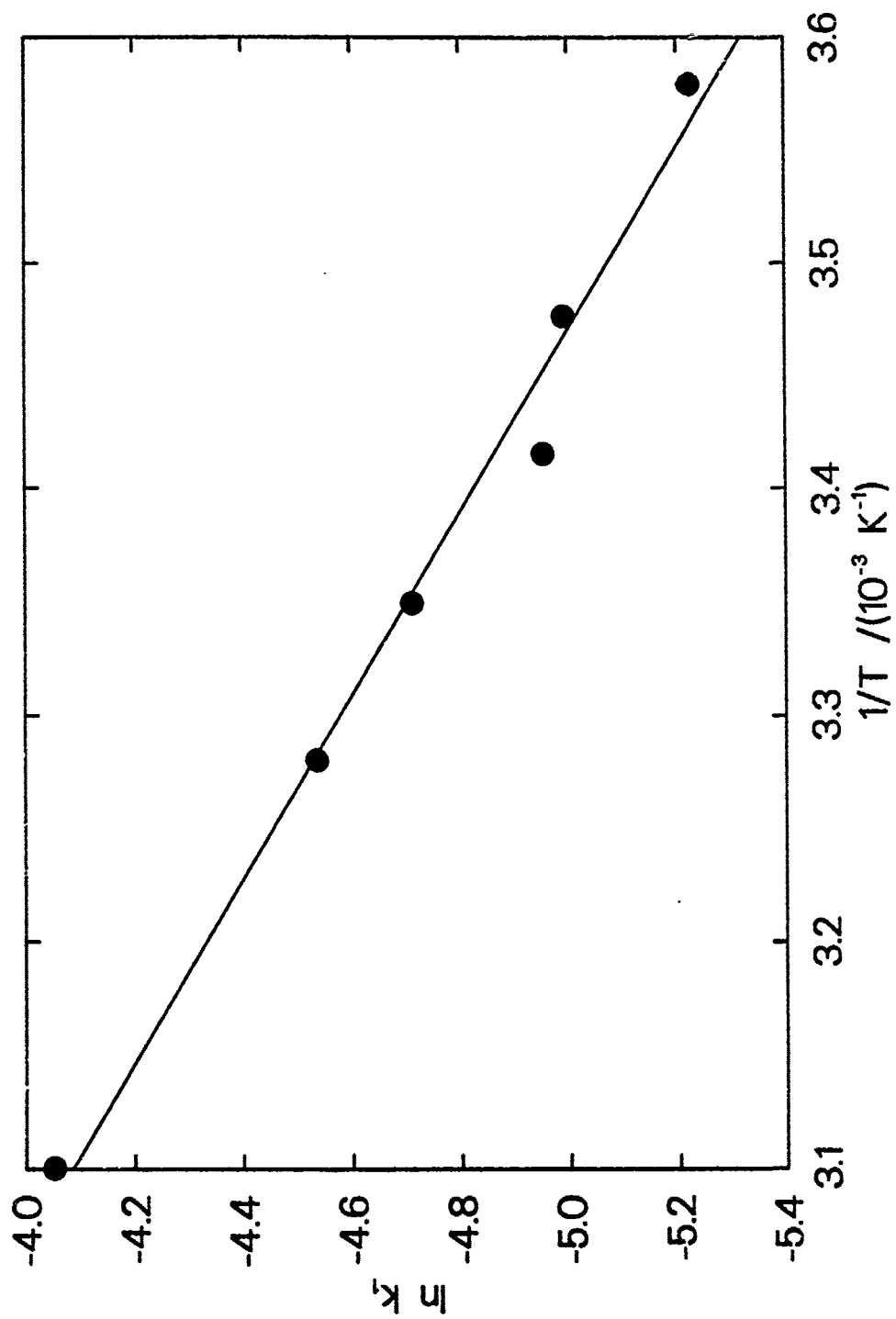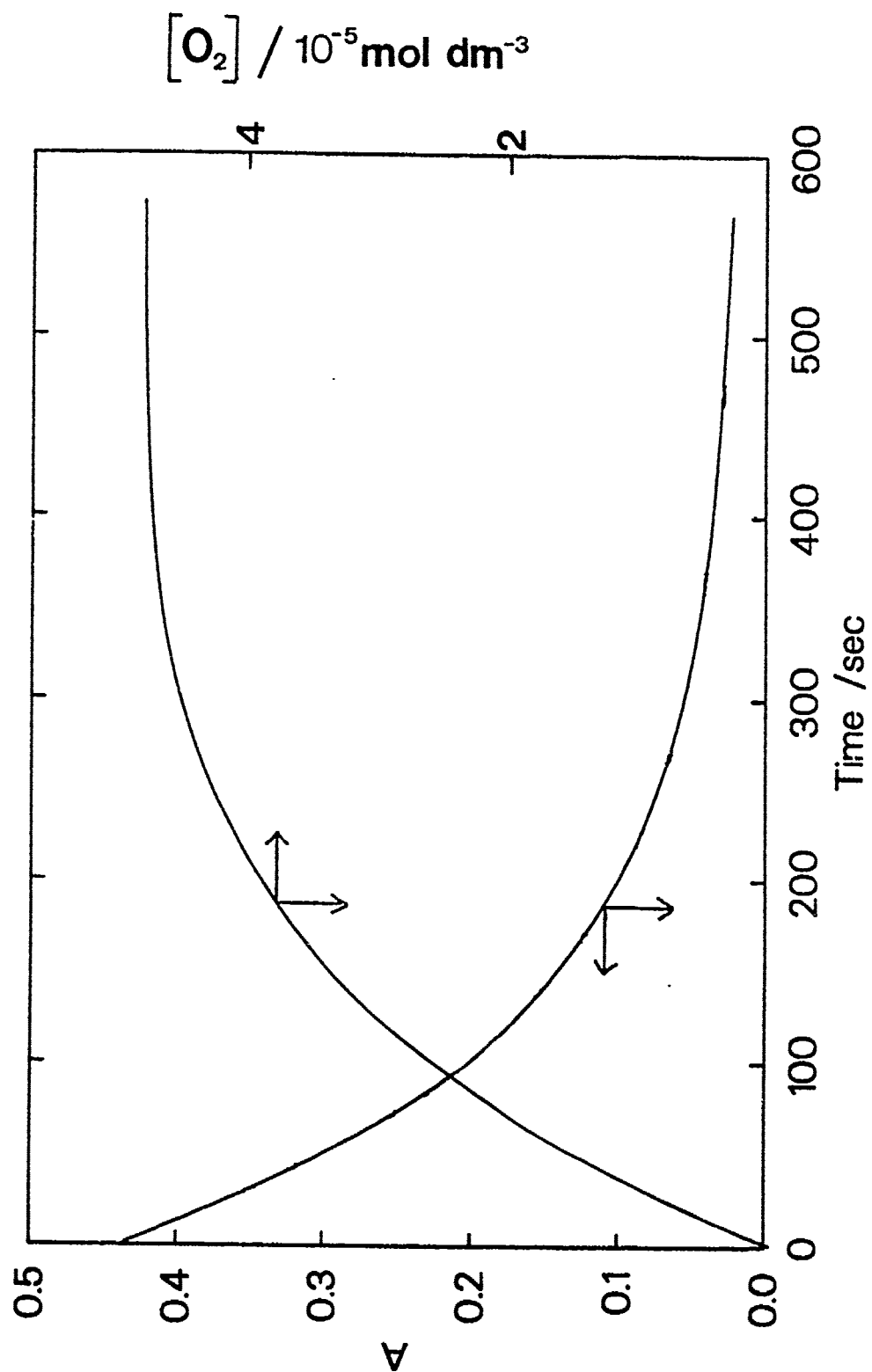
III-113

(25) **Synthesis and photoelectrochemical reactions
of Cadmium Sulfide in micellar solutions:**

M.P.Pileni[1,2], L.Motte[2], T.Jain[1], C.Petit[1,2] and F.Billoudet[1]

1- Université P. et M. Curie, Laboratoire S.R.I. bâtiment de Chimie Physique
   11 rue P. et M. Curie 75005 Paris, France

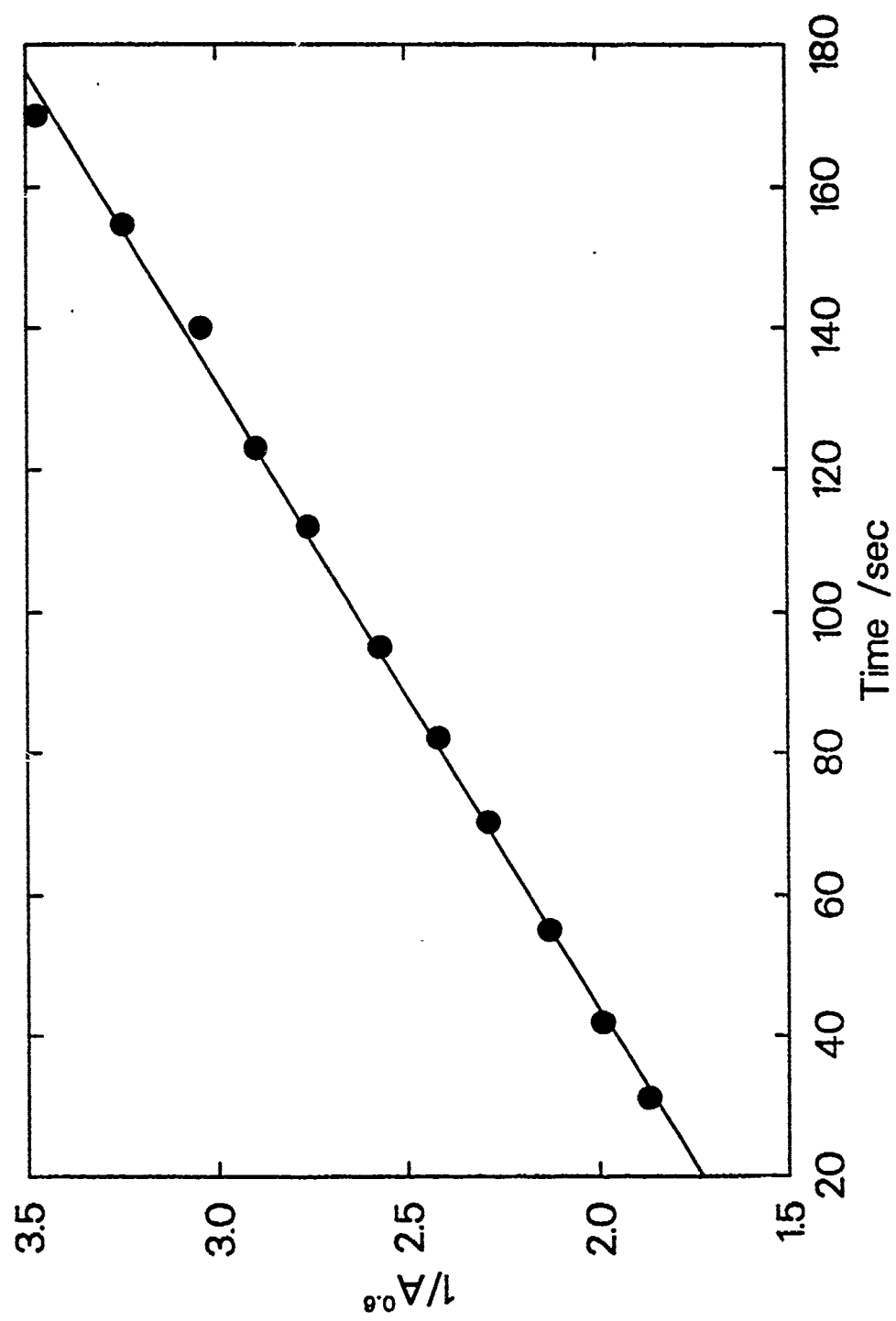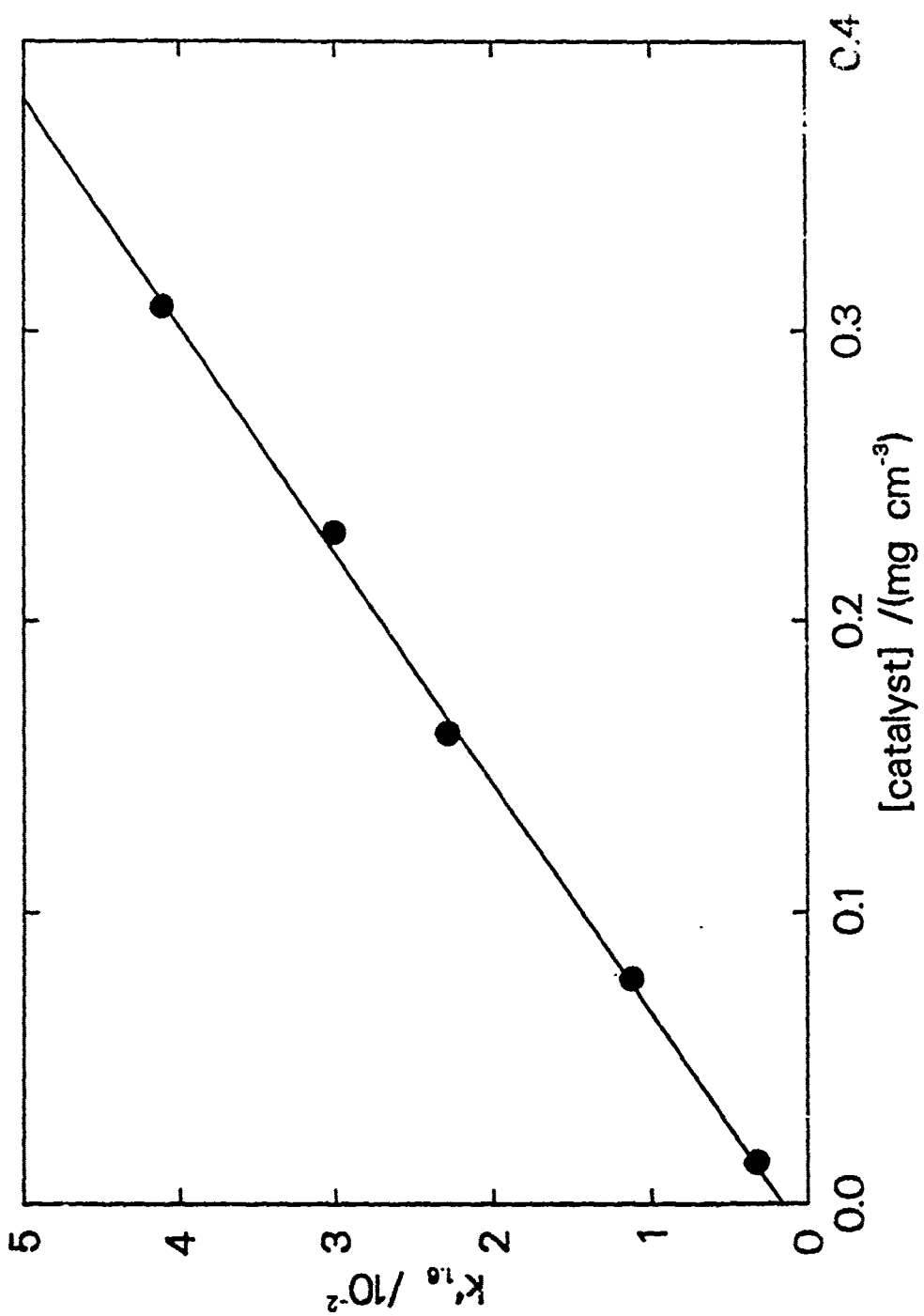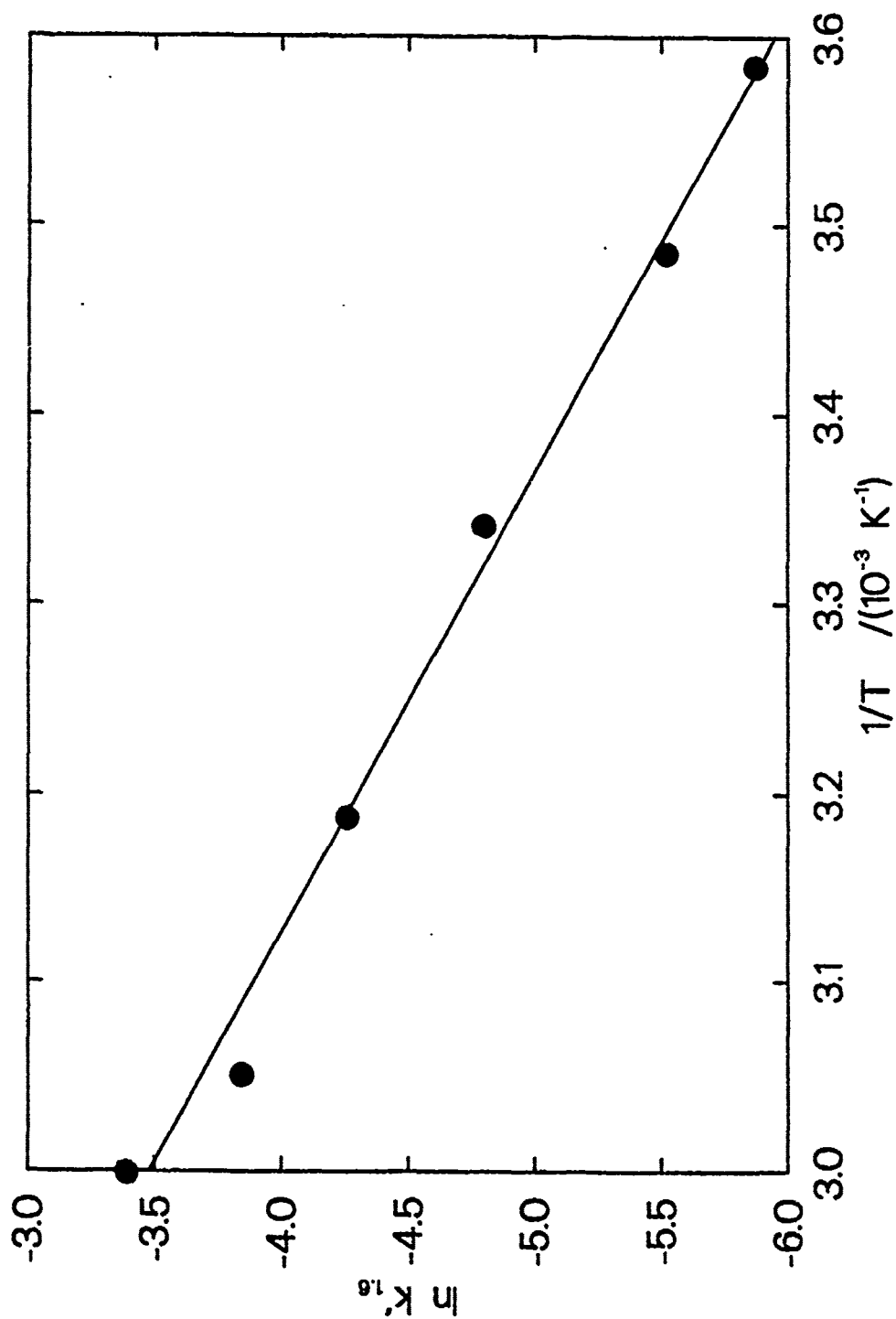2- C.E.N. Saclay, DRECAM.-S.C.M, 91191 Gif sur Yvette, France

Abstract: In this paper it is presented the results obtained by using either reverse
or normal to control the size of the CdS semiconductor particles. The use of mixed
sodium and cadmium di ethyl-2-hexyl sulfosuccinate (sodium and cadmium AOT)
reverse micelles favours the formation of monodispersed particles. By increasing
the water content, the size of the particle increases. Photoelectron transfer reactions
depend on the relative amount of cadmium and sulphur ions ($x=[Cd^{2+}]/[S^{2-}]$). At
low water content, reverse micelles prevent CdS semiconductor against
photocorrosion. By increasing the water content, photocorrosion process depends
on x value

Introduction

The use of dispersed media to solubilize or synthesise microparticles in situ has made considerable progress in the last few years: Langmuir-Blodget films, vesicles, polymerised vesicles, double layers or reverse micelles have been used as the incorporation media for microparticles, colloids or semiconductors[0].

Surfactants dissolved in organic solvents, form spheroidal aggregates called reverse micelles[1]. Water is readily solubilized in the polar core, forming a so called "water pool", characterised by w, w=[H2O]/[AOT]. For AOT as a surfactant, the maximum amount of bound water in the micelle corresponds to a water-surfactant molar ratio w = $[H_2O]$ /[AOT] of about 10. Above w 15, the water pool radius is found linearly dependent on the water content[0]. Another property of reverse micelles is their dynamic characters[1]. They can exchange the content of their water pools by a collision process.

Cadmium sulphide has been synthesised in AOT reverse micelles[0], with very high concentrations of surfactant (AOT = 0.5M) and in the presence of small quantities of water. These authors[0] were able to observe a reduced size distribution and an increase of the size of the particles by increasing the amount of water solubilized in the reverse micelle. The value of the ratio w = $[H_2O]$/[AOT] is always low (w<10).

Photocorrosion, observed in the presence of oxygen, is due to the photodissolution of CdS particles. The photochemical reaction is the following:

$$O_2 + CdS + 2h^+ \xrightarrow{h\nu} Cd^{2+} + S + H_2O_2$$
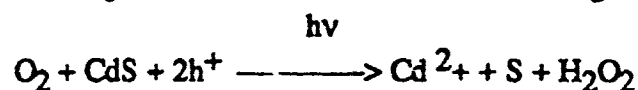
Such process can be blocked by trapping the holes, h^+, formed during the irradiation of the particles either by adding an external electron donor or by the presence of an excess of sulphur ions which is oxidised by the holes.

In the present paper we compare the micellar effect in the formation of CdS semiconductors. It is shown that using reverse micelles, the size of the particle increases with the size of the droplet whereas one size of particle is observed by using oil in water micellar solution.

Experimental section:

1- Products:

Sodium di (ethyl-2-hexyl) sulfosuccinate is produced by Fluka and sodium sulphide Na_2S by Janssen. The synthesis of functionalized surfactant has been previously described(7). The various dialkylviologens have been synthetized as described previously(8).

2-Synthesis of CdS in reverse micelles:

i) water in oil micellar solution: The synthesis is carried out by mixing two micellar solutions with the same ratio of water (w=$[H_2O]$/[AOT]), one containing a solution   in   which   the   sulphur   ions

17/06/91

(Na_2S) are solubilized and the other in which cadmium ions are present. The cadmium ions are obtained from cadmium di ethyl-2- hexyl sulfossucinate. The respective concentrations are, in general, the same, 3.10^{-4} mole.l^{-1}. The mixing is produced by rapid injection of a variable volume of solutions of cadmium ions and sulphide ions of the same concentration.A mixed sodium and cadmium AOT in isooctane reverse micelles were prepared. The concentrations are 0.1M and 3.10^{-4} mole.l^{-1}.

ii) oil in water micellar solution: A micellar solution of cadmium lauryl sulfate is formed and sulphur ions solution is added.

3- Preparation of samples for electron microscopy experiments:
i)reverse micelles:
An equal volume of water-acetone is added to the mixed micellar solution containing CdS particles. A two phases transition takes place and CdS particles migrate to the interface. A drop of a suspension of extracted CdS particles in acetone is pull on a copper plate with a carbon film The solvent is removed by vacuum.

ii) Oil in water micelles: Acetonitrile is added to the micellar solution. A precipitation takes place and the CdS particles are dried under vacuum. The powder is then dispersed in aqueous solution and a pull on a copper plate with carbon film.

4- Apparatus:
The small-angle X-ray scattering was done on a GDPA30 goniometer with copper $K\alpha$ radiation (1.54 Å). The experimental arrangement used has been described previously(9).
The absorption spectra were obtained with a Perkin-Elmer lambda 5 and Hewlett Packard spectrophotometer and the fluorescence spectra with a Perkin-Elmer LS5 spectrofluorimeter.
A Philips electron microscope (model CM 20,200 kV) was used to obtain pictures.
Continuous irradiation was performed using 1000watts Oriel lamp with 20cm water filter and 385nm cutoff filter.
Flash photolysis experiments were performed using an Applied Photophysics apparatus.

5- Stuctural study of mixed sodium-cadmium di ethyl-2-hexyl sulfosuccinate:
Using sodium AOT reverse micelles it has been shown[0]a linear dependence of the water pool radius with the water content (R_w=1.5 W) previously. In pure

Cadmium AOT reverse micelles, it has been shown[0] very strong changes in the phase diagram $Cd(AOT)_2$-isooctane-water. Using mixed micelles (sodium-cadmium AOT, in the experimental conditions in which CdO particles are synthetized, no structural changes compared to sodium AOT reverse micelles is observed: a linear relationship between the water pool and the water content (R_w =

1.5w)

Results and Discussions:

I In reverse micelles:

The synthesis of CdS in AOT reverse micelles are obtained for various water contents (w=[H$_2$O]/[AOT]) and various x (x=[Cd^{2+}]/[S^{2-}]) values.

1. Size determination:

In the presence of an excess of cadmium ion (x=2), figure 1 shows a red shift in the absorption spectra by increasing w. Below the absorption onset several bumps are observed (figure 1) and can be clearly recognised in the second derivative (inserts figure 1). These weak absorption bands correspond to the excitonic transitions and result in a perturbation of electron structure of the semiconductor due to the change in the particles size. This gives a widening of the forbidden band and therefore a shift of the absorption threshold as the size decreases. The average size of the particles is then deduced from the absorption onset[]. At low water content the first excitonic pic is well resolved and is followed by a bump (figure 1A). The second derivative shows a very high intensity of this bump (insert 1A). With small crystallite, according to the data previously published[], several bumps due to several excitonic pics are expected. Insert figure 1A shows only one bump. This is due to the fact that the others are blue shifted and are not observable in our experimental conditions. By increasing the water content, that is to say by increasing the size of the particles, several bumps are observed (insert figure 1B). This confirms the fact that, at w=5, the bumps are blue shifted and indicates a very narrow distribution in the size of the particles. The intensity of these bumps decreases with the water content, w (inserts figure 1). This indicates a decrease in the number of excitonic transitions with the size of the particle. This is in agreement to the theoretical calculations previously published for the Q-particles[].

The size of CdS particle, the average radius, r, is deduced. Figure 3 shows a change in the size of the particle with the relative ratio of cadmium and sulphide ions (x = [Cd^{2+}]/[S^{2-}]). The biggest sizes are obtained for x=1 and the smallest for x=2. It can be noticed that the size of CdS is always smaller when one of the two reactants are in excess (x=1/4, 1/2, 2). This confirm that the crystallisation process is faster when one of the species is in excess[].

Electron microscopy has been performed using a sample synthesised at w=10, x=2, in mixed reverse micelles, characterised by 430 nm absorption onset corresponding to a CdS radius equal to 25A. The micrograph picture (figure 2A) shows spherical and monodispersed particles. From micrograph picture the average size is in the range of 40 ± 20Å. The electron rays diffraction shows concentrical circles (figure 2B). This is compared to a simulated diffractogram of bulk CdS and a good agreement between the two spectra is obtained indicating the particles keep ZnS crystalline structure (c.c.f) with a lattice constant equal to 5.83A. From the simulated curve, it can be noticed the absence of (200) line. The microanalysis study shows the characteristic line of sulphur and cadmium ions indicating that the observed particles are CdS semiconductor cristallites. The radius of the particle can be deduced from the line widening of the diffraction signals given by the following

17/06/91

ZII-118

relationship[()]: $2r = \lambda L / \Delta R$ where λ is electron wavelength ($\lambda = 0.251$nm), L is

~~~~~~ l~~~~ll. (L—1000......) ~~~ ΔR ~~ ~~~ ~~~~~~~~ ~~~.(ΔR —9......). The radius
determined from such calculation is equal to 41A . The differences in the size of the
particles deduced from the absorption onset and obtained from electron microscopy
are probably due to the extraction of CdS from the droplets with formation of
aggregates.

2- Polydispersity:

As the fluorescence is dependent on the size of the particles a shift of the excitation
threshold with the emission wavelength indicates the presence of particles of
different sizes in the solution: this is then a measurement of the polydispersion of

the aggregates[0]. In the case where this excitation spectrum is analogous to the
absorption spectrum, the threshold is a measure of the average size of the emitting
particles.

Figure 4 C,D shows the fluorescence spectra at various water content. The

unchanged spectra ($\Delta\lambda = 2$ nm) with the excitation wavelength indicates strong
monodispersity. The shift of the maximum of the emission with the water content,
w, can be related to the average size of the particles. For a sample synthetized in
the given experimental condition (fixed w and x value) the fluorescence excitation
spectra obtained are unchanged with the emission wavelength. This confirms the
monodispersity in the size of the CdS particles.

3- Photochemical reaction:
i- Photocorrosion:

The yield of photocorrosion is followed by observing the change in the absorption
spectrum of CdS particles at 300nm. Figure 5 shows the relative photocorrosion
yield determined under continuous irradiation at various water content.

In the presence of an excess of sulphur ions ($x=1/2$) a shift of the absorption
threshold to longer wavelengths is observed showing an increase in the size of the
aggregates. This phenomenon favouring the formation of large particles correspond

to a greater thermodynamic stability (Ostwald's ripening[0]). Figure 5A shows an
increase in the photocorrosion yield with the water content.

In the presence of an excess of cadmium ions ($x=2$), figure 5B shows the high

value of the photocorrosion yield. Because of the sulphur vacancies the holes (h^+)
can easily react with CdS particles, in the presence of oxygen. However at low
water content micelles play the role of protecting agent: at $w=5$, the size of the CdS
particles and the water droplets are similar. This indicates that the surfactants
molecules totally surrounds the CdS particles. By increasing the water content, the
photocorrosion yield is very large

B- Photoelectron Transfer:

The photoelectron transfer from CdS to various dialkylviologens, {$(Cn)2V2+$},
has been studied by flash photolysis. The size of the particles remains unchanged
either by adding viologen before or after CdS synthesis.

In the presence of an excess of sulphur ($x=1/2$), figure 6 shows a decrease in the

5

IV-119

JUN 17 '91 19.56

yield of reduced dialkylviologen with the water content. This can be related to the fact that, at low water content, figure 2 shows a change in the absorption spectrum probably due to sulphur aggregates adsorbed at the CdS interface. Such sulphur ions are able to give an electron to the hole formed by light excitation and then prevent the back electron transfer reaction. The yield of reduced viologen increases with chain length of viologen. It can be attributed to an increase in the amount of viologen anchored the CdS semiconductor surface.

The photoelectron transfer rate constant increases with the water content and with the chain length of dialkylviologen. This can be explained in term of size effect: figure 2 shows that, at $x=1/2$, the size of CdS particle is strongly changed between $w=5$ ($R=12Å$) to $w=10$ ($R=13Å$). By increasing the water content, no drastic change in the size is obtained (for $15<w<40$, $R_{CdS} \neq 16Å$). The photoelectron transfer rate constant is more efficient by using small particle and long chain dialkylviologen.

In the presence of an excess of cadmium ions ($x=2$), the photoelectron transfer rate constant and the reduced viologen yield are constant and independent on the length of the alkylchain and to the water content. This can be attributed to the fact that there are no internal electron donor to prevent the back electron transfer reaction as it takes place in the presence of an excess of sulphide in which the latter play a role.

The addition of an external electron donor such as cysteine, adenine benzylnicotinamide does not prevent the back reaction. This could be explained in term on accessibility of the electron donor to the holes formed by CdS excitation. The back electron transfer takes place before the external electron donor can reach the CdS hole.

6

III-120

Figures:

Figure 1: Variation of the absorption spectrum of CdS in reverse micelles with the water content. [AOT- Na] =0,1M, [(AOT)$_2$Cd] =2.10^{-4}M, x = 2, A(w=5), B (w=10); C (w=20); D (w=40)

Figure 2: Variation of the absorption onset and the CdS radius with the water content [AOT- Na] =0.1M, for x value equal to1/4; 1/2; and [(AOT)$_2$Cd] = 10^{-4}

M and for x=2 [(AOT)$_2$Cd]=2.10^{-4}M

[x=1/4: (O);]; [x=1/2; (●)]; [x=1; (□)]; [x=2; (■)]
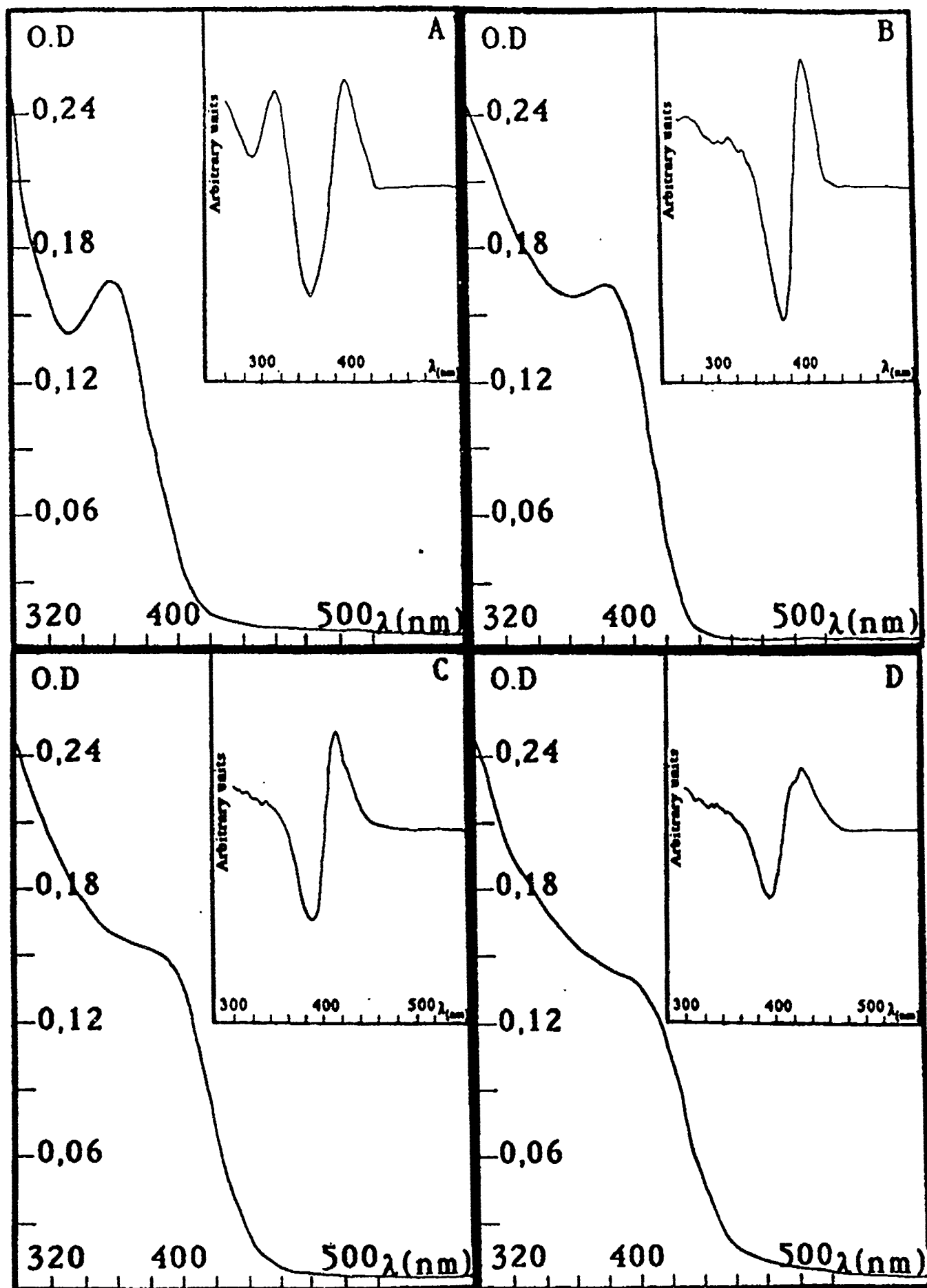
Figure 3:
-A- Electron microscopy of a sample after extraction from a micellar solution
-B- Electron diffraction spectrum of CdS particle

Figure 4: Variation of the relative fluorescence spectra (normalized at the emission maximum) with the water content at various excitation wavelength;
[AOT] =0,1 M, x = 2; [(AOT)$_2$Cd] =2.10^{-4}M , (λexc:△ = 380 nm ; ■ = 400 nm; + = 420 nm) w=10 (A); w=10 (B); w=20 (C) and w=40 (D)

Figure 5: Variation of the relative photocorrosion yield with time at various water content w=5 (■); w=10 (O); w=20 (△); and w=40 (+)

Figure 6: Variation of the reduced viologen yield (A x=1/2; B x=2) and the rate constant of the electron transfer (C X=1/2; D X=2) with the length of various alkyl chain at various water content.
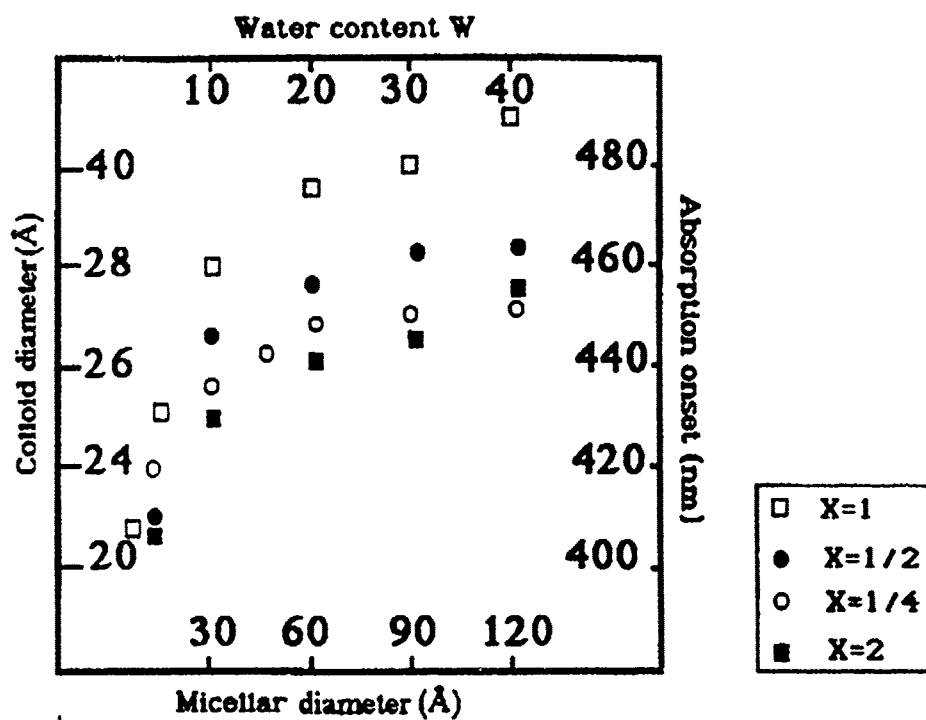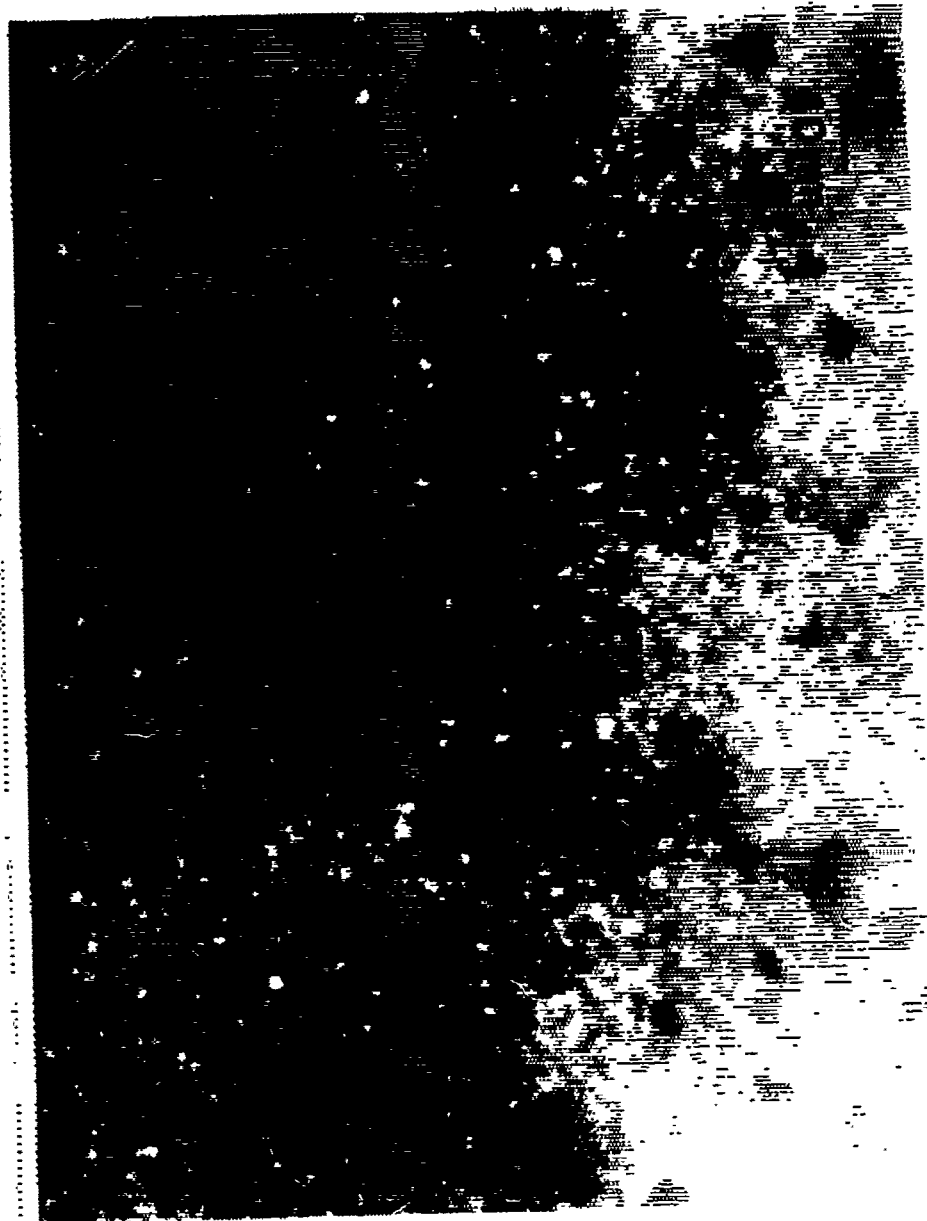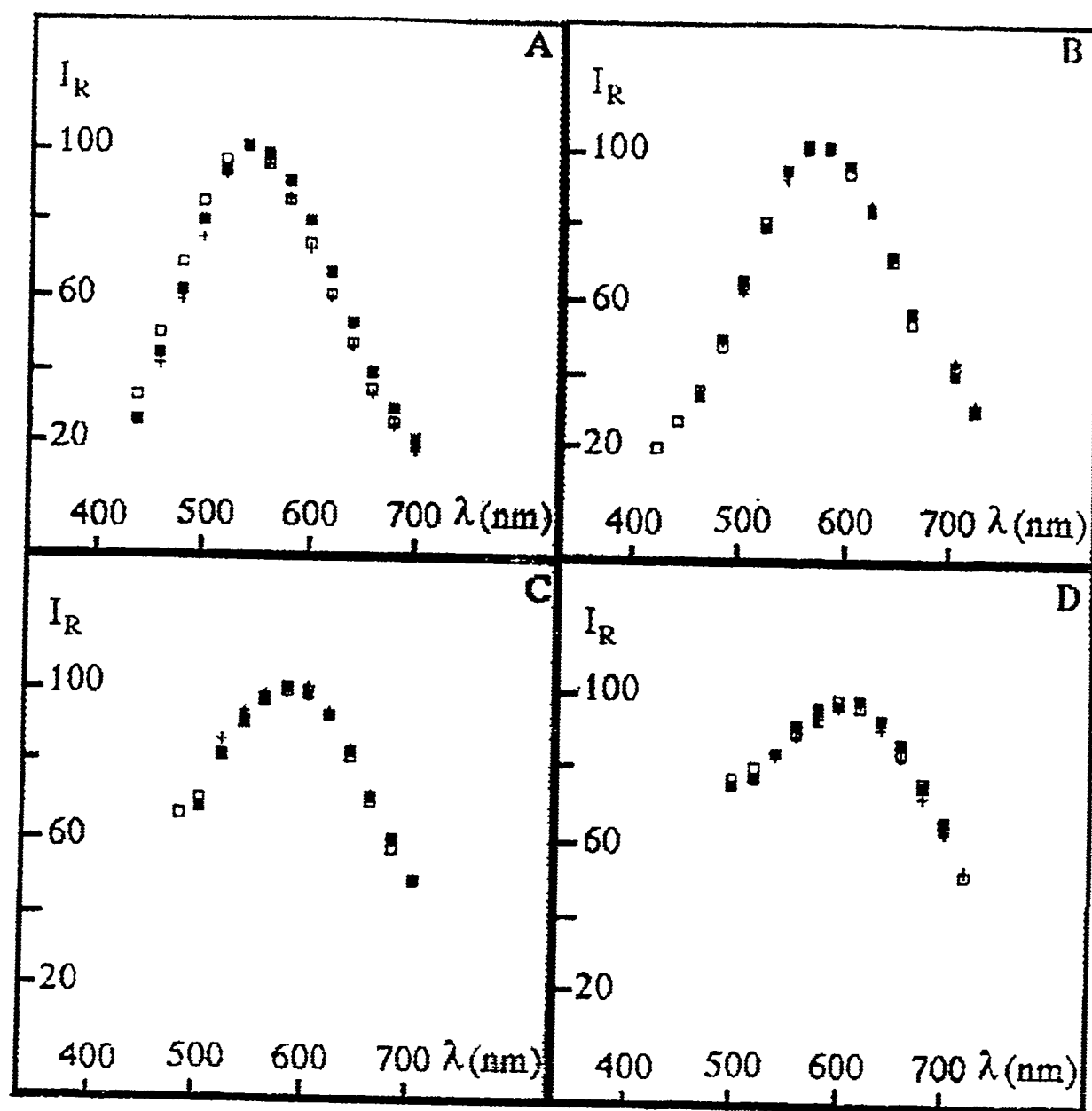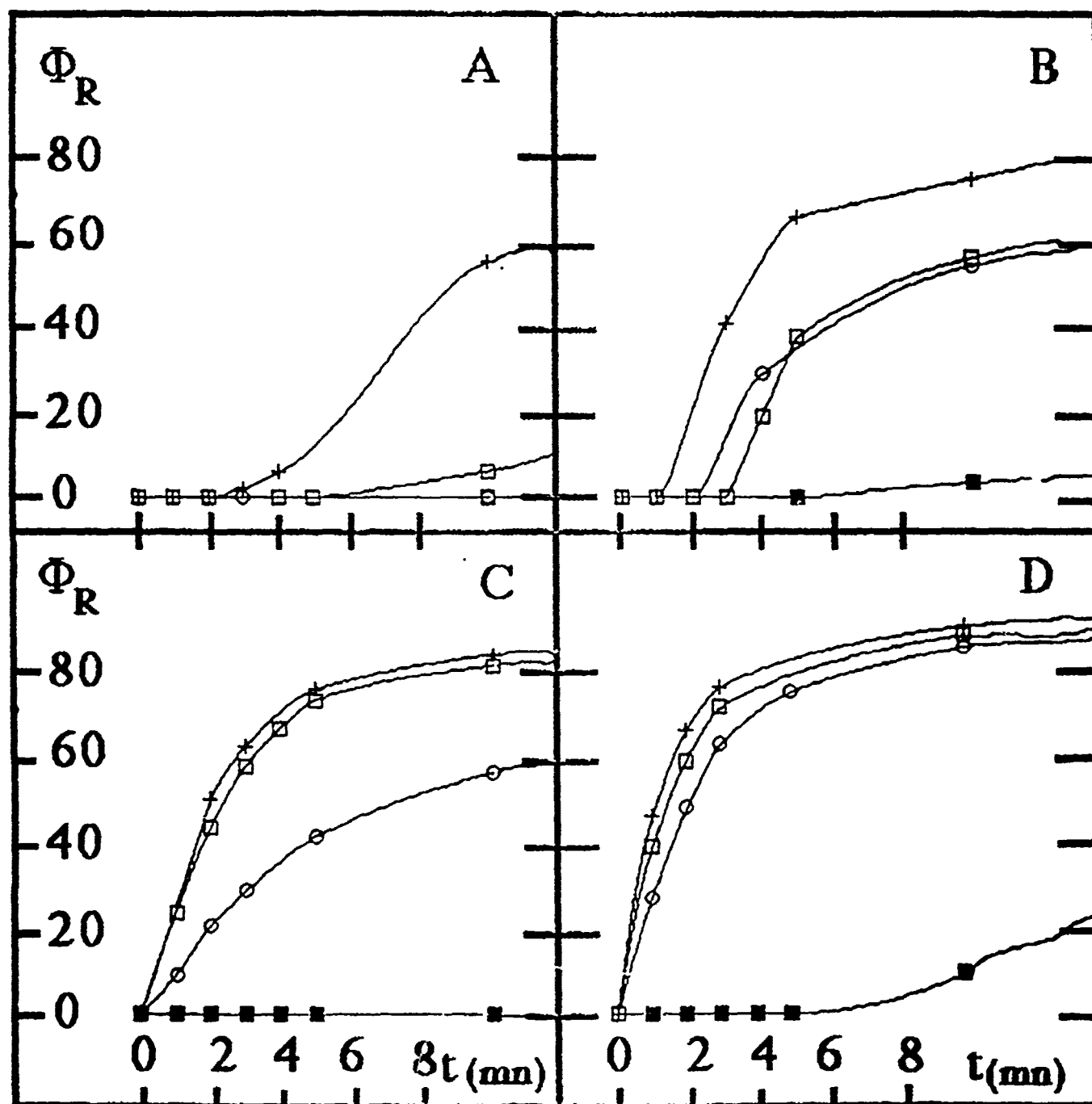
III-122   Figure 1

Water content W

Figure 2

III-124

Figure 4

$A=1/4$ $B=1/2$

$C=1$ $D=2$

figure 8.

(26) Sensitized Charge Injection in Large Bandgap Semiconductor Colloids

Prashant V. Kamat[*] and Brian Patrick

Radiation Laboratory
University of Notre Dame
Notre Dame, IN 46556

2

Abstract

The mechanistic and kinetic details of charge injection into the conduction band of TiO_2 and ZnO colloids from the exicted thionine and CdS colloids are investigated. The participation of singlet and triplet excited states of thionine in sensitizing TiO_2 and ZnO colloids are elucidated with picosecond and nanosecond laser flash photolysis. The reverse electron transfer between the injected charge and the dye cation radical is the major limiting factor in controlling the efficiency net charge transfer. Better charge separation can be achieved by coupling the two semiconductor systems.

1. Introduction

Photosensitization of a stable, large-bandgap semiconductor has important applications in imaging science and photoelectrochemical conversion of solar energy. This phenomenon often serves the purpose of selectively extending the absorptive range of the semiconductor materials. The principle of a dye sensitization process is illustrated in Figure 1 [1,2]. One of the intriguing aspects of the photosensitization process is the poor efficiency (often less than 1%) of net charge transfer although some recent reports have indicated efficiencies of 30-80% [3-6]. In recent years several researchers have investigated the charge injection from excited dye into the semiconductor particles and electrodes by employing various fast kinetic spectroscopy techniques. These include, emission [7-10], nanosecond [8-11] and picosecond [12-15] laser flash photolysis, resonance Raman [16,17], microwave absorption [18], diffuse reflectance laser flash photolysis [19,20], and internal reflection flash photolysis [21].

Another interesting approach for achieving photosensitization would be to replace the sensitizing dye with a short bandgap semiconductor. Coupling with a short bandgap semiconductor would thus enable sensitization of a large bandgap semiconductor. For example, in a CdS-TiO$_2$ system, CdS (E$_g$ = 2.4 eV) can be excited with visible light and photogenerated electrons can then be injected into the TiO$_2$ semiconductor [22,23]. The difference in energy levels of the two semiconductor systems plays an important role in controlling the charge injection process. In recent years, charge injection processes in several mixed semiconductor colloids,

4

CdS-TiO$_2$ [23-25], CdS-ZnO [25], Cd$_3$P$_2$-TiO$_2$ and Cd$_3$P$_2$-ZnO [26], AgI-Ag$_2$S [27] and ZnO-ZnS [28] have been reported.

Both dye-sensitized and short bandgap semiconductor sensitized charge injection into a large bandgap semiconductor have now been carried out by us to elucidate the mechanistic and kinetic details of charge injection processes in colloidal semiconductor suspensions. In the present study, we have chosen thionine dye and CdS semiconductor colloid as sensitizers and TiO$_2$ and ZnO colloids as large bandgap semiconductors. The transparency of the colloidal suspension facilitates direct detection of transients by picosecond and nanosecond laser flash photolysis. Ultrafast charge transfer processes that control the efficiency of photosensitization will be addressed here.

2. Experimental

2.1 Materials:

Thionine (Fluka) was purified over a chromatography column of neutral alumina. Colloidal TiO$_2$ was prepared by the hydrolysis of Titanium(IV)-2-propoxide (Alfa products) in acetonitrile [29]. ZnO colloids were prepared by the hydrolysis of a Zn-complex precursor with LiOH as described by the method of Spanhel and Anderson [30].

2.2 Optical Measurements

Absorption and emission spectra were recorded with a Perkin-Elmer 3840 diode array spectrophotometer. Emission spectra were recorded with a SLM S-8000 spectrofluorometer.

III-132

Nanosecond laser flash experiments were performed with a 532-nm laser pulse (8 mJ, pulse width 6 ns) from a Quanta Ray Nd:YAG laser system. The experiments were performed in a rectangular quartz cell and all the solutions were deaerated with high purity nitrogen.

Picosecond laser flash photolysis were performed in a flow cell using a mode-locked 355-nm laser pulse from Quantel YG-501 DP Nd:YAG laser system (2-3 mJ/pulse, pulse width ~ 18 ps) as the excitation source. The white continuum was generated by passing the residual fundamental output through a D_2O/H_2O solution. The time zero in these experiments corresponds to the end of the excitation pulse. All the experiments were performed at room temperature (296 ± 1 K).

3. Results and Discussion

3.1 Dye Semiconductor System:

Recently, there have been several reports which address the interfacial charge transfer at the excited dye and the semiconductor [12-21]. As indicated in Fig. 1, both triplet and singlet excited states of a sensitizing dye are capable of injecting charge into the semiconductor. Most of the earlier studies have indicated that excited singlet state of the dye is the major species that participate in the charge injection process and the rate constant for the charge injection process is greater than 5×10^{10} s^{-1}. However, little effort has been made to elucidate the role of triplet excited state as the donor in the dye sensitization process. Because of the longer lifetime (often in microseconds) it should be
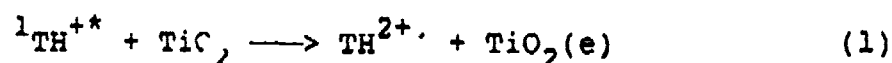
$III - 133$

6

advantageous to utilize the triplet excited state in injecting charge into the semiconductor. We now discuss the role of singlet and triplet excited states of the dye in governing the mechanism of photosensitization process. We have chosen a thiazine dye as the sensitizing dye since it yields both singlet and triplet excited states in detectable amounts. Also its energetics (E_{ox} = 1.25 V vs NHE) facilitate charge injection into the conduction band of the semiconductor.

3.1.1 Thionine-TiO$_2$ System:

The absorption and emission spectra of thionine in aceto-nitrile and in colloidal TiO$_2$ suspension are shown in Figure 2. A red shift in the absorption maximum of thionine was observed in colloidal TiO$_2$ suspension. As shown earlier [29], such a red shift represents charge transfer interaction between TiO$_2$ surface and thionine. The negatively charged $-OH^-$ groups on the TiO$_2$ surface influences the interaction between TiO$_2$ and positively charged dye. The equilibrium constant for such a charge transfer inter-action is found to be quite high (K_a = 2.75 x 10^5 M^{-1} [29]).

Such a charge transfer interaction between thionine and TiO$_2$ colloid resulted in the decrease of the fluorescence yield. This is evident from the emission spectra recorded in Fig. 2B. This decrease in fluorescence yield (> 60%) is attributed to the quench-ing of singlet excited state. As shown earlier, the quenching of excited singlet state proceeds by charge transfer to the semicon-ductor colloid (reaction 1).

III—139

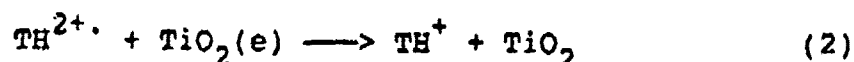$$^1TH^{+*} + TiO_2 \longrightarrow TH^{2+\cdot} + TiO_2(e) \qquad (1)$$

Picosecond laser   photolysis experiments were carried out
to probe the ultrafast charge transfer events that might occur on
the surface of colloidal TiO_2. Figure 3 shows transient absorption
spectra of thionine in acetonitrile and in colloidal TiO_2 suspen-
sion recorded immediately after the 532-nm laser pulse (pulse dura-
tion, 18 ps) excitation. The transient absorption spectrum in
acetonitrile which is attributed to singlet excited state exhibits
maximum at 450 nm and a shoulder around 500 nm. The lifetime of
$^1TH^{+*}$ as determined from the first order decay of the 450 nm
absorption was 450 ps in ethanol. However, in colloidal TiO_2 sus-
pension a similar absorption spectrum but with decreased intensity
was observed. It is likely that the excited singlet state of the
unassociated dye dominates the absorption in spectrum b (Figure
3). Although one would have expected to see formation of $TH_2^{2\cdot+}$
with absorption in the region of 500 nm, such a transient absorp-
tion is likely to be buried in the singlet-singlet absorption of
free dye. If the lifetime of dye cation-radical is very short
(i.e. less than the lifetime of singlet excited state) it will be
difficult to time-resolve the transient absorption spectra for
characterizing $^1TH^*$ and $TH^{2+\cdot}$ species. We have recently shown [15]
in the case of TiO_2-squaraine that the dye cation radical formed
during the charge injection process was short lived (270 ps) than
the singlet excited state (3 ns). A high rate constant (3.7×10^9
s^{-1}) for the reverse electron transfer between injected charge and
dye cation-radical was a limiting factor in controlling the effi-

ciency of net charge transfer.

While the quenching of thionine fluorescence by TiO_2 colloid was efficient, we failed to detect any transient absorption of cation-radical in the laser flash photolysis experiments. This shows that the reverse electron transfer (reaction 2)

$$TH^{2+\cdot} + TiO_2(e) \longrightarrow TH^+ + TiO_2 \qquad (2)$$

occurs faster than the decay of the excited singlet state. Because of the strong interaction between the dye and TiO_2, static quenching processes dominate both the forward and reverse electron transfer processes.
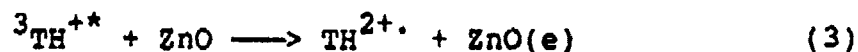
3.1.2 Thionine-ZnO System:

ZnO colloids prepared in ethanol have pH around 9.0. We maintained a pH of 8.2 in our ZnO suspension so that the surface is slightly positive. As a result of this, no direct interaction between TH^+ and ZnO colloid was seen. The absorption spectrum of thionine remained unaltered when ZnO colloids were added to the dye solution. Similarly, no change in the fluorescence yield was seen in colloidal ZnO suspensions. Hence, the participation of excited singlet state in the charge injection process can be ruled out.

A more interesting picture emerged when the laser flash photolysis experiment was carried out with a nanosecond laser. The transient absorption spectra recorded 5 μs after 532-nm laser pulse excitation are shown in Figure 4. In neat ethanol, we observe transient absorption with a maximum around 420 nm arising as a

result of triplet-triplet absorption. However, a growth of a new transient with a maximum at 500 nm is seen in ZnO suspensions. The spectral features as observed in earlier studies confirm this transient to be $TH^{2+}\cdot$. The monophotonic formation of $TH^{2+}\cdot$ (see dose dependence in the insert of Figure 4) is the result of a charge transfer interaction between $^3TH_2^{+*}$ and ZnO (reaction 3).

$$^3TH^{+*} + ZnO \longrightarrow TH^{2+}\cdot + ZnO(e) \qquad (3)$$

The growth in the 500 nm absorption matched well with the decay of dye triplet at 420 nm. The rate constant for the quenching of $^3TH^{+*}$ by ZnO was 6.8×10^4 s^{-1}. Control experiments were carried out to rule out the possibility of $TH^{2+}\cdot$ formation via excited state annihilation and self quenching processes.

These experiments clearly confirm the participation of triplet excited state in the charge injection process. Because of the excess positive charge on the ZnO surface, TH^+ are located away from the ZnO surface, across the double layer (Figure 5). In order to interact with the ZnO colloid, it is necessary for the dye to diffuse through the double layer. The lifetime of singlet excited state is too short to promote a diffusional charge transfer process. However, the triplet dye which is sufficiently long-lived ($\tau = 88$ µs) interacts with ZnO via diffusional process. Other parameters, such as surface potential of the semiconductor colloid, and charge of the dye molecule could well influence such a diffusion controlled charge transfer mechanism. Further studies to understand these aspects are currently being undertaken in our

laboratory.

The reverse electron transfer between injected electron and TH^{2+}· was rather slow, but was dependent on the concentration of ZnO colloids. The rate constant for the decay of TH^{2+}· increased from $8.6 \times 10^4 \ s^{-1}$ to $3.2 \times 10^5 \ s^{-1}$ when colloidal ZnO concentration was increased from 50 µM to 2 mM. Interparticle recombination process is expected to dominate at high ZnO concentrations. Contributions of intraparticle and interparticle recombination processes to the decay of dye cation radical has been illustrated earlier for the TiO_2-eosin system [8].

We have presented here two examples in which the participation of singlet and triplet excited states of the dye in the charge injection process are described. The interaction between the dye and the semiconductor, as described in Figure 5, is an important factor that governs the mechanism of photosensitization. In the case of thionine-TiO_2 system, the strong interaction between the dye and semiconductor leads to the static quenching of singlet excited state. However, in the absence of any direct interaction between the dye and semiconductor (e.g. thionine-ZnO system), triplet excited state can participate in the charge injection process.

3.2 Semiconductor-Semiconductor Systems:

By coupling a large bandgap semiconductor colloid with a short bandgap semiconductor colloid it should be possible to extend its photoresponse into the visible. The feasibility of this approach has been demonstrated with CdS-TiO_2 and several other semiconductor systems. Such systems not only extend the photoresponse into the

TF-128

visible but also improve the efficiency of charge separation (see Fig. 6). An enhancement in the efficiency of methyl viologen reduction has been observed upon increasing the colloidal TiO_2 content in a $CdS-TiO_2$ system.

We have recently made an effort to probe the charge transfer processes in colloidal $CdS-TiO_2$ system [23]. The interaction between the two colloidal semiconductor systems can be studied by monitoring the emission spectra. CdS colloids prepared in aceto-nitrile exhibit red emission at wavelengths greater than 550 nm. The red emission which arises as a result of sulfur vacancy can be readily quenched by electron acceptors such as thiazine dyes [31]. One would also expect to see quenching of CdS emission in a $CdS-TiO_2$ system if the interaction between the two semiconductor colloid results in the transfer of photogenerated electron from CdS to TiO_2. Figure 7 shows the dependence of CdS emission yield on the the concentrations of colloidal TiO_2 and AgI. Only a small amount of TiO_2 (or AgI) is sufficient to quench nearly 90% of the CdS emission. This raises the possibility of a single TiO_2 par-ticle being able to quench many excited CdS molecules . TEM analysis have confirmed that several of small size CdS particles (<50 Å) can interact with a single TiO_2 particle (~ 300 Å) and participate in the charge injection process [23].

Picosecond laser flash photolysis experiments were performed to probe the injected charge in TiO_2 colloids. The transient absorption spectra recorded immediately after 355-nm laser pulse excitation ($\Delta t = 0$ ps) are shown in Figure 8. The excitation of CdS colloids in the presence of TiO_2 colloids led to the transient

absorption in the region of 550-750 nm. These absorption features
matched well with the absorption of trapped electrons at the TiO_2
surface. The absorption spectrum of trapped charge carriers was
recorded separately by direct excitation of TiO_2 colloids with 266-
nm laser pulse. The absorption in the 550-760 nm region increased
with increasing concentration of colloidal TiO_2 as an increasing
amount of colloidal CdS interacted with TiO_2 colloids. No such
transient absorption was detected when CdS alone or TiO_2 alone was
excited with 355-nm laser pulse.

The trapping of charge carriers at the TiO_2 surface was com-
pleted within the laser pulse duration. This indicated that the
charge injection process from excited CdS into TiO_2 occurs with a
rate constant greater than 5×10^{10} s^{-1}. These trapped charge
carriers were also found to survive for a long period of time
(~ 1 μs). Charge transfer processes in other coupled semi-
conductors and semiconductor triads are currently being inves-
tigated.

3.3 Dye Sensitization of Coupled Semiconductors

In the earlier sections we described two modes of achieving
sensitization of large bandgap semiconductors with a dye and a
short bandgap semiconductor. The question now arises whether one
could incorporate both these principles and design a system such as
TiO_2-CdS-dye. Attachment of a red sensitive dye to the short band-
gap semiconductor would then extend the photoresponse of the large
bandgap semiconductor further into the red region. The principle
of such a configuration is illustrated in Figure 9.

III- /40

Figure 10(a) shows the emission spectra of thionine in the absence and presence of ZnO colloids. As described earlier (section 3.1.2) the ZnO colloids do not quench the emission of thionine. However, CdS colloids are able to interact with the dye thionine and quench its fluorescence emission. As can be seen in Figure 10(b), this quenching is partial, but the quenching efficiency increases if we add a small amount of ZnO colloids. Since ZnO colloids interact with CdS, the electrons injected from excited thionine into CdS would then migrate into ZnO colloids. This is indicated by the fact that quenching efficiency observed in the ZnO-CdS-thionine is greater than CdS-thionine system. These preliminary experiments demonstrate the feasibility of sensitizing coupled semiconductors with dyes. Rectification properties of coupled semiconductor system is expected to achieve better charge separation, thereby retarding the process of reverse electron transfer. Ultrafast charge transfer events associated with ZnO-TiO_2-thionine system are currently being investigated.

Conclusions

Ultrafast photochemical events associated with dye sensitization and short-bandgap semiconductor sensitization have been elucidated. The dye sensitization proceeds via singlet excited state when the dye interacts directly with the semiconductor surface. The participation of triplet excited state in the sensitization of a large bandgap semiconductor can be seen when the semiconductor-dye interaction is poor. Large bandgap semiconductors can also be sensitized with a short bandgap semiconductor and such

14

systems can also be coupled with red sensitive dyes to improve the overall efficiency of photosensitization.

Acknowledgment

III-142

15

References

1. Gerischer, H.; Willig, F. Top Curr. Chem. 1976, 61, 31.

2. Meir, H. Photochem. Photobiol. 1972, 16, 219.

3. Brachnou, E.; Vlachopoulos, N.: Grätzel, M. J. Chem. Soc., Chem. Commun. 1987, 68.

4. Vlachopoulos, N.; Liska, P.; Augustynski, J.; Grätzel, M. J. Am. Chem. Soc. 1988, 110, 1216.

5. De Silverstro, J.; Grätzel, M.; Kevan, L.; Moser, J. J. Am. Chem. Soc. 1985, 107, 2988.

6. Spitler, M.; Parkinson, B. A. Langmuir 1986, 2, 549.

7. Kamat, P. V.; Fox, M. A. Chem. Phys. Lett. 1983, 102 379.

8. Moser, J.; Grätzel, M. J. Am. Chem. Soc. 1984, 106 6559.

9. Kamat, P. V. J. Phys. Chem. 1989, 93 859.

10. Kamat, P. V.; Chauvet, J.-P.; Fessenden, R. W. J. Phys. Chem. 1989, 90, 1389.

11. Kalyansundaram, K.; Vlachopoulos, N.; Krishnan, V.; Monnier, A.; Grätzel, M. J. Phys. Chem. 1987, 91, 2342.

12. (a) Kirk, A. D.; Langford, C. H.; Joly, C. S.; Lesagi, R.; Sharma, D. K. J. Chem. Soc., Chem. Commun. 1984, 961; (b) Arbour, C; Sharma, D. K.; Langford, C. H. J. Phys. Chem. 1990, 94, 331.

13. Moser, J.; Grätzel, M.; Sharma, D. K.; Serpone, N. Helv. Chim. Acta 1985, 68, 1686.

14. Kamat, P. V. Langmuir 1990, 6, 512.

15. Kamat, P. V.; Das, S.; Thomas, K. G.; George, M. V. Chem. Phys. Lett. 1991, 178, 75.

IY-143

16

16. Rossetti, R.; Brus, L. E. J. Am. Chem. Soc. 1984, 106, 4336.

17. Umapathy, S.; Cartner, A. M.; Parkei, A. W.; Hester, R. J. Phys. Chem. 1990, 94, 8880.

18. Fessenden, R. W.; Kamat, P. V. Chem. Phys. Lett. 1984, 123, 233.

19. Kamat, P. V.; Gopidas, K. R.; Weir, D. Chem. Phys. Lett. 1986, 149, 491.

20. Gopidas, K. R.; Kamat, P. V. J. Phys. Chem. 1989, 93, 6428.

21. Ryan, M. A.; Fitzgerald, E. C.; Spitler, M. T. J. Phys. Chem. 1989, 93, 6150.

22. Gerischer, H.; Lübke, M. J. Electroanal. Chem. 1986, 204, 225.

23. Gopidas, K. R.; Bohorquez, M.; Kamat, P. V. J. Phys. Chem. 1990, 94, 6435.

24. Serpone, N.; Borgarello, E.; Grätzel, M. J. Chem. Soc., Chem. Commun. 1983, 342.

25. Spanhel, L.; Henglein, A.; Weller, H. J. Am. Chem. Soc. 1987, 109, 6632.

26. Spanhel, L.; Henglein, A.; Weller, H. Ber. Bunsenges. Phys. Chem. 1987, 91, 1359.

27. Henglein, A.; Gutierrez, M.; Weller, H. Ber. Bunsenges. Phys. Chem. 1989, 93, 593.

28. Rabani, J. J. Phys. Chem. 1989, 93, 7707.

29. Kamat, P. V. J. Photochem. 28, 513 (1985).

30. Spanhel, L.; Anderson, M. A. J. Am. Chem. Soc. 1991, 113, 2826.

31. Kamat, P. V.; Dimitrijević, N. M. J. Phys. Chem. 1987, 91, 396.

ZI-144

Figure Captions

Fig. 1: Schematic diagram illustrating the principle of dye sensi-
tization process.

Fig. 2: A. Absorption and B. emission spectra of 5 μM thionine in
acetonitrile containing (a) 0 M and (b) 0.45 mM colloidal
TiO_2.

Fig. 3: Transient absorption spectra recorded immediately ($\Delta t = 0$
ps) after 532-nm laser pulse excitation of 10 μM thionine
in 70% acetonitrile, 20% ethanol and 5% 2-propanol: (a) no
colloidal TiO_2 and (b) 1 mM colloidal TiO_2.

Fig. 4: Transient absorption spectra recorded 5 μs after 532-nm
laser pulse excitation of thionine (-o-) and thionine +
ZnO (-Δ-) in ethanol. Insert shows the dependence of
$TH^{2+\cdot}$ yield on the excitation intensity.

Fig. 5: Two possible modes of interaction between semiconductor
and the sensitizing dye.

Fig. 6: Sensitization of large bandgap semiconductor by coupling
it with a short bandgap semiconductor.

Fig. 7: Quenching of colloidal CdS emission by (a) TiO_2 and
(b) AgI colloids in acetonitrile ([CdS] = 2 mM).

Fig. 8: Transient absorption spectra recorded immediately after 355-nm laser pulse excitation of 0.75 mM CdS colloids in acetonitrile containing (a) 0, (b, 0.63 and (c) 1.75 mM TiO_2 colloids.

Fig. 9: Sensitization of a coupled semiconductor system with a dye.

Fig. 10: A. Emission spectra of 10 μM thionine in the presence and in the absence of ZnO colloids. B. Emission spectra of 10 μM thionine in acetonitrile (a) No colloids; (b) after adding CdS colloids to solution in (a); and (c) after addition of ZnO colloids to solution in (b).

III-146

Fig. 1

III-147

Fig 2

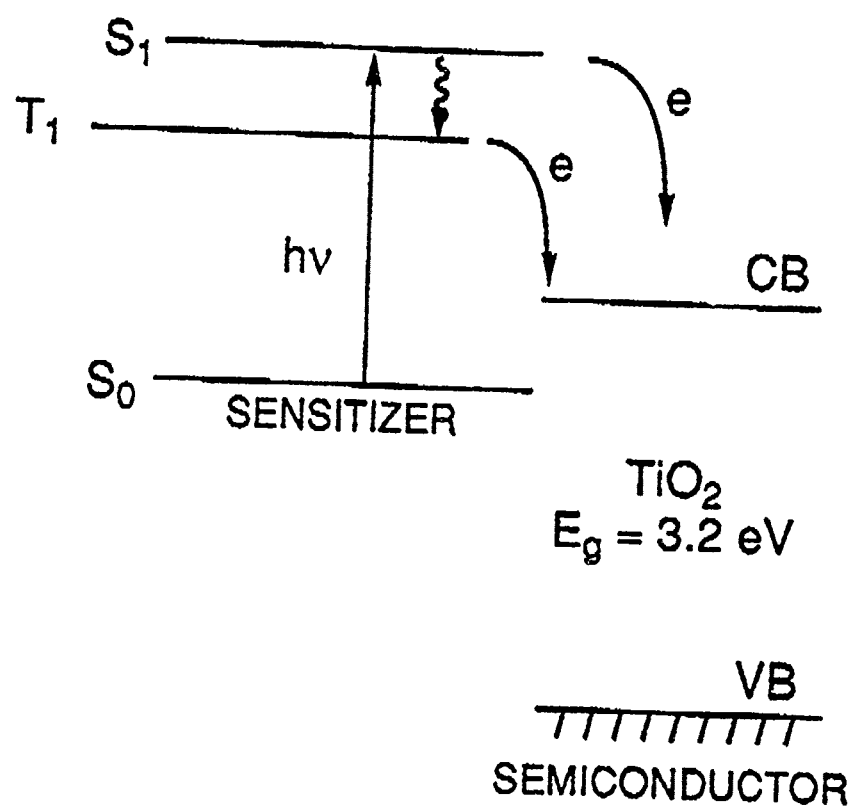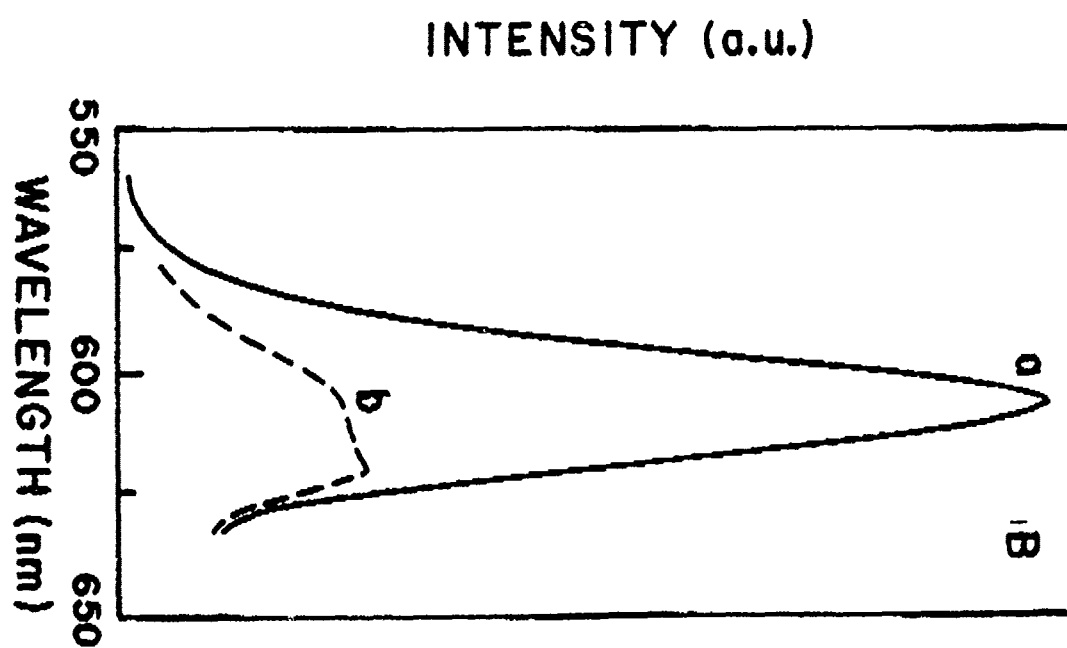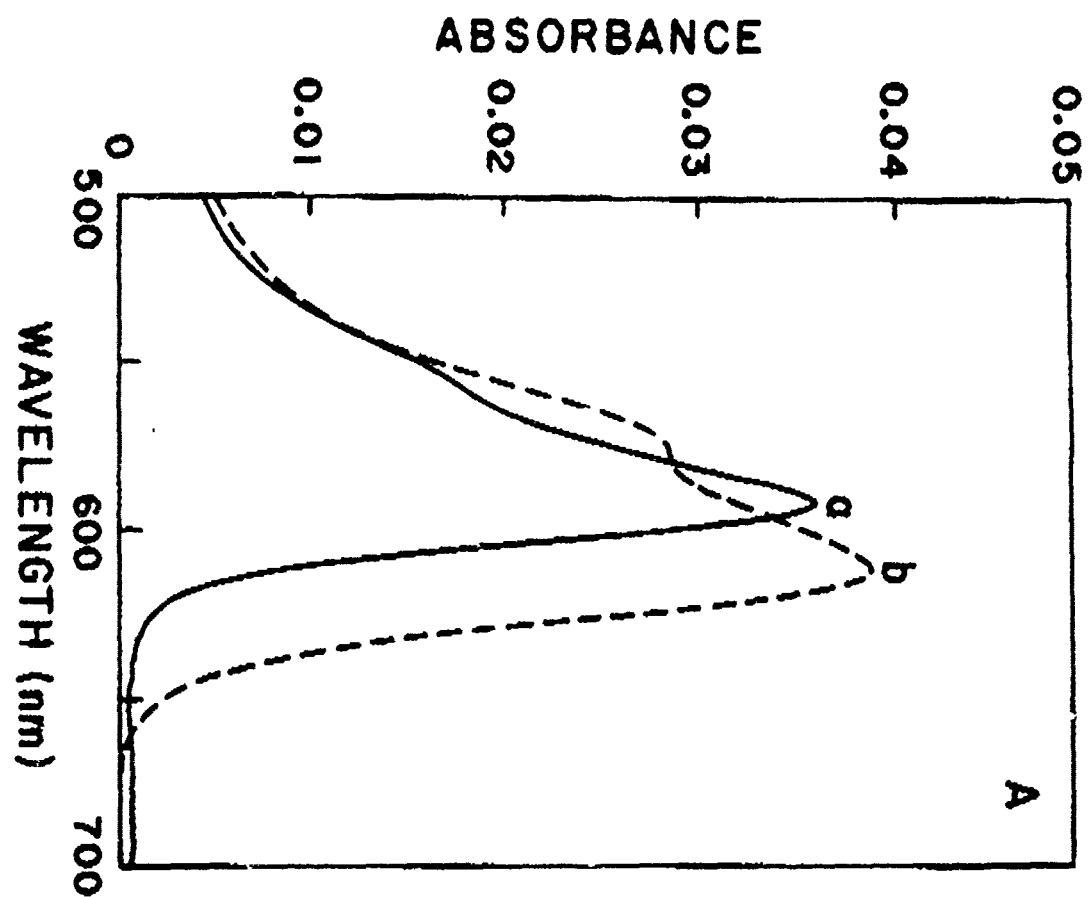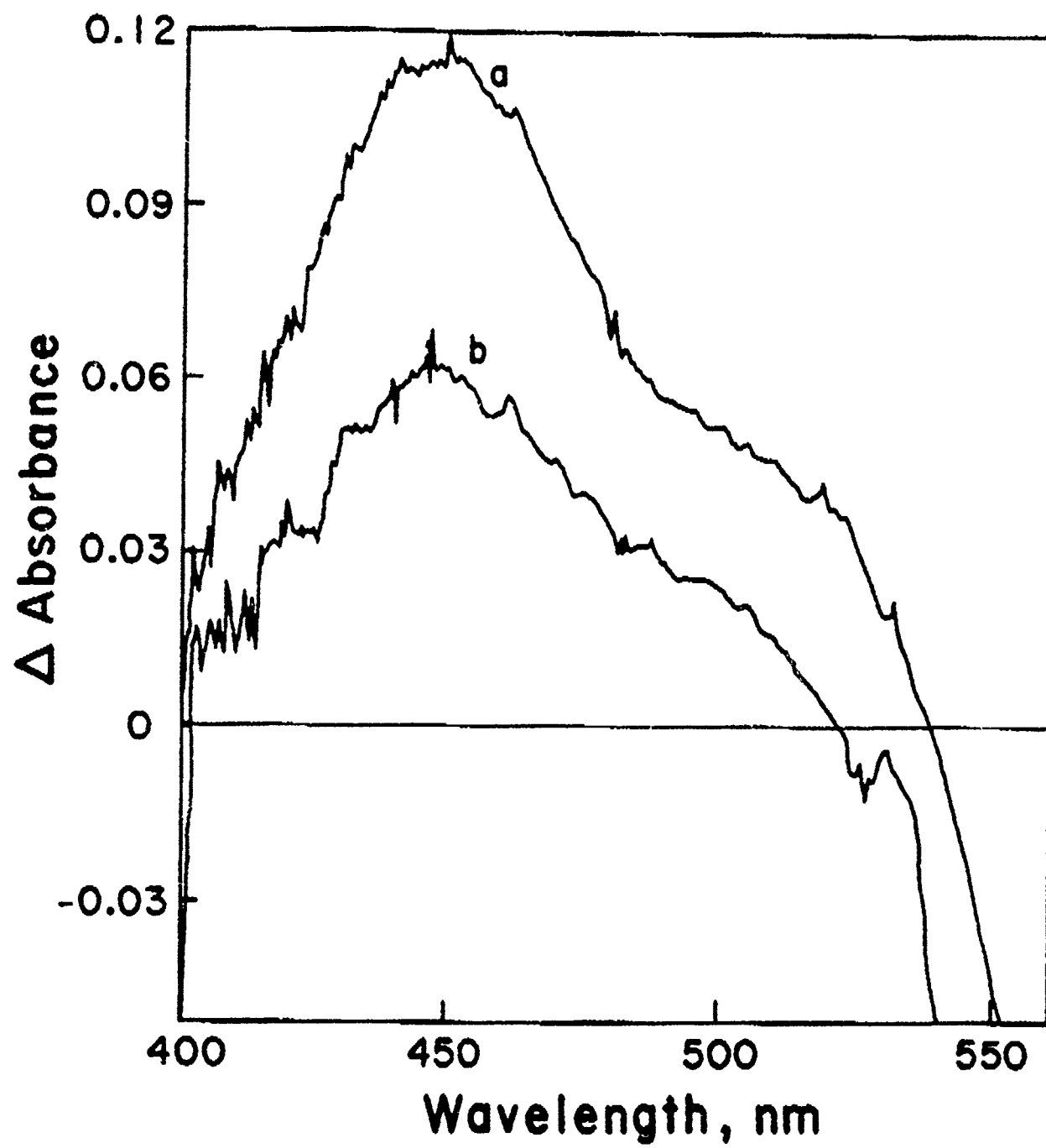III-148

Fig 3

III - 149

Fig. 4

III-15D

a. With Interaction/
Adsorption

b. With no direct
interaction

Fig. 5

Ⅳ-151

CdS   TiO$_2$

Fig 6

Ⅶ-152

Fig. 7
IV-153

III-151

Fig 8

Thionine – CdS – ZnO

Fig 9 Ⅲ-155

Fig 10

Ⅲ-156

(27) Diffusion- and Activation-controlled Photoredox Reactions Sensitised by
Colloidal Semiconductors

Andrew Mills*, P. Douglas, M. Garley, A. Green and G. Williams

Department of Chemistry, University College of Swansea,

Singleton Park, Swansea, SA2 8PP, U.K.

Abstract

The recent application of two specific but related kinetic models to
interpret the kinetics of photo-induced electron transfer between a
semiconductor and a redox agent, observed in μs flash-photolysis studies of
colloidal TiO_2 and CdS, is reviewed. A central feature of both kinetic
models is the assumption that the distribution of colloid particle sizes
fits a log-normal distribution law. The first kinetic model further
assumes that the electron-transfer reaction is activation-controlled, the
redox quencher is in large excess and that for any particle the rate
depends directly upon its surface area. The activation-controlled, log-
normal kinetic model can be used to interpret the complex kinetics observed
upon flash-photolysis of colloidal TiO_2 in the presence of methyl viologen
and, those for colloidal CdS in the presence of O_2 or Cd^{2+} ions. The
second kinetic model assumes that the electron transfer reaction is
diffusion-controlled and that the number of trapped electrons
photogenerated on a CdS particle directly after flash is much greater than
unity. The diffusion-controlled, log-normal kinetic model can be used to
interpret the very different to activation-controlled kinetics observed
upon flash-photolysis of colloidal CdS in the presence of methyl viologen
or methyl orange.

- 1 -

Ⅶ-/44

Ⅶ-/58

Introduction

The area of photoredox reactions sensitised by semiconductor dispersions
has attracted a great deal of attention over the last decade. In the early
eighties research centred on their use as sensitisers in solar to chemical
energy conversion systems, *eg.* for water splitting [1], or carbon dioxide
fixation [2]. Although work in this area continues, other research themes,
such as the use of semiconductor dispersions as photosensitisers in organic
synthesis [3], or water purification [4], have become increasingly
important. In this work, a better understanding of the processes involved
can be gained if the photoinduced redox reactions which occur at the
semiconductor-electrolyte interface can be monitored directly. In the case
of semiconductor powders this is often not possible. However, with
optically transparent semiconductor colloids, the fundamental reactions can
often be monitored using the well-established time-resolved techniques,
such as flash-photolysis [5], fluorescence [6] and resonance Raman
spectroscopy [7].

A number of studies have been carried using such techniques out on the
photochemistry of semiconductor colloids. In some cases it has proved
possible to observe one or more of the products of photo-induced electron
transfer from the semiconductor to the quencher, *eg.* reduced methyl
viologen ($MV^{\cdot+}$) in the flash photolysis of colloidal TiO_2 [8-10]. In other
cases, transient absorptions or bleachings have been assigned to trapped
photogenerated holes [8, 11, 12], or electrons [8, 13-16], *eg.* the photo-
induced transient bleaching in absorption spectrum of colloidal CdS has
been assigned to trapped photogenerated electrons [13-15]. On the whole,
however, most investigators have confined themselves to a qualitative

- 2 -

interpretation of the results of their time-resolved work and not attempted
a more rigorous interpretation of the often complex kinetics. In this
paper we review the recent and very successful use of a simple kinetic
model, developed initially for the interpretation of dispersed kinetics in
heterogeneous systems [16], in the analysis of the kinetics of the
transients generated upon flash-photolysis of colloidal semiconductor
dispersions, such as TiO_2 or CdS, in the presence or absence of various
redox quenchers [10, 13-16].

Colloid kinetics: some general points

In a large number of flash-photolysis studies of semiconductor colloids the
central photo-induced reaction often involves the transfer of electrons
from the colloidal particles to redox quenchers, *i.e.*

$$Q + e^- ---------> Q^- \qquad (1)$$

This process can be considered to occur *via* two stages, *i.e.* the diffusion
of Q to the colloidal particle, followed by the tranfer of an electron
across the semiconductor/electrolyte interface. The kinetics for this
sequence of events has been considered by several workers [17-19] and the
following expression has been derived for the overall bimolecular rate
constant for electron transfer

$$1/k_{obsd} = 1/k_{het} + 1/k_{diff} \qquad (2)$$

- 3 -

where, $k_{het} = k_{et}.4\pi r^2 L$ and $k_{diff} = 4\pi r L D$. The term k_{et} is the rate constant for the transfer of an electron from the conduction band of the semiconductor particle across the Helmholtz layer to Q and has units of m s^{-1}; L is Avogadros number and D is the sum of the diffusion coefficients for the CdS particle and Q, and, effectively, is the diffusion coefficient of Q, typically 10^{-9} m^2 s^{-1}.

If the overall electron transfer reaction is activation-controlled then $k_{et} \ll D/r$ and, therefore,

$$k_{obsd} = k_{het} = k_{et}.4\pi r^2 L \qquad (3)$$

From the Tafel equation, at 25°C,

$$\log(k_{et}/k_{et}^\circ) = -(1-\alpha).\eta/0.059 \qquad (4)$$

where k_{et}° is the rate constant when $\eta = 0$, α is the transfer coefficient (usually taken as 0.5) and η is the overpotential, i.e. the difference between the redox potential of the conduction band of the semiconductor and the Q/Q$^-$ couple

$$\eta = E_{CB}(SC) - E^\circ(Q/Q^-) \qquad (5)$$

Thus the value of k_{et} and, therefore, k_{obsd}, will depend upon the overvoltage available to drive the interfacial electron-transfer process.

If the overall electron transfer reaction is diffusion-controlled then $k_{et} \gg D/r$ and, therefore,

- 4 -

III - 160

$$k_{obsd} = k_{diff} = 4\pi r DL \qquad (6)$$

Given the large value for k_{diff} for most colloids (*eg*. $k_{diff} = 6.1\times10^{10}$ mol^{-1} dm^3 s^{-1} for colloid particles of 8 nm) it is often considered most likely that a photo-induced redox reaction, such as reaction (1), will be activation-controlled and, therefore, the bimolecular rate constant for the rate-determining step will be dependent upon particle area (see eqn. (3)) [9, 10, 13].

In typical flash-photolysis experiments involving TiO_2 or CdS colloids and methyl viologen as the redox quencher the number of moles of reduced methyl viologen photogenerated generated has usually been found to be much gre r than the number of moles of colloid particles, thereby implying that the average number of photogenerated electrons produced on flashing either colloidal TiO_2 or CdS is much greater than unity; typical values of 500 and 800 per average particle of TiO_2 and CdS, respectively, have been reported [10, 13]. Other relevant characteristics of the TiO_2 and CdS colloids which form the basis of this review are given in table 1 [20].

The number of moles of photogenerated electrons, δ, produced on flashing a semiconductor particle of radius r will depend in some way upon flash intensity, I. If a very efficient sacrificial electron donor is present it can be shown that δ would be $\propto$ I [10] whereas if charge recombination is the dominant process occuring within the flash then δ wil be $\propto I^{1/2}$ [14]. In addition, if the semiconductor particles are optically dilute, as is often the case, then the amount of light absorbed by a typical semiconductor particle (and, therefore, it value of δ) will be proportional to the volume of the particle ($= 4\pi r^3/3$).

It follows from the above arguments that directly after the flash,

$\overline{II} - 161$

i.e. at t=0, the total concentration of electrons photogenerated by *n* semiconductor particles of radius r will be given by [16]

$$[e^-]_o = K_1 r^3 I^\alpha n / V_6 \qquad (7)$$

where K_1 is a proportionality constant, V_6 is the volume of solution and α is the power term for flash intensity ($\alpha = 1$ for the TiO_2/PVA colloids, and $\alpha = \frac{1}{2}$ for the CdS/hexametaphosphate colloids). The term $K_1 r^3$ is = δ, the number of moles of photogenerated electrons on each of the *n* semiconductor particles of radius r directly after flash.

Simple activation-controlled kinetics and initial observations

If the semiconductor colloid was a monodispere and the interfacial electron transfer quenching reaction was activation-controlled, then at any time t the rate of reaction would be given by

$$-d[e^-]_t/dt = k_{et} 4\pi r^2 L[e^-]_t[Q] \qquad (8)$$

In the presence of a large excess of quencher the kinetics of reaction will be pseudo first-order and, therefore, the modified and integrated form of eqn (8) becomes

$$[e^-]_t = [e^-]_o \exp(-k_\alpha t) \qquad (9)$$

where k_α is the pseudo-first-order rate constant and is equal to $k_{et} 4\pi r^2 L[Q]$.

- 6 -

III-162

Detailed μs flash photolysis kinetic studies have been carried out on two different semiconductor colloids in particular, *i.e.* TiO_2 and CdS [10, 14-16], and different quenchers, but under conditions in which it was considered likely that the kinetics of photoinduced electron transfer would be activation-controlled. In the flash-photolysis of a TiO_2/PVA colloid using methyl viologen a quencher, the kinetics of MV^{+} were usually monitored [10, 16], whereas in the flash-photolysis of a CdS/hexametaphosphate colloid, using O_2 as a quencher, the kinetics of recovery of the CdS absorption spectrum were monitored (and assumed to provide a direct measure of the kinetics of photoinduced electron transfer) [14, 15]. In both cases a plot of the data in the form $\ln(\Delta A/\Delta A_{t=o})$ *vs.* t did not give a good straight line as expected for a simple first-order reaction and eqn (9). However, for each of the two different semiconductor systems the plots of the kinetic data derived from a series of experiments using the same conditions as before but in which the initial flash intensity was varied, when plotted in the form of $\ln(\Delta A/\Delta A_{t=o})$ *vs.* t, generated a series of superimposable curves which are illustrated in figs. 1 [10] and 2 [15]. The ability to superimpose these plots is typical of first-order kinetics even if the kinetics appear initially not to be first-order. In a higher order reaction, i.e. > 1, any increase in $\Delta A_{t=o}$ (initial absorbance change) would decrease the initial half-life thus making the $\ln(\Delta A/\Delta A_{t=o})$ *vs.* t plots non-superimposable.

Activation-controlled kinetics and the log-normal model

It is possible to rationalise the curved, normalised first-order plots of the observed data for TiO_2 and CdS colloids, illustrated in figs. i and 2,

- 7 -

respectively, by assuming not only that the reactions are activation-controlled, but also that the semiconductor colloids are polydispersed with a distribution in particle size adequately described by the log-normal distribution law, *i.e.*

$$n = \bar{n}.\exp(-x^2) \qquad (10)$$

and

$$\rho x = \ln(r/\bar{r}) \qquad (11)$$

where, n is the number of particles of radius r, $\bar{n}$ is the number of particles with the average radius $\bar{r}$, and ρ is a measure of the width of the distribution. The variation in the shape of the distribution as a function of ρ is illustrated in fig. 3.

It follows from eqns. (7) and (11) that for n particles of semiconductor of radius r, the concentration of electrons in the solution directly after flash, *i.e.* t=0, will be

$$[e^-]_{t=o} = K_2.\bar{r}^3.\exp(3\rho x).I^\alpha.\bar{n}.\exp(-x^2)/V_{\blacksquare} \qquad (12)$$

with the total concentration of photogenerated e$^-$'s given by

$$C_{t=o}(\text{Total}) = \sum_{x=-\infty}^{x=\infty} [e^-]_{t=o} \qquad (13)$$

In addition, the total concentration of e$^-$'s in the solution at any time, t, after the flash, *i.e.* C_t(Total), will be

III-169

$$C_t(\text{Total}) = \sum_{x=-\infty}^{x=\infty} [e^-]_t \qquad (14)$$

where, $[e^-]_t$ is given by

$$[e^-]_t = [e^-]_{t=0} \cdot \exp(-k_{e^-}4\pi[Q]L.\bar{r}^2.\exp(2\rho x)t) \qquad (15)$$

Using equations (12), (13), (14) and (15) it can be shown that

$$\theta_\tau = \frac{C_\tau(\text{Total})}{C_{\tau=0}(\text{Total})} = \frac{\displaystyle\sum_{x=-\infty}^{x=\infty} \exp(3\rho x).\exp(-x^2).\exp(-\tau.\exp(2\rho x))}{\displaystyle\sum_{x=-\infty}^{x=\infty} \exp(3\rho x).\exp(-x^2)} \qquad (16)$$

where,

$$\tau = k_{e^-}4\pi[Q]L.\bar{r}^2.t \qquad (17)$$

A useful parameter to introduce at this stage is ψ_τ, the ratio at time, τ, of the concentration of electrons per unit volume of solution due to *n* particles of semiconductor, of radius r, to the total concentration of electrons directly after flash, *i.e.* $\psi_\tau = [e^-]_{\tau, r}/C_{\tau=0}(\text{Total})$. Fig. 4 provides a typical illustration of the model predicted variation in ψ_τ as a function of time (τ) and $r/\bar{r}$ for ρ is = 0.75.

Fig. 5(a) illustrates a sectioned version of the same plot as fig. 4. Given that the area under each section in fig. 5(a), corresponding to a

- 9 -

particular τ value, is $= \theta_\tau$, it is possible, therefore, to plot θ_τ vs. τ for $\rho = 0.75$ or, for that matter, for any value of ρ, as illustrated by the modelled curves in fig. 5(b). Assuming the applicability of the kinetic model to the flash photolysis of semiconductor colloids, since τ and time are directly related, *via* eqn. (17), the parameter θ_τ has physical significance as it is equivalent to the normalised kinetic data at time t, *i. e.*

$$\Delta A_t / \Delta A_{o \; or \; \infty} = C_t(\text{Total})/C_{t=o}(\text{Total}) = C_\tau(\text{Total})/C_{\tau=o}(\text{Total}) \quad (18)$$

Thus, if the kinetic model is applicable, then the distribution width of the semiconductor colloid under investigation can be obtained by plotting $\Delta A_t / \Delta A_{t=o \; or \; \infty}$ *vs.* ln(t) and then matching up the curve obtained with a theoretical θ_τ *vs.* ln(τ) curve calculated for a certain value of ρ, such as one of those illustrated in fig. 5(b). After matching the two curves, at any common values of θ_τ and $\Delta A/\Delta A_{t=o}$ the rate constant for particles with the number average radius $\bar{r}$, *i. e.* $\bar{k}_Q$, can be obtained from the difference between the two x-co-ordinated (ln(τ) and ln(t), respectively), *i. e.*

$$\ln(\bar{k}_Q) = \ln(k_{\infty t} 4\pi[Q]L\bar{r}^2) = \ln(\tau) - \ln(t) \quad (19)$$

In fact, from the theoretical plots, for a wide range of ρ, it appears that when $\theta_\tau = \exp(-1)$, $\tau. \exp(3\rho^2) = 1$. Thus, for an observed kinetic trace, $\bar{k}_Q$ can be estimated *via* the expression

$$\bar{k}_Q = \exp(-3\rho^2)/t_{1/\infty} \quad (20)$$

- 10 -

where, $t_{1/e}$ is the time taken for $\Delta A_t / \Delta A_{t=0}$ or ⸱ to fall from 1 to exp(-1).

An important feature of this kinetic model is the curvature (with a positive deviation) in the first-order plots of the predicted, normalised kinetic data for moderate to large ρ values. The solid lines in figs. 1 and 2 correspond to the best fit model predicted curves for the TiO_2 and CdS colloids, respectively, using the ρ values given in table 1. In a very elegant piece of work Darwent *et al.* showed that the ρ values for two different TiO_2 colloids ($\bar{r}$ = 18 and 6 nm), given in table 1 and derived from kinetic data arising from their flash-photolysis in the presence of methyl viologen as the redox quencher and assuming the above, log-normal kinetic model, were in very close agreement to those predicted for the same colloids from dynamic light scattering experiments [10].

Probably the most important feature of the model is the predicted invariance in shape of the plot of θ_τ vs. τ as a function of flash intensity for any given ρ value. Thus, for a particular semiconductor colloid and, therfore, a set ρ value, the different kinetic traces obtained as a function of flash intensity, once normalised should be superimposable, according to the kinetic model. This feature was, of course, one of the most striking details associated with the flash-photolysis kinetic studies of the TiO_2 and CdS colloids [10, 14-16], as illustrated by the data contained in figs. 1 and 2, and thus provides confirmaton of the applicability of the kinetic model to these two semiconductor photosystems.

Diffusion-controlled kinetics and the log-normal model

In some recent work on the μs flash-photolysis of colloidal CdS using methyl viologen, or methyl orange, as a quencher [14, 15], the kinetics of

- 11 -

$ZII-II?$

recovery in CdS absorption spectrum appeared much faster than those usually found for activation-controlled reactions. In addition, the condition of superimposability for the normalised first-order plots of the kinetic data obtained as a function of flash intensity, which is usually assumed, *via* the kinetic model, as indicative of activation-controlled kinetics, was not satisfied as illustrated by the kinetic data contained in fig. 6 [15]. These results led us to develop the following diffusion-controlled, log-normal kinetic model which helps to provide a rationale [15].

For some reactions, involving photogenerated electrons and an added redox quencher, the rate of reaction will depend upon the rate of diffusion of the quencher to the semiconductor colloidal particles. Under these conditions, for a semiconductor particle of radius r, k_Q will depend directly upon its radius, *i.e.*

$$k_Q = k_{diff}.[Q] = 4\pi rDL[Q] \tag{21}$$

where k_{diff} is the diffusion-controlled rate constant for particles of radius r. If the number of electrons generated per semiconductor particle is $\gg 1$ then, for a diffusion-controlled reaction, the rate of loss of e^-'s on a CdS particle will be zero order with respect to the concentration of e^-'s on that particle. Thus, for n semiconductor particles of radius r, the rate of change in the number of moles of photogenerated e^-'s per unit volume of solution will be

$$d[e^-]/dt = k_{diff}[Q]n/V_mL = 4\pi D[Q]n/V_mN_A \tag{22}$$

Integration of this equation generates the following equation

- 12 -

$$[e^-]_t = [e^-]_{t=o} - 4\pi r D n t / V_\bullet \tag{23}$$

for $0 < t < [e^-]_{t=o} / (4\pi r D[Q] n / V_\bullet)$. Using eqns. (11) and (12) the above equation can be rewritten as

$$([e^-]_\tau) / ([e^-]_{\tau=o}) = 1 - \tau . \exp(-2\rho x) \tag{24}$$

where,

$$\tau = 4\pi D[Q] t / (\bar{r}^2 . K, I^\alpha) \tag{25}$$

For the full distribution of radii, equation (24) coupled with equations (13) and (14) yields the following:

$$\theta_\tau = \frac{C_\tau (total)}{C_{\tau=o} (Total)} = \frac{\sum\limits_{x=-\infty}^{x=\infty} \exp(3\rho x) . \exp(-x^2) . (1 - \tau . \exp(-2\rho x))}{\sum\limits_{x=-\infty}^{x=\infty} \exp(3\rho x) . \exp(-x^2)} \tag{26}$$

Since τ and the real time, t, for any decay trace are directly related, then the experimentally measurable quantity $\Delta A_t / \Delta A_{t=o}$ will be equal to θ_τ, i.e.

$$\theta_\tau = \Delta A_t / \Delta A_{t=o} \text{ or } \infty = C_t(Total) / C_{t=o}(Total) = C_\tau(Total) / C_{\tau=o}(Total) \tag{27}$$

Fig. 7 illustrates how, ψ_τ, the ratio of the concentration of electrons on the semiconductor particles, of radius, r, to the total concentration of electrons at time, τ, i.e. $\psi_\tau = [e^-]_{\tau, x} / C_\tau(Total)$, varies with τ and $r/\bar{r}$, for $\rho = 0.75$. Once again, the area under the ψ_τ vs. $r/\bar{r}$ curve at any time,

- 13 -

$$\text{III} - 169$$

τ, is θ_τ, which is proportional to $C_\tau(\text{Total})/C_{\tau=0}(\text{Total})$. Thus, at $\tau = 0$, $\theta_\tau = 1$ and at $\tau = \infty$, θ_τ is zero. Fig. 8(a) illustrates a sectioned version of the 3D peofile illustrated in fig. 7 and fig. 8(b) illustrates the plot of θ_τ vs. $\ln(\tau)$ for ρ values from (a) 1 to (e) 0 in steps of 0.25. One way in which the the distribution width of the CdS colloid, ρ, may be found is to plot $\Delta A_t/\Delta A_{t=0}$ vs. $\ln(t)$ and to match up the curve obtained with a theoretical θ_τ vs. $\ln(\tau)$ curve, calculated for a certain value of ρ, such as one of those illustrated in fig. 8.

The rate constant for particles with the number average radius $\bar{r}$ is $\bar{k}_{Q\star}$, where

$$\bar{k}_{Q\star} = 4\pi D[Q]/(\bar{r}^2 . K_1 I^\alpha) = \tau/t \qquad (28)$$

Once the experimental decay data has been plotted in the form $\Delta A_t/\Delta A_{t=0}$ or $\_$ vs. $\ln(t)$ and matched up with a theoretical curve for a particular value of ρ, of the type illustrated in fig. 8, then $\bar{k}_{Q\star}$ may be determined by the difference between the $\ln(\tau)$ and $\ln(t)$ values, since, from equation (28), $\ln(\tau) - \ln(t) = \ln(\bar{k}_{Q\star})$.

We have already seen that for an activation-controlled reaction the $\Delta A_t/\Delta A_{t=0}$ vs. time profiles will be independent of flash intensity and the plots will be superimposable, since τ, is independent of I. However, for a diffusion-controlled reaction τ and, therefore, $[e^-]_t/[[e^-]_{t=0}$, will be dependent upon I^α, via equations (12) and (23). As a result, the predicted different plots of θ_τ (and, therefore, $\Delta A_t/\Delta A_{t=0}$) vs. time τ (or, t) for the different flash intensities should not be superimposable. In practical terms the rate constant for the decay of $[e^-]$ will appear to decrease with increasing I, i.e. the time-scale of the decay will appear to increase with

- 14 -

increasing flash intensity. This predicted behaviour in kinetics provides a good description of the observed kinetics for the colloidal CdS-methyl viologen (or methyl orange) photosystem (see fig. 6). However, according to the diffusion-controlled, log-normal model although the plots of $\ln(\Delta A_t / \Delta A_{t=o})$ vs. t will not be superimposable, plots of $\ln(\Delta A_t / \Delta A_{t=o})$ vs. ln(t) will be superimposable and this prediction is confirmed for the kinetics of the CdS-methyl viologen system, as illustrated by the plot in fig. 9 [15].

Conclusion

Activation-controlled, and diffusion-controlled, log-normal kinetic models can be used to interpret the kinetics for interfacial electron transfer, observed upon flashing colloids of TiO_2 and CdS in the presence of a variety of different electron acceptors. Table 1 summarises the major findings reported revealed using the appropriate log-normal kinetic model to analyse data arising from different flash photolysis studies carried out on colloidal TiO_2 and CdS. Both log-normal kinetic models are likely to find increasing application as more semiconductor photosystems are investigated. In this respect, the recent application of the activation-controlled, log-normal model in the analysis of the kinetics of photooxidation of thiocyanate, sensitised by a TiO_2 powder dispersion and monitored by diffuse reflectance spectroscopy appears to be a particularly important recent development [21].

Acknowledgement

- 15 -

$III - 171$

References

(1)   Kalyanasundaram, K.; Grätzel, M; Pelizzetti <u>Coord. Chem. Rev.</u> 1986, <u>69</u>, 57-125.

(2)   Halmann, M. In<u>Energy Resources through Photochemistry and Catalysis</u>, Grätzel, M., Ed.; Academic Press, New York, 1983, pp 507-534.

(3)   Fox, M-A. <u>Proc. Electrochem. Soc.</u> 1988, <u>88-14</u>, 9-15.

(4)   Matthews, R. In <u>Photochemical Conversion and Storage of Solar Energy</u>: Pelizzetti, E.; Schiavelo, M., Eds., Kluwer Academic Publishers: Dordrecht; pp 427-450.

(5)   Henglein, A.; Kumar, A.; Janata, E.; Weller, H. <u>Chem. Phys. Lett.</u> 1986, <u>132</u>, 133-136.

(6)   Kuczynski, J.P.; Milosavljevic, B.H.; Thomas, J.K. <u>J. Phys. Chem.</u> 1983, <u>87</u>, 3368-3370.

(7)   Metcalfe, K.; Hester, R.E. <u>J. Chem. Soc., Chem. Commun</u> 1984, 90-92.

(8)   Bahnemann, D.; Henglein, A.; Lilie, J.; Spanhel, L. <u>J. Phys. Chem.</u> 1984, <u>88</u>, 709-711.

(9)   Duonghong, D.; Ramsden, J.; Grätzel M. <u>J. Am. Chem. Soc.</u>, 1982, <u>104</u>, 2977-2985.

- 16 -

III-172

References (contd.)

(10) Brown, G. T.; Darwent, J. R.; Fletcher, P. D. I. <u>J. Am. Chem. Soc.</u>, 1985, <u>107</u>, 6446-6451.

(11) Dimitrijevic, N. M.; Kamat, P. V. <u>J. Phys. Chem.</u> 1987, <u>91</u>, 396-401.

(12) Kamat, P. V.; Dimitrijevic, N. M. <u>J. Phys. Chem.</u> 1989, <u>93</u>, 4259-4263.

(13) Albery, W. J.; Brown, G. T.; Darwent, J. R.; Saievar-Iranizad, E. <u>J. Chem. Soc., Faraday Trans. 1</u> 1985, <u>81</u>, 1999-2007.

(14) Mills, A.; Douglas, P.; Williams, G. <u>J. Photochem. Photobiol., A: Chem.</u> 1989, <u>48</u>, 397-417.

(15) Mills, A.; Green, A.; Douglas, P. <u>J. Photochem. Photobiol., A: Chem.</u> 1990, <u>53</u>, 127-137.

(16) Albery, W. J.; Bartlett, P. N.; Wilde, C. P.; Darwent, J. R. <u>J. Am. Chem. Soc.</u> 1985, <u>107</u>, 1854-1858.

(17) Albery, W. J.; Bartlett, P. N. <u>J. Electroanal. Chem.</u> 1982, <u>139</u> 57-68.

(18) Grätzel, M. and Frank, A. <u>J. Phys. Chem.</u> 1982, <u>86</u>, 2964-2967.

(19) Spiro, M.; Freund, A. J. <u>J. Chem. Soc., Faraday Trans. 1</u> 1983, <u>79</u>, 1649-1658.

- 17 -

References (contd.)

(20)   Moser, J; Grätzel, M. <u>J. Am. Chem. Soc.</u> 1983, <u>105</u>, 6547-6555.

(21)   Draper, R.B.; Fox, M.A. <u>J. Phys. Chem.</u> 1990, <u>94</u> 4628-4634.

Ⅶ-174

Colloid Characteristics

	TiO$_2$	CdS
method of preparation	TiCl$_4$ hydrolysis (ammonia [5], or cold water [20])	Cd(ClO$_4$)$_2$ + Na$_2$S [14]
typical concentration	5×10^{-4} (mol dm^{-3})	5×10^{-4} (mol dm^{-3})
support	PVA (M$_r$ 72000) (0.1 w/v %)	sodium hexametaphosphate (5×10^{-3} mol dm^{-3})
average particle radius	18 nm (ammonia) or 6 nm (cold water) (dynamic light scattering [10])	8 nm (electron microscopy [14])
particle size* distribution (ρ)	0.55 (18 nm) or 0.9 (6 nm)	0.9-1.0

*: determined from an analysis of the flash-photolysis kinetic data using the activation-controlled (TiO$_2$ [10]) or diffusion-controlled (CdS [14,15]), log-normal models and methyl viologen as the quencher.

Table 2: Quenching Rate Constants and Activation Energies*

Quencher	$\bar{k}_{het}$ (/M^{-1} s^{-1})	$\bar{k}_{diff}$ (/M^{-1} s^{-1})	E_a (/kJ mol^{-1})
TiO_2 [10]			
MV^{2+}	1.8×10^6 (18 nm)	–	–
MV^{2+}	1.0×10^6 (6 nm)		
CdS [14, 15]			
O_2	3.8×10^4	–	82 ± 6
Cd^{2+}	3.0×10^4	–	–
MV^{2+}	–	1.1×10^{11}	21 ± 1
methyl orange	–	2.1×10^{10}	19 ± 1

*: arising from an analysis of the kinetics using either the activation-controlled, log-normal model (gives $\bar{k}_{het}$) or the diffusion-controlled, log-normal model (gives $\bar{k}_{diff}$) [10, 14, 15].

$\bar{k}_{het}$: heterogeneous rate constant for the number average particle.

$\bar{k}_{diff}$: diffusion-controlled rate constnat for the number average particle.

III-176

Figure Legends

(1) Typical time profiles for a TiO_2 colloid ($r = 18$ nm), showing electron transfer to methyl viologen for a range of flash intensity with the final concentration of $MV^{\cdot+}$ = (●) 0.4, (■) 1.2, (O) 2.4, and (▲) 4.8×10^{-c} mol dm^{-3}. Reprinted with permission from Brown, G.T.; Darwent, J.R.; Fletcher, P.D.I. J. Am. Chem. Soc., 1985, 107, 6446-6451. Copyright 1985 American Chemical Society.

(2) Transient decay curves recorded using different flash energies on a colloid of CdS containing ascorbic acid (10^{-2} mol dm^{-3}) as the sacrificial electron donor and O_2 as the quencher (1.3×10^{-4} mol dm^{-3}). The decay curves are plotted in the form of $-\ln(\Delta A_t / \Delta A_{t=0})$ vs. t. The flash energies used were as follows: ● 28 J, O 61 J, ▲ 113 J, ■ 153 J, Δ 200 J. The solid line is a plot of $\ln(C_\tau(Total)/C_{\tau=0}(Total))$ vs. t, calculated using eqn (11) of the 'first-order' model for $\rho = 1.0$ and t (ms) = 90.τ. Reprinted with permission from Mills, A.; Douglas, P.; Williams, C. J. Photochem. Photobiol., A: Chem. 1989, 48, 397-417. Copyright 1989 Elsevier Sequoia S.A.

(3) Log-normal distributions predicted using eqns. (10) and (11) for the following ρ values: (a) 0, (b) 0.5, (c) 1 and (d) 2.

(4) Activation-controlled, log-normal model: calculated variation of ψ_τ (= $[e^-]_{\tau,r}/C_\tau(Total)$) with τ, for $\rho = 0.75$ using eqns. (13) and (15).
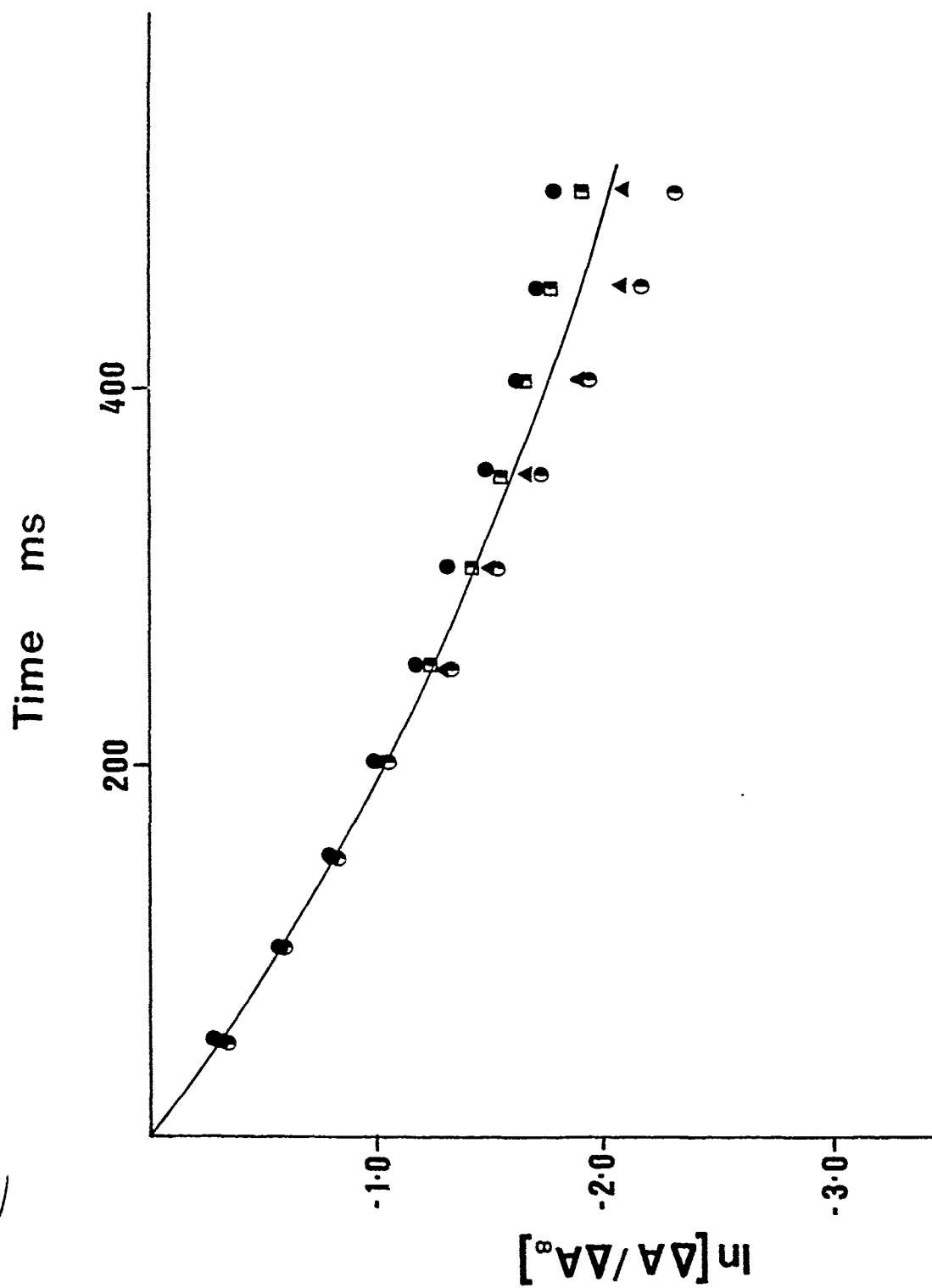
IV-177

(5) (a) Sectioned version of the plot in fig. 4 and (b) subsequent plots of θ_τ vs. τ for ρ = (a) 1, (b) 0.75, (c) 0.5, (d) 0.25 and (e) 0 calculated for the activation-controlled, log-normal model.

(6) Transient decay curves recorded using different flash energies on a colloid of CdS containing cysteine (10^{-2} mol dm^{-3}) as the sacrificial electron donor and methylviologen as the quencher (10^{-6} mol dm^{-3}). The decay curves are plotted in the form of $\ln(\Delta A_t/\Delta A_{t=o}$ vs.$)$ t. The flash energies used were as follows: Δ 32 J, o 66 J, $\blacktriangle$ 105 J, $\bullet$ 145 J, $\blacksquare$ 200 J. Reprinted with permission from Mills, A.; Green, A.; Douglas, P. J. Photochem. Photobiol., A: Chem. 1990, 53, 127-137. Copyright 1990 Elsevier Sequoia S. A.

(7) Diffusion-controlled, log-normal model: calculated variation of ψ_τ (= [e$^-$]$_{-,\tau}$ C_τ(Total) with τ, for ρ = 0.75 using eqns. (13) and (23).

(8) (a) Sectioned version of the plot in fig. 4 and (b) subsequent plots of θ_τ vs. $\ln(\tau)$ for the following values of ρ: (a) 1, (b) 0.75, (c) 0.5, (d) 0.25 and (e) 0 calculated for the diffusion-controlled, log-normal model.
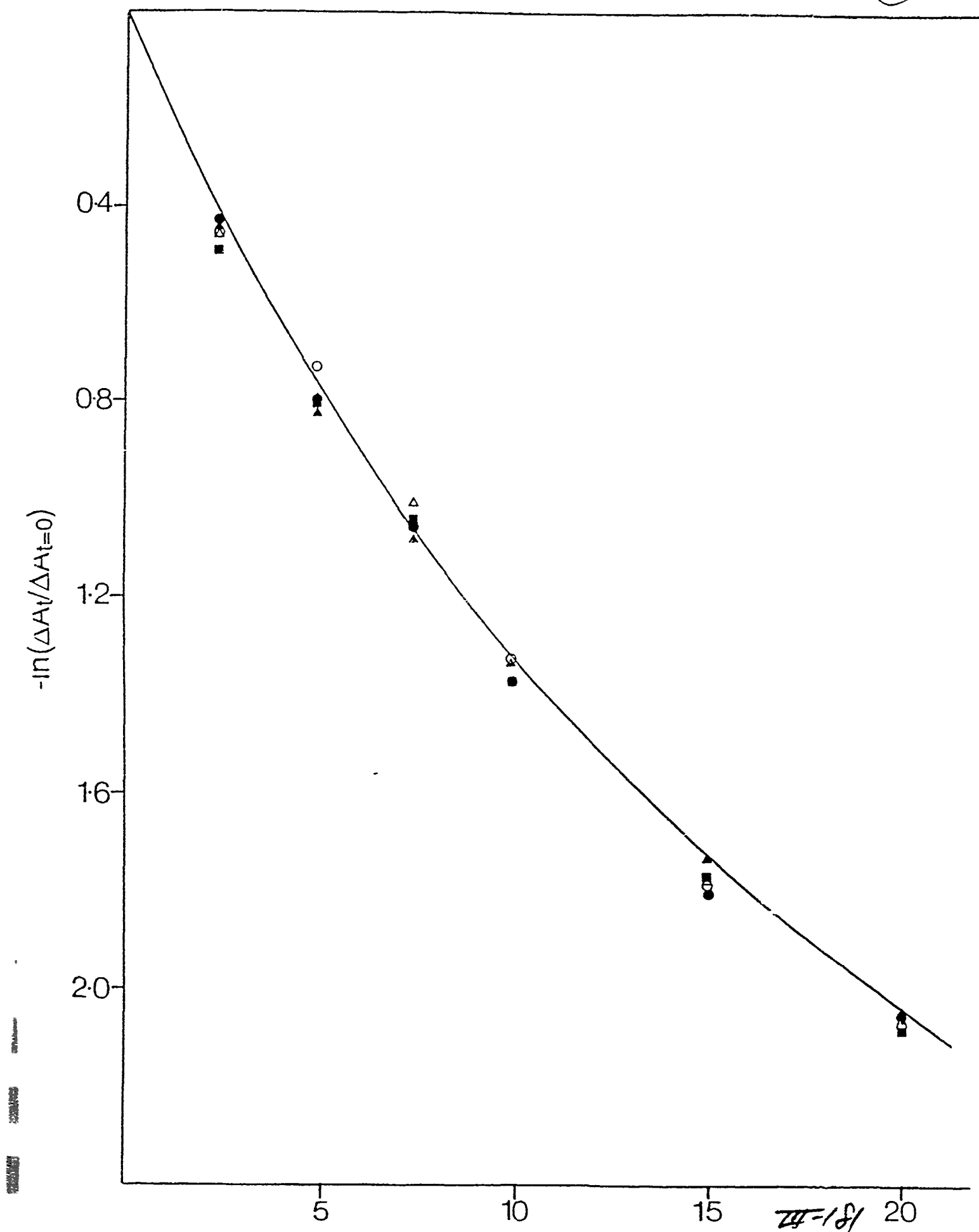
Figure Legends (contd.)

(9)   Same transient decay data as illustrated in fig. 6 but plotted in the form
of $\Delta A_t/\Delta A_{t=o}$ *vs.* $\ln T$ (or $(x + \ln t)$ where $x = \ln\{4\pi D[Q]/(\bar{r}^2 K_1 I^{1/2})$; see eqn
28).   The solid line is a plot of C_T(Total)$/C_{T=o}$(Total) *vs.* $\ln T$,
calculated using eqn (26) of the diffusion-controlled, log-normal kinetic
model for $\rho = 0.9$.   Reprinted with permission from Mills, A.; Green, A.;
Douglas, P. J. Photochem. Photobiol., A: Chem. 1990, 53, 127–137.
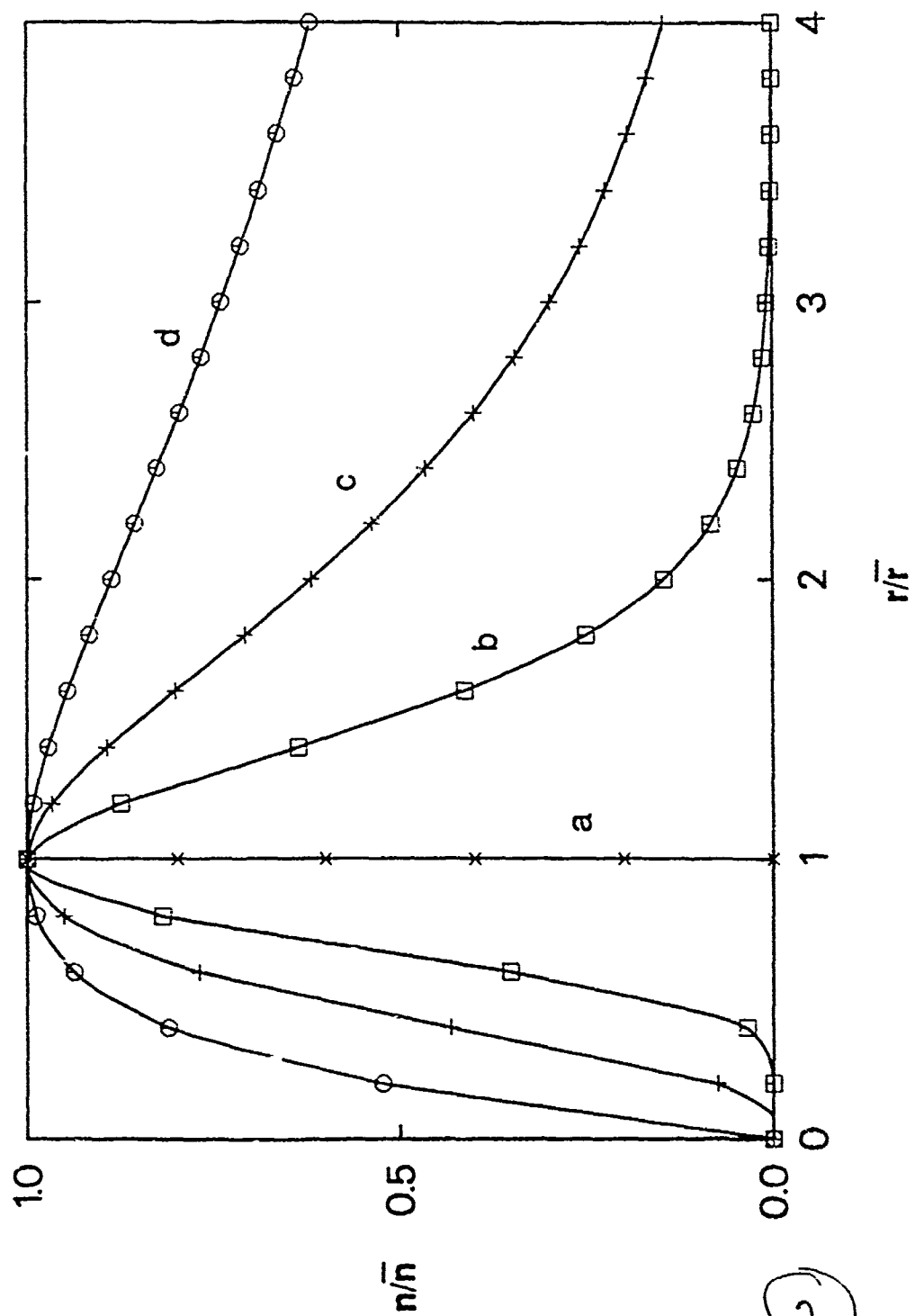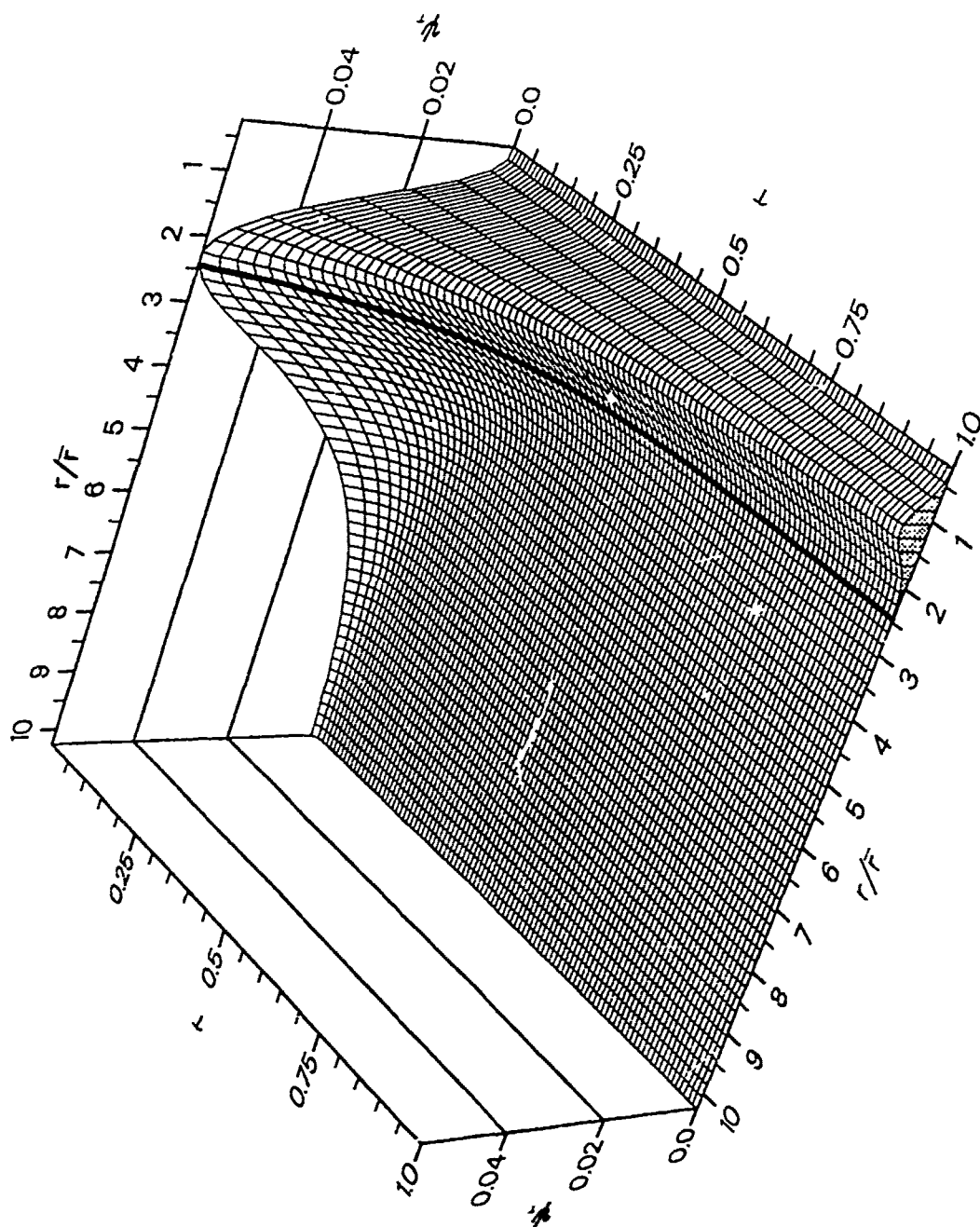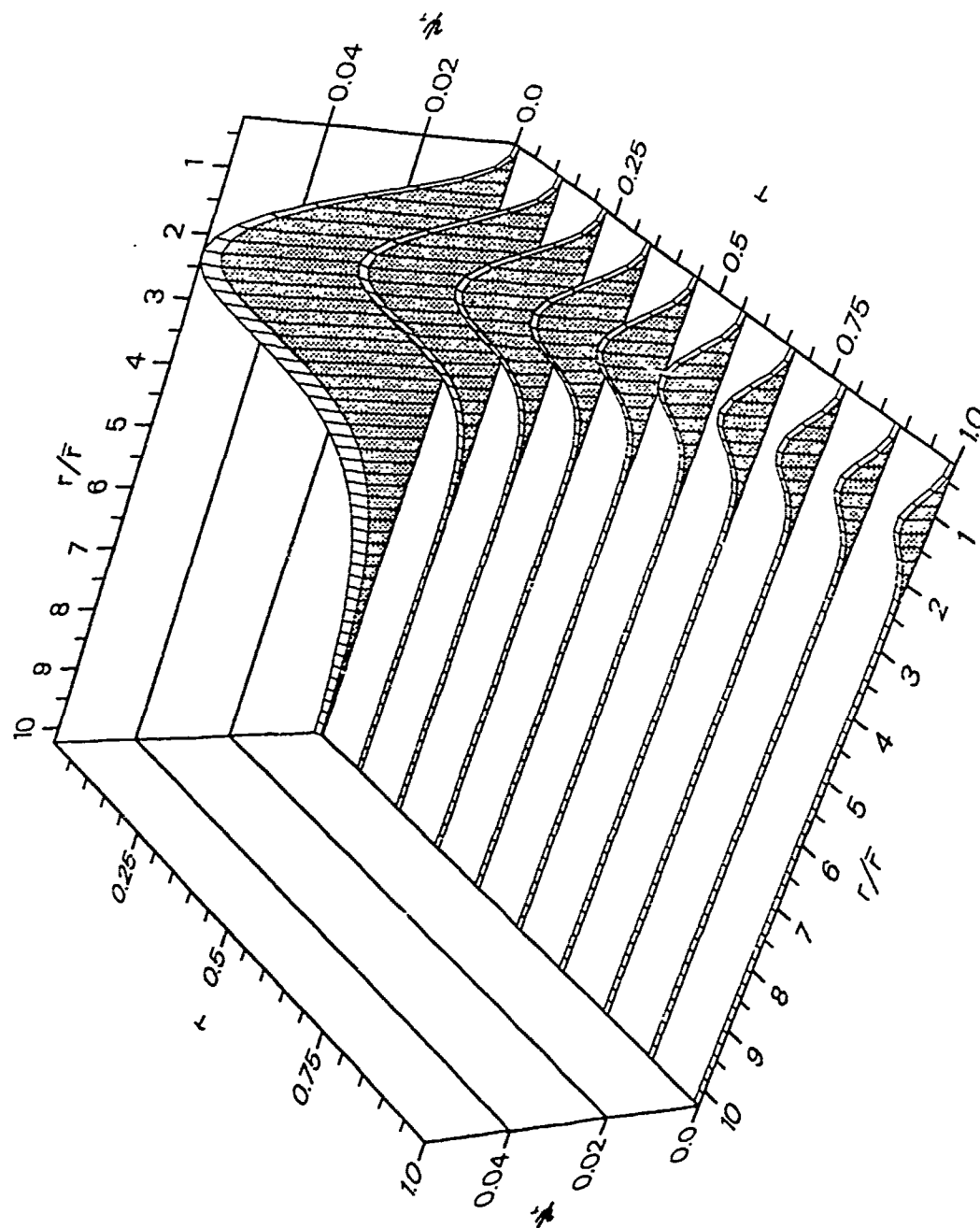Copyright 1990 Elsevier Sequoia S. A.

Ⅶ-184

(5a) Fig 5a

Fig. 56.

III-185

Fig. 8a

Fig. 8b

$\ln(\tau)$

θ_T

$\Pi - 189$

Fig. 9.

INFLUENCE OF SURFACE PROPERTIES ON CHARGE CARRIER DYNAMICS OF QUANTIZED SEMICONDUCTOR COLLOIDS

Olga I.Mićić, Tijana Rajh, and Mirjana V.Čomor

Boris Kidrič Institute, Vinča, P.O.Box 522, 11001 Belgrade, Yugoslavia

1

XII-191

ABSTRACT. Electron transfer reactions between different electron donors end metal chalcogenide semiconductor colloidal particles were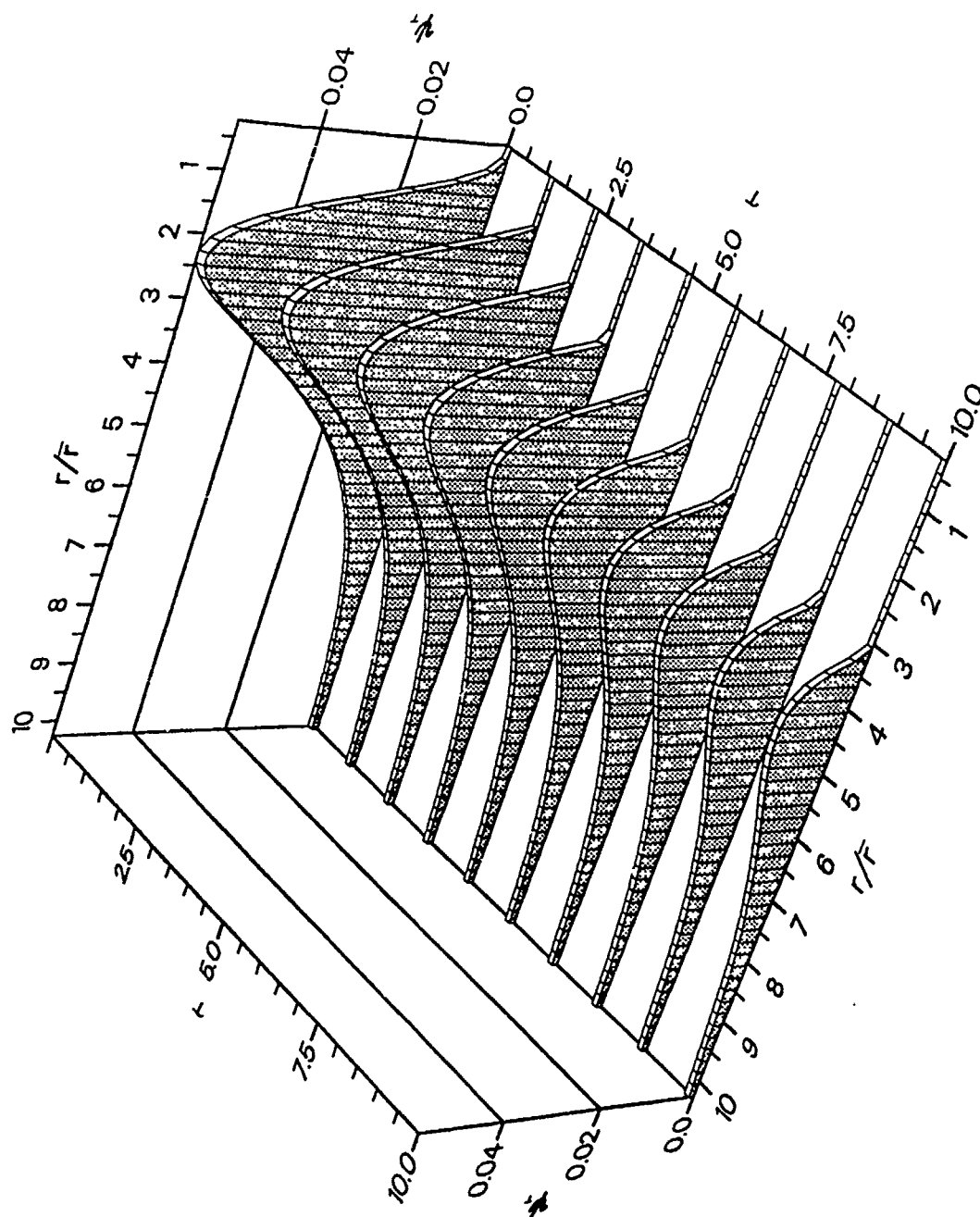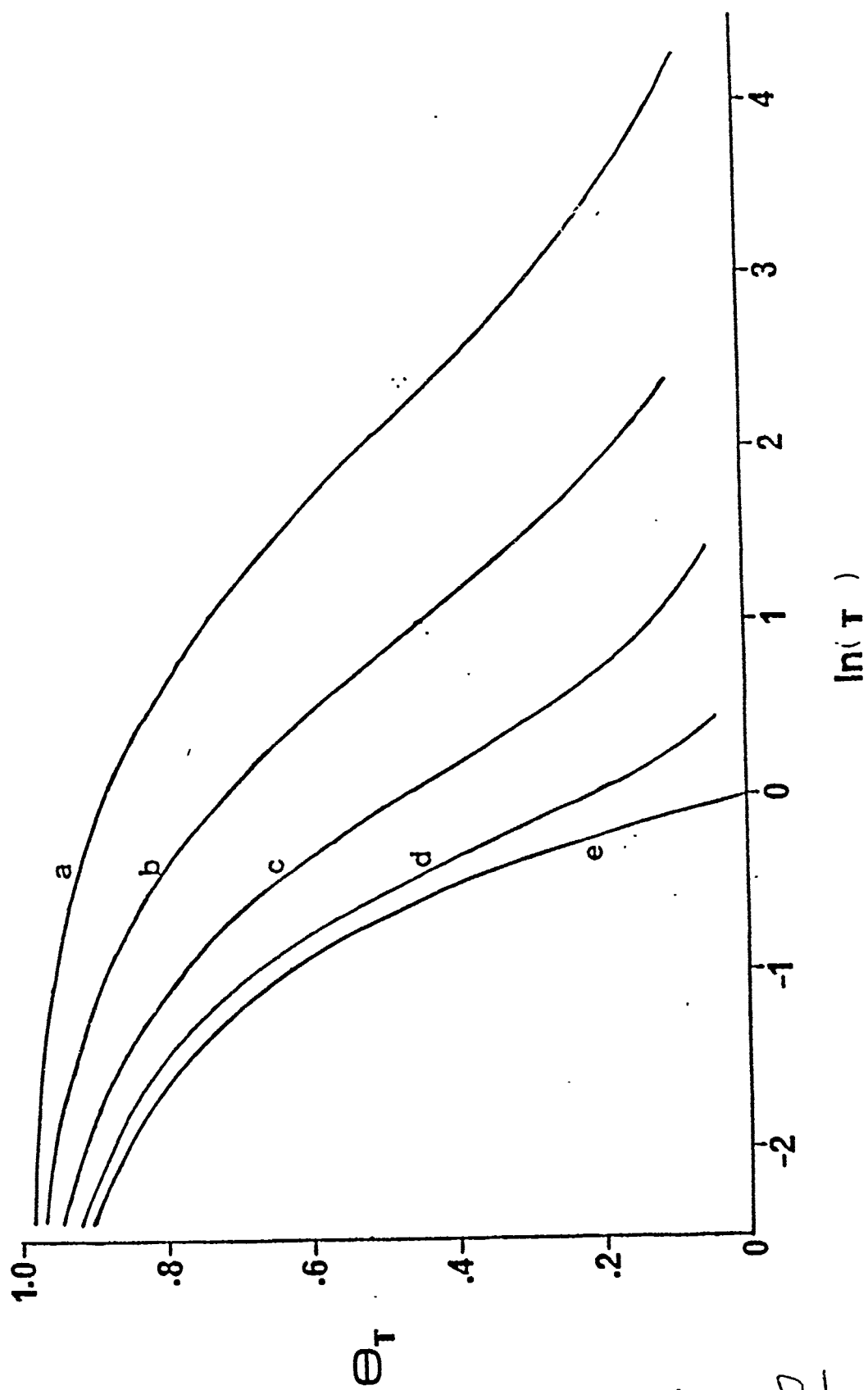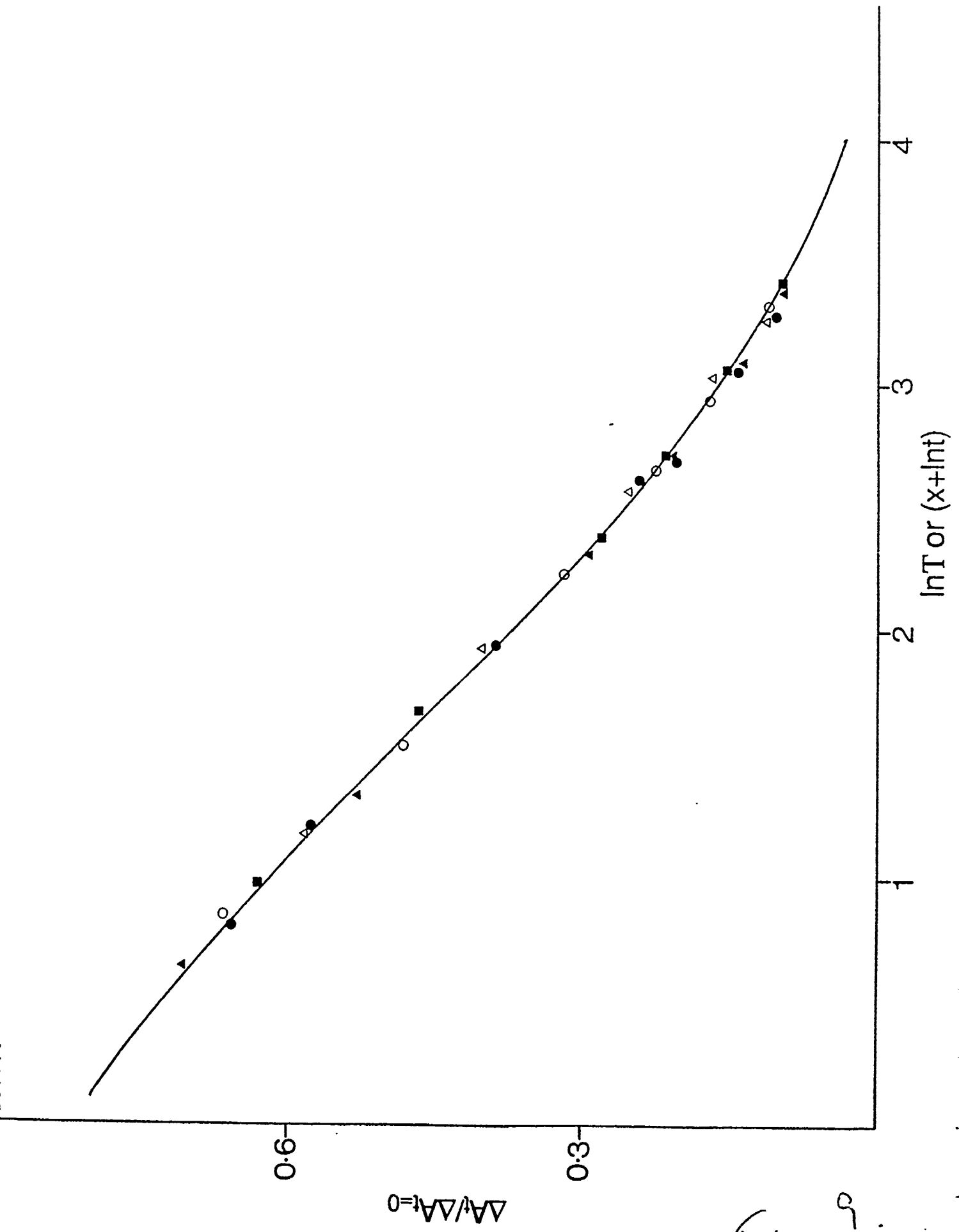 studied by the pulse radiolysis technique. Equilibrium concentrations of the reactants were exploited to derive the potential of the lowest empty electronic state of the quantized semiconductor colloids. For metal chalcogenide particles which contain a small number of molecules in microcrystallites, empty coordination sites at the crystal boundaries can be filled by OH⁻ or other complexing agents. This kind of chemical modification of the surface affects the nature and density of the trapped sites on the surface. Electron transfer reactions from hydrous titanium oxides to different strong oxidizing agents such as SO_4^-, OH and Tl^{2+} were also studied. Different spectroscopic properties were found for OH and hole adducts of hydrous titanium oxides in the alkaline colloidal solution. The potentials of holes located in mid-gap levels of TiO_2 colloids were determined in solutions of different pH.

INTRODUCTION

In recent years there has been much interest in the nature of nanometer-scale semiconductor particles that exhibit quantization effects (1-4). Due to the confinement of the electron and hole in small clusters the physical and chemical properties are appreciably modified from their bulk behaviour. Of particular interest is their ability to enhance photoredox chemistry (5). A large increase of several eV in the effective band gap in quantized particles leads to an undesirable inherent instability of the particles, since cathodic and anodic corrosion potentials have new positions relative the band edges; the cathodic corrosion potential lies below the lowest empty electronic state and the anodic above the highest filled state. Information about the energy levels of the semiconductor particles in the solution can be obtained by studying interfacial charge transfer reactions in these microheterogeneous systems (6,7).

III - 182

2

In this work the pulse radiolysis technique was used to study the chemical reaction on the surface. Radicals produced by the pulse radiolysis can accept or donate electrons to the semiconductor particles. The potentials of the lowest empty electronic state of a number of quantized metal chalcogenide particles was determined. Hole injection into titanium hydrous oxide colloids was also studied.

REDOX DEGRADATION POTENTIAL OF EXTREMELY SMALL PARTICLES

The physical nature of the particles prevents the investigation of the electronic energy levels by impedance measurements such as have been used for single crystal semicond··.tor electrodes. Radiation chemical processes, however, enable the electronic energy levels in the particulate semiconductor to be determined, since transient species with strong negative redox potentials can be created in the solutions, resulting in a charge transfer between the redox couple and the semiconductor particles:

$$M^{(n-1)+} + coll \longrightarrow M^{n+} + (e^-)coll \qquad (1)$$

In reaction (1), $(e^-)coll$ represents electrons injected into the semiconductor colloid. $M^{(n-1)+}$ is produced by the radiation chemistry processes following the electron pulse, and electron transfer to the colloids is followed via transient spectrophotometry.

In the presence of the $M^{n+}/ M^{(n-1)+}$ couple, the lowest available energy level in the particle equilibrates in time with the redox potential of the couple. This potential is a measure of the reducing power of the semiconductor material, and is related to the electron affinity of the semiconductor and the charge density at the surface.

The potential of the particles, $E(e^-)coll$, and that of the solution are equilibrated.

III-193

$$E(e^-)coll = E^\circ(M^{n+}/M^{(n-1)+}) + 0.059 \log\{[M^{n+}]/[M^{(n-1)+}]\} \qquad (2)$$

For large particles at equilibrium this potential should be equal to the Fermi-level potential of the particles (7,8). Although identity is only valid if the particles retain the band structure of the bulk material, it is generally accepted that semiconductor particles with relatively large effective masses and with diameters above 50 Å do exhibit bulk properties (1).

The quantized particles have no conduction and valence states near the Brillouin zone center, which is associated with long range cristallinity (9). For these particles the potential of the lowest empty electronic state is equilibrated with the redox couple in the solution; all bulk and surface traps that lie below this state are filled. The lowest empty electronic state of quantized colloids was determined by observing which redox couples could inject electrons into the semiconductor particles. The results are summarized in Figure 1, which shows the redox couples studied and the deduced positions of the empty electronic states for CdTe (10), CdSe (11), CdS (12), PbSe (5), HgSe (5) and PbS (13). In this figure, only redox couples above the indicated energy levels of the measured semiconductors could inject electrons into the respective colloids; the uncertainty in the electronic energy levels of the semiconductors is also indicated in the figure.

Size quantization in small particles creates energy levels that lie above the corrosion level. All colloids presented in Figure 1, with exception of 40-Å PbS, undergo cathodic corrosion by injection of electrons. For 40-Å PbS the redox potential of a particle was found to be -0.07 V (vs.NHE) which is more positive than the cathodic corrosion potential of PbS, -0.91 V (vs. NHE).

We chose zwitterionic viologen radicals, ZV⁻(E° = -0.37 V), to determine the position of the lowest empty electronic states of 40-Å PbS. For example, the variation of redox potential with the concentration of injected electrons is shown in Figure 2. The density of the electrons

III-194

in our experiments (10^{19}-10^{21} e$^-$/cm^3) is sufficiently large to fill all bulk and surface traps that lie below the band edge. At the same time, trapped electrons slightly increase the band gap (14,9), which we observed as band edge movement in the cathodic direction.

EXCESS CHARGE ON QUANTIZED PARTICLES

The nature of the electrons injected into the semiconductor colloids is of general interest. In large particles, electrons move freely in the conduction band. However, in quantized particles the situation is different since the exciton only is formed and this is trapped as an electron/hole pair at random positions on the particle surface (9). Excess electrons or holes which are injected into particle are also localized at different defect sites on the surface. On the other hand, the methods used for preparation of extremely small particles usually create high densities of defects and disorder on the surface as well as imperfection in lattice. Corrosion processes on the semiconductor begin with localization of electrons or holes at defect sites on surface. In order to suppress corrosion and non- radiative recombination it is important to block the defect sites on surface and to allow the excitonic recombination to occur.

The semiconductor CdTe is a promising material for use in optoelectronics (16). We prepared quantized CdTe colloidal particles with a very sharp excitonic peak (Figure 3, curve a) in the presence of thiol which is a complexing agent for Cd^{2+} ions (15). The colloids were prepared in two different ways and have the onset of absorption shifted towards the UV region. The absorption spectrum with sharp peak (Curve a) is associated with 35 Å particles, prepared in the presence of thiols. For these colloids partial passivation with thiols and OH$^-$ ions can be achieved and luminescence with a high quantum yield of 0.2 was observed. Some ions which are strongly bound to surface can cover defect sites on the surface. In very small particles containing a small number of molecules, empty coordination sites at the crystal boundaries are filled by
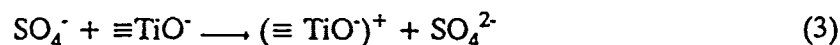
5

species present in the environment. For example, CdTe particles with the cubic zinc blende structure and a diameter of 35 Å contain 90 cell units and about 250 cadmium atoms on surface, which can be bound by species present in the solution. In an alkaline medium, the small OH⁻ ions can enter the crystal faces and bind to these sites. As a result, the layer of cadmium hydroxide on the CdTe surface removes the surface sites at which non-radiative recombination of charge carriers takes place, increases the luminescence quantum yield and shifts the emission towards higher energy. It was found for CdS (14), PbS (13) and CdTe (10) colloids that long-lived bleaching created by trapped charge disappeared in alkaline solution. However, CdTe particles with a diameter of about 35 Å are very sensitive to corrosion due to large shifts in the position of the lowest empty electronic state to a very negative value grater then -1.9 V (Figure 1) which favours the reductive corrosion process. The formation of free cadmium atoms by injection of excess electrons into 20-Å CdTe was observed in pulse radiolysis experiments (10). The first step involves an intermediate state which equilibrates with the level of lowest empty electronic state that is a precursor to a second- step reduction of CdTe to Cd^0.

HOLE INJECTION INTO TiO_2 COLLOIDS

Hole injection into semiconductor particles was observed via interfacial electron transfer from titanium oxide colloids to strong oxidizing agents. We chose titanium oxide because it has good properties for the photooxidation of a wide variety of organic and inorganic substrates (17). SO_4^-, OH and Tl^{2+} were used as oxidizing agents because of their large positive redox potentials. SO_4^- is an oxidizing radical with a potential $E(SO_4^-/SO_4^{2-}) = 2.4$ V (vs. NHE) (18) which is even higher than that of OH radical [$E(OH/OH^-) = 1.9$ V (vs. NHE)] (19). In a solution of 2.75×10^{-3} M TiO_2 (average diameter 25 Å, particle concentrationt ~1.2×10^{-5} M) at pH 10, SO_4^- radicals inject holes directly into particles. The transparent solution of TiO_2 with

a particle size of 25 Å in water shows a small spectral blue-shift which corresponds to a band gap of 3.4 eV, slightly higher than the 3.2 eV for bulk anatase TiO_2. Bahnemann et al. (20) found that these small particles also have the anatase titanium dioxide structure. It is known that hydrous titanium oxide is slightly soluble in water (21). However, in neutral and alkaline solutions the reaction of monomers or low weight aggregates of titanium hydroxide is negligible since the particle concentration is higher. In acidic solution (pH < 3), the concentration of TiO^{2+} ions and oligomers is higher than the concentration of particles, and they can also react with oxidizing radicals (22).

In neutral and alkaline solutions hydroxylated TiO_2 is dissociated on the surface as $\equiv TiO^-$

$$SO_4^- + \equiv TiO^- \longrightarrow (\equiv TiO^-)^+ + SO_4^{2-} \tag{3}$$

$$(\equiv TiO^-)^+ \longrightarrow \equiv TiO \tag{4}$$

Brown and Darwent (23) assumed that surface radicals $\equiv TiO$ are formed during photooxidation of colloidal TiO_2. This radical should also be formed by he reaction of the SO_4^- radical. The reaction of SO_4^- with TiO_2 is very fast and we obtained $k_3 = 3.75 \times 10^{10}$ $M^{-1}s^{-1}$ at pH 10, which is very close to the rate predicted for diffusion-controlled reactions. In these experiments the concentration of SO_4^- species was 2.7×10^{-6} M and, on average, every fifth particle reacts with one hole. However, the transient absorption spectrum is the same even when two holes react with one particle. Figure 4a ʳhows the broad absorption spectrum of the transient formed by the SO_4^- reaction, which has an onset at about 460 nm and rises steeply towards the UV region. This absorption spectrum shows a slight blue shift if compared with the spectrum for trapped holes reported by Henglein and co-workers (24) and obtained by flash photolysis, but it is in close agreement with the spectrum for the product of the OH reaction with TiO_2 at pH 3 (25). The same absorption spectrum as that in Figure 4a was found at pH 3 and 6. We also found

7

that the absorption spectrum is not sensitive to the method of the colloid preparation. However, the halflife of the transient decay was found to be of poor reproducibility due to the difficulty of strictly controlling the surface chemistry during the colloid preparation. Halflife ranging from tens of microseconds to several milliseconds were observed, depending on the mode of colloid preparation.
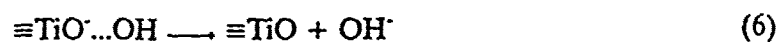
Figure 4b shows the absorption spectrum of the hydroxyl adduct which formed in the reaction of OH radicals with titanium hydrous oxide at pH 10. The initial absorption spectrum, observed 10 μs after the pulse, has a band in the visible wavelength range with a maximum at 620 nm. It can be seen that the OH adduct has a completely different absorption spectrum than that of the hole adduct formed in the SO_4^- reaction.

We assume that OH can be added as a ligand at one of the vacant position of the $\equiv TiO^-$ groups on surface.
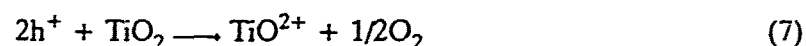
$$OH + TiO^- \longrightarrow \equiv TiO^-...OH \qquad (5)$$

The observed growth in the absorption yields $k_5=1.8 \times 10^{10}\ M^{-1}s^{-1}$.

The transient absorption shown in Figure 4b changes in a complex manner in time. For the absorption spectrum with a maximum at 620 nm two transients with different kinetics ($\tau_{1/2}$ = 25 μs and 160 μs) are probably responsible for resulting decay at 620 nm. The transient with $\tau_{1/2}$ = 350 μs which absorbs below 460 nm is very similar to the absorption of the product formed in the reaction of SO_4^- with TiO_2.

$$\equiv TiO^-...OH \longrightarrow \equiv TiO + OH^- \qquad (6)$$

III-198

However, the absorption below 460 nm is very weak and precise identification of the product is very difficult. Here again the decay lifetimes are poorly reproducible due to difficulty to strictly controlling the surface chemistry. Completely different decay rates were obtained when $Ti(ClO)_4$ was replaced by $TiCl_4$ as the starting material for the preparation of TiO_2. All decay processes are significantly slower (~millisecond) in the presence of Cl^- ions ($2x10^{-2}$ M). Both OH and SO_4^- reactions with TiO_2 lead to anodic dissolution of TiO_2 ($E_D^0 = 1.4$ V vs. NHE).

$$2h^+ + TiO_2 \longrightarrow TiO^{2+} + 1/2O_2 \qquad (7)$$

The position of the level in which holes can be injected into the 25-Å TiO_2 colloid was determined by observing which redox couples could accept electrons from the semiconductor particles. These results are summarized in Figure 5 which shows the redox couples studied and the deduced position of the highest electronic filled state of TiO_2 colloids. Only oxidizing species whose potential is below the indicated energy levels could accept electrons from the colloids. Thus, for example SO_4^-, and Tl^{2+} can inject hole, where as Br_2^-, $(SCN)_2^-$ and I_2^- radicals cannot do that. The OH radical and the $TlOH^+$ ion reacts with TiO_2 to form an OH adduct which can in the presence of H^+_{aq} at pH 3, be transformed to a product that is the same as that formed in the SO_4^- reaction. The pH variation of the valence band edge of the bulk anatase TiO_2 is also presented in Figure 5. This variation shows a normal protonic equilibrium that occurs on oxide surfaces in aqueous solution. It can be seen that the 25-Å titanium hydrous oxide has a less positive potential than the TiO_2 anatase crystal. The photoelectrochemistry of the bulk anatase TiO_2 has been interpreted in terms of the classical band model which was originally developed for highly ordered macrocrystallline materials. This treatment is not valid for small colloids which have a large surface to bulk ratio and surface states may therefore be especially important in the interpretation of the photoelectrochemical behaviour of colloids. The intermediate state

9

III-199

where hole injection occurs lies in mid-gap level. This intermediate state equilibrates relatively rapidly with oxidizing agents and then provides holes at a slower rate for the oxidation step of TiO_2 (reaction (7)).

REFERENCES

1. Brus, L.E. J.Chem.Phys. 1983, 79, 5566; J.Chem.Phys. 1984, 80, 4403; J.Phys.Chem. 1986, 90, 2555.

2. Rossetti, R.; Elison, J.L.; Gibson, J.M.; Brus, L.E. J.Chem. Phys. 1984, 8, 4464.

3. Fojtik, A.; Weller, H.; Koch, U.; Henglein A. Ber. Bunsenges.Phys.Chem. 1984, 88, 969; Weller, H.; Koch, U.; Gutierrez, M.; Henglein , A. ibid., 1984, 88, 4464.

4. Nozik, A.; Williams, F.; Nenadovic, M.; Rajh, T.; Micic, O.I. J.Phys.Chem. 1985, 89, 397; Micic, O.I.;Nenadovic, M.T.; Peterson, M.W.; Nozik, A. J. J.Phys.Chem.1987, 91, 1295.

5. Nedeljkovic, J.M.; Nenadovic, M.T.; Micic, O.I.; Nozik, A.J. J.Phys.Chem. 1986, 90, 12

6. Duonghoung, D. ; Ramsden, J.; Gratzel, M. J.Am.Chem.Soc. 1982, 104, 2977

7. Dimitrijevic, N.M. ; Savic, D.; Micic,O.I.; Nozik, A.J. J.Phys.Chem. 1984, 88, 4278.

8. Nenadovic, M.T.; Rajh, T.; Micic, O.I.; Nozik, A.J. J.Phys.Chem. 1984, 88, 5827.

9. Wang, Y.; Suna, A; McHugh, J.; Hilinski,E.F.; Lucas, P.A.; Johnson, R.D. J.Chem.Phys. 1990, 92, 6927.

10. Comor, M. I.; Micic, O.I.; Nozik, A.J. to be published.

11. Dimitrijevic, N.M. J.Chem.Soc.Faraday.Trans.I 1987, 83, 1193.

12. Kamat, P.V.; Dimitrijevic, N.M.; Fessenden, R.W. J.Phys. Chem. 1987, 91, 396.

13. Nenadovic, M.T.; Comor, M.I.; Vasic, V.; Micic, O.I. J.Phys.Chem. 1990, 94, 6390.

14. Henglein, A.; Kumar, A.; Janate, E.; Weller, H. Chem. Phys.Lett. 1986, 132, 133.

15. Hayes, D.; Micic, O.I.; Nanadovic, M.T.; Swayambunathan, V.; Meisel, D. J.Phys.Chem. 1989, 93, 4601.

16. Esch, V.; Fluegel, B.; Khitrova, G.; Gibbs, H.M.; Jiajin, Xu.; Kang, K.; Koch, S.W.; Liu, L.C.; Risbud, S.H.; Peyghambarian, N. Phys.Rev.B 1990, 42, 7450.

11

II-201

17. Serpone, N.; Ah-Zou. J.K.; Harris, R.; Pelizzetti, E.; Hidaka, H. Sol. Energy 1987, 39, 491.

18. Stanbury, D.M. Adv.Inorg.Chem. 1989, 33, 69.

19. Schwardz, H.A.; Dodson, R.W. J.Phys.Chem. 1984, 88, 3643.

20. Kormann, C.; Bahnemann, D.W.; Hoffmann, M.R. J.Phys.Chem. 1988, 92, 5196.

21. Baes, Jr.C.F.; Mesmer, R.E. The Hydrolysis of Cations, John Wiley & Sons, New York, 1976, p. 147.

22. Rajh, T.; Saponjic, Z.M.; Micic, O.I. to be published.

23. Brown, G.T.; Darwent, J.R. J.Phys.Chem. 1984, 88, 4955.

24. Bahnemann, D.; Henglein, A.; Lilie, J.; Spanhel, L. J.Phys.Chem. 1984, 88, 709.

25. Lawless, D.; Serpone, N.; Meisel, D. J.Phys.Chem. 1991, in press.

LEGEND TO FIGURES

Figure 1. Energy level diagram for equilibration of quantized metal chalcogenide semiconductor particles with redox couple potentials in aqueous solution.
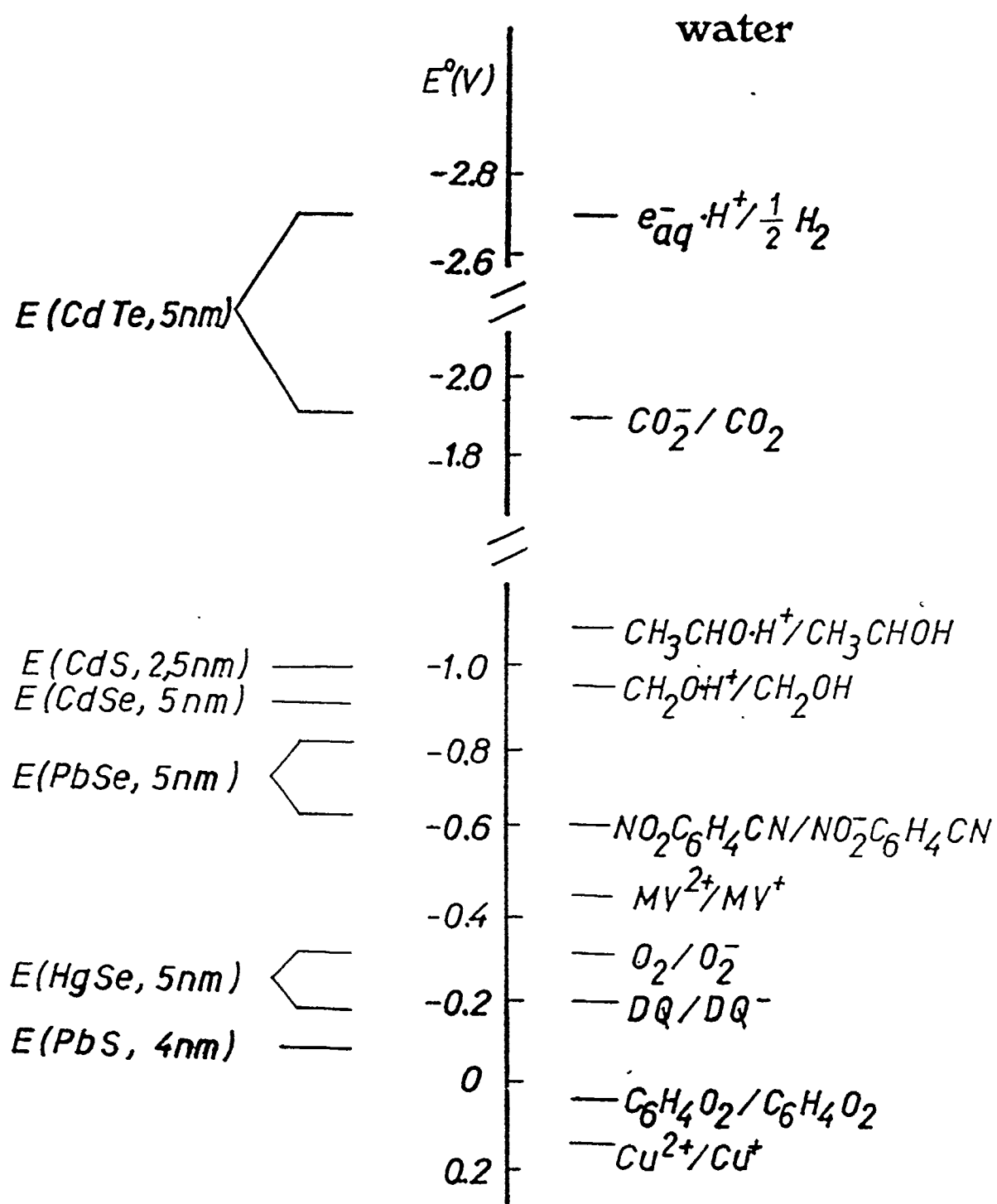
Figure 2. Redox potential of PbS colloids as a function of electron number injected into particles. Solutions contained 0.1 M 2-propanol, $5x10^{-3}$M ZV, and PbS colloids with different concentrations: ($\bullet$) $4.5x10^{-4}$M, ($\blacktriangle$) $3.5x10^{-4}$ M, (x) $2x10^{-4}$M. and (o) 1×10^{-4} M. The concentration of ZV^- was $2.2x10^{-6}$ - $7.2x10^{-5}$ M.

Figure 3. Absorption and emission spectra of CdTe colloids. (a) $2x10^{-4}$ M CdTe prepared in the presence of 3-mercapto- 1,2 propanediol, $5x10^{-4}$ M hexamethaphosphate, pH=10 and excess of cadmium ions; (b) $2.5x10^{-4}$ M CdTe in the presence of 0.1% poly(vinyl alcohol).

Figure 4. (a) Absorption spectrum of excess holes on titanium hydrous oxide measured in argon saturated solution of TiO_2 ($2.75x10^{-3}$M) at pH 10 in the presence of $5x10^{-3}$M $Na_2S_2O_8$ and 0.01 M tert-butanol after 10 μs. The concentration of SO_4^- was 2.8×10^{-6}M. (b) Absorption spectrum of OH adduct of titanium hydrous oxide measured in N_2O saturated solution of TiO_2($2.75x10^{-3}$M) at pH 10 and different times after the pulse. The concentration of OH was $1.1x10^{-5}$ M.

Figure 5. Energy level diagram for equilibration of 25-Å TiO_2 with redox couple potentials in aqueous solution.
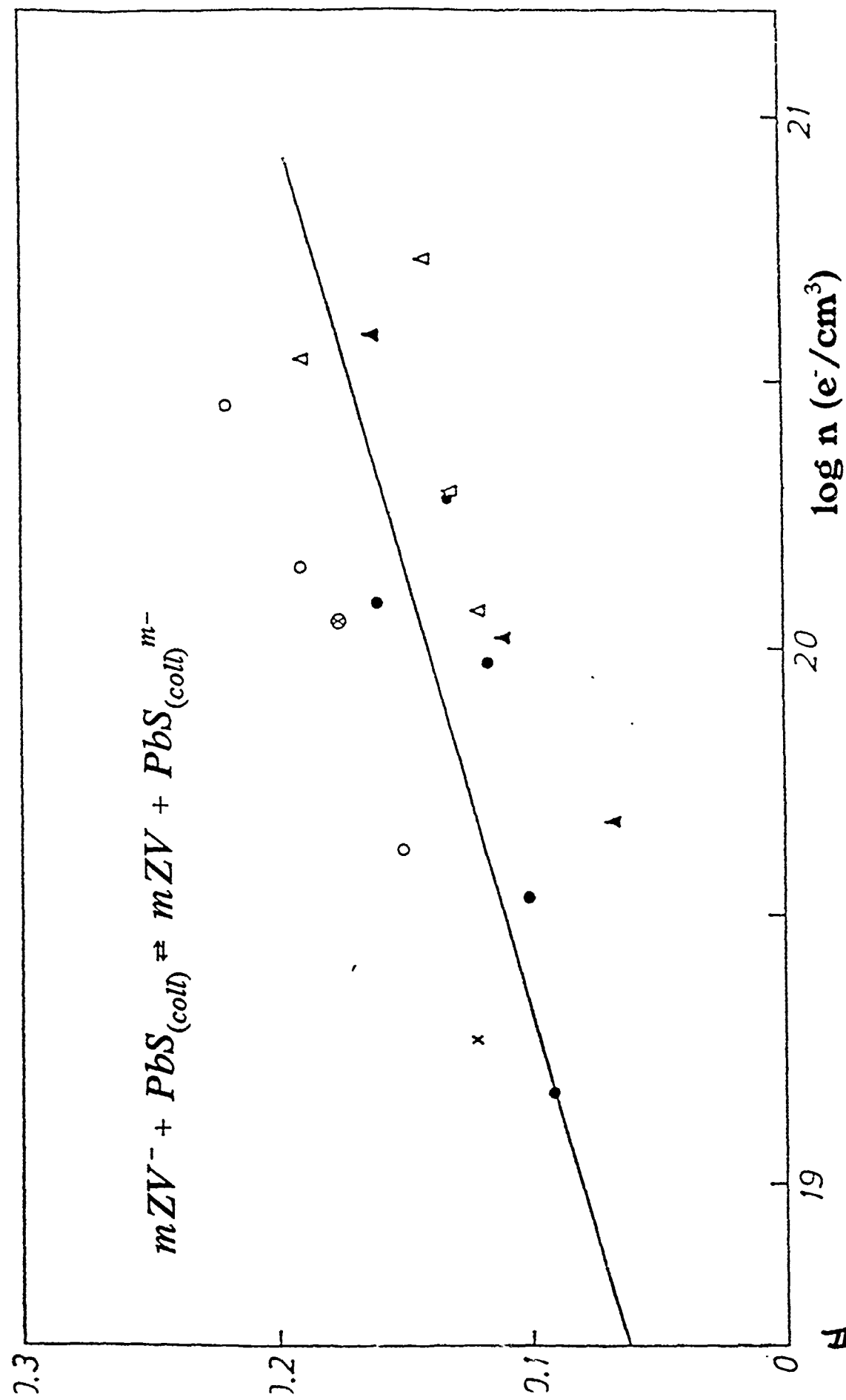
III-203

Figure 1

water

$E^0(V)$

-2.8 — $e^-_{aq} \cdot H^+/\frac{1}{2} H_2$

-2.6

$E(CdTe, 5nm)$

-2.0 — CO_2^-/CO_2

-1.8

$E(CdS, 2.5nm)$ — $CH_3CHO \cdot H^+/CH_3CH\dot{O}H$

$E(CdSe, 5nm)$ -1.0 — $CH_2\dot{O}H^+/CH_2OH$

$E(PbSe, 5nm)$ -0.8

-0.6 — $NO_2C_6H_4CN/NO_2^-C_6H_4CN$

-0.4 — MV^{2+}/MV^+

$E(HgSe, 5nm)$ — O_2/O_2^-

-0.2 — DQ/DQ^-

$E(PbS, 4nm)$

0 — $C_6H_4O_2/C_6H_4O_2$

0.2 — Cu^{2+}/Cu^+

Firgure 2

$$mZV^- + PbS_{(coll)} \rightleftharpoons mZV + PbS_{(coll)}^{m-}$$

log n (e⁻/cm³)

Figure 3

CdTe colloid spectra

a

$SO_4^- \cdot + TiO_2 \, {}_{(coll)}$

10 μs

b

$OH \cdot + TiO_2 \, {}_{(coll)}$

10 μs

200 μs

500 μs

Absorbance

Wavelength (nm)

III-207

Figure 5

(29) # KINETIC EFFECTS OF ZETA POTENTIAL ON INTERFACIAL ELECTRON TRANSFER

Dan Meisel[a], Franz Grieser[b] and Paul Mulvaney[c]

[a]Argonne National Laboratory, Argonne, Illinois USA

[b]University of Melbourne, Melbourne, Victoria, Australia

[c]Hahn-Meitner-Institut, Berlin Germany

INTRODUCTION

Electrostatic interactions between charged solution species have significant effects on rates of chemical reactions. The diffusional encounter of the reacting ionic species is given (in units of M^{-1} s^{-1}) by: [1]

$$k_{diff} = 4\pi N_0\, a_{ij}\, (D_i + D_j)\, \Phi_{ij} \times 10^{-3} \qquad (3)$$

In this equation, a_{ij} is the distance of closest approach of the reaction partners i and j, D_i and D_j are the corresponding diffusion coefficients, and N_o is Avogadro's number. The function Φ_{ij} depends on the potential of interaction between i and j, $z_i e_0 \psi_j$, and is given by:

$$\Phi_{ij} = \left(a_{ij} \int_{a_{ij}}^{\infty} \exp\left(\frac{z_i e_0 \psi_j}{kT}\right) \frac{dr}{r^2} \right)^{-1} \qquad (4)$$

In a solution containing a background electrolyte, the Debye-Hückel treatment for the potential energy of interaction yields:

$$\psi_j(r) = \frac{z_j e_0}{4\pi \varepsilon \varepsilon_0 r} \exp(-\kappa r) \qquad (5)$$

For a 1:1 electrolyte and at 25°C, $\kappa = 0.329 c^{1/2}$ ($Å^{-1}$), where c is the concentration (in mole/l) of the electrolyte. The Debye length, $1/\kappa$, is the distance at which the interaction potential between the reactive charged species has fallen to $1/e$ of the value at contact. For a 1:1 electrolyte at a concentration of 0.001M $1/\kappa$ is about 100 Å. At higher electrolyte concentrations the interaction range between charged reactants is of course reduced due to increased screening of the potential by the counter-ions. At a 1:1 electrolyte concentration of 0.1 M, $1/\kappa$ of about 10 Á is

obtained. The rate constant of the elementary reaction between hydrated electrons and protons, for example, decreases by approximately 20% over the electrolyte concentration mentioned [2].

Perhaps a more interesting area in which to consider the effects of Coulombic interactions is in reactions occurring in microheterogeneous systems, i.e., reactions between charged colloids and ionic oxidants or reductants. Due to the larger interaction potentials that can exist between charged colloids and charged reactants, electrostatic effects can be far more pronounced than for simple ion-ion interactions.

Generally, a colloid can be considered to be a globular polymer, micelle, or a solid metallic or semiconductor particle particle. The random generation of reactive species by, say, an excitation light pulse or a pulse of ionizing radiation, in a colloidal dispersion can lead to chemical reactions between the colloid and the reactive solution species. The rate of these reactions are highly dependent on the charge on the colloid, the charge on the reactant and on the background electrolyte concentration of the dispersion. If the chemical reactions in question are diffusion controlled, then the above parameters are quantitatively taken into account in equation (3). The one modification that needs to be made is that the potential profile between the colloid and the ion must be found from the numerical solution of the Poisson-Boltzmann equation:

$$\nabla^2 \psi = \frac{1}{r^2}\frac{d}{dr}\left(r^2\frac{d\psi}{dr}\right) = \frac{8\pi c e_0}{\varepsilon} \sinh\left(\frac{e_0\psi}{kt}\right) \tag{6}$$

where r is the distance from the surface and the other symbols have their usual meaning. Although equations (4) and (6) are clumsy to work with, they can nevertheless be readily solved numerically. The influence of Coulombic interactions between a colloid and a charged reactant has been recognized in micellar systems [3,4], polyelectrolyte solutions [5] and semiconductor particle dispersions [6-10].

Often the reaction between the solution species and the solid particle is slower than the diffusion controlled limit, i.e. the diffusional encounter between the colloidal particle and the solution species does not lead to a reaction on each encounter. Electron transfer, between the

semiconductor particle and solution species is in general activation controlled. To treat activation controlled reactions and still allow for Coulombic interactions between the colloid and solution reactant requires a significant embellishment to equation (3). To illustrate the consequences of this treatment, we will concentrate in the forthcoming discussion on electron transfer reactions between semiconductor colloids and charged redox reactants in solution.

INTERFACIAL ELECTRON TRANSFER REACTIONS

Before developing the equations involved in electron transfer across the colloid-solution interface, it is necessary to adopt a model describing the electrostatic potential profile ($\psi(r)$) between the charged particle surface and the bulk solution. A useful and widely used model is the Gouy-Chapman-Stern (GCS) model which is depicted in Figure 1. The diagram shows that for a negatively charged surface with a surface potential, ψ_0, there will be an immobile layer of oppositely charged ions immediately next to the surface (the Stern layer), and a diffuse distribution of mobile ions at further distance from the surface. In this electrical double layer (EDL) there is overall, of course, an equal number of positive and negative charges. The electrostatic potential extending from the surface into the bulk solution will have the profile as shown in the figure.
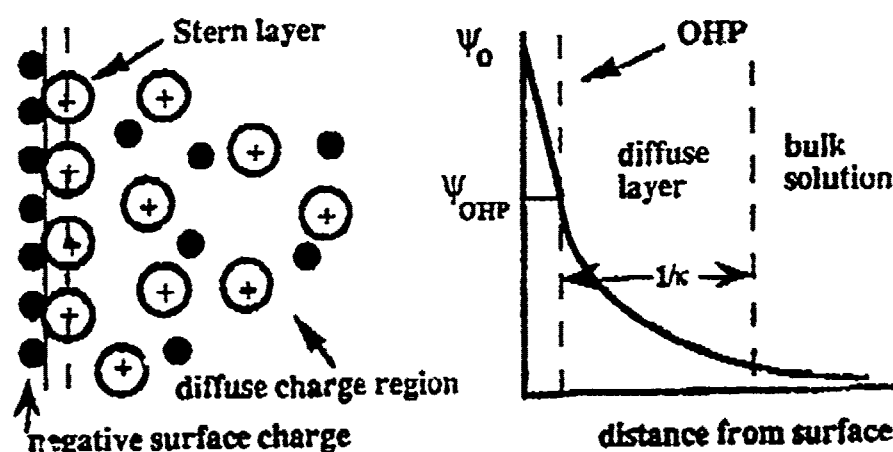

Figure 1. Schematic diagram of the GCS model for the EDL of a charged surface in an aqueous electrolyte solution, with the corresponding electrostatic potential profile.

6/20/91   DRAFT   5

For a colloidal semiconductor metal oxide, the electrostatic surface potential is controlled by the net surface charge density, composed of positive $-OH_2^+$ and negative $-O^-$ sites. Since these sites are in equilibrium with solution protons, a change in the pH of the solution will affect the surface charge density and hence the electrostatic surface potential. The pH at which there is an equal number of positive and negative sites on the oxide is known as the pzc; at this point the electrostatic surface potential will be zero. At a pH above the pzc, the surface will be negative, and below the pzc the surface will be positive.

Armed with this model of the electrostatic surface of a colloidal semiconductor metal oxide, electron transfer reactions can now be considered. For anodic electron transfer (electron transfer from a solution species to the colloid) the rate constant, using the electrochemical Tafel approximation, can be expressed as:

$$k_{et} = k^\circ \exp\left[\frac{\beta F(E_f - E_{redox})}{RT}\right] \qquad (7)$$

where k° is the rate constant when the system is at equilibrium, i.e, $E_f - E_{redox} = 0$. E_f is the electrochemical potential of the Fermi level of the semiconductor and is assumed to lie at the bottom of the conduction band. E_{redox} is the electrochemical reduction potential of the reactive solution species. In the treatment followed in this article, both these potentials are taken relative to the NHE.

At the pzc, the rate constant for electron transfer is

$$k_{pzc} = k^\circ \exp\left[\frac{\beta F(E_f^{pzc} - E_{redox})}{RT}\right] \qquad (8)$$

6/20/91   DRAFT   6

As indicated earlier, a change in pH will affect the electrostatic potential at the surface of the semiconductor oxide. This can be incorporated into equation (8) by using the following two equations:

$$E_f = E_f^{pzc} + \Psi_0 \tag{9}$$

$$\Psi_0 = 2.3 \frac{RT}{F} (pH - pH_{pzc}) \tag{10}$$

Substituting equations (9) and (10) into equation (8) gives:

$$\log\left(\frac{k_{et}}{k_{pzc}}\right) = -\beta (pH - pH_{pzc}) \tag{11}$$

Equation (11) assumes that the reaction occurs at the surface. It is commonly believed, however, that the plane at which electron transfer occurs is at the Outer Helmholtz Plane (OHP) [11]. At this plane the electrostatic potential is no longer Ψ_0 but rather Ψ_{OHP}. Only at high ionic strength (or, trivially, at the pzc) will the two coincide. For a finite potential at the OHP and taking into account that the concentration of reactive species (of charge z_R) at the OHP is now determined by a Boltzmann distribution, produces equation (12) [9,10],

$$\log\left(\frac{k_{et}}{k_{pzc}}\right) = -\beta(pH - pH_{pzc}) - (\beta + z_R)\frac{\Psi_{OHP}}{2.3RT} \tag{12}$$

The validity of this equation has been tested for the reaction of both negatively and positively charged radicals, reducing colloidal iron oxide [9,10]. To show its more universal application we now turn to the case of electron transfer from the colloid to a solution species. For a cathodic electron transfer process, β in equation (12) is replaced by $-(1-\beta)$, and this gives equation (13).

$$\log\left(\frac{k_{et}}{k_{pzc}}\right) = (1-\beta)(pH-pH_{pzc}) - (z_R + \beta - 1)\frac{\Psi_{OHP}}{2.3RT} \tag{13}$$

III-214

Although a number of reactions have been studied involving electron transfer from a semiconductor colloid to a solution species, EDL effects have not in general been recognized. Little data actually exists in the literature that allows the treatment of the data by equation (13). An exception is the work of Darwent and co-workers [6-8] using TiO_2 as the electron donor and methylviologen (MV^{++}) as the solution acceptor. Their rate constant data at different pH is plotted in Figure 2 relative to the value at the pH_{pzc}.
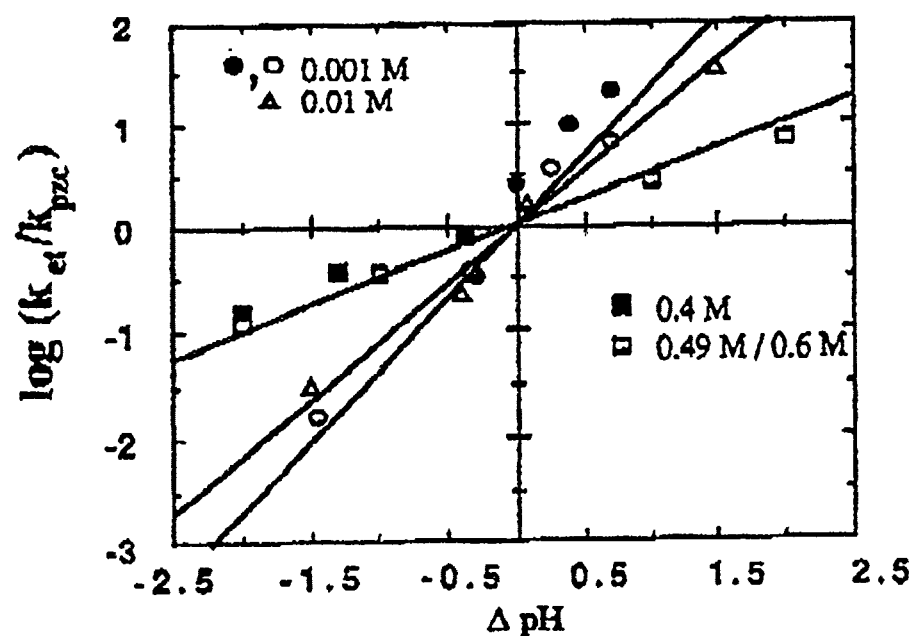

Figure 2. Experimental and theoretical plots of $\log(\frac{k_{et}}{k_{pzc}})$ vs. ΔpH (= pH - pHpzc) for electron transfer from TiO_2 to MV^{++}. Data points are from references 6 and 7. Solid lines have been calculated using equation (13) and ζ values taken from Figure 3. In these calculations, $\beta = 0.5$ and $z_R = 2$.

The overlap of the data in Figure 2 for the different higher electrolyte concentrations implies that $\Psi_{OHP} = 0$ in this concentration regime. The solid line passing through the data points for 0.4M, 0.49M and 0.6M, 1:1 electrolyte has therefore been generated using the cathodic version of equation (11), i.e., equation (13) with $\psi_{OHP} = 0$. The choice of $\beta = 0.5$ is consistent with other

measurements on TiO_2 colloids [9,10,12,13]. In order to calculate theoretical lines through the other data points shown requires a knowledge of the variation in the OHP potential of TiO_2. Accepting that Ψ_{OHP} is equal to the ζ potential [14], the data of Wiese and Healy [15] can be used to generate the two curves shown in Figure 3. The original data of Wiese and Healy reports only ζ potentials at pH values greater than the pH_{pzc}. However, since electrophoretic potentials are symmetric about the pzc (provided no specific ion adsorption occurs) the full curves, as shown, can be generated.
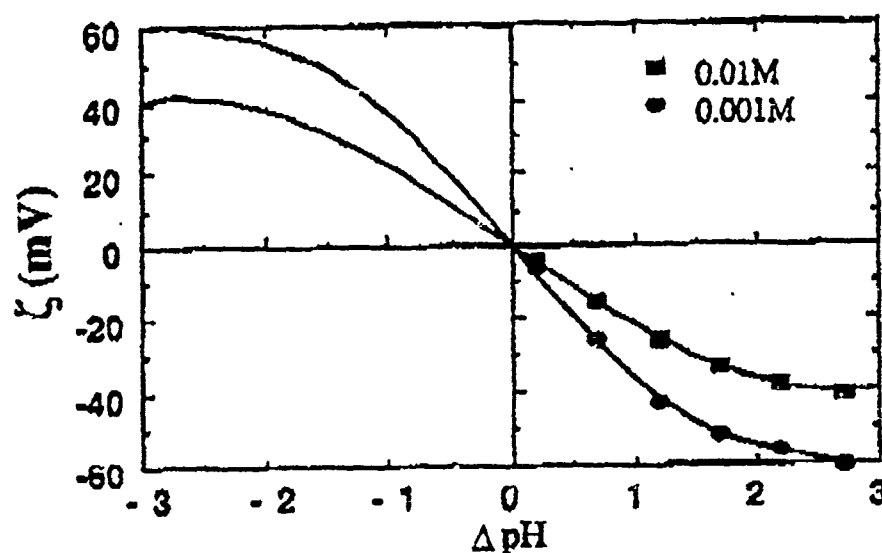

Figure 3. The electrophoretic ζ potential on TiO_2 colloids as a function of ΔpH and background electrolyte (KNO_3) concentration. Data from reference 15.

Using the data of Figure 3 and equation (13) generates the solid lines in Figure 2, which essentially follow the 0.01 M and 0.001 M data. As can be seen, there is excellent correspondence between theory and the 0.01 M experimental data and a reasonably good correlation between the two data sets for 0.001 M. A possible reason that the experimental points at pH values greater than the pH_{pzc} for the 0.001 M data are slightly higher than the theoretical line may be due to specific adsorption of MV^{++} onto colloidal iron oxide [10] under similar conditions. At higher electrolyte levels, as with the 0.01 M data, ion exchange effects reduce the amount of adsorbed MV^{++} as we

6/20/91   DRAFT   9

have observed on colloidal SnO_2 [16], and consequently in this case, theory and experiment agree very well.

A final point to discuss is the situation in which activation controlled reactions overlap with diffusion limited reactions, a situation that can occur if an electron transfer reaction is followed over a wide pH range. The appropriate rate constant, k, is then give by:

$$\frac{1}{k} \approx \frac{1}{k_{diff}} + \frac{1}{k_{et}} \tag{14}$$

An example of a system in which this was found to occur was in our study of the reduction of colloidal iron oxide [10].

SUMMARY

Electrostatic field effects around a colloidal semiconductor metal oxide can have a pronounced effect on the rate of interfacial electron transfer, both to and from the colloid. A quantitative understanding of the effect can be gained based on available models of the electrical double layer surrounding a colloid in solution and the treatment of interfacial electron transfer using athe electrochemical Tafel approach.

ACKNOWLEDGMENTS

6/20/91   DRAFT   10

REFERENCES

1.   M. Eigen, *Progress in Reaction Kinetics*, 2, 285-319 (1962).

2.   E. J. Hart and M. Anbar, *The Hydrated Electron*, Wiley-Interscience, New York, 1970.

3.   M. Grätzel and J. K. Thomas, *J. Phys. Chem.*, 78, 2248-2254 (1974).

4.   A. Henglein and Th. Proske, *Ber. Bunsenges. Phys. Chem.* 82, 471-476 (1978).

5.   D. Meisel, M. S. Matheson and C. D. Jonah, *J. Phys. Chem.* 83, 257-264 (1979).

6.   G. T. Brown and J. R. Darwent, *J. Chem. Soc., Chem. Commun.* 98-100 (1985).

7.   J. R. Darwent and A. Lepre, *J. Chem. Soc., Faraday Trans. II*, 82, 2323-2335 (1986).

8.   G. T. Brown, J. R. Darwent and P. D. I. Fletcher, *J. Am. Chem. Soc.* 107, 6446-6451 (1985).

9.   P. Mulvaney ,V. Swayambunathan, F. Grieser and D. Meisel, *J. Phys. Chem.* 92, 6732-6740 (1988).

10. P. Mulvaney ,V. Swayambunathan, F. Grieser and D. Meisel, *Langmuir* 6, 555-559 (1990).

11. A. J. Bard and L. R. Faulkner, *Electrochemical Methods - Fundamentals and Applications*, Wiley, New York, 1980.

12. M. Grätzel and A. J. Frank, *J. Phys. Chem.* 86, 2964-2967 (1982).

13. J. Möser and M. Grätzel, *J. Am. Chem. Soc.* 105, 6547-6555 (1983).

14. R. J. Hunter, *Zeta Potential in Colloid Science*, Academic Press, London, 1981.

15. G. R. Wiese and T .W. Healy, *J. Colloid Interface Sci.* 51, 427-433 (1975).

16. P. Mulvaney, F. Grieser and D. Meisel, *Langmuir* 6, 567-572 (1990).

III-218